

**REGULATION AND EVOLUTIONARY ADAPTATIONS OF THE OSMOTIC  
STRESS RESPONSE IN *VIBRIO PARAHAEMOLYTICUS***

by

Gwendolyn J. Gregory

A dissertation submitted to the Faculty of the University of Delaware in partial fulfillment of the requirements for the degree of Doctor of Philosophy in Biological Sciences.

Summer 2020

© 2020 Gregory  
All Rights Reserved

**REGULATION AND EVOLUTIONARY ADAPTATIONS OF THE OSMOTIC  
STRESS RESPONSE IN *VIBRIO PARAHAEMOLYTICUS***

by

Gwendolyn Gregory

Approved: \_\_\_\_\_  
Velia M. Fowler, Ph.D.  
Chair of the Department of Biological Sciences

Approved: \_\_\_\_\_  
John A. Pelesko, Ph.D.  
Dean of the College of Arts and Sciences

Approved: \_\_\_\_\_  
Douglas J. Doren, Ph.D.  
Interim Vice Provost for Graduate and Professional Education and  
Dean of the Graduate College

I certify that I have read this dissertation and that in my opinion it meets the academic and professional standard required by the University as a dissertation for the degree of Doctor of Philosophy.

Signed:

---

E. Fidelma Boyd, Ph.D.  
Professor in charge of dissertation

I certify that I have read this dissertation and that in my opinion it meets the academic and professional standard required by the University as a dissertation for the degree of Doctor of Philosophy.

Signed:

---

M. Ramona Neunuebel, Ph.D.  
Member of dissertation committee

I certify that I have read this dissertation and that in my opinion it meets the academic and professional standard required by the University as a dissertation for the degree of Doctor of Philosophy.

Signed:

---

Salil A. Lachke, Ph.D.  
Member of dissertation committee

I certify that I have read this dissertation and that in my opinion it meets the academic and professional standard required by the University as a dissertation for the degree of Doctor of Philosophy.

Signed:

---

Sharon Rozovsky, Ph.D.  
Member of dissertation committee

I certify that I have read this dissertation and that in my opinion it meets the academic and professional standard required by the University as a dissertation for the degree of Doctor of Philosophy.

Signed:

---

Karl R. Schmitz, Ph.D.

Member of dissertation committee

## ACKNOWLEDGMENTS

I would like to start by thanking my doctoral advisor Dr. E. Fidelma Boyd. Re-entering science after a ten-year hiatus was no easy feat, and would have been impossible without her willingness to take a chance on me. She provided me the opportunity to enter a new discipline of science and was patient with me as I learned new techniques and approaches. She also allowed me the freedom to enhance my training by seeking collaborations with other laboratories and to make the most of the scientific resources available at the University of Delaware. She was dedicated to helping me produce the best work possible and to become the best scientist that I can be, as evidenced in the time we spent reviewing every presentation, abstract, poster and manuscript that I generated.

I would also like to thank my committee for their support and guidance throughout my graduate studies. Dr. Sharon Rozovsky kindly allowed me to complete a rotation in her lab and enabled me to expand my scientific toolkit to include biochemical techniques. Dr. Ramona Neunuebel was always available to answer questions and challenged me to think outside the box. Dr. Karl Schmitz took the time to work with me on assay development that was critical to the publication of two of my manuscripts. Dr. Salil Lachke provided invaluable feedback on my research.

Throughout my time in graduate school, the members of the Boyd laboratory were always available to offer guidance on research and balancing the many responsibilities of a grad student. Dr. Nathan McDonald mentored me in my first few years, and I am grateful to him for his patience and support. Dr. Megan Carpenter was

also a mentor, tolerated constant questions, and has remained a friend. Dr. Sai Kalburge had a significant impact on my research, and his work enabled me to develop my dissertation project. Dr. Abish Regmi was always available to answer questions and to provide feedback on my work. Jessica Tague has acted as a sounding board for my ideas, has always been available for troubleshooting, and many, many rounds of edits. Her insights have made me a better scientist and have helped me to hone my own critical thinking and problem-solving skills. Most importantly, she has been a true friend, always encouraging me when I needed it most. I had the opportunity to mentor Daniel Morreale on his senior thesis work, and am so grateful for this opportunity. I could not have asked for a better trainee, as he was always eager, prepared, careful, diligent, and hard-working.

Without a doubt, my graduate career would not have been successful without the constant and unfailing support of my husband, Adam Gregory. He was always willing to listen to one more presentation, read through one more document, or entertain the kids so I could work on an assignment. Many people asked me how I was able to pursue my PhD with three children at home. My answer was always the same: “My mother helps so much!”. She took care of so many things so that I could focus on my research, and I would have not been able to succeed without her support and love. I have been in graduate school for as long as my three boys can remember. They have always been understanding when I needed to work, and would excitedly accompany me to the lab to set up an experiment. Now they all love science as much as I do.

I am so grateful to all my friends who have provided support and acted as cheerleaders as I have worked through my graduate career. In particular, I would like to thank Ashley Petrino, Rhonda Asplen, Anna Smith, Aly Snider, Jean Wilcox, Pat

White, Michele Chynoweth, Michele Maughan and Brittney Schoenberger for their unwavering support and friendship.

## TABLE OF CONTENTS

LIST OF TABLES .....	xii
LIST OF FIGURES .....	xiii
ABSTRACT .....	xvii
 Chapter	
1 INTRODUCTION .....	1
Osmotic Stress Response in Bacteria.....	1
Biosynthesis of Compatible Solutes.....	5
Transport of Compatible Solutes.....	8
<i>Vibrio parahaemolyticus</i> a Marine Halophile.....	9
<i>Vibrio parahaemolyticus</i> Contains Multiple Compatible Solute Biosynthesis and Transporter Systems. ....	10
Regulation of Compatible Solute Biosynthesis.....	12
Regulation of Compatible Solute Transporters.....	14
Quorum Sensing in <i>Vibrio</i> .....	16
Dissertation Work.....	19
2 QUORUM SENSING REGULATORS APHA AND OPAR CONTROL EXPRESSION OF THE OPERON RESPONSIBLE FOR BIOSYNTHESIS OF THE COMPATIBLE SOLUTE ECTOINE .....	24
Introduction .....	24
Materials and Methods .....	27
Bacterial strains, media and culture conditions.....	27
Construction of the <i>cosR</i> deletion mutant. ....	28
RNA isolation and quantitative real-time PCR (qPCR).....	29
Protein purification of AphA, OpaR, and CosR.....	30
Electrophoretic Mobility Shift Assay.....	32
Transcriptional reporter Assays.....	33
Growth pattern analysis.....	35
Bioinformatics analysis.....	36
Results .....	36
Expression of <i>ectABCasp_ect</i> and quorum sensing regulator genes throughout the growth cycle.....	36
Ectoine biosynthesis genes are differentially regulated in quorum sensing mutants. ....	38
The <i>aphA</i> mutant has a growth defect in high salt. ....	41

	OpaR and AphA bind upstream of the ectoine biosynthesis operon.....	41
	OpaR and AphA directly regulate transcription of <i>ectABCasp_ect</i> .....	44
	CosR is a repressor that binds directly to the <i>ectABCasp_ect</i> regulatory region.....	46
	CosR is activated by OpaR and AphA.....	48
	Quorum sensing regulation of ectoine biosynthesis genes in <i>Vibrionaceae</i> .....	52
	Discussion.....	53
3	<b>COSR IS A GLOBAL REGULATOR OF THE OSMOTIC STRESS RESPONSE WITH WIDESPREAD DISTRIBUTION AMONG BACTERIA</b> .....	60
	Introduction .....	60
	Materials and Methods .....	64
	Bacterial strains, media and culture conditions .....	64
	Construction of the <i>betI</i> deletion mutant .....	64
	RNA isolation and qPCR.....	65
	Protein purification of CosR.....	66
	Electrophoretic Mobility Shift Assay .....	66
	Reporter Assays.....	68
	Bioinformatics and phylogenetic analyses .....	69
	Results .....	70
	Compatible solute biosynthesis and transport genes are downregulated in low salinity .....	70
	CosR represses compatible solute biosynthesis and transport genes in low salinity .....	73
	CosR binds directly to the promoter of the <i>betIBaproXWV</i> operon and represses transcription .....	75
	CosR binds directly to the promoter of <i>bccT1</i> and <i>bccT3</i> and is a direct repressor of <i>bccT3</i> .....	77
	CosR is a direct repressor of <i>proVWX1</i> .....	81
	CosR is not autoregulated.....	83
	BetI represses its own operon <i>betIBA</i> .....	85
	The quorum sensing LuxR homolog OpaR is a positive regulator of <i>betIBaproXWV</i> in <i>V. parahaemolyticus</i> .....	88
	Motif identification and phylogenetic distribution of CosR.....	89
	Discussion.....	94

4	INVESTIGATIONS OF DIMETHYLGLYCINE (DMG), GLYCINE BETAINE AND ECTOINE UPTAKE BY A BCCT FAMILY TRANSPORTER WITH BROAD SUBSTRATE SPECIFICITY IN <i>VIBRIO SPECIES</i> .....	103
	Introduction .....	103
	Materials and Methods .....	108
	Bacterial strains, media and culture conditions .....	108
	Growth analysis .....	108
	Functional complementation of <i>E. coli</i> strain MKH13 with VP1456, VP1723, VP1905, and VPA0356 .....	110
	Homology modeling of BCCT1 and docking of glycine betaine, DMG and ectoine.....	111
	Bioinformatics and phylogenetic analyses .....	112
	Results .....	113
	<i>V. parahaemolyticus</i> can utilize a wide range of compatible solutes.....	113
	DMG is an important compatible solute for <i>Vibrio</i> species.....	115
	BCCTs are responsible for transport of DMG .....	118
	BccT1 sequence homology to structurally characterized BCCTs.....	123
	Structural Modelling of BccT1.....	127
	Docking analysis of DMG and ectoine binding residues in BccT1. ....	132
	Site directed mutagenesis of BccT1 uncovers ectoine binding pocket. ...	133
	Distribution of BCCT1 .....	136
	Discussion.....	138
5	UTILIZATION OF DIMETHYLSULFONIOPROPIONATE (DMSP) AS AN OSMOLYTE BY <i>VIBRIO SPECIES</i> .....	146
	Introduction .....	146
	Materials and Methods .....	150
	Bacterial strains, media and culture conditions .....	150
	Growth analysis .....	151
	Functional complementation of <i>E. coli</i> strain MKH13 with VP1456, VP1723, VP1905, and VPA0356 .....	151
	Bioinformatics and phylogenetic analyses .....	152
	Results .....	152

	<i>Vibrio parahaemolyticus</i> can utilize dimethylsulfoniopropionate (DMSP) as a compatible solute.....	152
	DMSP is utilized as an osmolyte by <i>Vibrio</i> species .....	154
	DMSP is not a carbon source for <i>V. parahaemolyticus</i> .....	155
	A BCCT transporter is required for DMSP uptake .....	156
	Distribution and Phylogenetic Analysis .....	160
	Discussion.....	165
6	IDENTIFICATION OF NOVEL REGULATORS OF THE ECTOINE BIOSYNTHESIS OPERON.....	168
	Introduction .....	168
	Materials and Methods .....	171
	Bacterial strains, media and culture conditions .....	171
	DNA affinity chromatography/mass spectrometry .....	171
	Construction of <i>nhaR</i> , <i>torR</i> , and <i>ompR</i> , deletion mutants.....	173
	Reporter assays.....	174
	Results .....	176
	Identification of putative novel regulators of the ectoine biosynthesis operon .....	176
	LeuO, NhaR, OmpR and TorR are regulators of <i>ectABCasp_ect</i> in <i>V. parahaemolyticus</i> .....	177
	Investigation of NhaR as a direct regulator of <i>ectABCasp_ect</i> in <i>V. parahaemolyticus</i> .....	179
	Discussion.....	180
	REFERENCES .....	189
	Appendix	
A	THE ROLE OF OSCR AND LEUO IN LOW SALT REGULATION IN <i>VIBRIO PARAHAEMOLYTICUS</i> .....	211
B	ALIGNMENT OF <i>VIBRIO PARAHAEMOLYTICUS</i> BCCT-FAMILY TRANSPORTERS .....	221
C	PERMISSION LETTER .....	225
D	PERMISSION LETTER .....	226

## LIST OF TABLES

Table 1	Strains and Plasmids used in this study.....	56
Table 2	Primers used in this study.....	57
Table 3	Putative OpaR binding sites in the ectoine regulatory region of <i>Vibrio</i> species.....	59
Table 4	Strains and plasmids used in this study.....	99
Table 5	Primers used in this study.....	100
Table 6	Strains and plasmids used in this study.....	142
Table 7	Primers used in this study.....	144
Table 8	Results of the docking study showing free energy change upon substrate binding and a list of BccT1 residues mediating interactions with each substrate. ....	145
Table 9	Strains and plasmids used in this study.....	167
Table 10	Strains and plasmids used in this study.....	183
Table 11	Primers used in this study.....	185
Table 12	Candidate proteins ranked by score.....	186
Table 13	Candidate transcriptional regulators.....	188
Table 14	Primers used in this study.....	220

## LIST OF FIGURES

Figure 1	Structures of common compatible solutes.....	4
Figure 2	Compatible solute systems in <i>V. parahaemolyticus</i> , <i>V. cholerae</i> and <i>E. coli</i> .....	12
Figure 3	Quorum sensing in <i>Vibrio parahaemolyticus</i> .....	18
Figure 4	Expression analysis of <i>ectA</i> , <i>asp_ect</i> , <i>aphA</i> and <i>opaR</i> .....	38
Figure 5	Expression and growth analyses of quorum sensing mutants. ....	40
Figure 6	OpaR binds to <i>ectABC-asp_ect</i> promoter region. ....	42
Figure 7	AphA binds to <i>ectABCasp_ect</i> promoter region. ....	44
Figure 8	$P_{ectA-gfp}$ reporter assays in <i>E. coli</i> . ....	45
Figure 9	CosR binds to and represses <i>ectABCasp_ect</i> promoter region.....	48
Figure 10	<i>cosR</i> is regulated by OpaR. ....	50
Figure 11	<i>cosR</i> is regulated by AphA. ....	51
Figure 12	A model of ectoine biosynthesis gene regulation by quorum sensing regulators. ....	55
Figure 13	Expression of osmotic stress response genes is salinity dependent. ....	72
Figure 14	CosR represses osmotic stress response genes in low salinity.....	74
Figure 15	CosR binding to <i>betIBAprOXWV</i> promoter region. ....	76
Figure 16	CosR binds to <i>bccT1</i> promoter region.....	78
Figure 17	CosR binds to <i>bccT3</i> promoter region.....	80
Figure 18	CosR bind to <i>proVWX</i> promoter region. ....	82
Figure 19	CosR does not autoregulate. ....	84
Figure 20	BetI autoregulates in <i>V. parahaemolyticus</i> .....	87
Figure 21	OpaR binds to <i>betIBAprOXWV</i> promoter region. ....	89

Figure 22	CosR MEME analysis. ....	90
Figure 23	Genomic context of CosR in Vibrionaceae species. ....	92
Figure 24	Phylogenetic analysis of CosR distribution.....	94
Figure 25	A model of CosR regulation of the osmotic stress response. ....	98
Figure 26	BCCT-family transporters in <i>Vibrio parahaemolyticus</i> .....	107
Figure 27	Growth analyses of $\Delta$ <i>ectB</i> mutant in phenotypic microarray plate .....	114
Figure 28	Growth analyses of $\Delta$ <i>ectB</i> mutant with selected osmolytes .....	115
Figure 29	Growth analyses of <i>Vibrio</i> strains with DMG.....	117
Figure 30	Growth analyses of <i>Vibrio</i> species with DMG as carbon source .....	118
Figure 31	Growth analyses of quadruple <i>bccT</i> mutant with DMG.....	119
Figure 32	Growth analyses of triple <i>bccT</i> mutants with DMG.....	121
Figure 33	Functional complementation of <i>E. coli</i> with DMG .....	122
Figure 34	Functional complementation of <i>E. coli</i> with BccT1 .....	124
Figure 35	Hydropathy profile of <i>V. parahaemolyticus</i> BccT1 .....	125
Figure 36	BccT1 alignment with <i>Corynebacterium glutamicum</i> BCCT-family transporters .....	126
Figure 37	Verification of the overall quality of our predicted BccT1 models with Verify3D.....	128
Figure 38	Ramachandran plots verifying stereochemical properties of our BccT1 models.....	129
Figure 39	Predicted overall structure of BCCT1 and its active site interactions with different substrates. ....	131
Figure 40	Functional complementation of <i>E. coli</i> with BccT1 mutants .....	135
Figure 41	Phylogenetic distribution of BccT1 .....	137
Figure 42	BCCTs in <i>Vibrio parahaemolyticus</i> . ....	150

Figure 43	Growth analyses with DMSP .....	153
Figure 44	Growth analyses of <i>Vibrio</i> species with DMSP. ....	155
Figure 45	Growth of <i>Vibrio</i> species with DMSP as sole carbon source. ....	156
Figure 46	Growth analysis of <i>bccT</i> null strain with DMSP.....	157
Figure 47	Growth analyses of triple <i>bccT</i> mutants with DMSP. ....	158
Figure 48	Functional complementation of <i>E. coli</i> MKH13 with <i>bccT</i> . ....	160
Figure 49	Phylogenetic analysis of BccT2 distribution within Vibrionaceae. ....	162
Figure 50	<i>Halomonas</i> sp. HTNK1 DddT alignment with homologs found in <i>V. vulnificus</i> , <i>V. fluvialis</i> and <i>V. harveyi</i> . ....	163
Figure 51	Phylogenetic analysis of the evolutionary relationships among five BccTs present in <i>Vibrio</i> species. ....	164
Figure 52	Protein separation via SDS-PAGE. ....	177
Figure 53	Expression of a $P_{ectA}$ - <i>gfp</i> transcriptional fusion in wild-type (WT) <i>V. parahaemolyticus</i> $\Delta leuO$ , $\Delta nhaR$ , $\Delta ompR$ , and $\Delta torR$ mutants. ....	178
Figure 54	Expression of a $P_{ectA}$ - <i>gfp</i> transcriptional fusion in <i>E. coli</i> strain $\Delta nhaR$ . ....	180
Figure 55	Model of regulation of ectoine biosynthesis genes in low salinity and high salinity growth conditions. ....	182
Figure 56	Swarming assay on HI plates supplemented with 0.5% NaCl .....	213
Figure 57	Swarming assay on HI plates supplemented with 3% NaCl .....	214
Figure 58	Colony morphology and CPS production.....	215
Figure 59	Swimming assay on soft-agar 0.5% NaCl plates.....	216
Figure 60	Swimming assay on soft-agar 3% NaCl plates.....	217
Figure 61	OpaR binds <i>oscR</i> promoter region. ....	218
Figure 62	Putative OpaR binding sites in <i>leuO</i> regulatory region.....	219

Figure 63 Alignment of BccTs with structurally-characterized BCCT-family transporters ..... 223

## ABSTRACT

Bacteria have evolved mechanisms that allow them to adapt to changes in osmolarity and some species have adapted to live optimally in high salinity environments such as the marine ecosystem. Many bacteria that live in high salt environments do so by the biosynthesis or uptake of compatible solutes, small organic molecules, that maintain the turgor pressure of the cell by balancing the internal and external osmolarity. The mechanisms by which bacteria regulate osmoadaptations in response to osmotic stress is poorly understood. *Vibrio parahaemolyticus* is a marine halophile that grows optimally at 0.5M NaCl, and also encounters changes in osmolarity, both hypo- and hyper-salinities. The bacterium copes with hyper-salinity by accumulating a range of compatible solutes by uptake from the environment via multiple compatible solute transporters: four betaine-carnitine-choline transporter (BCCT) family transporters and two ATP-Binding Cassette (ABC)-family transporters, ProU1 and ProU2. In addition, *V. parahaemolyticus* contains the compatible solute biosynthesis operons ectoine (*ectABC-asp\_ect*) and glycine betaine (*betIBA*). This is triple the number of systems compared to those present in *Escherichia coli* and *V. cholerae*. We hypothesized that *V. parahaemolyticus* can grow optimally in high salinity conditions due to the presence of multiple compatible solute systems. The work in this dissertation seeks to elucidate how these evolutionary adaptations are coordinated and regulated at the transcriptional level and how these adaptations allow halophiles such as *V. parahaemolyticus* to thrive in high salinity environments. Chapter 2 focuses on the role of the quorum sensing regulatory system in controlling ectoine biosynthesis. Using genetic and biochemical analyses, we determined that low cell density regulator AphA was a direct positive regulator of

ectoine biosynthesis, whereas the high cell density regulator OpaR was a direct negative regulator of the operon. This study also identified an additional regulator CosR that repressed the ectoine biosynthesis operon. In addition, CosR was positively regulated by the quorum sensing master regulators AphA and OpaR. This regulation mechanism formed a feed-forward loop to tightly control expression of ectoine.

In chapter 3, we demonstrated that the CosR repressor is a global regulator of the osmotic stress response. We showed that CosR was a repressor of multiple compatible solute transporters and both biosynthesis operons. DNA binding assays demonstrated that CosR binds directly to each of the regulatory regions of these osmotic stress response genes. Plasmid-based reporter assays in *E. coli* demonstrated that CosR directly represses *bccT3*, both *proU* operons, and the glycine betaine operon. CosR distribution is widespread within *Vibrionaceae*, and in Gamma-proteobacteria in general, indicating that CosR regulation of the osmotic stress response is pervasive among bacteria.

In chapter 4, we demonstrated for the first time that N-N dimethylglycine (DMG), dimethylsulfoniopropionate (DMSP), trimethylamine-N-oxide (TMAO), and  $\gamma$ -amino-N-butyric acid (GABA), amongst others, are effective compatible solutes for *V. parahaemolyticus*. DMG was a highly effective osmoprotectant and we show that it is also utilized as an osmoprotectant by *V. harveyi*, *V. fluvialis*, *V. cholerae* and *V. vulnificus*. We determined that, with the exception of BccT4, all of the BccTs in *V. parahaemolyticus* could uptake DMG. Of the four BCCT-family transporters present in *V. parahaemolyticus*, BccT1 had the broadest substrate uptake ability in terms of number and diversity of compounds. To determine how substrate coordination and transport by BccT1 has evolved, we examined amino acid residues known to be

important for coordination of glycine betaine. Utilizing mutagenesis and functional complementation approaches, our results showed the binding pocket for glycine betaine is more flexible than for ectoine and DMG.

In chapter 5, we examined the role of DMSP in *Vibrio* osmoprotection. DMSP is an organosulfur compound produced by phytoplankton in huge quantities in the marine environment and used as an osmoprotectant. Whether marine bacteria also use DMSP as an osmoprotectant is largely unknown. Our work demonstrated that DMSP is a highly effective compatible solute used by *Vibrio* species. Our work showed that DMSP is transported into bacterial cells using a single BCCT transporter BccT2 with high efficiency.

In chapter 6, we set out to identify novel ectoine biosynthesis regulators. To accomplish this, we performed a DNA affinity chromatography-pulldown with the regulatory region of the *ectABCasp\_ect* operon as a bait. Pulldowns were performed under inducing conditions and non-inducing conditions to capture both positive and negative regulators of the *ectABCasp\_ect* operon. In total, we identified 37 candidate proteins that bound to the regulatory region. Four proteins were examined further, regulators NhaR, TorR, LeuO, and OmpR. Our work showed that NhaR is a repressor while LeuO is an activator of the *ectABCasp\_ect* operon.

## Chapter 1

### INTRODUCTION

#### Osmotic Stress Response in Bacteria.

Halophilic bacteria such as *Vibrio parahaemolyticus* encounter a range of osmolarities in the aquatic environment. As a free-living marine organism, *V. parahaemolyticus* encounters fluctuations in osmolarity to which it must rapidly respond to prevent cell lysis. Growth of bacteria in high NaCl concentrations lowers the turgor pressure of the cell due to efflux of water across the osmotic gradient. To combat this loss of turgor pressure, bacteria have developed two strategies for osmotic stress adaptation. The salt-in-the-cytoplasm response was first discovered in *Halobacteriaceae* (1). Extremely halophilic members of this *Archaea* family (2) as well as anaerobic halophilic *Bacteria* of the order *Haloanaerobiales* (3) have cellular machinery adapted to this strategy and can accumulate inorganic ions up to a reported 7 M concentration (4). In non-extreme halophiles and those in the domain *Bacteria*, osmoadaptation occurs in two stages. The initial and short-term response is characterized by the uptake of potassium ions in response to increased external osmolarity, exemplified in *Escherichia coli* and *Bacillus subtilis* (5). The strong positive charge of the potassium ( $K^+$ ) ions must be balanced to prevent damage to biological molecules and processes. Gram-negative bacteria biosynthesize or uptake from the environment organic anions, such as glutamate, to counterbalance the charge of the accumulating  $K^+$ . In contrast, the counter ion that balances  $K^+$  accumulation in Gram-positive bacteria is unknown, as intracellular glutamate only minimally increases or decreases (5, 6).

High concentrations of  $K^+$  have deleterious effects on cellular processes and therefore a secondary long-term osmoadaptation strategy involving uptake or biosynthesis of compatible solutes is employed (5). It was proposed that accumulated  $K^+$  and glutamate act as a trigger of this secondary response (7-10). This was demonstrated in the halophilic bacterium *Halobacillus halophilus*, where  $K^+$  glutamate accumulation induces proline biosynthesis (11). Compatible solutes, as the name suggests, are organic compounds that are compatible with the molecular machinery and processes of the cell. Typically compatible solutes carry no net charge at physiological pH and do not interact with proteins or nucleic acids (12). Compatible solutes are taken up from the environment and/or biosynthesized from various precursors in response to osmotic stress. Compatible solutes can be classified into a few structural categories and include compounds such as trehalose (a sugar), glycerol and mannitol (polyols), proline, glutamate and glutamine (free amino acids), ectoine (amino acid derivative), glycine betaine (GB) and carnitine (quarternary amines), dimethylglycine (DMG, a tertiary amine), choline-*O*-sulfate (sulfate ester), dimethylsulfoniopropionate (DMSP, a tertiary sulfonium), N-acetylated diamino acids and small peptides, among others (**Figure 1**) (5, 13-20). Bacteria can accumulate compatible solutes in molar concentrations without affecting the molecular processes of the cell. This accumulation also causes an increase in free water in the cell which is a major determining factor in growth and division (21). Accumulation of compatible solutes thus allows cells to continue to grow and divide even in unfavorable environments (22). It has been shown that compatible solutes also protect proteins, nucleic acids and other vital molecular machinery by increasing the hydration shell around these molecules (23). Accumulation of osmolytes can be accomplished either

by uptake via primary ABC-type transporters, secondary transporters of the BCCT family or biosynthesis.

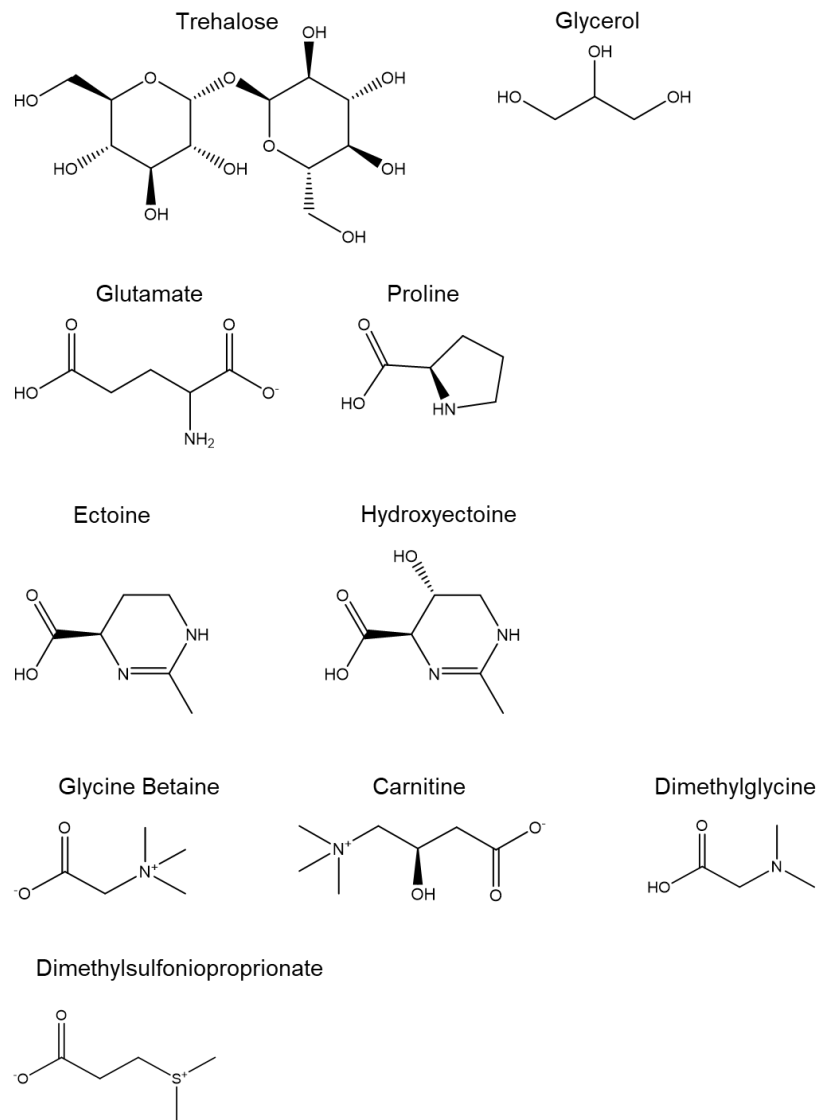


**Figure 1 Structures of common compatible solutes**  
 Examples of structural categories of compatible solutes include: trehalose (sugar), glycerol (polyol), proline and glutamate (free amino acids), ectoine and hydroxyectoine (amino acid derivatives), glycine betaine (GB), and carnitine (quarternary amines), dimethylglycine (DMG, tertiary amine), and dimethylsulfonylpropionate (DMSP, tertiary sulfonium).

### **Biosynthesis of Compatible Solutes.**

Osmoadaptative mechanisms include systems for compatible solute biosynthesis and many bacterial species can biosynthesize proline, glutamate, glutamine and trehalose in response to osmolarity changes. These compounds are also utilized in different metabolic pathways in the cell and as carbon sources, therefore their usage as osmolytes can lead to an energy sink. Some compatible solutes are widespread among bacteria such as glycine betaine, trehalose and glutamate while others are more confined. Glycine betaine (N,N,N-trimethylglycine) was considered the main compatible solute produced by halophilic phototrophic bacteria (24-26) and archaeal methanogens (27). While ectoine (1,4,5,6-tetrahydro-2-methyl-4-pyrimidinecarboxylic acid) was suggested as the main compatible solute produced by aerobic heterotrophic bacteria (28-31). A recent bioinformatics study showed that ectoine and hydroxyectoine genes were present predominantly in *Bacteria* and only a few *Archaea* and *Eukarya* (32-34). Among 6,428 microbial genomes examined, 440 species (7%) had ectoine biosynthesis genes and of these, 272 were predicted to synthesize hydroxyectoine as well (32). Trehalose is also a compatible solute used by members of the phylum *Proteobacteria* as well as several Gram-positive bacteria including *Bacillus* species and members of the order *Actinomycetes* (28). In the absence of preferred compatible solutes glycine betaine and proline, trehalose is biosynthesized by *E. coli* and *Salmonella typhimurium* (35, 36). Trehalose can also be utilized as a carbon source and therefore biosynthetic and catabolic pathways are tightly controlled in an osmolarity-dependent manner (5, 37). Most members of the family *Vibrionaceae* can biosynthesize and catabolize trehalose.

Ectoine is biosynthesized *de novo* from endogenous cellular aspartic acid. EctA, EctB, and EctC encoded by the operon *ectABC* convert aspartic acid to ectoine

and this operon is evolutionarily conserved in Gram-positive and Gram-negative bacteria (38-40). Several species that produce ectoine also encode a specialized aspartokinase (Ask) specific to the ectoine biosynthesis pathway and clustered with the *ectABC* genes (41-44). For example, the halophile *Vibrio parahaemolyticus* encodes a specific aspartokinase (Asp\_ect) in the same operon as the *ectABC* genes (45). Ask/Asp\_ect converts aspartic acid to  $\beta$ -aspartyl phosphate, which is then converted to L-aspartate- $\beta$ -semialdehyde by aspartate semialdehyde dehydrogenase (Asd). This intermediate product in the aspartic acid pathway, L-aspartate  $\beta$ -semialdehyde, is then funneled into the ectoine biosynthesis pathway and converted to L-2,4-diaminobutyrate by L-2,4-diaminobutyrate transaminase (EctB). This product is then acetylated by L-2,4-diaminobutyrate N<sup>γ</sup>-acetyltransferase (EctA) and N<sup>γ</sup>-acetyldiaminobutyrate is formed. Finally, L-ectoine synthase (EctC) performs the cyclic condensation reaction to produce tetrahydropyrimidine ectoine, or ectoine (40). The ectoine derivative 5-hydroxyectoine also a compatible solute, requires an additional enzyme EctD, an ectoine hydroxylase, which converts ectoine to 5-hydroxyectoine (46).

Production of glycine betaine takes place in a two-step oxidation from the precursor choline and is not a *de novo* biosynthetic reaction. True *de novo* biosynthesis of glycine betaine is rare and has been identified in a limited number of halophilic bacteria: *Actinopolyspora halophila*, *Halorhodospira halochloris*, *Aphanothece halophytica*, *Synechococcus* sp. WH8102, *Myxococcus xanthus* and *Methanohalophilu sportucalensis* (47-54). The two-step oxidation proceeds with choline conversion to glycine betaine by the products of two genes *betB* and *betA*, which encode betaine-aldehyde dehydrogenase and choline dehydrogenase, respectively. In *E. coli*, these

genes are encoded by the operon *betIBA*; *betI*, is a repressor of its own operon (55, 56). Choline is oxidized by choline dehydrogenase (BetA) to produce betaine aldehyde. Betaine aldehyde is then oxidized to glycine betaine by betaine-aldehyde dehydrogenase (BetB) (57, 58). In all *Vibrio* species that biosynthesize betaine, the *betIBA* genes are in an operon with the *proXWV* genes, which encode a ProU transporter (45, 59, 60). We also recently demonstrated that BetI is a repressor of its own operon in *V. parahaemolyticus*, and this has also been demonstrated in *V. harveyi*, indicating this mechanism is conserved (61, 62). Within the family *Vibrionaceae*, neither ectoine or glycine betaine are used as carbon and energy sources and are considered bona fide osmolytes. It was shown that nearly 70% of *Vibrio* species produced ectoine and greater than 60% produced both ectoine and glycine betaine (59).

Dimethylglycine (DMG) is produced as an intermediate compound during *de novo* glycine betaine biosynthesis. It is also produced as an intermediate of glycine betaine metabolism and is utilized as a compatible solute by several bacterial species, including *V. parahaemolyticus* (20, 63-68). DMSP is an organosulfur compound abundant in marine surface waters produced by phytoplankton and some halophytic vascular plants in large quantities and used by these primary producers as an osmoprotectant (69-73). We recently demonstrated that DMSP is utilized as an osmoprotectant by *V. parahaemolyticus* and other *Vibrio* species (Gregory & Boyd, unpublished data). Many of the compatible solutes or precursors in use by *Vibrio* species are available in the marine environment, including glycine betaine, ectoine, choline, DMG, and DMSP (13, 64, 65, 70, 72, 74).

### **Transport of Compatible Solutes.**

It is energetically favorable to the cell to uptake compatible solutes from the environment rather than to synthesize them *de novo* (5, 30, 75). Therefore, *Bacteria* and *Archaea* encode osmoregulated transporters to uptake compatible solutes (76-80). One family of compatible solute transporters is the betaine-carnitine-choline transporter (BCCT) family; the founding member, BetT, was first discovered in *E. coli* and transports choline with high-affinity (81). Other members of the BCCT family include an L-carnitine transporter, CaiT, in *E. coli*, and glycine betaine transporters in *Bacillus subtilis* (OpuD) and *Corynebacterium glutamicum* (BetP), among many others (77, 78, 82-84). The BCCT family uses a proton- or sodium-motive force to transport substrates into the cell (77, 78, 80, 85). The BcctT protein is organized into 12 transmembrane domains (TM to TM12) (85), with TM8 comprised of a stretch of tryptophan residues, thought to be involved in substrate binding (86). BCCTs have been shown to be induced in high osmolarity conditions (60, 61, 82).

*Bacteria* and *Archaea* also utilize osmoregulated ATP-binding cassette (ABC) transporters to import exogenous compatible solutes into the cell (77-80, 87). Examples of ABC-type transporters include ProU in *E. coli*, OpuA in *Lactococcus lactis*, OpuA, OpuB and OpuC in *B. subtilis*, and OpuC in *Pseudomonas syringae* (77-80, 88-92). The ABC transporters are made up of a transmembrane domain (TMD), a nucleotide-binding domain (NBD) and a substrate-binding protein (SBP). Several ABC transporters contain a cystathionine- $\beta$ -synthase (CBS) on the C-terminus of the NBD. The CBS is required for osmoregulatory function of the ABC transporters in *L. lactis* and *P. syringae* (90, 91, 93). The NBD is encoded by the *proV* gene, while *proW* encodes the TMD and *proX* encodes the SBP (88, 94-96). The *E. coli* ProU was shown to bind glycine betaine with high affinity and to be osmoregulated (88, 97, 98). We

have also recently demonstrated that both ProUs present in *V. parahaemolyticus* are osmoregulated (61).

### ***Vibrio parahaemolyticus* a Marine Halophile**

*Vibrio parahaemolyticus* is a Gram-negative rod-shaped moderately halophilic bacterium, a member of the sub-phylum gamma-proteobacteria and the family *Vibrionaceae*. All species belonging to the family *Vibrionaceae* are cosmopolitan in their distribution in the marine environment, present in salt marshes, deep-sea sediments, throughout the water column and associated with marine flora and fauna. *Vibrionaceae* are the most significant consumers of chitin ( $\beta$ 1,4-linked *N*-acetylglucosamine), the second most abundant polymer in the ocean. Chitin makes up the major structural component of the exoskeletons of crustaceans and marine zooplankton. Estimates of chitin production range from  $\sim 10^{10}$ – $10^{11}$  tons globally, which is rapidly recycled primarily by *Vibrionaceae* highlighting the importance of this bacterial family to ocean health. *Vibrio parahaemolyticus* is also the leading bacterial cause of seafood-related gastroenteritis worldwide (99, 100), frequently associated with the consumption of raw or undercooked seafood (101, 102). The CDC estimates that around 80,000 cases of vibriosis occur each year in the U.S. alone, with approximately 45,000 of those cases caused by *V. parahaemolyticus*; however cases frequently are not reported (103). *V. parahaemolyticus* has several virulence factors including thermostable direct hemolysin (TDH), TDH related hemolysin (TRH), and two contact-dependent secretion systems Type Three Secretion System-1 and 2 (T3SS-1, T3SS-2) (104). All isolates encode a T3SS-1, which is considered a mechanism for environmental survival (105). Clinical isolates contain the T3SS-2,

found on a pathogenicity island on chromosome 2 and is essential for infections in humans (104).

### ***Vibrio parahaemolyticus* Contains Multiple Compatible Solute Biosynthesis and Transporter Systems.**

*Vibrio parahaemolyticus* is a moderate halophile that has an absolute requirement for NaCl and can grow at a range of NaCl concentrations in the marine and estuarine environments (45, 59). For example, *V. parahaemolyticus* can grow optimally in nutrient rich media at 0.1M to 3M NaCl and at temperatures ranging from 18°C to 42°C (45, 59). It was demonstrated that growth in 3% NaCl allowed better survival in sublethal and lethal acid shock conditions, as well as persistence in high- and low-temperature conditions (106, 107). Thus, growth in high salt protects against other abiotic stresses. *Vibrio parahaemolyticus* possesses biosynthesis pathways for trehalose, proline, glutamate, glutamine, ectoine and glycine betaine (Figure 2) (45, 59). However, Ongagna and colleagues showed that neither ectoine nor glycine betaine can be utilized as a carbon source making them *bona fide* compatible solutes. Ectoine and glycine betaine biosynthesis genes in *V. parahaemolyticus* are induced by NaCl during exponential phase (59). However, ectoine production was shown to be essential for growth in minimal media supplemented with 6% NaCl when no other compatible solutes or precursors are available (59). It was demonstrated that compatible solutes showed the following effectiveness when provided exogenously: glycine betaine>proline> ectoine>glutamate (59).

Four BCCTs encoded by VP1456 (*bccT1*), VP1723 (*bccT2*), VP1905 (*bccT3*), and VPA0356 (*bccT4*) are present in *V. parahaemolyticus* strains (45). BccT1 transports, glycine betaine, choline, DMG, proline, and ectoine (60, 68). BccT2

transports glycine betaine, choline, DMG, DMSP and proline, BccT3 transports glycine betaine, choline, DMG, and proline while BccT4 transports proline and choline (60, 68). In addition to ectoine and glycine betaine, we showed that the compatible solutes DMG, the N-dimethyl derivative of glycine, and DMSP are *bona fide* compatible solutes for *V. parahaemolyticus* (68). The full complement of compatible solutes that are imported by BCCTs in *V. parahaemolyticus* has not been investigated. *V. parahaemolyticus* also possesses two putative ProU transporters of the ABC-type transporter family, one on each chromosome. ProU1 (VP1726-VP1729) is encoded by *proVWX*, and ProU2 (VPA1112-VPA1114) is encoded by *proXWV* (45). ProU1 is a homolog of the *E. coli* K-12 ProU. ProU2 is part of the same operon which encodes the glycine betaine biosynthesis genes, *betIBA-proXWV*, and is a homolog of the *P. syringae proVXW* (45).

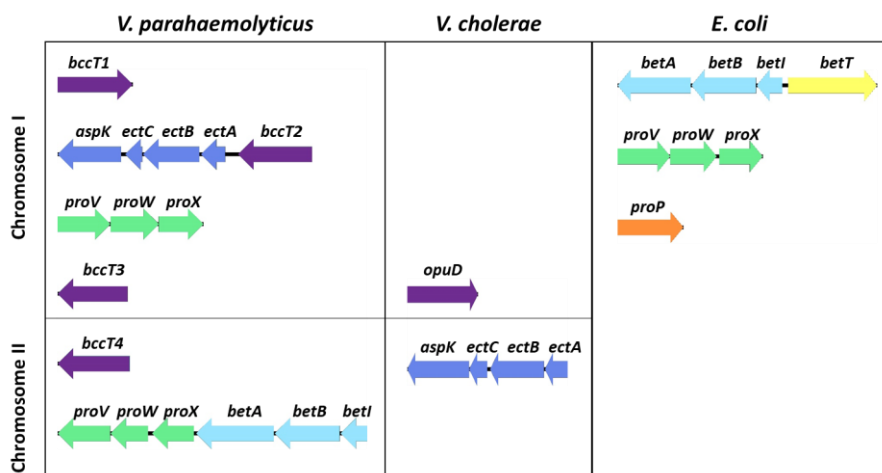


**Figure 2** Compatible solute systems in *V. parahaemolyticus*, *V. cholerae* and *E. coli*.

*V. parahaemolyticus* has two compatible solute biosynthesis systems and at least six dedicated compatible solute transporters, *V. cholerae* has one transporter and the ectoine biosynthesis system, and *E. coli* possesses two dedicated compatible solute transporters and a glycine betaine biosynthesis system.

### Regulation of Compatible Solute Biosynthesis.

Several studies have demonstrated that ectoine and glycine betaine biosynthesis can be directly controlled by transcriptional regulators CosR and BetI, respectively (55, 61, 62, 108, 109). In *V. cholerae*, the transcriptional regulator CosR, a member of the multiple antibiotic resistance (MarR)-type regulators, was identified as a repressor of ectoine biosynthesis genes (109). *cosR* is divergently transcribed from *opuD*, a homolog of *bccT3* in *V. parahaemolyticus*, and CosR was also a negative regulator of *opuD* (109). The *V. parahaemolyticus* homolog of *cosR* (ORF VP1906) is divergently transcribed from *bccT3* (ORF VP1905), sharing 70% identity with *V. cholerae*. In *V. parahaemolyticus* CosR was found also to be a direct repressor of the ectoine biosynthesis genes in both 1% and 3% NaCl (61, 108). EctR1, another

MarR-type regulator present in the halotolerant methanotroph *Methylmicrobium alcaliphilum*, shares 51% sequence identity to CosR, and repressed expression of the *ectABC-ask* operon in response to salinity (110). It was also demonstrated in *V. parahaemolyticus* that the quorum sensing low cell density regulator AphA directly activates while the high cell density regulator OpaR directly represses *ectABC-asp\_ect*. In addition, these two quorum sensing regulators both activate *cosR* expression, forming a feed-forward loop that tightly controls expression of *ectABCasp\_ect*, resulting in the highest expression at low cell density, with levels decreasing across the growth cycle (108).

Regulation of glycine betaine biosynthesis has been studied in several species, but few direct mechanisms of direct regulation have been shown. BetI is a direct transcriptional regulator of its own operon *betIBA* in *E. coli*, and expression analyses demonstrated that repression is relieved in the presence of choline (55, 56). This mechanism of regulation is conserved in both *V. harveyi* and *V. parahaemolyticus* where the operon is comprised of *betIBA-proXWV* (61, 62). In *Vibrio harveyi*, a closely related species to *V. parahaemolyticus*, expression analyses demonstrated that the quorum sensing regulator LuxR activates expression of *betIBA-proXWV* (62). A follow-up study demonstrated that IHF works synergistically with LuxR to activate transcription of *betIBA-proXWV* (111). Our recent study found that the *V. parahaemolyticus* LuxR homolog OpaR also regulates *betIBA-proXWV* directly, suggesting this mechanism of regulation is widespread among *Vibrio* species (61). Additionally, we showed that CosR bound directly to the regulatory region of the *betIBA-proXWV* in *V. parahaemolyticus*, and this binding lead to direct repression in low salinity conditions (61).

Compatible solute biosynthesis genes were shown to be osmotically regulated in several species (59, 61, 112, 113). Ectoine biosynthesis genes in *V. parahaemolyticus* are induced by NaCl, indicating they are osmoregulated (59, 61). Recently it was determined that the ectoine promoter of *Pseudomonas stutzeri* is osmotically regulated and induced by both ionic and non-ionic osmolytes, with transcriptional activity increasing linearly with osmolarity (113). Glycine betaine biosynthesis genes are also regulated by osmolarity at the transcriptional level. Transcription of *betIBA* in *E. coli* was upregulated during growth in high-osmolarity medium. This effect was seen after addition of NaCl, KCl, and sucrose, indicating the genes are osmoregulated and not just regulated by salinity (112). In *V. vulnificus*, glycine betaine biosynthesis genes VVA0506 and VVA0508 were upregulated in hyperosmotic conditions (114). Glycine betaine biosynthesis genes are also induced by salinity in *V. parahaemolyticus* (59, 61).

### **Regulation of Compatible Solute Transporters.**

Compatible solute transporters can be regulated via a combination of direct regulation, indirect regulation via exogenous compatible solutes and/or osmotic stress (77-80). Direct regulation of compatible solutes transporters by the transcriptional regulator BetI was demonstrated in several species. In *E. coli*, BetI regulates the gene *betT*, a BCCT family transporter, which is divergently transcribed from *betIBA* (55). In *Acinetobacter baylyi*, which contains the *betIBA* operon, BetI was found to repress the transcription of two choline transporter genes, *betT1* and *betT2*. Unlike in *E. coli*, DNA binding assays revealed BetI released the regulatory region in the presence of choline. Levels of *betT1* and *betT2* were induced after growth in minimal media supplemented with choline over levels measured without choline, indicating

repression by BetI is relieved (115). In *Pseudomonas aeruginosa*, expression of *betI* and *betT3* were upregulated in a *betI* mutant when grown in low salinity conditions, suggesting that BetI represses the expression of these transporter genes. Expression levels of these transporter genes in the wild type increased in the presence of choline, indicating that choline relieves the repression by BetI (116). As detailed previously in *V. harveyi* and *V. parahaemolyticus*, LuxR and OpaR respectively are positive regulators and BetI is a negative regulator of the *betIBA-proXWV* operon(61, 62). Additionally, it was shown that CosR is a direct repressor of this operon, *bccT3* and *proU1*, while CosR indirectly represses *bccT1*. *cosR* is clustered with compatible solute transporters or biosynthesis systems in many species of the family *Vibrionaceae*, suggesting CosR is a global regulator of osmotic stress response genes (61). Nucleoid associated proteins have also been shown to play a direct role in compatible solute transporter regulation. A recent study showed that repression of the ProU promoter by H-NS in *E. coli* was relieved by IHF binding, which modifies the DNA secondary structure and activates transcription at the *proU* locus (117).

Transporters are also regulated at the level of transcription by osmolarity (77-80). Transcription of *betT* in *E. coli* was upregulated during growth under osmotic stress. This osmoregulation was seen after growth in NaCl, KCl and sucrose, indicating that the transporter gene is controlled by osmolarity, not just salinity (112). In *B. subtilis*, the *opuD* gene encoding a BCCT-family transporter is osmoregulated on the transcriptional level (82). In *V. parahaemolyticus*, three of the four BCCTs are upregulated in exponential and stationary phase by upshock into 6% NaCl, indicating that these genes are osmoregulated. The *bccT2* gene (VP1723) was unaffected by salt upshock (60). Similar results were demonstrated in a study that examined expression

of the BCCTs in low salinity conditions. Only *bccT2* was not repressed in low salinity (1% NaCl), while the other three BCCTs were significantly repressed in 1% NaCl as compared to 3% NaCl (61). Osmotic stress also has been shown to upregulate the ABC-type family of transporters. The *E. coli* ProU was shown to bind glycine betaine with high affinity and to be osmoregulated (88, 97, 98). In *Vibrio vulnificus*, the genes encoding a ProU transporter, which uptakes choline and glycine betaine, were upregulated by hyperosmotic conditions (114). Both ProUs in *V. parahaemolyticus* are osmoregulated, and are significantly upregulated in 3% NaCl as compared to 1% NaCl (61).

### **Quorum Sensing in *Vibrio*.**

Quorum sensing is a form of bacterial communication used to coordinate behaviors in response to changing cell density. The quorum sensing circuitry has been studied extensively in *V. harveyi*, and a similar system with a LuxR homolog, OpaR, has been demonstrated in *V. parahaemolyticus* (107, 118-121). Vibrios synthesize and secrete compounds known as autoinducers (AIs) that act as signals for a population of bacteria. *V. harveyi* produces and senses HAI-1 (*V. harveyi* autoinducer 1), an acyl homoserine lactone (AHL), AI-2 (autoinducer 2) and CAI-1 (*V. cholerae* autoinducer 1) (122, 123). HAI-1 is produced via the synthase LuxM and sensed via the cognate transmembrane histidine kinase LuxN (121, 124-127). The precursor for AI-2, 4,5-dihydroxy-2,3-pentanedione (DPD), is produced by LuxS and sensed via LuxPQ histidine kinases (121, 127-131). CAI-1 is produced by the synthase CqsA and sensed by CqsS histidine kinase (121, 132, 133). These autoinducers are sensed via the cognate transmembrane histidine kinases in the periplasm, which trigger a phosphorelay cascade. At low cell density, the concentration of AIs in the

environment is low and therefore the histidine kinases are not stimulated. They act as kinases and phosphorylate LuxU, a phosphotransfer protein (134). A phosphate is then transferred by LuxU to the response regulator, LuxO, thereby activating LuxO (134, 135). LuxO interacts with the sigma factor RpoN that activates the transcription of five small quorum regulatory RNAs (Qrrs). These Qrrs hybridize with transcripts and promote their translation or degradation (136). Translation is promoted when the Qrr base-pairs with the target mRNA and a change in secondary structure reveals the ribosomal binding site. Negative regulation is achieved via base-pairing of the Qrr at or near the ribosomal binding site of the target mRNA which occludes ribosomal binding (137). The Qrrs stabilize the translation of the low cell density transcriptional regulator AphA and destabilize the translation of the high cell density regulator LuxR (OpaR homolog) (119, 122, 138). LuxR positively regulates transcription of *qrr2-qrr4* in *V. harveyi*, and OpaR positively regulates transcription of *qrr2-qrr4* in *V. parahaemolyticus* (139, 140). This feedback loop enables the transition from LCD to HCD and leads to the downregulation of LuxR production by the Qrrs (140). Qrrs have been reported to have targets outside of the quorum sensing regulatory network such as those involved in metabolism, chemotaxis and transcription in *V. harveyi* (141). In *V. harveyi*, the Qrrs have additive functionality. In *V. harveyi*, the *qrr genes* were found to be differentially expressed by varying degrees at low cell density: *qrr4* is the most highly expressed (25-fold), followed by *qrr2* (18-fold), *qrr3* (14-fold), *qrr1* (eight-fold), while *qrr5* did not show density-dependent expression. These expression levels correspond to degree of repression of *luxR* by each Qrr, with Qrr 4 repressing *luxR* the most (142).

At high cell density, receptors are activated as the AI concentration increases in the environment and binds receptors. The receptors then act as phosphatases and reverse the phosphorylation of LuxO, inactivating it. The *qrr genes* are no longer transcribed, and LuxR, the high cell density master regulator, can be transcribed and translated (119, 122, 135, 143, 144). In *V. harveyi*, LuxR has been shown to regulate 625 genes while AphA was shown to regulate 296 genes in one study (138) and 167 in another (143). This regulatory cascade is conserved in *V. parahaemolyticus* (Figure 3). It was shown that OpaR negatively transcriptionally regulates *aphA* production and also autoregulates (139). In *V. parahaemolyticus*, OpaR has been shown to regulate approximately 500 genes (118, 119). It is known that LuxR/OpaR and AphA are autoregulators and negatively regulate each other (138, 139, 142, 143, 145-148).

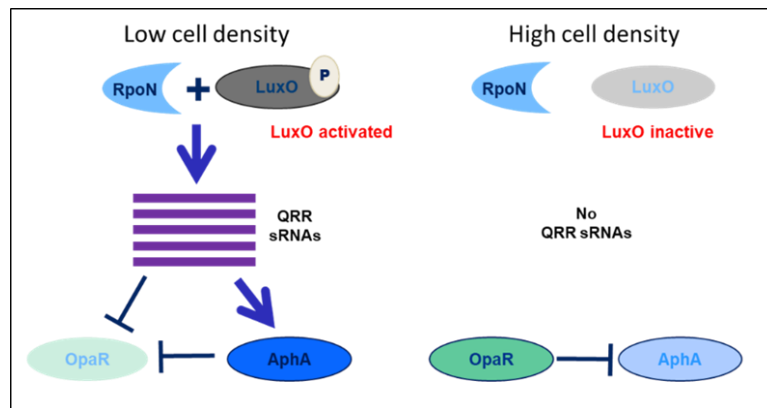


**Figure 3** **Quorum sensing in *Vibrio parahaemolyticus*.**  
 The quorum sensing response regulator LuxO is phosphorylated at low cell density when autoinducer concentrations are low. AphA negatively regulates *opaR* expression. At high cell density when autoinducer concentrations are high, LuxO is inactive, OpaR is highly expressed and negatively regulates *aphA* expression.

Regulation of osmotic stress response systems via direct mechanisms and osmotic induction was demonstrated in several species of bacteria, but there is still much unknown about how these processes are coordinated. We utilized *V. parahaemolyticus* as a model organism due to the multiple osmotic stress response systems that it possesses. We hypothesize that *V. parahaemolyticus* optimally controls expression of these systems to enable cells to uptake or biosynthesize compatible solutes when they are required. We sought to elucidate the mechanisms by which *V. parahaemolyticus* regulates the osmotic stress response systems and the evolutionary adaptations that enable *V. parahaemolyticus* to survive in high salinity conditions utilizing gene expression, phenotypic and biochemical analyses. We also utilize phylogenetic analyses to predict whether these mechanisms are widespread among bacteria.

### **Dissertation Work**

To maintain the turgor pressure of the cell under high osmolarity, bacteria accumulate small organic compounds called compatible solutes, either through uptake or biosynthesis, in a process known as the osmotic stress response. *Vibrio parahaemolyticus*, a marine halophile and an important human and shellfish pathogen, needs to adapt to abiotic stresses such as changing salinity. *Vibrio parahaemolyticus* contains multiple compatible solute biosynthesis and transporter systems including the *ectABC-asp\_ect* operon required for *de novo* ectoine biosynthesis. Ectoine is a highly effective compatible solute whose biosynthesis genes are widespread among bacteria; however, little is known about the mechanism of regulation of the *ect* genes. In chapter 2, we investigated the role of the quorum sensing master regulators OpaR and AphA in *ect* gene regulation. In an *opaR* deletion mutant, transcriptional reporter

assays demonstrated that *ect* expression was induced, which indicates that OpaR is a negative regulator of the *ect* genes. In an electrophoretic mobility shift assay (EMSA), we showed that purified OpaR bound to the *ect* regulatory region indicating direct regulation by OpaR. In an *aphA* deletion mutant, expression of the *ect* genes was repressed, and purified AphA bound upstream of the *ect* genes. These data indicate that AphA is a direct positive regulator. CosR, a Mar-type regulator known to repress *ect* expression in *V. cholerae*, was found to repress *ect* expression in *V. parahaemolyticus*. In addition, we identified a feed-forward loop in which OpaR is a direct activator of *cosR*, while AphA is an indirect activator of *cosR*. Regulation of the ectoine biosynthesis pathway via this feed-forward loop allows for precise control of ectoine biosynthesis genes throughout the growth cycle to maximize fitness. Ectoine is an industrially important compound that is harvested from bacteria and utilized in pharmaceuticals and cosmetics. The results of this study further the understanding of ectoine regulation and may be useful in engineering better ectoine-producer strains, given that the mechanisms of regulation we have uncovered appears to be widespread in bacteria.

In Chapter 3, we investigated whether CosR has a broader role in the osmotic stress response. Previously, it was shown that CosR, a multiple antibiotic resistance (MarR-type) regulator, was a direct repressor of *ectABC-asp\_ect* in *Vibrio* species. Expression analyses demonstrated that *betIBA-proXWV*, *bccT1*, *bccT3*, *bccT4* and *proVWX* are repressed in low salinity. Examination of an in-frame *cosR* deletion mutant showed expression of these systems is de-repressed in the mutant at low salinity compared to wild-type. DNA binding assays demonstrated that purified CosR binds directly to the regulatory region of both biosynthesis systems and four

transporters. In *Escherichia coli* GFP reporter assays, we demonstrated that CosR directly represses transcription of *betIBA-proXWV*, *bccT3*, and *proVWX*. These data show that CosR is a global regulator of osmotic stress response. Similar to *V. harveyi*, we showed *betIBA-proXWV* was directly activated by the quorum sensing LuxR homolog OpaR, suggesting a conserved mechanism of regulation among *Vibrio* species. Phylogenetic analysis demonstrated that CosR is ancestral to the *Vibrionaceae* family and bioinformatics analysis showed widespread distribution among *Gamma-Proteobacteria* in general. Incidentally, in *Aliivibrio fischeri*, *A. finisterrensis*, *A. sifiae* and *A. wodanis*, an unrelated MarR-type regulator named *ectR* was clustered with *ectABC-asp*, which suggests the presence of another novel ectoine biosynthesis regulator. Collectively, these data suggest that CosR is an unrecognized global regulator of the osmotic stress response that is widespread in bacteria, controlling more systems than previously demonstrated.

Chapter 4 focused on transport of compatible solutes by *V. parahaemolyticus* and other species of *Vibrio*. The full range of compatible solutes transported by *V. parahaemolyticus* has yet to be determined. Thus, an *ectB* mutant strain, which has a growth defect in high salt in the absence of osmolytes was grown on an osmolyte phenotypic microarray plate to identify osmolytes that can be utilized. These analyses expanded the number of known osmolytes used by *V. parahaemolyticus* to include N-N dimethylglycine (DMG),  $\gamma$ -amino-N-butyric acid (GABA), trimethylamine-N-oxide (TMAO), and creatine. Growth pattern analysis showed that DMG was a highly effective osmoprotectant in several *Vibrio* species and none could grow on DMG as a carbon source. Using a combination of osmolyte-transporter mutant strains, we showed that *V. parahaemolyticus* requires a BCCT transporter for DMG uptake.

Growth pattern analysis of four triple-*bccT* mutants, possessing only one functional BCCT, indicated that BccT1 (VP1456), BccT2 (VP1723), and BccT3 (VP1905) transported DMG, which was confirmed by functional complementation in *E. coli* strain MKH13. BccT1 was unusual in that it could uptake both compounds with methylated head groups (DMG, choline, and glycine betaine (GB)) and cyclic compounds (ectoine and proline) compounds. Using bioinformatics analysis, we identified the potential coordinating residues (Trp 203, Trp 208, Tyr 211, and Trp 384) for glycine betaine. Using site-directed mutagenesis, we showed that a strain with all four residues mutated resulted in loss of uptake of GB, DMG and ectoine. We showed three of the four residues were essential for ectoine uptake whereas only one of the residues was important for GB uptake. Overall, we have shown that DMG is an effective compatible solute for *V. parahaemolyticus* and other *Vibrio* species, and we have elucidated the residues in BCCT-family transporters that are important for coordination of DMG and ectoine.

Chapter 5 investigated *Vibrio* species usage of DMSP, a key component of the global geochemical sulfur cycle and a secondary metabolite produced in large quantities by marine phytoplankton as an osmoprotectant. Bacterial DMSP lyases convert DMSP to dimethylsulfide (DMS) a climate active compound that is released from oceans into the atmosphere. Whether marine bacteria can use DMSP as an osmoprotectant has not been examined extensively. Bacteria accumulate compatible solutes in the cytoplasm to maintain the turgor pressure of the cell in response to high external osmolarity. We found that DMSP is used as an osmoprotectant in *V. parahaemolyticus* and this ability was present in several *Vibrio* species tested. DMSP was not catabolized by these species indicating it is a *bona fide* osmoprotectant. A

*bccT* null mutant was not rescued by DMSP in high salinity growth conditions indicating that a BCCT transporter was required for uptake. Using *bccT* triple mutants possessing only one functional BCCT in growth pattern assays, we identified two BCCT transporters that were carriers of DMSP. Functional complements in *E. coli* strain MKH13 corroborate the findings that BCCT2 is the main transporter of DMSP in *V. parahaemolyticus*.

Chapter 6 focused on identifying and characterizing novel regulators of the ectoine biosynthesis operon in *V. parahaemolyticus*. Ectoine biosynthesis is essential for growth in high salinity environments but is unnecessary and energetically costly for the cell in low salinity. Therefore, the ectoine biosynthesis operon, *ectABC-asp\_ect*, is under tight regulation by the cell to prevent energy waste. Previously, we have shown that quorum sensing regulators AphA and OpaR, together with the repressor CosR, participate in a feed-forward loop to produce a gradient of *ectABC-asp\_ect* mRNA when ectoine production is required. In addition, CosR acts as a repressor in low salinity conditions, when ectoine production is not required. We performed a DNA affinity pulldown with the regulatory region of the ectoine operon to identify novel regulators of the ectoine biosynthesis operon via tandem mass spectrometry. We identified several putative regulators of the *ect* genes including NhaR, TorR, LeuO, and OmpR. Expression analyses in regulator deletion mutants showed that the *ect* genes are upregulated in an *nhaR* mutant and downregulated in a *leuO* mutant, indicating that NhaR is a negative regulator and LeuO is a positive regulator. This study further demonstrates that *Vibrio* species utilize a number of regulators to precisely control compatible solute biosynthesis and uptake, which is an energetically costly process for the cell.

## Chapter 2

# **QUORUM SENSING REGULATORS APHA AND OPAR CONTROL EXPRESSION OF THE OPERON RESPONSIBLE FOR BIOSYNTHESIS OF THE COMPATIBLE SOLUTE ECTOINE**

The work in this chapter was published in *Applied and Environmental Microbiology*

## **Quorum Sensing Regulators AphA and OpaR Control Expression of the Operon Responsible for Biosynthesis of the Compatible Solute Ectoine**

Gregory GJ; Morreale DP; Carpenter MR; Kalburge SS; Boyd EF

Appl. Env. Microb. 2019 Oct 30;85(22). doi: 10.1128/AEM.01543-19.

### **Introduction**

In response to osmotic stress, bacteria have developed a strategy that involves accumulation of compatible solutes through uptake from the environment or biosynthesis from available precursors to maintain the turgor pressure of the cell. Compatible solutes are small organic compounds, which bacteria can accumulate in the cell without disrupting cellular processes to counteract increased external osmolarity (13-15). As a marine organism, *Vibrio parahaemolyticus*, a halophile, encounters fluctuations in osmolarity to which it must rapidly respond to prevent cell lysis. *Vibrio parahaemolyticus* has biosynthesis pathways for compatible solutes ectoine (*ectABCasp-ect*) and glycine betaine (*betIBA*) and at least six transporters for compatible solute uptake (45, 59, 60).

Aspartic acid is the precursor for ectoine, which can be biosynthesized *de novo*. Aspartic acid is converted to ectoine by EctA, EctB, and EctC encoded by the operon *ectABC*, which is evolutionarily conserved in Gram-positive and Gram-negative bacteria (38-40). Several species that produce ectoine also encode a dedicated aspartokinase (Ask) specific to the ectoine biosynthesis pathway, which is clustered with the *ectABC* genes (41-44). All *Vibrio* species contain an aspartokinase (Asp-Ect) in the same operon as the *ectABC* genes (45). Ectoine production was shown to be essential for growth of *V. parahaemolyticus* in minimal media supplemented with 6% NaCl when no other compatible solutes or precursors are available (59). Ectoine is a *bona fide* compatible solute and is not used as a carbon source by *V. parahaemolyticus*. Ectoine biosynthesis genes in *V. parahaemolyticus* are induced by NaCl upshock during exponential phase and repressed in stationary phase, however the mechanism of transcriptional control remains unknown (59). EctR1 and CosR were identified as local regulators of ectoine biosynthesis in *Methylobacterium alcaliphilum* and *V. cholerae*, respectively (109, 110). EctR1, a member of the multiple antibiotic resistance (MarR)-type regulators, in the halotolerant methanotroph *M. alcaliphilum*, repressed expression of the *ectABCasp-ect* operon in response to salinity (110). In *V. cholerae*, CosR shared 51% sequence identity to EctR1, and also was identified as a repressor of ectoine biosynthesis genes in low salinity conditions (109).

Quorum sensing is a form of bacterial communication used to coordinate behaviors in response to changing cell density. The quorum sensing circuitry has been studied extensively in *V. harveyi*, and a similar system with a LuxR homolog, OpaR, has been demonstrated in *V. parahaemolyticus* (107, 118-121, 139, 148). Quorum

sensing involves the synthesis of autoinducers (AIs), which bind to receptors, triggering a phosphorelay pathway, that activates LuxO, the master response regulator. In *V. harveyi*, at low cell density, the concentration of AIs in the environment is low and therefore the receptors act as kinases, leading to the phosphorylation of LuxO (134, 135). LuxO is an activator of the sigma factor RpoN, which activates the transcription of five homologous small regulatory RNAs (sRNAs) named quorum regulatory RNAs (Qrr1 to Qrr5) (142, 149). Qrr sRNAs hybridize with *aphA* and *opaR* transcripts to promote their translation or degradation, respectively (119, 122, 136, 138). AphA is therefore upregulated at low cell density and regulates 100s of genes (143). At high cell density, LuxO is inactive, no Qrr sRNAs are transcribed, and LuxR, the high cell density master regulator, is produced to regulate 100s of genes. In addition, LuxR and AphA are autoregulators and negatively regulate each other (119, 122, 135, 138, 143, 144). Previously, it was shown that LuxR in *V. harveyi*, positively regulates glycine betaine biosynthesis genes (62). In *V. parahaemolyticus*, it was demonstrated that the ectoine biosynthesis genes were repressed in a *luxO* mutant (where OpaR levels are high) compared to wild-type (107).

In this study, we determined the role of global and local regulators in the control of expression of the ectoine biosynthesis operon *ectABCasp-ect*. We examined expression of ectoine biosynthesis genes across the growth cycle in *V. parahaemolyticus* RIMD2210633 and determined expression in quorum sensing deletion mutants  $\Delta luxO$ ,  $\Delta aphA$ ,  $\Delta opaR$  and double mutants  $\Delta opaR/\Delta aphA$  and  $\Delta luxO/\Delta opaR$  using plasmid-based transcriptional fusion reporter assays. We demonstrated a role for AphA and OpaR in ectoine gene expression and used DNA binding assays to determine whether regulation was direct or indirect. We examined

the *V. parahaemolyticus* CosR (VP1906) regulator and uncovered a feed-forward loop involving both AphA and OpaR. This study demonstrates that the quorum sensing regulators AphA and OpaR, as well as CosR, play a role in transcriptional regulation of the *ectABCasp-ect* operon.

## Materials and Methods

### Bacterial strains, media and culture conditions.

All strains and plasmids used in this study are listed in Table 1. A previously described streptomycin-resistant clinical isolate of *V. parahaemolyticus* RIMD2210633 was used as the wild-type (WT) strain (104). Strains were grown in either lysogeny broth (LB) (Fisher Scientific, Fair Lawn, NJ) supplemented with 3% NaCl (wt/vol) (LB3%) or in M9 minimal medium (47.8 mM Na<sub>2</sub>HPO<sub>4</sub>, 22 mM KH<sub>2</sub>PO<sub>4</sub>, 18.7 mM NH<sub>4</sub>Cl, 8.6 mM NaCl) (Sigma-Aldrich, USA) supplemented with 2 mM MgSO<sub>4</sub>, 0.1 mM CaCl<sub>2</sub>, 20 mM glucose as the sole carbon source (M9G) and 3% or 6% NaCl (wt/vol) (M9G3%, M9G6%). *E. coli* strains were grown in LB supplemented with 1% NaCl (wt/vol) (LB1%) or M9G supplemented with 1% NaCl (M9G1%) where indicated. *E. coli*  $\beta$ 2155  $\lambda$ pir, a diaminopimelic acid (DAP) auxotroph, was supplemented with 0.3 mM DAP and grown in LB1%. All strains were grown at 37°C with aeration. Antibiotics were used at the following concentrations (wt/vol) as necessary: ampicillin (Amp), 50  $\mu$ g/ml; chloramphenicol (Cm), 12.5  $\mu$ g/ml; streptomycin (Str), 200  $\mu$ g/ml; and tetracycline (Tet), 1  $\mu$ g/mL. Ectoine was added to media to a final concentration of 100  $\mu$ M, when indicated.

### Construction of the *cosR* deletion mutant.

A Gibson Assembly protocol, using NEBuilder HiFi DNA Assembly Master Mix (150) (New England Biolabs, Ipswich, MA), was used to generate an in-frame truncated, non-functional *cosR* gene in the suicide vector pDS132 (pDS $\Delta$ *cosR*). This was followed by allelic exchange to generate a *cosR* (VP1906) in frame deletion mutant in *V. parahaemolyticus* RIMD2210633 (151). Primers pairs were designed to create a 60-bp truncated PCR product of the 477-bp *cosR* gene (Table 2). PCR amplification, using genomic DNA from *V. parahaemolyticus* RIMD2210633 as template and primer sets SOEcosRA/SOEcosRB and SOEcosRC/SOEcosRD, was performed to produce two fragments, AB and CD, of the *cosR* gene. Complementary regions for Gibson assembly are indicated in lower case letters in the primer sequence in Table 2. AB and CD fragments were ligated with pDS132 vector linearized with SacI, via Gibson assembly to generate pDS $\Delta$ *cosR*. pDS132 harboring the truncated version of *cosR*, which was transformed into the *E. coli* strain  $\beta$ 2155  $\lambda$ *pir*, followed by conjugation into *V. parahaemolyticus*. For the pDS $\Delta$ *cosR* suicide vector to be maintained in the cell, the vector undergoes homologous recombination into the genome, as *V. parahaemolyticus* does not contain the *pir* gene required for replication of the pDS $\Delta$ *cosR* plasmid. Positive colonies were selected on chloramphenicol plates to contain a single crossover of pDS $\Delta$ *cosR* in the genome. A culture was grown overnight in the absence of chloramphenicol to induce a second recombination event, leaving behind either the truncated mutant *cosR* allele or the wild-type allele in the genome. Colonies were plated on sucrose for selection. Colonies of cells that still contain the plasmid appeared soupy on the sucrose plate due to the presence of the *sacB* gene on the pDS $\Delta$ *cosR* plasmid. Colonies were screened via PCR assays for the

presence of a mutant allele. Positive colonies were sequenced to confirm an in-frame deletion of the *cosR* gene.

#### RNA isolation and quantitative real-time PCR (qPCR).

*Vibrio parahaemolyticus* RIMD2210633 was grown overnight at 37°C with aeration in LBS. Cells were then washed 2 times with 1X PBS, diluted 1:50 into 50 mL of M9G3% and grown with aeration at 37°C. Cells were harvested at an optical density (OD<sub>595</sub>) of 0.15, 0.25, 0.4, 0.5, 0.8, and 1.0. For the 0.15 OD sample, RNA was isolated from 5 mL of culture. For all other samples, RNA was isolated from 1 mL of culture. Following manufacturer's protocol, total RNA was extracted using Trizol (Invitrogen, Carlsbad, CA). The concentrations of RNA were determined using a NanoDrop spectrophotometer (Thermo Scientific, Waltham, MA). The samples were then treated with Turbo DNase (Invitrogen). Superscript IV reverse transcriptase (Invitrogen) was used to synthesize cDNA from 500 ng of RNA by priming with random hexamers. cDNA samples were then diluted 1:25, and quantitative real-time PCR (qPCR) was performed using cDNA. PowerUp SYBR Green master mix (Life Technologies, Carlsbad, CA) was used and samples were run on an Applied Biosystems QuantStudio6 fast real-time PCR system (Applied Biosystems, Foster City, CA). Reactions were set up with primer pairs: 16SFwd/Rev, for normalization, *ectAFwd/Rev*, *asp-ectFwd/Rev*, *aphAFwd/Rev* and *opaRFwd/Rev* (Table 2). The qPCR primer efficiency was determined for each primer pair using a standard curve. The efficiency of each pair was as follows: *opaR* 101.96%, *aphA* 102.81%, *ectA* 98.09%, *asp-ect* 98.73%, 16S 95.99%. Cycle threshold (C<sub>T</sub>) values were used to determine expression levels and all samples were normalized to 16S rRNA.

Expression levels were calculated relative to the OD<sub>595</sub> 0.15 sample, using the  $\Delta\Delta\text{CT}$  method, as described previously (152).

#### Protein purification of AphA, OpaR, and CosR.

*Vibrio parahaemolyticus* RIMD2210633 OpaR was purified as previously described (107). The 540-bp *aphA* (VP2762) gene was cloned into a pMAL-c5x vector with a hexahistidine-tagged maltose binding protein tag and TEV protease cleavage site upstream of the multiple cloning site. Full-length *aphA* was amplified from *V. parahaemolyticus* RIMD2210633 genomic DNA using primer pair NcoIaphAFwd/BamHIaphARev, which included restriction cut sites in the 5' end of the primers (Table 2). The pMAL vector and the purified PCR fragment were digested with NcoI and BamHI and ligated with T4 ligase (Invitrogen). The pMAL*aphA* plasmid was transformed into *E. coli* Dh5 $\alpha$ , purified, and sequenced. The pMAL*aphA* plasmid was then transformed into *E. coli* BL21 (DE3) cells. MBP-AphA was then expressed and purified. Ten milliliters of overnight culture was used to inoculate 1 L LB supplemented with 0.2% glucose at 37°C. This culture was induced with 0.5 mM isopropyl-1-thio- $\beta$ -d-galactopyranoside (IPTG) at OD<sub>595</sub> 0.5. Growth continued overnight at 18°C. Cells were harvested by centrifugation (5,000 x *g* for 20 min at 4°C) and were resuspended in amylose column buffer (50 mM sodium phosphate, 200 mM NaCl, pH 7.5) supplemented with 1 mM phenylmethanesulfonyl fluoride (PMSF) and 0.5 mM benzamidine. Bacterial cells were lysed on ice using a high-pressure homogenizer (EmulsiFlex-C5, Avestin, Ottawa, Canada). Cell debris was removed by centrifugation (15,000 x *g* for 1 h at 4°C). The supernatant was diluted 1:6 with amylose column buffer and was passed through a column containing 20 mL of amylose resin (New England BioLabs). The column was washed with 10 column

volumes (CVs) of amylose wash buffer. The fusion protein, MBP-AphA, was eluted with three CVs amylose elution buffer (50 mM sodium phosphate, 200 mM NaCl, 20 mM maltose, pH 7.5). After purification, the MBP tag was removed by overnight incubation of the eluent at 4° C with a hexahistidine-tagged Tobacco Etch Virus (TEV) protease (gift from Dr. Sharon Rozovsky, UD) in a 1:10 molar ratio. The cleavage mixture was then adjusted to 20 mM imidazole and subjected to Immobilized Metal Affinity Chromatography (IMAC) using HisPur Ni-NTA resin (ThermoFisher) to remove the hexahistidine-tagged TEV protease, the hexahistidine-tagged MBP protein, and any uncleaved MBP-AphA. AphA was further purified using size exclusion chromatography by passing over a GE HiPrep Sephacryl S100 column, analyzed for purity by SDS-PAGE and molecular weight was confirmed using mass spectrometry.

The 477-bp *cosR* (VP1906) gene was cloned into pET-28a (+) (Novagen) with a C-terminal hexahistidine tag using primer pair NcoIcosRFwd/XhoIcosRRev (Table 2). The pET28a (+) vector and the purified PCR fragment were digested with NcoI and XhoI and ligated via sticky-end ligation with T4 ligase (Invitrogen). The pET*cosR* plasmid was transformed into *E. coli* Dh5 $\alpha$ , purified, and sequenced. The pET*cosR* plasmid was transformed into *E. coli* BL21 (DE3) cells. CosR-His expression was induced with 0.5 mM IPTG at 0.4 OD<sub>595</sub> and grown overnight with aeration at 25° C. Cells were then pelleted, resuspended in lysis buffer (50 mM sodium phosphate, 200 mM NaCl, 20 mM imidazole, pH 7.4, 1.0 mM phenylmethanesulfonyl fluoride, 0.5 mM benzamidine) and lysed using a microfluidizer. Debris was pelleted through centrifugation at 24,000 x g for 35 mins at 4°C. Clarified supernatant was subjected to

IMAC using a column packed with HisPur Ni-NTA resin (ThermoFisher) and equilibrated with column buffer (50 mM sodium phosphate, 200 mM NaCl, 20 mM imidazole, pH 7.4). The column was washed with 20 CVs of column buffer, 20 CVs of a buffer containing 40 mM imidazole, and 10 CVs of buffer containing 100 mM imidazole to remove any remaining contaminants. CosR-His was eluted using three CVs of 500 mM imidazole buffer. After elution, the samples dialyzed overnight at 4°C in sodium phosphate buffer to remove any excess salts. Protein purity was estimated at 95% using SDS-PAGE.

#### Electrophoretic Mobility Shift Assay.

Two overlapping DNA fragments designated *PectA* probe 1 (323-bp) and probe 2 (329-bp) were amplified using primer sets VPectAFwd1A/Rev1C and VPectAFwd1C/Rev2. Probe 1 was split into three similarly sized probes 1A (125-bp), 1B (137-bp), and 1C (106-bp). These probes were amplified using primer sets VPectAFwd1A/Rev1A, VPectAFwd1B/Rev1B, and VPectAFwd1C/Rev1C (Table 2). Two overlapping DNA fragments, 105-bp and 142-bp, were amplified from *V. parahaemolyticus* RIMD2210633 using the primer sets VPcosRFwdA/VPcosRRevA and VPcosRFwdB/VPcosRRevB, comprising 220-bp of the *cosR* regulatory region. An additional probe, probe C, 188-bp in length, which contained a putative AphA binding site was amplified using primer set VPcosRCFwd/VPcosRCRev (Table 2). Protein concentration was determined using Bradford reagent. Various concentrations of purified OpaR, AphA, or CosR were incubated for 20 minutes with 30 ng of each DNA fragment in OpaR/CosR binding buffer (10 mM Tris, 150 mM KCl, 0.1 mM dithiothreitol, 0.1 mM EDTA, 5% polyethylene glycol (PEG) [pH 7.9 at 4°C]) or

AphA binding buffer (10 mM Tris, 150 mM KCl, 0.1 mM dithiothreitol, 0.1 mM EDTA, 5% polyethylene glycol (PEG) [pH 7.5 at 4°C]). A 6% native acrylamide gel was pre-run for 2 hours at 4°C (200 V) with Tris-acetate-EDTA (TAE) buffer (pH 8.4 for OpaR and CosR, pH 7.5 for AphA at 4°C). The DNA:protein mixtures (10 µl) were loaded onto the gel and run for 2 hours at 4°C (200V) in 1X TAE buffer. Gels were then stained for 20 minutes in an ethidium bromide bath (0.5 µg/ml).

#### Transcriptional reporter Assays.

GFP reporter plasmids were constructed by cloning the regulatory region of interest upstream of a promoterless *gfp* gene in the parent vector pRU1064, which contains both tetracycline and ampicillin resistance cassettes (153). The *PectA* regulatory region was amplified from *V. parahaemolyticus* RIMD2210633 genomic DNA with primer pairs listed in Table 2. The *PectA* region encompasses 514 bp upstream of *ectA* including 224 bp of ORF coding region of VP1723. *PectA* was cloned into pRU1064 via digestion with HindIII and SpeI and ligation with T4 ligase to produce the pRUP<sub>*ectA-gfp*</sub> reporter plasmid. The *PcosR* regulatory region was amplified from *V. parahaemolyticus* RIMD2210633 genomic DNA using primer pairs listed in Table 2 generating a 397 bp probe. pRU1064 was linearized with SpeI and ligated with *PcosR* via Gibson assembly protocol to produce the pRUP<sub>*cosR-gfp*</sub> reporter plasmid (150). Complementary regions for Gibson assembly are indicated in lower case letters in the primer sequence (Table 2). The plasmids were transformed into *E. coli* Dh5 $\alpha$ , purified, and sequenced. The reporter plasmids were subsequently transformed into *E. coli*  $\beta$ 2155  $\lambda$ *pir* and conjugated into WT and quorum sensing mutant strains. Wild-type and single deletion mutants of each quorum sensing regulator  $\Delta$ *luxO*,  $\Delta$ *opaR*, and  $\Delta$ *aphA*, as well as the double deletion mutants

$\Delta luxO/\Delta opaR$ , and  $\Delta opaR/\Delta aphA$  containing pRUP<sub>ectA-gfp</sub>, pRUP<sub>cosR-gfp</sub> or the promoterless parent reporter vector pRU1064 were grown overnight in LB3% with tetracycline (1  $\mu$ g/mL), washed twice with 1X PBS and then diluted 1:100 into M9G3% media and grown for 20 hours under tetracycline selection to an OD<sub>595</sub> between 0.9 and 1.1. Reporter expression over the growth cycle was determined by measuring GFP fluorescence with excitation at 385 nm and emission at 509 nm in black, clear-bottom 96-well plates on a Tecan Spark microplate reader with Magellan software (Tecan Systems, Inc., San Jose, CA). Specific fluorescence was calculated for each sample by dividing fluorescence intensity by OD<sub>595</sub>. Three biological replicates were performed for each experiment.

GFP reporter assays were conducted in the *E. coli* strain MKH13 [F *araD139* (*argFlac*) *U169 rpsL150 relA1 deoC1 ptsF25 rbsR flbB5301*] (94). A full-length copy of *opaR*, *cosR* or *aphA* was cloned into the pBBR1MCS expression vector, which contains an IPTG-inducible promoter, using the primer pairs opaRCFwd/opaRCRev, cosRCFwd/cosRCRev, and aphACFwd/aphACRev (Table 2). pBBR1MCS was linearized via digestion with KpnI and BamHI. Purified PCR fragments were ligated with linearized pBBR1MCS via Gibson assembly protocol to generate pBBR*opaR*, pBBR*cosR*, or pBBR*aphA*. Complementary regions for Gibson assembly are indicated in lower case letters in the primer sequence in Table 2. The plasmids were transformed into *E. coli* Dh5 $\alpha$ , purified, and sequenced. The purified plasmids, along with empty pBBR1MCS expression vector, were transformed into *E. coli* strain MKH13. The reporter plasmids pRUP<sub>ectA-gfp</sub> and pRUP<sub>cosR-gfp</sub> were then transformed into the

MKH13 strains containing pBBR*opaR*, pBBR*cosR*, pBBR*aphA* or pBBR1MCS empty vector. Strains containing the pRUP<sub>*ectA*</sub>-*gfp* reporter plasmid and pBBR*cosR* were grown overnight in LB1% with ampicillin (25 µg/mL) and chloramphenicol (12.5 µg/mL), washed twice with 1X PBS, and diluted 1:1000 into M9G1%. pBBR*cosR* was then induced with 250 µM IPTG and strains were grown overnight under antibiotic selection to an OD<sub>595</sub> between 0.9 and 1.1. Strains containing the pRUP<sub>*cosR*</sub>-*gfp* reporter plasmid and pBBR*opaR* or pBBR*aphA* were grown overnight in LB1% with ampicillin (25 µg/mL) and chloramphenicol (12.5 µg/mL), washed twice with 1X PBS, and diluted 1:50 into M9G1%. pBBR*opaR* or pBBR*aphA* was then induced with 10 µM IPTG and strains were grown for 20 hours under antibiotic selection to an OD<sub>595</sub> between 0.9 and 1.1. Reporter expression was determined by measuring GFP fluorescence with excitation at 385 nm and emission at 509 nm in black, clear-bottom 96-well plates on a Tecan Spark microplate reader with SparkControl Magellan software (Tecan Systems, Inc., San Jose, CA). Specific fluorescence was calculated for each sample by dividing fluorescence intensity by OD<sub>595</sub>. At least two biological replicates were performed for each experiment.

#### Growth pattern analysis.

Cultures were grown overnight in M9G1% and subsequently diluted 1:50 into new medium. Cultures were grown for 5 hours and inoculated 1:40 into M9G supplemented with 6% NaCl in 96-well plates. Cultures were grown overnight with intermittent shaking in a Tecan Sunrise microplate reader and Magellan software

(Tecan Systems, Inc., San Jose, CA). Ectoine was added to a final concentration of 100  $\mu$ M where indicated. At least two biological replicates were performed for each experiment. Statistics were calculated using a one-way ANOVA with a Tukey-Kramer post hoc test.

#### Bioinformatics analysis.

Protein sequences of OpaR orthologs were downloaded from NCBI database and aligned using the ClustalW algorithm in MEGA10. NCBI accession numbers for each protein are BAC60779.1, AGV17442.1, AEH34083.1, OFJ17407.1, AGU95396.1, YP\_205560.1, EEZ87352.1, WP\_017108721.1, ADT86079.1, WP\_000340102.1, EAS63745.1, EGA66814.1, EEX95356.1. FASTA sequences for each ectoine regulatory region were downloaded from NCBI database with accession numbers listed in Table 3. Sequences were examined by the Motif Occurrence Detection Suite (MOODS) of algorithms with a given p-value and position frequency matrix for *V. parahaemolyticus* OpaR (139, 154). Log-odds scores returned by the algorithm are the natural log of odds. The probability of binding in a given regulatory region is calculated from the odds using the formula  $\text{probability} = \text{odds} / (1 + \text{odds})$ .

### Results

Expression of *ectABCasp\_ect* and quorum sensing regulator genes throughout the growth cycle.

Previously, we showed that in a quorum sensing  $\Delta luxO$  deletion mutant the *ect* genes were repressed compared to wild-type (107). To determine the expression pattern of the ectoine biosynthesis operon *ectABCasp\_ect* in *V. parahaemolyticus* across the growth curve, we examined expression levels in M9G3% at OD<sub>595</sub> of 0.15,

0.25, 0.4, 0.5, 0.8 and 1.0. We found that ectoine biosynthesis genes *ectA* and *asp\_ect* are most highly expressed in early-exponential phase cells (OD<sub>595</sub> 0.15) and expression levels decrease with increasing OD (**Figure 4A and 4B**). Next, we examined expression levels of *aphA* and/or *opaR* under the same conditions and at the same growth time-points to determine whether there was a correlation with ectoine gene expression. We found that *aphA* is most highly expressed during early-exponential phase and *opaR* is most highly expressed in late-exponential and stationary phase (**Figure 4C and 4D**). These data suggest that the *ect* genes could be under the control of the quorum sensing master regulators AphA and OpaR.

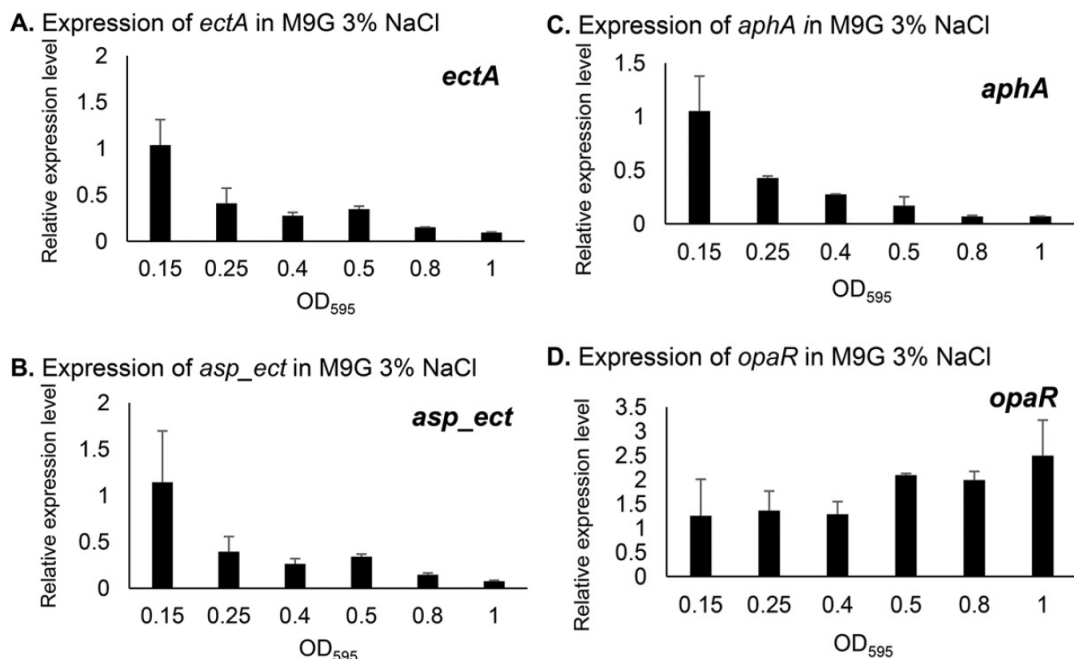


**Figure 4** **Expression analysis of *ectA*, *asp\_ect*, *aphA* and *opaR*.** Expression analysis of *ectA*, *asp\_ect*, *aphA* and *opaR* across the growth curve by quantitative real time PCR (qPCR). RNA was isolated from WT at OD<sub>595</sub> of 0.15, 0.25, 0.4, 0.5, 0.8 and 1.0 after growth in M9G3%. qPCR was performed using primer sets for (A) *ectA*, (B) *asp\_ect*, (C) *aphA*, (D) *opaR* and 16S was used for normalization. Expression levels shown are relative to levels for each gene at OD<sub>595</sub> 0.15. Mean and standard error for at least two biological replicates are shown.

Ectoine biosynthesis genes are differentially regulated in quorum sensing mutants.

We investigated the contribution of AphA and OpaR to ectoine biosynthesis gene expression by measuring transcriptional activity of the *ect* regulatory region using a transcriptional fusion GFP reporter assay. The *P<sub>ectA</sub>-gfp* reporter was examined in WT and quorum sensing deletion mutants  $\Delta luxO$ ,  $\Delta aphA$ , and  $\Delta opaR$ . Strains were grown overnight in M9G3%, and relative fluorescence intensity was then normalized to OD<sub>595</sub>. In the  $\Delta luxO$  mutant, overall *P<sub>ectA</sub>-gfp* activity was unchanged compared to WT, whereas *P<sub>ectA</sub>-gfp* expression levels in the  $\Delta aphA$  mutant were significantly

downregulated (**Figure 5A**). Compared to WT,  $P_{ectA-gfp}$  expression levels in the  $\Delta opaR$  mutant were significantly upregulated (**Figure 5A**). Since AphA and OpaR are negative regulators of each other, these data could indicate that OpaR is a negative regulator and/or that AphA is a positive regulator of ectoine biosynthesis gene expression. To investigate this further, we determined the overall  $P_{ectA-gfp}$  expression in both  $\Delta opaR/\Delta aphA$  and  $\Delta luxO/\Delta opaR$  double deletion mutants (**Figure 5A**). The  $P_{ectA-gfp}$  expression level was significantly downregulated (3.10-fold) in the  $\Delta opaR/\Delta aphA$  double mutant as compared to levels in the  $\Delta opaR$  mutant (**Figure 5A**), which demonstrates that AphA is a positive regulator. When *opaR* is deleted in the  $\Delta luxO$  mutant background,  $P_{ectA-gfp}$  activity in this double mutant is increased 10.73-fold compared to WT and 8.64-fold compared to the  $\Delta luxO$  single mutant (**Figure 5A**). These data demonstrate that OpaR is a negative regulator of the *ectABCasp\_ect* operon.

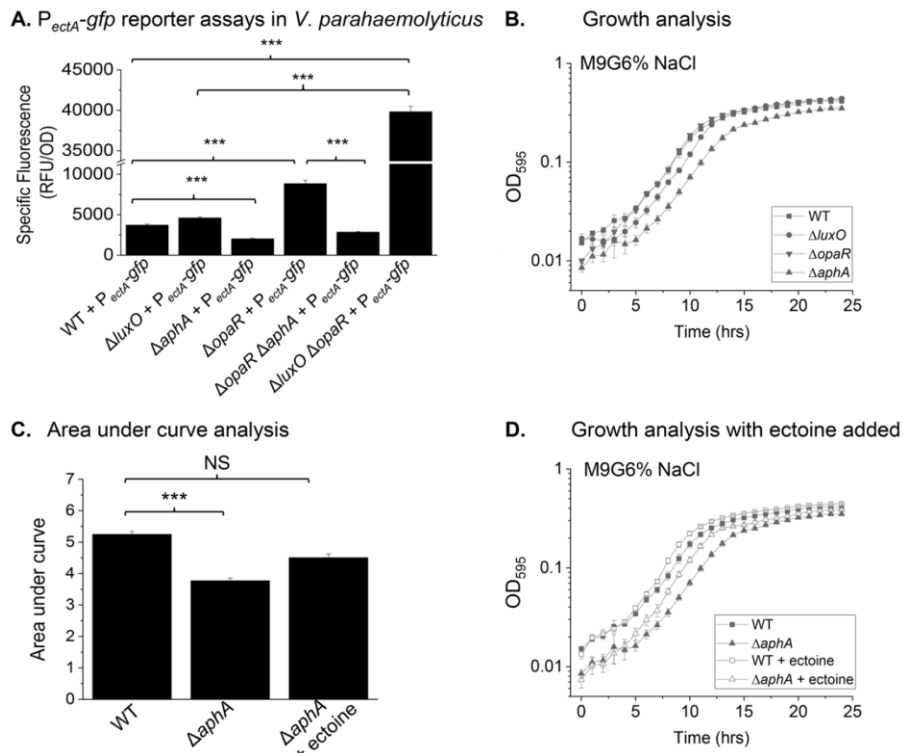


**Figure 5 Expression and growth analyses of quorum sensing mutants.** (A) Expression of a  $P_{ectA}$ -gfp transcriptional fusion in wild-type (WT) *V. parahaemolyticus* and  $\Delta luxO$ ,  $\Delta aphA$ ,  $\Delta opaR$ ,  $\Delta opaR/\Delta aphA$ , and  $\Delta luxO/\Delta opaR$  mutants. Cultures were grown overnight in M9G3% and relative fluorescence intensity (RFU) was measured. Specific fluorescence was calculated by dividing RFU by OD. Mean and standard deviation of at least two biological replicates are shown. Statistics were calculated using a one-way ANOVA with a Tukey-Kramer post hoc test; \*\*\* =  $P < 0.001$ . (B) Growth analysis of WT,  $\Delta luxO$ ,  $\Delta aphA$ , and  $\Delta opaR$  mutant strains was conducted in M9G6% (C) The area under the curve of WT and  $\Delta aphA$  after 24-hours growth in M9G6% in the growth analysis was calculated using Origin 2018 and compared to area under the curve of  $\Delta aphA$  grown in M9G6% with the addition of 100  $\mu$ M ectoine. Mean and standard error were plotted. Statistics were calculated using a one-way ANOVA with a Tukey-Kramer post hoc test; \*\*\* =  $P < 0.001$ , NS = not significant. (D) Growth analysis of WT and  $\Delta aphA$  in M9G6% or M9G6% supplemented with 100  $\mu$ M ectoine. Mean and standard error were plotted with two biological replicates shown.

The *aphA* mutant has a growth defect in high salt.

To grow in high salinity media without exogenous compatible solutes, *V. parahaemolyticus* needs to produce ectoine (59). We investigated the growth of each of the quorum sensing mutant strains compared to growth of WT under high salt stress conditions (M9G6%). The  $\Delta opaR$  mutant strain grew similarly to WT (**Figure 5B**), whereas the  $\Delta aphA$  mutant strain had a growth defect in M9G6% (**Figure 5B**). The  $\Delta luxO$  mutant also had a defect but it was not as pronounced as in the  $\Delta aphA$  mutant. We quantified the growth defect by calculating the area under the curve for both WT and the  $\Delta aphA$  mutant and found there was a significant difference, indicating a reduced osmotic tolerance in the  $\Delta aphA$  mutant (**Figure 5C**). When the  $\Delta aphA$  mutant was supplemented with exogenous ectoine in the growth media, there was no longer a significant difference in growth between the two strains (**Figure 5C and 5D**). This suggests that reduced ectoine production is responsible for the reduced osmotic tolerance of the  $\Delta aphA$  mutant.

OpaR and AphA bind upstream of the ectoine biosynthesis operon.

To further demonstrate that AphA and OpaR are regulators of the ectoine biosynthesis genes, we performed bioinformatics analysis to identify putative binding sites for each regulator in the *ect* operon regulatory region. To accomplish this, we utilized a suite of algorithms MOODS, which uses a known position frequency matrix for each regulatory protein to calculate the probability of binding to a given sequence of DNA (139, 148, 154). We determined that OpaR has a putative binding site 166-bp to 187-bp upstream of the *ectA* translation start (**Figure 6A**). To test whether OpaR binds directly to the regulatory region, electrophoretic mobility shift assays (EMSAs) were performed using purified protein and DNA probes containing the putative

binding site. OpaR bound to *PectA* Probe 1, which includes the entire intergenic region between ORFs VP1722 (*ectA*) and VP1723 (**Figure 6B**). This suggests direct regulation by OpaR. The 323 bp *PectA* probe 1, which includes the first 33 bp of the *ectA* gene and 290 bp of the upstream regulatory region, was then divided into three smaller probes, *PectA* 1A, 1B and 1C, and the EMSA was performed again with purified OpaR. OpaR bound to probe 1B indicating specificity of binding to the probe containing the putative OpaR binding site (**Figure 6C**).

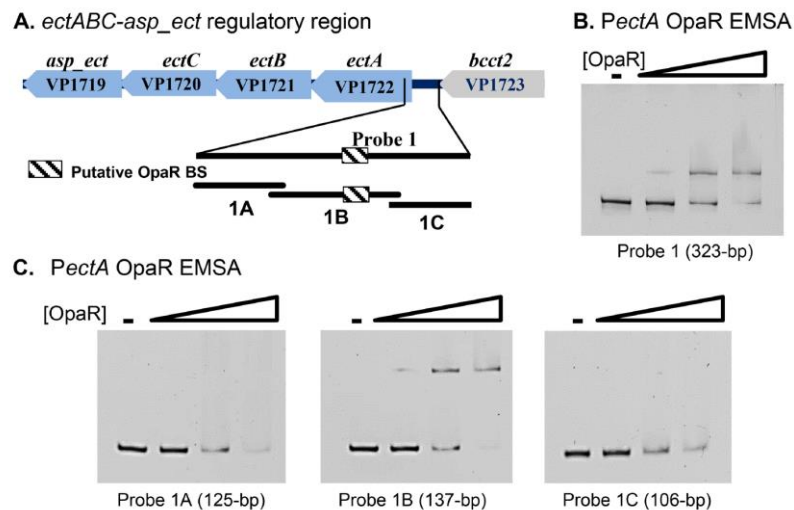


**Figure 6 OpaR binds to *ectABC-asp\_ect* promoter region.** (A) The region upstream of *ectABCasp\_ect* (*PectA*) is shown with a putative OpaR binding site 166 bp upstream of the translational start. *PectA* Probe 1, 323-bp in length, comprises the entirety of the *ectABCasp\_ect* regulatory region (+33 to -290 relative to the ATG) and contains the putative OpaR binding site. *PectA* probe 1 was then subdivided into three similarly sized probes, with probe 1B containing the putative OpaR binding site. An EMSA was performed with various concentrations of purified OpaR protein (0 to 0.87  $\mu$ M) and 30 ng of (B) probe 1 or (C) probes 1A, 1B, and 1C, 125-bp, 137-bp, 106-bp in length, respectively, with DNA:protein ratios of 1:0, 1:1, 1:10, and 1:20.

Bioinformatics analysis did not identify an AphA binding site within the intergenic region of VP1722 (*ectA*) and VP1723 (*bccT2*), however, a binding site was present within the coding region of VP1723 (Figure 4A). EMSAs were performed using purified AphA protein, *PectA* probe 1 (previously used in the OpaR *PectA* EMSA) as a negative control (no putative binding site) and *PectA* probe 2, which contained the putative AphA binding site (**Figure 7A**). Probe 2 extends from 185-bp to 513-bp upstream of the ATG, overlapping with *PectA* probe 1 by 106-bp. AphA bound to *PectA* probe 2 (**Figure 7B**), which indicates that the location of AphA binding is within the coding region of VP1723.

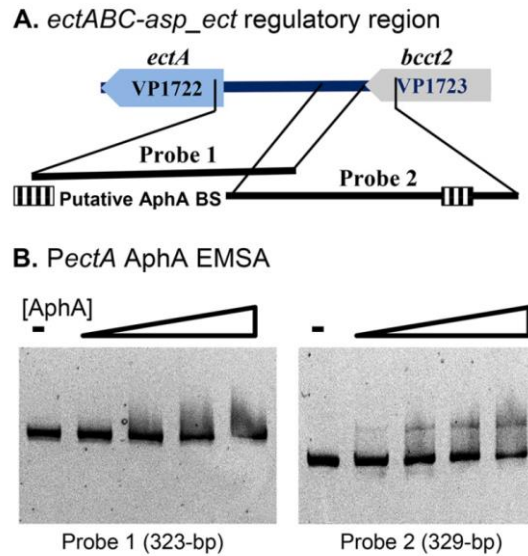


**Figure 7** **AphA binds to *ectABCasp\_ect* promoter region.** (A) The region upstream of *ectABCasp\_ect* (*PectA*) is shown with a putative AphA binding site 441-bp upstream of the translational start, with *PectA* probe 1 used in the OpaR EMSA and *PectA* probe 2. *PectA* probe 2 is 329-bp in length, contains the putative AphA binding site and extends from 185 bp to 513 bp upstream of the ATG. (B) An EMSA was performed with 30 ng of *PectA* probe 1 or probe 2 and purified AphA protein (0 to 0.84  $\mu$ M) with DNA:protein molar ratios of 1:0, 1:15, 1:30, 1:45, and 1:60.

OpaR and AphA directly regulate transcription of *ectABCasp\_ect*.

Since AphA and OpaR bind directly to the upstream region of *ectABCasp\_ect*, we next measured direct transcriptional regulation by both OpaR and AphA using a GFP reporter assay in *E. coli*. We expressed *opaR* or *aphA* from an expression plasmid (*popaR* or *paphA*) along with the  $P_{ectA}$ -*gfp* reporter plasmid in *E. coli* MKH13. *E. coli* lacks the *V. parahaemolyticus* quorum sensing components, therefore expressing *opaR* or *aphA* in this background will determine the direct effects of each regulator on transcription of *ectABCasp\_ect*. Specific fluorescence was determined after overnight

growth, and compared to specific fluorescence of a control strain harboring an empty expression vector (pBBR1MCS) and the  $P_{ectA}$ -*gfp* reporter.  $P_{ectA}$ -*gfp* activity in the *opaR*-expressing strain was significantly higher than the empty vector strain (**Figure 8A**) indicating that OpaR activates transcription of these genes in *E. coli*. Total  $P_{ectA}$ -*gfp* activity in the *aphA*-expressing strain was significantly lower as compared to the empty vector strain (**Figure 8B**), suggesting that AphA acts as a repressor of the ectoine operon in an *E. coli* background. These data are in contrast to the *in vivo*  $P_{ectA}$ -*gfp* reporter data (**Figure 5A**), which show that OpaR is a negative regulator and AphA is a positive regulator of the ectoine operon. Since OpaR and AphA reciprocally repress each other and each regulate the *qrr* sRNAs, the absence of these additional regulatory mechanisms in *E. coli* likely contributes to the differences between the *V. parahaemolyticus in vivo* data and the *E. coli* reporter assays.

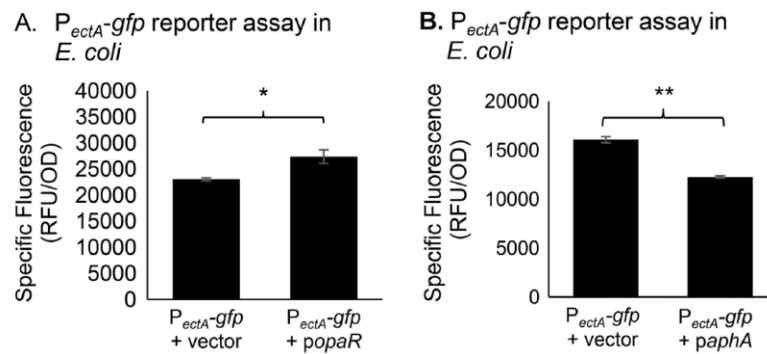


**Figure 8**  $P_{ectA}$ -*gfp* reporter assays in *E. coli*.

*E. coli* strain MKH13 harboring  $P_{ectA}$ -*gfp* and expression plasmid pBBR1MCS containing (A) *opaR* or (B) *aphA* under the control of an IPTG inducible promoter (*popaR* or *paphA*). Fluorescence intensity and OD were measured after overnight growth in M9G1% and compared to a strain with empty expression vector. Two biological replicates are shown. Statistics were calculated using a student's t-test; \* =  $P < 0.05$ , \*\* =  $P < 0.01$ .

CosR is a repressor that binds directly to the *ectABCasp\_ect* regulatory region.

Local regulators, CosR in *V. cholerae* and a homolog EctR1, in *M. alcaliphilum*, act as repressors of ectoine biosynthesis genes (109, 110). *Vibrio parahaemolyticus* encodes a homolog of CosR<sub>Vc</sub> encoded by VP1906 in strain RIMD2210633. CosR<sub>Vc</sub> and CosR<sub>Vp</sub> share 70% amino acid identity. Regulation of ectoine biosynthesis genes by CosR has not been investigated in *V. parahaemolyticus*. We determined whether CosR represses transcription of the *ect* operon by first constructing an in-frame deletion mutant of *cosR*. We then introduced the P<sub>ectA-gfp</sub> reporter plasmid into the  $\Delta$ *cosR* mutant and compared the reporter activity levels to that of WT harboring P<sub>ectA-gfp</sub> after growth in M9G3%. P<sub>ectA-gfp</sub> activity in the  $\Delta$ *cosR* mutant strain was significantly higher than in the WT strain indicating that CosR is a repressor (**Figure 9A**).

To determine whether regulation of the *ect* operon by CosR is direct, we purified CosR with a C-terminal hexahistidine tag. We first performed an EMSA with the full-length *PectA* Probe 1, utilized previously in the OpaR EMSA, and various molar ratios of purified CosR. CosR bound to the *PectA* Probe 1 (**Figure 9B**). A CosR consensus binding sequence is not available for *V. parahaemolyticus*, so we utilized the probes from our OpaR binding assay to narrow down potential binding sites and demonstrate specificity of binding (**Figure 6A**). EMSAs using these DNA probes were performed with various molar ratios of DNA probe:CosR. CosR bound specifically to probe 1A and probe 1B of the regulatory region (**Figure 9C**), indicating that CosR is a direct regulator of this operon. CosR did not bind to probe 1C demonstrating the binding specificity of CosR (**Figure 9C**).

A GFP reporter assay in *E. coli* was utilized to determine the effect CosR has on transcription of the *ectABCasp\_ect* operon by measuring transcriptional activity.

The assay used *E. coli* strain MKH13 harboring two plasmids: an expression plasmid with full-length *cosR* under the control of an inducible promoter (*pcosR*) and a  $P_{ectA}$ -*gfp* reporter plasmid. Performing this reporter assay in *E. coli* allowed us to assess the contribution of CosR to transcription at the *ectABCasp\_ect* promoter in the absence of other *V. parahaemolyticus* proteins that may affect transcriptional regulation. Relative fluorescence and OD were measured after growth in M9G1%. Specific fluorescence values were compared to a strain with an empty expression vector (pBBR1MCS).  $P_{ectA}$ -*gfp* reporter activity in the strain expressing CosR was 3.49-fold lower compared to the empty vector strain, indicating that CosR directly significantly represses transcription of the *ectABCasp\_ect* operon (**Figure 9D**).

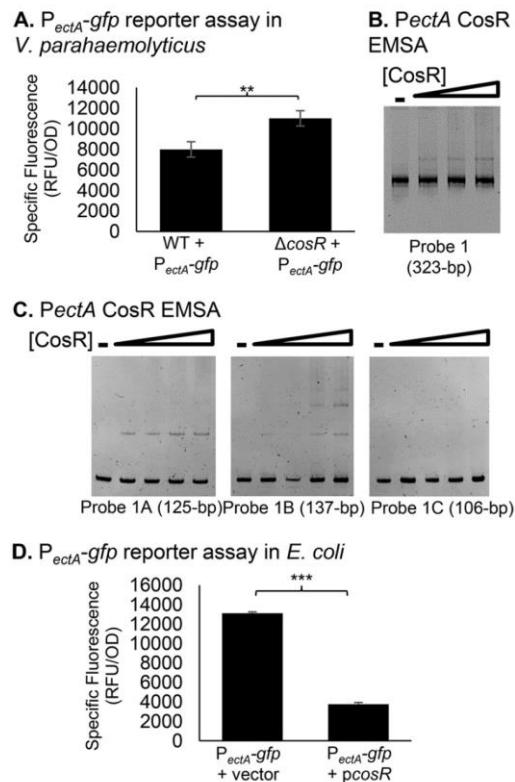


**Figure 9 CosR binds to and represses *ectABCasp\_ect* promoter region.** (A) A *P<sub>ectA-gfp</sub>* reporter assay in wild-type (WT) *V. parahaemolyticus* and the  $\Delta$ *cosR* mutant. (B) An EMSA was performed with 30 ng of the full-length *PectA* Probe 1 and purified CosR protein (0 to 0.27  $\mu$ M) with DNA:protein molar ratios of 1:0, 1:5, 1:10, and 1:20. (C) An EMSA was performed with 30 ng of each *PectA* probe 1A, 1B, or 1C and purified CosR protein (0 to 0.65  $\mu$ M), with DNA:protein molar ratios of 1:0, 1:1, 1:5, 1:10, and 1:15. (D) *P<sub>ectA-gfp</sub>* reporter assay in *E. coli* strain MKH13 containing expression plasmid pBBR1MCS with *cosR* under the control of an IPTG inducible promoter (*pcosR*). Cultures were induced and grown overnight in M9G1%. Specific fluorescence of the CosR-expressing strain was compared to a strain harboring empty pBBR1MCS. Mean and standard deviation of at three biological replicates are shown. Statistics were calculated using a student's t-test; \*\*\* =  $P < 0.001$ .

CosR is activated by OpaR and AphA.

We utilized a GFP reporter assay to investigate whether CosR is under the control of the quorum sensing master regulator OpaR. We constructed a *P<sub>cosR-gfp</sub>* reporter plasmid and introduced this into the WT strain and the  $\Delta$ *opaR* mutant strain to measure transcriptional activity. Relative fluorescence and OD were measured after growth in M9G3%. The *P<sub>cosR-gfp</sub>* reporter activity was significantly lower in the  $\Delta$ *opaR* mutant strain than in the WT strain indicating that OpaR is a positive regulator of the *cosR* gene (Figure 10A).

Bioinformatics analysis identified one putative OpaR binding site in the regulatory region of the *cosR* gene, located 180-bp to 199-bp upstream of the translation start (Figure 10B). We performed an EMSA with purified OpaR protein and two DNA probes comprising the upstream portion of the *cosR* regulatory region containing the putative binding site, and the region proximal to, and including, the ATG as a negative control (Figure 10B). OpaR bound directly to *P<sub>cosR</sub>* probe A, but

not to P<sub>cosR</sub> probe B (**Figure 10C**). This indicates that OpaR is a direct regulator of *cosR* that binds specifically to probe A of the *cosR* regulatory region.

To demonstrate that direct binding of OpaR to the *cosR* regulatory region activates transcription, a reporter assay was performed in *E. coli* MKH13 harboring P<sub>cosR-gfp</sub> and an expression vector harboring *opaR* under the control of an IPTG-inducible promoter. Specific fluorescence was calculated after growth in M9G1% and compared to a strain harboring an empty expression vector along with the P<sub>cosR-gfp</sub> reporter. In the OpaR-expressing strain, P<sub>cosR-gfp</sub> reporter activity was significantly higher than in the empty vector strain, indicating that OpaR directly activates transcription of *cosR* (**Figure 10D**).

We next determined whether AphA regulates transcription of *cosR*. Utilizing our P<sub>cosR-gfp</sub> reporter plasmid, we assessed P<sub>cosR-gfp</sub> activity in WT and  $\Delta$ *aphA*. Relative fluorescence and OD were measured after growth in M9G3%. The P<sub>cosR-gfp</sub> reporter activity was significantly lower in the  $\Delta$ *aphA* mutant strain than in the WT strain indicating that AphA is a positive regulator of the *cosR* gene (**Figure 11A**). Using bioinformatics analysis, we identified a putative AphA binding site in the *cosR* regulatory region (**Figure 11B**). An EMSA was performed with probe A (188 bp) containing the putative binding site and probe B (142 bp) with no binding site. In this assay, AphA did not bind to either probe (**Figure 11C**). This suggests that AphA does not directly regulate *cosR* or that AphA requires an additional factor to bind.

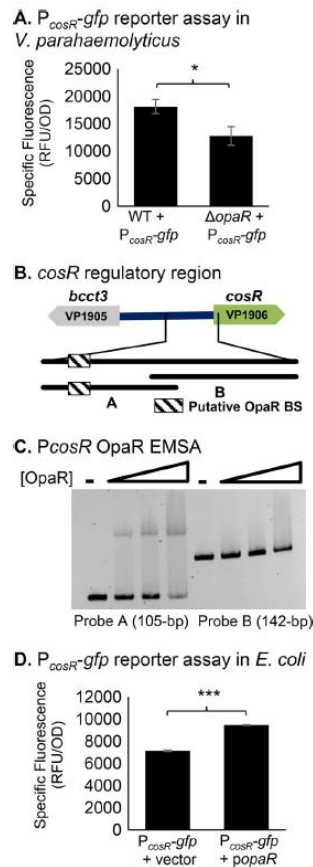
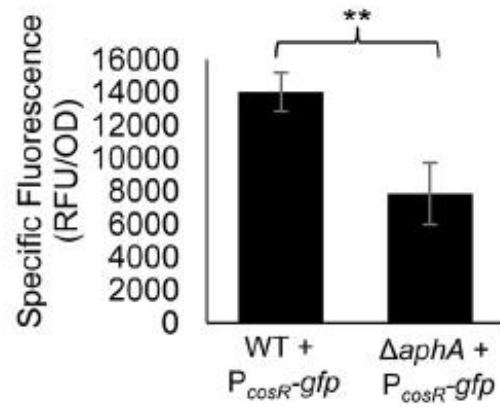


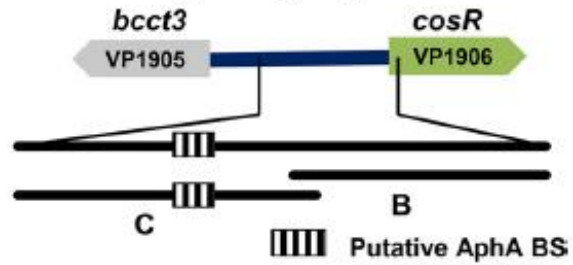
**Figure 10 *cosR* is regulated by OpaR.**

(A) A  $P_{cosR}$ -*gfp* reporter assay in wild-type (WT) *V. parahaemolyticus* and the  $\Delta opaR$  mutant harboring a  $P_{cosR}$ -*gfp* transcriptional fusion reporter plasmid. (B) A 224-bp region of the *cosR* regulatory region ( $P_{cosR}$ ; +4 to -220 relative to ATG) was divided into two similarly sized probes A and B, 105-bp and 142-bp in length, respectively. A putative OpaR binding site is located 180 to 199 bp upstream of the translation start, within probe A. (C) An EMSA was performed with various concentrations of purified OpaR protein (0 to 0.88  $\mu$ M) and  $P_{cosR}$  probe A or B. Each lane contains 30 ng of DNA probe with molar ratios of DNA:protein of 1:0, 1:1, 1:10 and 1:20. (D) *E. coli* strain MKH13 harboring  $P_{cosR}$ -*gfp* and expression plasmid pBBR1MCS containing *opaR* under the control of an IPTG inducible promoter (*popaR*). Cultures were induced and grown overnight in M9G1%. Specific fluorescence of the OpaR-expressing strain was compared to a strain harboring empty expression vector. Mean and standard deviation of two biological replicates are shown. Statistics were calculated using a student's t-test; \*\*\* =  $P < 0.001$ .

**A.**  $P_{cosR}$ -*gfp* reporter assay in *V. parahaemolyticus*



**B.** *cosR* regulatory region



**C.**  $P_{cosR}$  AphA EMSA

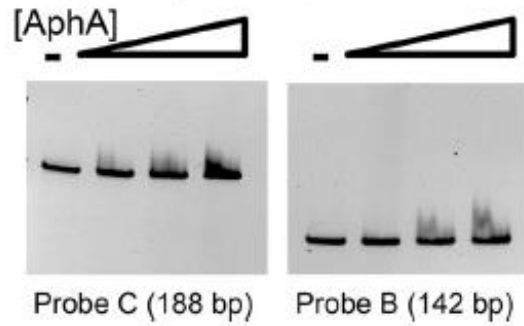


**Figure 11** *cosR* is regulated by AphA.

(A) A  $P_{cosR-gfp}$  reporter assay in wild-type (WT) *V. parahaemolyticus* and the  $\Delta aphA$  mutant harboring a  $P_{cosR-gfp}$  transcriptional fusion reporter plasmid. Cultures were grown overnight in M9G3% and specific fluorescence was determined by dividing RFUs by OD. Mean and standard deviation of three biological replicates are shown. Statistics were calculated using a student's t-test; \*\* =  $P < 0.01$  (B) The regulatory region of the *cosR* gene (+4 to -327 relative to the ATG) was divided into two similarly sized probes, probe B, used previously in the OpaR EMSA, and probe C, 142-bp and 188-bp in length, respectively. A putative AphA binding site is located 204 to 223-bp upstream of the ATG, within probe C. (C) An EMSA was performed with various concentrations of purified AphA protein (0 to 0.88  $\mu$ M) and *PcosR* probe B or C. Each lane contains 30 ng of DNA probe and DNA:protein molar ratios of 1:0, 1:15, 1:30 and 1:45.

#### Quorum sensing regulation of ectoine biosynthesis genes in *Vibrionaceae*.

The ability to biosynthesize ectoine is phylogenetically widespread among the *Vibrionaceae* family (59). It was determined previously through mutational analyses that three residues, I24, A51, and T52, within the DNA binding domains of LuxR are important for repression of target genes in *V. harveyi* ATCC BAA-1116 (143). We determined that homologs of LuxR in multiple *Vibrio* species also contained these conserved amino acids and therefore likely bind to target genes in the same manner (data not shown). We used the OpaR consensus binding motif to predict binding sites in the regulatory region of the ectoine biosynthesis genes in multiple *Vibrio* species. Putative binding sites, along with distance from the ATG, log odds score, probability of binding and a given p-value, are listed in Table 3. Only binding sites that were returned with a probability of 90% or greater are shown. The probability of a LuxR-type binding site in *V. alginolyticus*, the most closely related species to *V. parahaemolyticus*, is 99.1%, in *V. harveyi* 1DA3 and ATCC BAA-1116, 95% and in *V. splendidus* 92%, and each have one predicted binding site. Several species have

multiple predicted binding sites. Overall, this data suggests that quorum sensing control of the ectoine biosynthesis system is likely widespread among *Vibrio* species.

### Discussion

In this study, we investigated regulation of the ectoine biosynthesis operon by the quorum sensing regulators AphA and OpaR. Ectoine genes are most highly expressed in early exponential phase, and levels fall concurrently with AphA levels. This ensures that adequate transcripts are present to produce the enzymes necessary for conversion of aspartic acid to ectoine during exponential phase, when the cells are rapidly growing and dividing. We found that expression of the *ectABCasp\_ect* operon is activated by AphA and repressed by OpaR. This suggests that OpaR represses expression during late-exponential phase when the requirement for ectoine production begins to diminish, as the cells approach stationary phase and are no longer replicating. In addition, we show that AphA and OpaR activate transcription of CosR, which also represses *ectABCasp\_ect*. In this transcriptional motif, a feed-forward loop, a general transcription factor (OpaR or AphA) controls a specific transcription factor (CosR), and both transcription factors regulate the output of the effector operon (*ectABCasp\_ect*). This regulation scheme presumably results in precise control of energetically costly ectoine production across the growth cycle (**Figure 12**). The complexity of regulation of the *ectABCasp\_ect* operon likely explains the conflicting results of our *V. parahaemolyticus in vivo* and *E. coli* reporter assays. Here we have shown at least three regulators are involved in direct transcriptional control of the *ect* genes. Control by each regulator is more than likely affected by the other regulators. This could occur either via direct interactions at the regulatory region, or indirectly via transcriptional control of each other, as OpaR and AphA reciprocally repress each

other, and both activate CosR. Additionally, given the complexity of the quorum sensing regulatory circuit, it is probable that other regulators play a role in fine-tuning ectoine production via transcriptional, post-transcriptional, and enzyme-level regulation of ectoine biosynthesis. Due to an associated energy cost (75), it is reasonable that bacteria would utilize multiple levels of regulation to tightly control ectoine production in the cell.

The physiology of *V. parahaemolyticus* provides one explanation for quorum sensing control of ectoine production. In order to reach high cell density, *V. parahaemolyticus* grows optimally in high salinity, which requires accumulation of compatible solutes. Therefore, integration of quorum sensing regulators with osmotic tolerance would allow *V. parahaemolyticus* to respond to environmental stressors and to maximize production of compatible solutes at both low and high cell densities. Quorum sensing has been linked with multiple stress responses in bacteria. In *V. cholerae*, it was shown that HapR (LuxR homolog) activates *rpoS*, the general stress response sigma factor, increasing survival under environmental stress (155). A study in *Burkholderia glumae* revealed that quorum sensing functions to maintain bacterial osmolality by negatively regulating glutamate uptake and nitrogen metabolism (156). In *V. harveyi*, a closely related species to *V. parahaemolyticus*, the quorum sensing master regulator LuxR was shown to directly regulate the transcription of the glycine betaine biosynthesis operon (62).

*Vibrio* thrive in warmer temperatures and increased salinity, and cause infections mostly in the warmer months of the year. High salinity enables *V. parahaemolyticus* to adapt to other abiotic stresses, such as temperature (157, 158). This, along with warming ocean temperatures, has facilitated the expansion of the

range of *V. parahaemolyticus* as far north as Alaska (159), with infection rates in the US increasing over the last several years (160). *V. parahaemolyticus* poses a growing threat to the shellfish industry, where despite strict guidelines for handling, high incidence rates persist (161, 162). This work furthers the understanding of osmotic stress response regulation in *V. parahaemolyticus* and is an important step in understanding increased *Vibrio* proliferation in warmer ocean temperatures when salinity is elevated.

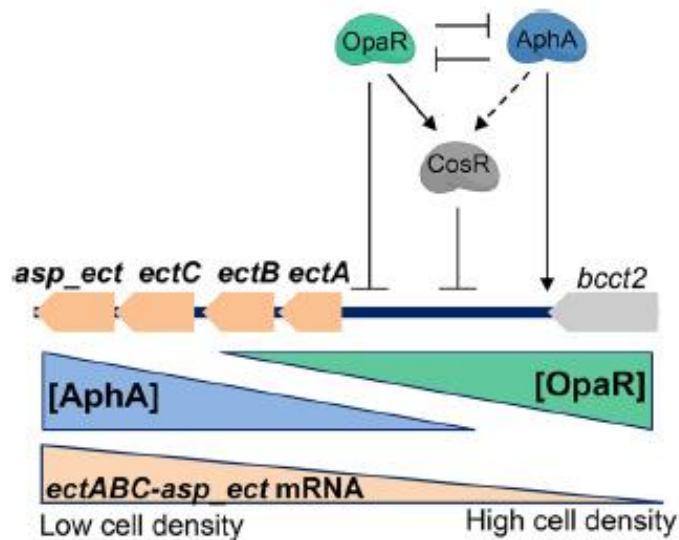


**Figure 12 A model of ectoine biosynthesis gene regulation by quorum sensing regulators.** Dashed line indicates indirect regulation while solid lines indicate direct regulation. AphA is activated at low cell density and activates transcription of *ectABCasp\_ect*. OpaR is activated during the transition from low cell density to high cell density. As levels of OpaR increase, levels of AphA decrease, and OpaR represses *ectABCasp\_ect* transcription. OpaR and AphA activate transcription of *cosR*. CosR participates in a feed-forward loop to repress *ectABCasp\_ect* transcription. This regulatory loop produces a gradient of *ectABCasp\_ect* transcripts across the growth cycle

Table 1 Strains and Plasmids used in this study.

Strain	Genotype	Source
<i>Vibrio parahaemolyticus</i>		
RIMD2210633	O3:K6 clinical isolate, StrR	(104, 157)
SSK2099 ( $\Delta luxO$ )	RIMD2210633 $\Delta luxO$ (VP2099), StrR	(107)
SSK2516 ( $\Delta opaR$ )	RIMD2210633 $\Delta opaR$ (VP2516), StrR	(107)
SSK2762 ( $\Delta aphA$ )	RIMD2210633 $\Delta aphA$ (VP2762), StrR	(107)
SSK9916 ( $\Delta luxO/\Delta opaR$ )	RIMD2210633 $\Delta luxO \Delta opaR$ , StrR	(107)
SSK1662 ( $\Delta opaR/\Delta aphA$ )	RIMD2210633 $\Delta opaR \Delta aphA$ , StrR	(107)
$\Delta cosR$	RIMD2210633 $\Delta cosR$ (VP1906), StrR	This study
<i>Escherichia coli</i>		
DH5 $\alpha$ $\lambda$ pir	$\Delta lac$ pir	ThermoFisher Scientific
$\beta$ 2155 $\lambda$ pir	$\Delta dapA::erm$ pir for bacterial conjugation	(163)
BL21(DE3)	Expression strain	ThermoFisher Scientific
MKH13	MC4100 ( $\Delta betTIBA$ ) $\Delta (putPA)101$ $\Delta (proP)2 \Delta (proU)$ ; SpR	(94)
<b>Plasmids</b>		
pDS132	Suicide plasmid, cmR, sacB (sucrose intolerant), R6Kg origin	(164)
pDS $\Delta cosR$	pDS132 harboring truncated <i>cosR</i> allele	This study
pBBR1MCS	Empty expression vector, <i>lacZ</i> promoter, CmR, pBBR1 origin	(165)
pBBR $opaR$	pBBR1MCS harboring full-length <i>opaR</i> (VP2516)	This study
pBBR $cosR$	pBBR1MCS harboring full-length <i>cosR</i> (VP1906)	This study
pBBR $aphA$	pBBR1MCS harboring full-length <i>aphA</i> (VP2762)	This study
pRU1064	promoterless- <i>gfp</i> UV, AmpR, TetR, IncP origin	(153)
pRU $PectA$	pRU1064 with <i>PectA-gfp</i> , AmpR, TetR	This study
pRU $PcosR$	pRU1064 with <i>PcosR-gfp</i> , AmpR, TetR	This study
pMAL-c5x	Empty expression vector, TEV site; AmpR	(166)
pMAL $aphA$	pMAL harboring <i>aphA</i> , AmpR	This study
pET28a+	Empty expression vector, 6xHis; KanR	Novagen
pET $cosR$	Pet28a+ harboring <i>cosR</i> , KanR	This study

Table 2 Primers used in this study

Primer	Sequence (5'-3')	Length (bp)
Mutant		
SOEVPcosRA	accgcatcgatatcgagctTCAAAGCCCCACTTTTGAAC	511
SOEVPcosRB	tgatgctgccgatAATCGAGACCAATACTTCTTCG	
SOEVPcosRC	ggtctcgattATCGGCAGCATCACCAAAC	522
SOEVPcosRD	gtggaattcccgggagagctCAATCATGAATGGCATCG	
SOEVPcosRFLFwd	CCCATCCAATGCTGTCTTCG	1838
SOEVPcosRFLRev	CATGCAAGAACGTGTGGAGT	
Protein expression		
NcoIaphAFwd	TGCCCATGGGAATGTCATTACCACACGTAATC	540
BamHIaphARev	CTCGGATCCTTAACCAATCACTTCAAGTTCTGTTAGG	
NcoIcosRFwd	TACGGCGCCATGGACTCAATTGCAAAGAG	625
XhoIcosRRev	CACGAGCTCTTAGTGTTCGCGATTGTAGA	
EMSA		
VPectAFwd1A	CCAAGGTGCTGATGTGATCA	125
VPectARev1A	CACATTAATCCAGATTA AAAACGCAG	
VPectAFwd1B	CTGCGTTTTAATCTGGATTAATGTG	137
VPectARev1B	CCCACTGCATTCTGACTCAT	
VPectAFwd1C	ATGAGTCAGAATGCAGTGGG	106
VPectARev1C	GCCACGACGACAAA ACTAAC	
VPectARev2	GTAAAGTCGATGCGCCAACAC	
VPcosRFwdA	CAAATCTCCACACCATTAATTAG	105
VPcosRRevA	CGTCTTTGGTGATTTCTTTTTTATTCGC	
VPcosRFwdB	GCGAATAAAAAGAAATCACCAAAGACG	142
VPcosRRevB	CCAATTTTTTTCATCCAGTCTGTAGGG	
VPcosRFwdC	CCCGTGAAAGCGGAAGATC	188
VPcosRRevC	CGCTCGTGCAACTGAAACA	
Expression		
opaRCFwd	agggaacaaaagctgggtacAATGGCAAGGAAAATGGATATG	642
opaRCRev	cggccgctctagaactagtG GGCTTGTTTCGTGTTCAAATC	
cosRCFwd	agggaacaaaagctgggtacTTCCCTACAGACTGGATG	501
cosRCRev	cggccgctctagaactagtTTATTCTGGTTTGGTGATG	
aphACFwd	agggaacaaaagctgggtacGACCATTTGGATTGAAGAC	559
aphACRev	cggccgctctagaactagtTTAACCAATCACTTCAAGTTC	
GFP reporter		
PectAPFwd	CTCAAGCTTGTAAGTCGATGCGCCAAC	514
PectAPRev	TATACTAGTATCCTTTGACGTCTAATTA AATTTTC	
PcosRPFwd	tagatagagagagagagagaCGTTCCTCTCTATTTTTGTATTATTTTTTC	397
PcosRPRev	actcatttttctctccaAATTTTTTTCATCCAGTCTGTAGG	

Table 2 (continued)

<b>qPCR</b>		
opaRFwd	CCATGTTGTCCGTCAGTTCTCG	158
opaRRev	GAGTTGATGCGCTCCACTCG	
aphAFwd	AGCCACCAACAAGTTTACCG	140
aphARev	CATTCTCCAAGAGCGCTACG	
ectAFwd	CCAATGGCGGTTGTACTGCTGAAA	269
ectARev	TCACCGTGAATACACTCGATGCCA	
asp-ectFwd	CGATGATTCCATTCGCGACG	126
asp-ectRev	GTCATCTCACTGTAGCCCCG	
16SFwd	ACCGCCTGGGGAGTACGGTC	234
16SRev	TTGCGCTCGTTGCGGGACTT	

---

Table 3 Putative OpaR binding sites in the ectoine regulatory region of *Vibrio* species.

Species	Binding Site	Upstream ATG	Log odds score	P	p-value	Strain Accession No.
<i>V. parahaemolyticus</i>	AAATGATGCTTTAATAAATT	147 bp	3.69	0.976	0.003	GCA_000196095.1
<i>V. alginolyticus</i>	TAGGTGACTATTTAATAAAAT	179 bp	4.65	0.991	0.005	GCA_000354175.2
<i>V. harveyi</i> 1DA3	CAATTTATTTTTCACCCTAT	155 bp	2.96	0.951	0.005	GCA_000182685.1
<i>V. harveyi</i> ATCC BAA-1116	CGATTAATTTTTTACCCTAT	187 bp	3.03	0.954	0.005	GCA_000017705.1
<i>V. splendidus</i>	CAAAGTATTATTTAATACAT	129 bp	2.46	0.921	0.005	GCA_003049855.1
<i>V. brasiliensis</i>	CTGCTGACATTAATTAGAGT	330 bp	2.24	0.904	0.005	GCF_000189255.1
	TTAATTAGAGTTCTAACTAA	321 bp	3.19	0.961	0.0025	
	GTATTGTTTCTAAGGACTAA	211 bp	2.48	0.923	0.005	
	TTATTGAGTAAACCTTAGT	150 bp	5.69	0.997	0.0005	
	CTTTAGTTTTAACTCTAAAT	137 bp	4.43	0.988	0.001	
	ATAATGAATGTGAAATTTGT	16 bp	4.50	0.989	0.001	
<i>V. orientalis</i>	TTTTTATTTGACTCTAATT	386 bp	2.22	0.902	0.005	GCA_000176235.1
	TAATTAATAAATCGCATTAT	371 bp	5.67	0.997	0.0005	
	ATTAAATTAATTTGGTTAAT	322 bp	3.13	0.958	0.0025	
	AATTGGTTAATTTAGCATTAA	313 bp	4.41	0.988	0.001	
	CAAATGGCTAATCATTAAAGT	283 bp	2.39	0.916	0.005	
<i>V. anguillarum</i>	AATTGTGAACAAAGAGTATT	417 bp	2.25	0.904	0.005	GCA_000217675.1
	TTATATAGAGATTTTAAATT	36 bp	2.50	0.924	0.005	
	ATATAGAGATTTTAAATTAG	34 bp	2.16	0.897	0.005	
	TTAATTAGAGCTCTAACTAT	22 bp	4.06	0.983	0.005	
<i>V. furnissii</i>	ATATAGTGTGAACAAAATGT	427 bp	2.35	0.914	0.005	GCA_000184325.1
	CTAGTGATAGCAATGTAACT	217 bp	3.42	0.968	0.0025	
	GGTTTTATTGAATTATCCAT	87 bp	2.85	0.946	0.005	
	TTATTGAATTATCCATTATT	83 bp	4.58	0.990	0.001	
<i>V. mimicus</i>	GTAAAAATAGAAATATGATT	43 bp	4.59	0.990	0.001	GCA_001767355.1
* <i>V. parahaemolyticus</i> (upstream of <i>opaR</i> )	TAATGACATTACTGTCTATA	127 bp	9.94	1.00	0.00001	

## Chapter 3

# **COSR IS A GLOBAL REGULATOR OF THE OSMOTIC STRESS RESPONSE WITH WIDESPREAD DISTRIBUTION AMONG BACTERIA**

The work in this chapter was published in *Applied and Environmental  
Microbiology*

## **CosR Is a Global Regulator of the Osmotic Stress Response with Widespread Distribution among Bacteria**

Gregory GJ; Morreale DP; Boyd EF

Appl. Env. Microb. doi: 10.1128/AEM.00120-20.

### **Introduction**

Halophilic bacteria such as *Vibrio parahaemolyticus* encounter a range of osmolarities and have an absolute requirement for salt. To combat the loss of turgor pressure due to efflux of water in high osmolarity conditions, bacteria have developed a short-term “salt in” strategy requiring the uptake of K<sup>+</sup> and a long-term “salt out” strategy that involves the accumulation of compatible solutes in the cell (15, 78, 167). Compatible solutes, as the name suggests, are organic compounds that are compatible with the molecular machinery and processes of the cell, and include compounds such as ectoine, glycine betaine, trehalose, glycerol, proline, glutamate, and carnitine, among others (5, 13-18). Compatible solutes are taken up from the environment or biosynthesized from various precursors in response to osmotic stress, which allows

cells to continue to grow and divide even in unfavorable environments (9, 13, 22, 167).

Searches of the genome database demonstrated that ectoine biosynthesis genes are present in over 500 bacterial species (32). Most of the species that contain ectoine biosynthesis genes are halotolerant or halophiles. Previously, it was shown that ectoine biosynthesis is present in all halophilic *Vibrio* species including *Vibrio parahaemolyticus* and this species also possesses the genes for glycine betaine biosynthesis and multiple compatible solute transporters (45). *De novo* biosynthesis of ectoine requires aspartic acid as the precursor, which can be supplied by the cell (59). Aspartic acid is converted to ectoine by four enzymes, EctA, EctB, EctC and Asp\_Ect, encoded by the operon *ectABCasp\_ect* (40). Ectoine biosynthesis begins with L-aspartate- $\beta$ -semialdehyde, which is also pivotal to bacterial amino acid and cell wall synthesis (40). Asp\_Ect is a specialized aspartokinase dedicated to the ectoine pathway that, among Proteobacteria, is present only in alpha, gamma and delta species (41). Our recent study showed that the quorum sensing response regulators OpaR and AphA are a negative regulator and a positive regulator of *ectABC-asp\_ect* gene expression, respectively (108). In addition, we showed that OpaR and AphA are positive regulators of *cosR*, which encodes a MarR-type regulator CosR (108, 109). We showed that, similar to *V. cholerae*, CosR is a repressor of *ectABC-asp\_ect* indicating that control of ectoine biosynthesis is multilayered and stringent (108).

Production of glycine betaine is a two-step oxidation from the precursor choline, which is acquired exogenously. *De novo* biosynthesis of glycine betaine has been identified in only a few species of halophilic bacteria (47-51, 54). Choline is converted to glycine betaine by the products of two genes *betB* and *betA* (57, 58). In *E.*

*coli*, these genes are encoded by the operon *betIBA*, with the regulator BetI shown to repress its own operon (55, 56). In all *Vibrio* species that biosynthesize glycine betaine, the *betIBA* genes are in an operon with the *proXWV* genes, which encode an ATP-binding cassette (ABC)-type transporter named ProU2 (45, 59, 60). Regulation of glycine betaine biosynthesis has been studied in several species, but few direct mechanisms of regulation have been shown beyond BetI (55, 56, 62, 111, 112, 115). Recently, in *V. harveyi*, a close relative of *V. parahaemolyticus*, *betIBAproXWV* was shown to be positively regulated by the quorum sensing master regulator LuxR (62, 111).

It is energetically favorable to the cell to uptake compatible solutes from the environment rather than to biosynthesize them, and Bacteria and Archaea encode multiple osmoregulated transporters (5, 30, 75, 77, 168-170). ABC-type transporters are utilized to import exogenous compatible solutes into the cell and include ProU (encoded by *proVWX*) in *E. coli* and *Pseudomonas syringae*, OpuA in *Lactococcus lactis* and *B. subtilis*, and OpuC in *P. syringae* (88-91, 170, 171). *Vibrio parahaemolyticus* encodes two ProU transporters, one on each chromosome. ProU1 is encoded by *proVWX* (VP1726-VP1728) and ProU2 is encoded by the *betIBAproXWV* operon (VPA1109-VPA1114) (45). ProU1 is a homolog of the *E. coli* K-12 ProU, which in this species was shown to bind glycine betaine with high affinity (88, 97, 98). ProU2 is a homolog of the *P. syringae proVXW* (45).

The betaine-carnitine-choline transporters (BCCTs) are single component sodium- or proton coupled transporters, the first of which, BetT, discovered in *E. coli*, was shown to transport choline with high-affinity and is divergently transcribed from *betIBA* (81, 85). *Vibrio parahaemolyticus* contains four BCCTs, BCCT1-BCCT3

(VP1456, VP1723, VP1905), and BCCT4 (VPA0356) (45). The *bccT2* (VP1723) gene is the only *bccT* that is not induced by salinity in *V. parahaemolyticus* (59). All four BCCT transporters were shown to transport glycine betaine amongst other compatible solutes (60). A study in *V. cholerae* demonstrated that a *bccT3* homolog is repressed by the regulator CosR in low salt conditions (109).

To date there has been no single regulator identified that controls multiple compatible solute systems in bacteria. In this study, we examined whether CosR could have a broader role in the osmotic stress response. First, we examined expression of genes encoding osmotic stress response systems in low salinity and used quantitative real-time PCR to quantify expression of these genes in a  $\Delta\text{cosR}$  deletion mutant. This analysis showed that CosR was a negative regulator of both ectoine and glycine betaine biosynthesis systems and two different transporter systems; the ABC-type transporters ProU1 and ProU2 and the sodium-coupled transporters BCCT1 and BCCT3. These data indicate that the CosR regulon is larger than appreciated and expands the role of CosR to that of a global regulator of compatible solute systems. We determined whether CosR was a direct regulator using DNA binding assays and an *E. coli* plasmid-based reporter assay. We also examined whether *betIBAproXWV* was under the control of the quorum sensing regulator OpaR, which also regulates *cosR*. We showed that OpaR is an activator of *betIBAproXWV* in contrast to its repression of *ectABCasp\_ect*. Phylogenetic analysis of CosR showed it is ancestral to the *Vibrionaceae* family, present in all members of the group. Bioinformatics analysis indicated that CosR homologs are also prevalent among *Gamma-Proteobacteria* in general. Overall, the data show that CosR is a previously unrecognized global regulator of the osmotic stress response that is widespread among bacteria.

## Materials and Methods

### Bacterial strains, media and culture conditions

Listed in Table 1 are all strains and plasmids used in this study. A previously described streptomycin-resistant clinical isolate of *V. parahaemolyticus*, RIMD2210633, was used as the wild-type strain (104, 157). *Vibrio parahaemolyticus* strains were grown in either lysogeny broth (LB) (Fisher Scientific, Fair Lawn, NJ) supplemented with 3% NaCl (wt/vol) (LBS) or in M9 minimal medium (47.8 mM Na<sub>2</sub>HPO<sub>4</sub>, 22 mM KH<sub>2</sub>PO<sub>4</sub>, 18.7 mM NH<sub>4</sub>Cl, 8.6 mM NaCl) (Sigma-Aldrich, USA) supplemented with 2 mM MgSO<sub>4</sub>, 0.1 mM CaCl<sub>2</sub>, 20 mM glucose as the sole carbon source (M9G) and 1% or 3% NaCl (wt/vol) (M9G1%, M9G3%). *E. coli* strains were grown in LB supplemented with 1% NaCl (wt/vol) or M9G1% where indicated. *E. coli*  $\beta$ 2155, a diaminopimelic acid (DAP) auxotroph, was supplemented with 0.3 mM DAP and grown in LB 1% NaCl. All strains were grown at 37°C with aeration. Antibiotics were used at the following concentrations (wt/vol) as necessary: ampicillin (Amp), 50  $\mu$ g/ml; chloramphenicol (Cm), 12.5  $\mu$ g/ml; tetracycline (Tet), 1  $\mu$ g/mL; and streptomycin (Str), 200  $\mu$ g/ml. Choline was added to media at a final concentration of 1 mM, when indicated.

### Construction of the *betI* deletion mutant

An in-frame *betI* (VPA1114) deletion mutant was constructed as described previously (108). Briefly, the Gibson assembly protocol, using NEBuilder HiFi DNA Assembly Master Mix (New England Biolabs, Ipswich, MA), followed by allelic exchange, was used to generate an in-frame 63-bp truncated, non-functional *betI* gene (150, 151). Two fragments, AB and CD, were amplified from the RIMD2210633 genome using primers listed in Table 2. These were ligated with pDS132, which had

been digested with SphI, via Gibson assembly to produce suicide vector pDS132 with a truncated *betI* allele (pDS $\Delta$ *betI*). pDS $\Delta$ *betI* was transformed into *E. coli* strain  $\beta$ 2155  $\lambda$ *pir*, followed by conjugation with *V. parahaemolyticus*. The suicide vector pDS132 must be incorporated into the *V. parahaemolyticus* genome via homologous recombination, as *V. parahaemolyticus* lacks the *pir* gene required for replication of the vector. Growth without chloramphenicol induces a second recombination event which leaves behind either the truncated mutant allele or the wild-type allele. Colonies were plated on sucrose for selection, as pDS132 harbors a *sacB* gene, which makes sucrose toxic to cells still carrying the plasmid and colonies appear soapy. Healthy colonies were screened via PCR and sequenced to confirm an in-frame deletion of the *betI* gene.

#### RNA isolation and qPCR

*Vibrio parahaemolyticus* RIMD2210633 and  $\Delta$ *cosR* were grown with aeration at 37 °C overnight in LBS. Cells were pelleted, washed twice with 1X PBS, diluted 1:50 into M9G3% or M9G1% and grown with aeration to mid-exponential phase (OD<sub>595</sub> 0.45). RNA was extracted from 1 mL of culture using Trizol, following the manufacturer's protocol (Invitrogen, Carlsbad, CA). The samples were treated with Turbo DNase (Invitrogen), followed by heat inactivation of the enzyme as per manufacturer's protocol. Final RNA concentration was quantified using a Nanodrop spectrophotometer (Thermo Scientific, Waltham, MA). 500 ng of RNA were used for cDNA synthesis by priming with random hexamers using SSIV reverse transcriptase (Invitrogen). Synthesized cDNA was diluted 1:25 and used for quantitative real-time PCR (qPCR). qPCR experiments were performed using PowerUp SYBR master mix (Life Technologies, Carlsbad, CA) on an Applied Biosystems QuantStudio6 fast real-

time PCR system (Applied Biosystems, Foster City, CA). Reactions were set up with the following primer pairs listed in Table 2: VPbcct1Fwd/Rev, VPbcct2Fwd/Rev, VPbcct3Fwd/Rev, VPbcct4Fwd/Rev, VPectAFwd/Rev, VPasp\_ectFwd/Rev, VPproV1Fwd/Rev, VPAbetIFwd/Rev, VPAbetBFwd/Rev, VPaproXFwd/Rev, VPaproWFwd/Rev, and 16SFwd/Rev for normalization. Expression levels were quantified using cycle threshold (CT) and were normalized to 16S rRNA. Differences in gene expression were determined using the  $\Delta\Delta$ CT method (172).

#### Protein purification of CosR

CosR was purified as described previously (108). Briefly, full-length *cosR* (VP1906) was cloned into the protein expression vector pET28a (+) containing an IPTG-inducible promoter and a C-terminal 6x-His tag (Novagen). Expression of CosR-His was then induced in *E. coli* BL21 (DE3) with 0.5 mM IPTG at OD<sub>595</sub> of 0.4 and grown overnight at room temperature. Cells were harvested, resuspended in lysis buffer (50 mM NaPO<sub>4</sub>, 200 mM NaCl, 20 mM imidazole buffer [pH 7.4]) and lysed using a microfluidizer. CosR-His was bound to a Ni-NTA column and eluted with 50 mM NaPO<sub>4</sub>, 200 mM NaCl, 500 mM imidazole buffer [pH 7.4] after a series of washes to remove loosely bound protein. Protein purity was determined via SDS-PAGE. OpaR was purified as described previously (107).

#### Electrophoretic Mobility Shift Assay

Five overlapping DNA fragments, designated *PbetI* probe A (125-bp), probe B (112-bp), probe C (142-bp), probe D (202-bp) and probe E (158-bp), were generated from the *betIBaproXWV* regulatory region (includes 36 bp of the coding region and the 594-bp upstream intergenic region) using primer sets listed in Table 2. Three

overlapping DNA fragments, designated *Pbcct1* probe A (120-bp), probe B (110-bp), and probe C (101-bp), were generated from the *bccT1* regulatory region (includes 15 bp of the coding region and the 276-bp upstream intergenic region) using primer sets listed in Table 2. Two overlapping DNA fragments, designated *PbccT3* probe A (108-bp) and probe B (107-bp), were generated from the *bccT3* regulatory region (includes 17 bp of the coding region and 179-bp of the upstream intergenic region) using primer sets listed in Table 2. Four overlapping DNA fragments, designated *PproVI* probe A (160-bp), probe B (134-bp), probe C (108-bp), and probe D (109-bp), were generated from the *proVI* regulatory region (includes 9-bp of the coding region and the 438-bp upstream intergenic region) using primer sets listed in Table 2. Fragments designated *PbccT2* (233-bp) and *PbccT4* (244-bp) were generated from the *bccT2* and *bccT4* regulatory regions, respectively, using primers listed in Table 2. Two overlapping DNA fragments, designated *PcosR* probe A (105-bp) and probe B (142-bp), were generated from the *cosR* regulatory region (includes 4 bp of the coding region and 216-bp of the upstream intergenic region) using primer sets listed in Table 2. The concentration of purified CosR-His and OpaR was determined using a Bradford assay. CosR or OpaR was incubated for 20 minutes with 30 ng of each DNA fragment in a defined binding buffer (10 mM Tris, 150 mM KCl, 0.5 mM dithiothreitol, 0.1 mM EDTA, 5% polyethylene glycol [PEG] [pH 7.9 at 4°C]). A 6% native acrylamide gel was pre-run for 2 hours at 4C (200 V) in 1 X TAE buffer. Gels were loaded with the DNA:protein mixtures (10 µL), and run for 2 hours at 4°C (200 V). Finally, gels were stained in an ethidium bromide bath for 15 min and imaged.

## Reporter Assays

A GFP reporter assay was conducted using the *E. coli* strain MKH13 (94). GFP reporter plasmids were constructed as previously described (108). Briefly, each regulatory region of interest was amplified using primers listed in Table 2 and ligated via Gibson assembly protocol with the promoterless parent vector pRU1064, which had been digested with SpeI, to generate reporter plasmids with GFP under the control of the regulatory region of interest. Complementary regions for Gibson assembly are indicated in lower case letters in the primer sequence (Table 2). Reporter plasmid  $P_{betI-gfp}$  encompasses 594-bp upstream of the *betI**BA**proXWV* operon. Reporter plasmid  $P_{bccT1-gfp}$  encompasses 278-bp upstream of the *PbccT1* regulatory region. Reporter plasmid  $P_{bccT3-gfp}$  encompasses 397-bp upstream of the *PbccT3* regulatory region. Reporter plasmid  $P_{proVI-gfp}$  encompasses 438-bp upstream of the *PproVI* regulatory region. Reporter plasmid  $P_{cosR-gfp}$  encompasses 397-bp upstream of the *PcosR* regulatory region. The full-length *cosR* was then expressed from an IPTG-inducible promoter in the pBBR1MCS expression vector. Relative fluorescence (RFU) and OD<sub>595</sub> were measured; specific fluorescence was calculated by dividing RFU by OD<sub>595</sub>. Strains were grown overnight with aeration at 37°C in LB1% with ampicillin (50 µg/mL) and chloramphenicol (12.5 µg/mL), washed twice with 1X PBS, then diluted 1:1000 in M9G1%. Expression of *cosR* was induced with 0.25 mM IPTG, and strains were grown for 20 hours at 37°C with aeration under antibiotic selection. GFP fluorescence was measured with excitation at 385 and emission at 509 nm in black, clear-bottom 96-well plates on a Tecan Spark microplate reader with Magellan software (Tecan Systems Inc., San Jose, CA). Specific fluorescence was calculated for each sampled by normalizing fluorescence intensity to OD<sub>595</sub>. Two biological replicates were performed for each assay.

A GFP reporter assay was conducted in RIMD2210633 wild-type,  $\Delta betI$ ,  $\Delta opaR$ , or  $\Delta cosR$  mutant strains. The  $P_{betI}$ -*gfp* or  $P_{cosR}$ -*gfp* reporter plasmid was transformed into *E. coli*  $\beta$ 2155  $\lambda$ *pir* and conjugated into wild-type,  $\Delta betI$ ,  $\Delta opaR$ , or  $\Delta cosR$  mutant strains. Strains were grown overnight with aeration at 37°C in LB3% with tetracycline (1  $\mu$ g/mL). Cells were then pelleted, washed two times with 1X PBS, diluted 1:100 into M9G3% and grown for 20 hours with antibiotic selection. Choline was added to a final concentration of 1 mM, where indicated. GFP fluorescence was measured with excitation at 385 and emission at 509 nm in black, clear-bottom 96-well plates on a Tecan Spark microplate reader with Magellan software (Tecan Systems Inc.). Specific fluorescence was calculated for each sample by normalizing fluorescence intensity to OD<sub>595</sub>. Two biological replicates were performed for each assay.

#### Bioinformatics and phylogenetic analyses

Sequences of EMSA probes *PectA* A and B, *PbetI* A, B and D, *PbccT1* B, *PbccT3* A, and *PproV1* D to which CosR bound were input into the MEME (Multiple EM for Motif Elicitation) tool ([meme-suite.org/tools/meme](http://meme-suite.org/tools/meme)) (173). We set the parameters to search for one occurrence of one motif per sequence with a minimum width of 18-bp and a maximum width of 35-bp. The *V. parahaemolyticus* protein CosR (NP\_798285) was used as a seed for BLASTp to identify homologs in the *Vibrionaceae* family in the NCBI database. Sequences of representative strains were downloaded from NCBI and used in a Python-based program Easyfig to visualize gene arrangements (174). Accession numbers for select strains were: *V. parahaemolyticus* RIMD (BA00031), *V. crassotreae* 9CS106 (CP016229), *V. splendidus* BST398 (CP031056), *V. celticus* CECT7224 (NZ\_FLQZ01000088), *V.*

*lentus* 10N.286.51.B9 (NZ\_MCUE01000044), *V. tasmaniensis* LGP32 (FM954973), *V. cyclitrophicus* ECSMB14105 (CO039701), *Aliivibrio fischeri* ES114 (CP000021), *A. fischeri* MJ11 (CP001133), *A. wodanis* AWOD1 (LN554847), *A. wodanis* 06/09/160 (CP039701). The *V. parahaemolyticus* RIMD2201633 CosR and *A. fischeri* ES114 EctR protein sequences were retrieved from NCBI using accession numbers NP\_798285 and AAW88191.1, respectively, and input into the SWISS-MODEL workspace, which generated a 3D model of a homodimer to identify putative ligand-binding pockets (175-179). Evolutionary analysis was performed on the CosR protein from all species within the family *Vibrionaceae* with completed genome sequence and as an outgroup we used CosR from members of the genus *Aeromonas*. Protein sequences were obtained from NCBI database and aligned using the Clustal W algorithm (180). Aligned protein sequences were used to generate a Neighbor-Joining tree with a bootstrap value of 1000 (181, 182). The evolutionary distances were computed using the JTT matrix-based method [3] and are in the units of the number of amino acid substitutions per site (183). The rate variation among sites was modeled with a gamma distribution (shape parameter = 5). This analysis involved 96 amino acid sequences. All ambiguous positions were removed for each sequence pair (pairwise deletion option). There were a total of 173 positions in the final dataset. Evolutionary analyses were conducted in MEGA X (184).

## Results

Compatible solute biosynthesis and transport genes are downregulated in low salinity

We have previously shown that *V. parahaemolyticus* does not produce compatible solutes ectoine and glycine betaine during growth in minimal media

(M9G) supplemented with 1% NaCl (M9G1%) (45, 59). Here we quantified expression levels of both biosynthesis operons in M9G1% or M9G3%. RNA was isolated from exponentially growing wild-type *V. parahaemolyticus* RIMD2210633 cells, at optical density 595 nm (OD<sub>595</sub>) 0.45, after growth in M9G1% or M9G3%. Real time quantitative PCR (qPCR) showed that ectoine biosynthesis genes *ectA* and *asp\_ect* are differentially expressed in M9G1% as compared to expression in M9G3%. *ectA* is significantly downregulated 794.6-fold and *asp\_ect* is significantly downregulated 204.9-fold in M9G1% (**Figure 13A**). The *betIBAprOXWV* operon is also significantly repressed in M9G1%, with fold changes of 25.8-fold, 22-fold, 33.7-fold, and 52.8-fold for *betI*, *betB*, *proX*, and *proW*, respectively (**Figure 13B**).

Similarly, the expression of *bccT1*, *bccT3*, *bccT4*, and *proVI* are significantly repressed in M9G1%, 500-fold, 71.4-fold, 11.6-fold, and 2,786-fold, respectively, when compared with expression in M9G3% (**Figure 13C**). The *bccT2* gene remained unchanged. Previously, we reported that *bccT2* is not induced by salinity (60), and our data indicated that it has a basal level of transcription in the cell based on similar Ct values in both salinities tested (data not shown). Overall, the data demonstrate osmoregulation of *ectABCasp\_ect*, *betIBAprOXWV*, *bccT1*, *bccT3*, *bccT4* and *proVI*.

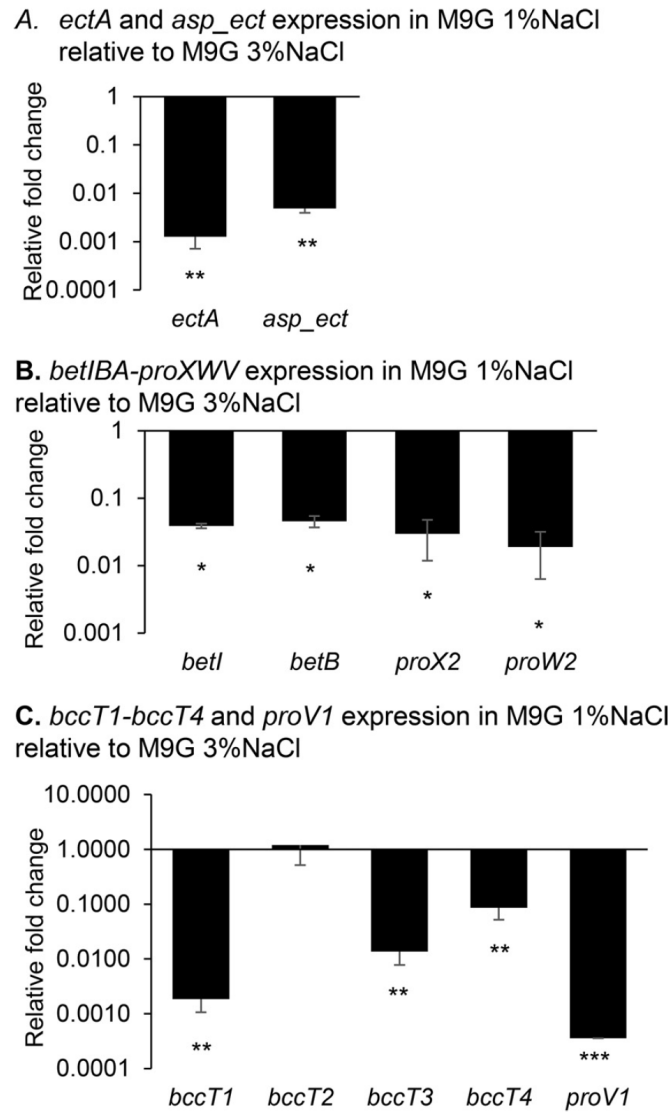
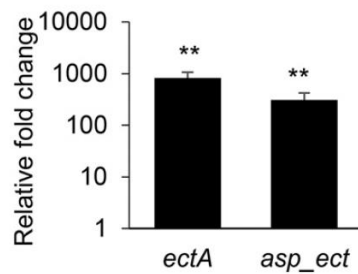


**Figure 13 Expression of osmotic stress response genes is salinity dependent.** RNA was isolated from RIMD2210633 after growth in M9G1%NaCl and M9G3%NaCl at an OD<sub>595</sub> of 0.45. Expression analysis of (A) *ectA*, *asp\_ect*, (B) *betI*, *betB*, *proX2*, *proW2* (C) *bccT1*, *bccT2*, *bccT3*, *bccT4* and *proV1* by quantitative real time PCR (qPCR). 16S was used for normalization. Expression levels shown are levels in M9G1% relative to M9G3%. Mean and standard error of two biological replicates are shown. Statistics were calculated using a Student's t-test (\*, P < 0.05; \*\*, P < 0.01; \*\*\*, P < 0.001).

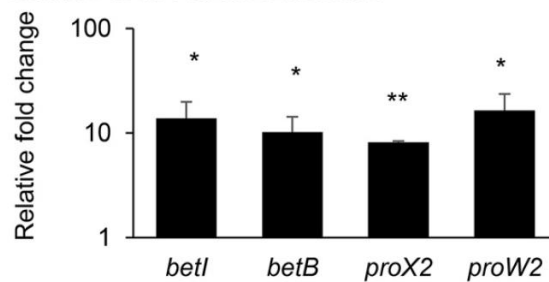
CosR represses compatible solute biosynthesis and transport genes in low salinity

We know CosR is a repressor of ectoine biosynthesis genes, and we wondered whether it played a broader role in the regulation of other osmotic stress response genes. Therefore, we examined expression in wild-type and an in-frame deletion mutant of *cosR*. RNA was isolated from the  $\Delta cosR$  mutant strain at mid-exponential phase (OD<sub>595</sub> 0.45) after growth in M9G1% and compared to wild-type grown under identical conditions. Using qPCR analysis, we determined the expression levels of *ectA* and *asp\_ect* and showed they are significantly upregulated, 818.5-fold and 308.2-fold, respectively, in a  $\Delta cosR$  mutant compared to wild-type in M9G1% (**Figure 14A**), indicating de-repression in the absence of CosR. Next, we examined expression levels of *betIBAprXWV* and showed these genes are significantly de-repressed in the  $\Delta cosR$  mutant (**Figure 14B**). Similarly, relative expression levels of *bccT1*, *bccT3* and *proV1* were significantly higher in  $\Delta cosR$  than wild-type, while levels of *bccT2* and *bccT4* were unchanged (**Figure 14C**). In sum, these data demonstrated that CosR is a repressor of *ectABCasp\_ect*, *betIBAprXWV*, *bccT1*, *bccT3* and *proVWX1* under low salinity conditions. Thus, CosR is a unique example of a regulator that controls multiple compatible solute systems.

**A. Expression of *ectA* and *asp\_ect* in  $\Delta\text{cosR}$  relative to WT in M9G1%NaCl**



**B. Expression of *betIBA-proXWV* in  $\Delta\text{cosR}$  relative to WT in M9G1%NaCl**



**C. Expression of *bccT1-bccT4* and *proV1* in  $\Delta\text{cosR}$  relative to WT in M9G1%NaCl**

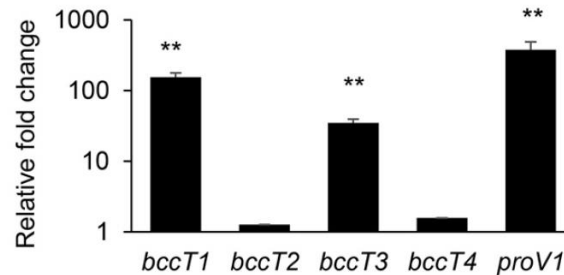


**Figure 14 CosR represses osmotic stress response genes in low salinity.** RNA was isolated from RIMD2210633 and  $\Delta\text{cosR}$  after growth in M9G1%NaCl at an  $\text{OD}_{595}$  of 0.45. Expression analysis of (A) *ectA*, *asp\_ect*, (B) *betI*, *betB*, *proX2*, *proW2* (C) *bccT1*, *bccT2*, *bccT3*, *bccT4* and *proV1* by qPCR. 16S was used for normalization. Expression levels shown are levels in  $\Delta\text{cosR}$  relative to wild-type. Mean and standard error of two biological replicates are shown. Statistics were calculated using a Student's t-test (\*,  $P < 0.05$ ; \*\*,  $P < 0.01$ ).

CosR binds directly to the promoter of the *betIBAprOXWV* operon and represses transcription

To determine whether CosR regulation of *betIBAprOXWV* is direct, we performed DNA binding assays with purified CosR protein and DNA probes of the regulatory region of this operon. The regulatory region was split into five overlapping probes, *PbetI* probes A-E (**Figure 15A**). CosR bound to probe A, which is directly upstream of the start codon for *betI*, and it also bound to probes B and D (**Figure 15B**). CosR did not bind to probes C and E, which demonstrated specificity of CosR binding (**Figure 15B**).

To demonstrate that direct binding by CosR results in transcriptional repression of the *betIBAprOXWV* operon, we performed a GFP-reporter assay in *E. coli* strain MKH13. Full-length *cosR* was expressed from a plasmid (pBBR*cosR*) in the presence of a *gfp*-expressing reporter plasmid under the control of the glycine betaine biosynthesis system regulatory region (*P<sub>betI-gfp</sub>*). Relative fluorescence and OD<sub>595</sub> were measured after overnight growth in M9G1%. Specific fluorescence was calculated by normalizing to OD and compared to specific fluorescence in a strain with an empty expression vector (pBBR1MCS) that also contained the *P<sub>betI-gfp</sub>* reporter plasmid. The activity of the *P<sub>betI-gfp</sub>* reporter was significantly repressed 4.84-fold as compared to the empty vector strain (**Figure 15C**). This indicates that CosR directly represses transcription of the *betIBAprOXWV* genes.

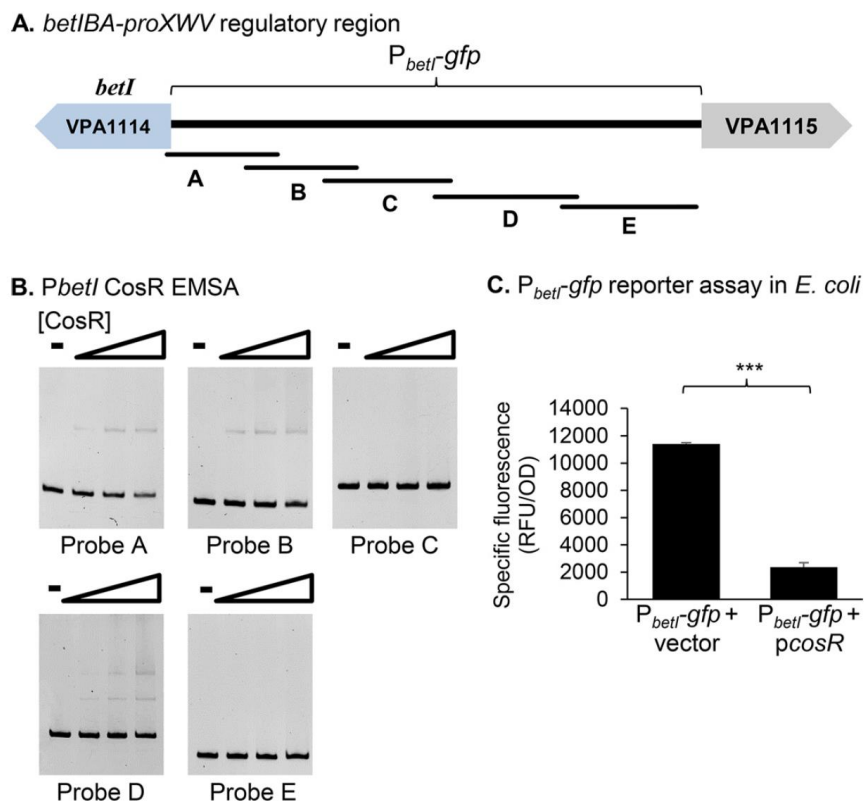


**Figure 15** **CosR binding to *betIBAproXWV* promoter region.** (A) The regulatory region of *betIBAproXWV* was divided into five probes for EMSAs, *PbetI* A-E, 125-bp, 112-bp, 142-bp, 202-bp and 158-bp, respectively. The regulatory region used for the GFP reporter assay is indicated with a bracket. (B) An EMSA was performed with purified CosR-His (0 to 0.62  $\mu$ M) and 30 ng of each *PbetI* probe, with DNA:protein molar ratios of 1:0, 1:1, 1:5, and 1:10. (C) A *PbetI-gfp* reporter assay was performed in *E. coli* strain MKH13 containing an expression plasmid with full-length *cosR* (*pcosR*). Specific fluorescence of the CosR-expressing strain was compared to a strain harboring empty expression vector. Mean and standard deviation of two biological replicates are shown. Statistics were calculated using a Student's t-test (\*\*\*,  $P < 0.001$ ).

CosR binds directly to the promoter of *bccT1* and *bccT3* and is a direct repressor of *bccT3*

Next, we wanted to investigate whether CosR repression of *bccT1* and *bccT3* was direct. We designed probes upstream of the translational start for *bccT1* and *bccT3*. The 291-bp regulatory region of *PbccT1*, which includes 15-bp of *bccT1* and 276-bp of the intergenic region, was split into three overlapping probes, *PbccT1* probes A, B, and C (**Figure 16A**). DNA binding assays were performed with increasing concentrations of CosR. CosR bound directly to the *PbccT1* probe B but did not bind to the other probes tested, which indicated direct and specific binding by CosR (**Figure 16B**). Next, we performed reporter assays in *E. coli* using a GFP expression plasmid under the control of the regulatory region of *bccT1* (*PbccT1-gfp*) and a CosR expression plasmid (pBBR*cosR*). Specific fluorescence in the presence of CosR was compared to a strain with empty expression vector (pBBR1MCS). The activity of the *PbccT1-gfp* reporter was not significantly different than the strain harboring empty expression vector, which indicates that CosR does not directly repress *bccT1* (**Figure 16C**). We speculate that CosR may still directly repress *bccT1*, but in our reporter assay the low level of activation of the *bccT1* regulatory region in *E. coli* may have affected the significance of the results. In the *E. coli* heterologous background, additional proteins, which are present in the native species, may be necessary for full repression of *bccT1* by CosR.

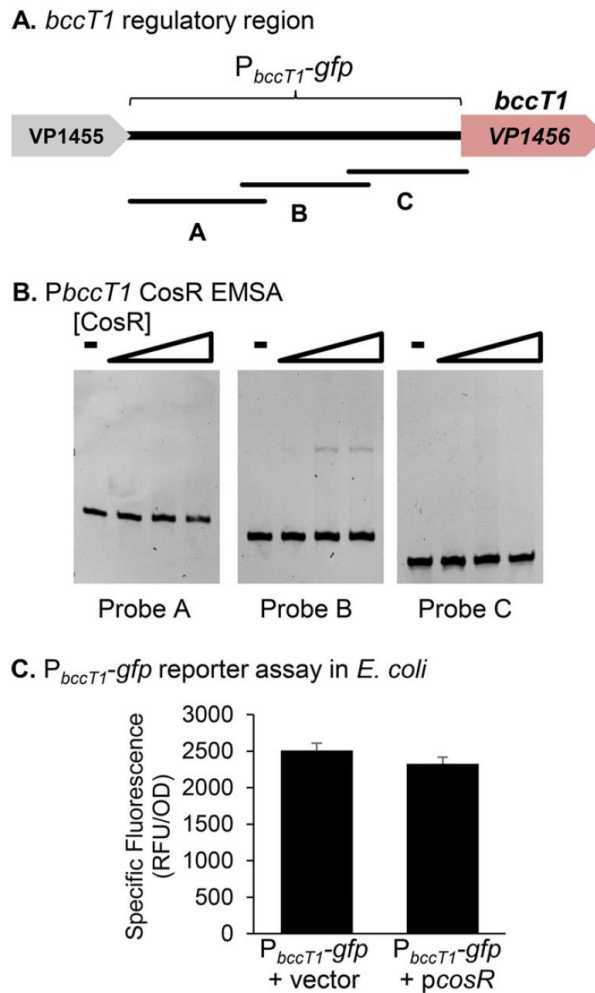


**Figure 16 CosR binds to *bccT1* promoter region.** (A) The regulatory region of *bccT1* was divided into three similarly sized probes for EMSAs, *P<sub>bccT1</sub>* A-C, 120-bp, 110-bp, and 101-bp, respectively. The regulatory region used for the GFP reporter assay is indicated with a bracket. (B) An EMSA was performed with purified CosR-His (0 to 0.69  $\mu$ M) and 30 ng of *P<sub>bccT1</sub>* probe with DNA:protein molar ratios of 1:0, 1:1, 1:5, and 1:10. (C) A *P<sub>bccT1-gfp</sub>* reporter assay was performed in *E. coli* strain MKH13 containing an expression plasmid with full-length *cosR* (*pcosR*). Specific fluorescence of the CosR-expressing strain was compared to a strain harboring empty expression vector (pBBR1MCS). Mean and standard deviation of two biological replicates are shown. Statistics were calculated using a Student's t-test (\*\*,  $P < 0.01$ ).

Two overlapping probes designated *PbccT3* probe A and B, were designed encompassing 196-bp of the regulatory region of *bccT3* (**Figure 17A**). Because *bccT3* is divergently transcribed from *cosR*, we used approximately half of the regulatory region for the *PbccT3* EMSA. An EMSA showed that CosR bound directly to the *PbccT3* probe A, which is proximal to the start of the gene, but not probe B (**Figure 17B**). We then performed reporter assays in *E. coli* using a GFP expression plasmid under the control of the regulatory region of *bccT3*, utilizing the entire 397-bp intergenic region between *bccT3* and *cosR*. Transcriptional activity of the *P<sub>bccT3</sub>-gfp* reporter is repressed in a CosR-expressing strain (**Figure 17C**), although not to the same extent that we saw in expression analyses in *V. parahaemolyticus*. This is not surprising, given that it appears the regulatory region of *bccT3* is not very active in an *E. coli* background, which made detection of repression more difficult. Additionally, other proteins are likely necessary for full repression of the regulatory region of *bccT3* that are not present in an *E. coli* background. The *E. coli* GFP assay did show a direct interaction between CosR and the *bccT3* regulatory region that resulted in repression of transcription. This result, in combination with expression analyses in a *cosR* mutant (**Figure 14C**) and binding assays which demonstrated direct binding (**Figure 17B**), indicate that CosR directly represses *bccT3*. In addition, we showed that CosR does not bind to the regulatory region of *bccT2* and *bccT4* (**Figure 17D and 17E**), which is in agreement with the *cosR* mutant expression data (**Figure 14C**). These data suggest that *bccT2* and *bccT4* are under the control of a yet to be described regulator.

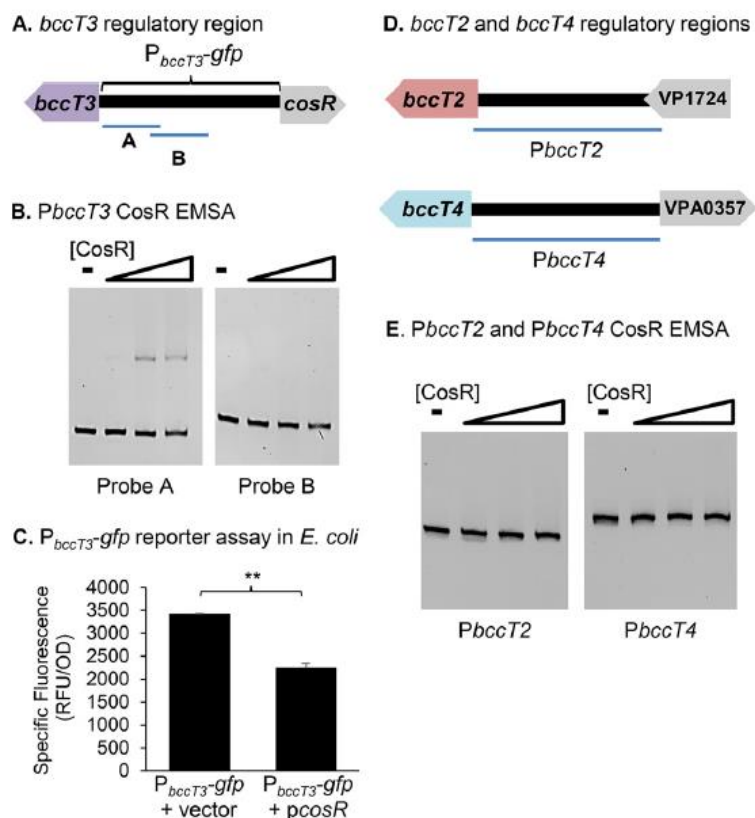


**Figure 17 CosR binds to *bccT3* promoter region.**

(A) A 196-bp portion of the regulatory region of *bccT3* was split into two probes for EMSAs, *P<sub>bccT3</sub>* A and B, 108-bp and 107-bp, respectively. The regulatory region used for the GFP reporter assay is indicated with a bracket. (B) An EMSA was performed with purified CosR-His (0 to 0.65 μM) and 30 ng of *P<sub>bccT3</sub>* probe with DNA:protein molar ratios of 1:0, 1:1, 1:5, and 1:10. (C) *P<sub>bccT3</sub>-gfp* reporter assay was performed in *E. coli* strain MKH13 containing an expression plasmid with full-length *cosR* (*pcosR*). Specific fluorescence of the CosR-expressing strain was compared to a strain harboring empty expression vector (pBBR1MCS). Mean and standard deviation of two biological replicates are shown. Statistics were calculated using a Student's t-test (\*\*, P < 0.01). (D) Diagrams indicating the regulatory regions of *bccT2* and *bccT4* that were used as probes in a CosR EMSA. (E) An EMSA was performed with CosR-His (0 to 0.18 μM) and probes of the regulatory regions of *bccT2* and *bccT4*. Each lane contains 30 ng of DNA and DNA:protein molar ratios of 1:0, 1:1, 1:5, and 1:10.

### CosR is a direct repressor of *proVWXI*

The regulatory region upstream of the *proVI* gene was divided into four probes (**Figure 18A**). A DNA binding assay was performed with increasing concentrations of CosR and 30 ng of each probe. A shift in the DNA bands of probe D, which is proximal to the start codon of *proVI*, indicated that CosR binds directly to this region (**Figure 18B**). CosR did not bind to the other probes tested, which indicated that CosR binding is specific.

We also performed a reporter assay in *E. coli* utilizing the *cosR* expression plasmid (pBBRcosR) and a GFP reporter plasmid ( $P_{proVI-gfp}$ ). In a CosR-expressing strain, expression of the  $P_{proVI-gfp}$  reporter was repressed when compared to an empty expression vector strain (**Figure 18C**). This repression was to a lesser extent than is seen in *V. parahaemolyticus* but recapitulation of the same magnitude of repression in the heterologous background is not to be expected given the potential absence of additional factors present in the native background. Overall, the results of the *E. coli* reporter assay, taken together with expression analyses in the native background (**Figure 14C**) and the DNA binding assay (**Figure 18B**), indicate that CosR is a direct repressor of the *proVWXI* operon.

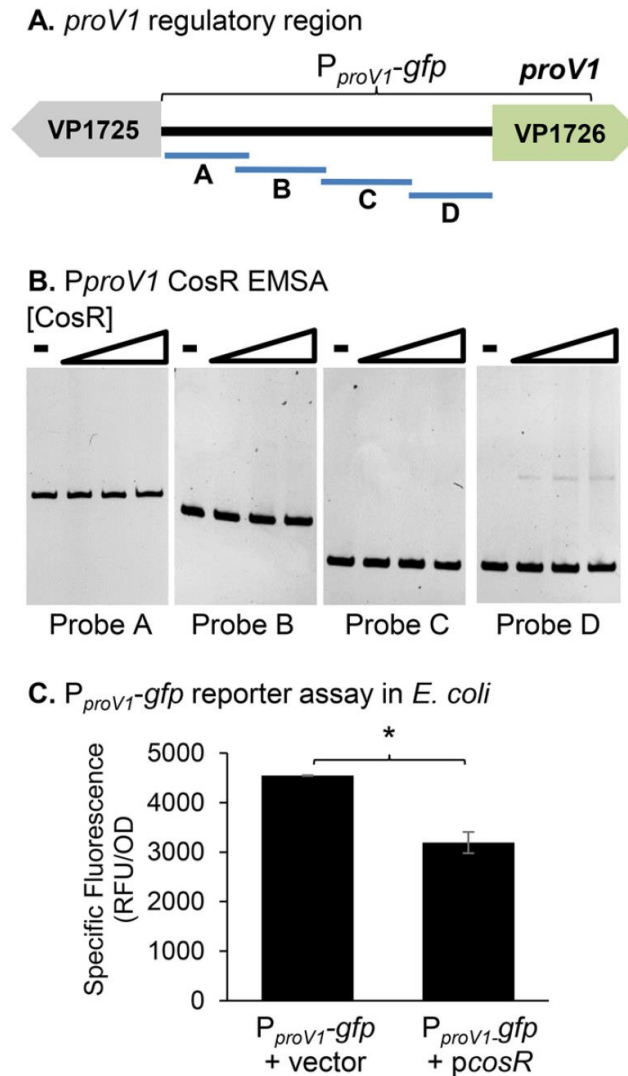


**Figure 18 CosR bind to *proVWX* promoter region.** (A) The 447-bp regulatory region of the *proV1* gene was divided into four probes for EMSAs,  $P_{proV1}$  A-D, 160-bp, 134-bp, 108-bp and 109-bp, respectively. The regulatory region used for the GFP reporter assay is indicated with a bracket. (B) An EMSA was performed with purified CosR-His (0 to 0.64  $\mu$ M) and 30 ng of each  $P_{proV1}$  probe with DNA:protein molar ratios of 1:0, 1:1, 1:5, and 1:10. (C) A reporter assay was conducted in *E. coli* MKH13 harboring the  $P_{proV1-gfp}$  reporter plasmid and the expression plasmid *pcosR*. Specific fluorescence of the CosR-expressing strain was compared to an empty vector strain. Mean and standard deviation of two biological replicates are shown. Statistics were calculated using a Student's t-test (\*,  $P < 0.05$ ).

## CosR is not autoregulated

In *V. cholerae*, expression levels of *cosR* were upregulated in 0.5 M NaCl as compared to levels in 0.2 M NaCl (109). It was suggested that one reason for the upregulation of *cosR* in higher salinity could be that it is involved in an autoregulatory feedback loop (109). In *V. parahaemolyticus*, we found that levels of *cosR* were not significantly upregulated in 3% NaCl as compared to 1% NaCl (data not shown). We have already shown that CosR binds to the intergenic region between *bccT3* and *cosR*, but the binding site location is proximal to the start codon of *bccT3*, more than 300-bp upstream of the *cosR* gene (**Figure 17A & 17B**). Therefore, to investigate CosR autoregulation, we designed two probes, 105-bp and 142-bp, which comprise a 220-bp portion of the regulatory region upstream of *cosR* (VP1906) (**Figure 19A**) and used this in a DNA binding assay with various concentrations of purified CosR (**Figure 19B**). There were no shifts observed in the binding assay, which indicated that CosR does not bind (**Figure 19B**). We then performed a GFP reporter assay in *E. coli*, utilizing the entire 397-bp intergenic region between *bccT3* and *cosR*, to determine if CosR directly represses transcription of its own gene. The transcriptional activity of  $P_{cosR-gfp}$  in the presence of CosR was not significantly different from the empty-vector strain ( $p=0.09$ ) (**Figure 19C**). Because we cannot assess expression of *cosR* in a  $\Delta cosR$  mutant, we examined this in a GFP reporter assay in wild-type and a  $\Delta cosR$  mutant after growth in M9G1%. We found that the activity of a  $P_{cosR-gfp}$  reporter was not different between wild-type and the *cosR* mutant (**Figure 19D**). Taken together, lack of CosR binding in the EMSA and both *in vivo* and *E. coli* reporter assays lead us to conclude that under these conditions, CosR does not autoregulate, and that the CosR binding site proximal to the *bccT3* gene does not affect transcription of the *cosR* gene.

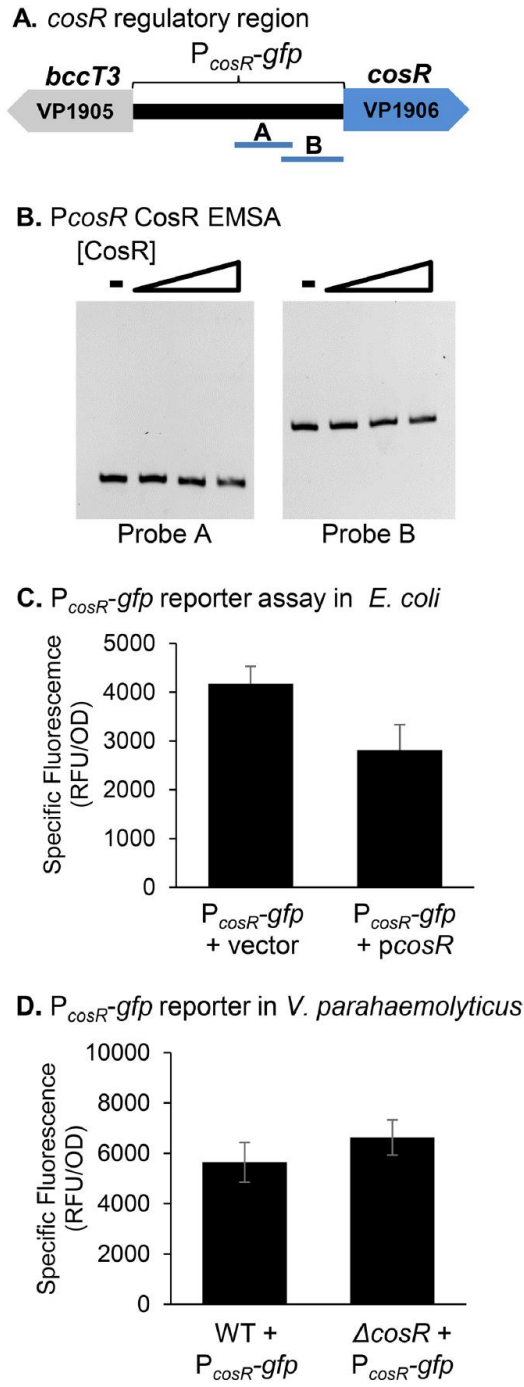


**Figure 19** CosR does not autoregulate.

(A) A 220-bp section of the regulatory region of *cosR* was split into two similarly sized probes for EMSAs, *PcosR* A and B, 105-bp and 142-bp, respectively. The regulatory region used for the GFP reporter assay is indicated with a bracket. (B) An EMSA was performed with increasing concentrations of purified CosR-His (0 to 0.66  $\mu$ M) and 30 ng of each probe with DNA:protein molar ratios of 1:0, 1:1, 1:5, and 1:10. (C) A *PcosR-gfp* reporter assay was performed in *E. coli* strain MKH13 the *pcosR* expression plasmid. Specific fluorescence of the CosR-expressing strain was compared to a strain harboring empty expression vector. Mean and standard deviation of two biological replicates are shown. (D) A *PcosR-gfp* reporter assay was performed in *V. parahaemolyticus* WT and  $\Delta$ *cosR* mutant strains. Mean and standard deviation of three biological replicates are shown.

### BetI represses its own operon *betIBA*

Previously, it was shown that BetI represses its own operon in several bacterial species and this repression is relieved in the presence of choline (55, 62, 115). To demonstrate BetI regulates its own operon in *V. parahaemolyticus*, we performed a reporter assay utilizing the *PbetI-gfp* reporter in wild-type and a  $\Delta$ *betI* mutant strain. Strains were grown overnight in M9G3%, with and without choline, and specific fluorescence was calculated. Expression of the reporter was de-repressed in the  $\Delta$ *betI* mutant when no choline was present, indicating that BetI is a negative regulator of its own operon (**Figure 20A**). In the presence of choline, there was no longer a difference in reporter activity between the wild-type strain and the  $\Delta$ *betI* mutant strain, indicating that repression by BetI was relieved (**Figure 20B**). To confirm regulation of *betIB* *proXWV* by BetI is direct, we performed a GFP reporter assay in *E. coli* MKH13 strain. The *PbetI-gfp* reporter was transformed into *E. coli* MKH13 (which lacks the *betIBA* operon) along with an expression vector harboring full-length *betI* under the control of an IPTG-inducible promoter. In the BetI-expressing strain, *PbetI*-

*gfp* expression was significantly repressed, which indicated that BetI is a direct repressor of its own operon in *V. parahaemolyticus* (**Figure 20C**).

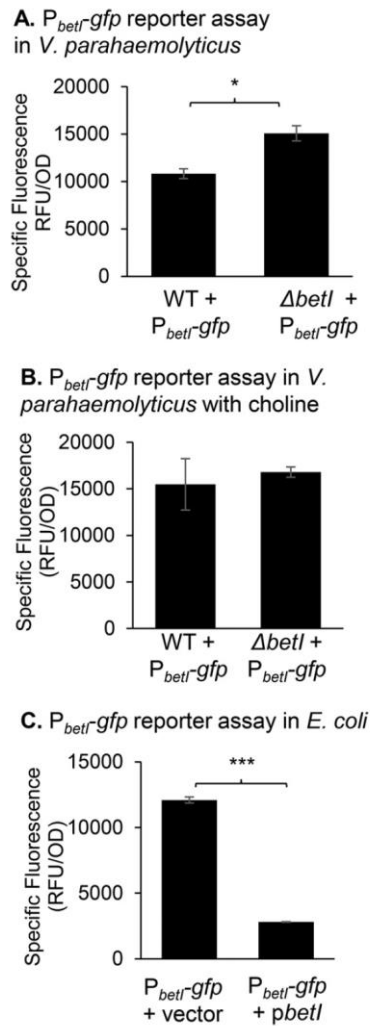
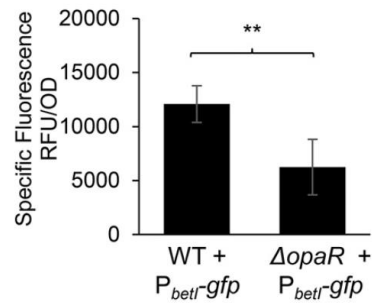


**Figure 20 BetI autoregulates in *V. parahaemolyticus*.** (A) Expression of a  $P_{betI-gfp}$  transcriptional fusion reporter in wild-type and a  $\Delta betI$  mutant. Relative fluorescence intensity (RFU) and  $OD_{595}$  were measured after growth in (A) M9G3% or (B) M9G3% with the addition of choline. Specific fluorescence was calculated by dividing RFU by OD. Mean and standard deviation of two biological replicates are shown. Statistics were calculated using a Student's t-test (\*,  $P < 0.05$ ). (C) A reporter assay was conducted in *E. coli* MKH13 using the  $P_{betI-gfp}$  reporter plasmid and an expression plasmid with full-length  $betI$  ( $pbetI$ ). The specific fluorescence was calculated and compared to a strain with an empty expression vector (pBBR1MCS). Mean and standard deviation of two biological replicates are shown. Statistics were calculated using a Student's t-test (\*\*\*,  $P < 0.001$ ).

The quorum sensing LuxR homolog OpaR is a positive regulator of *betIBAprXWV* in *V. parahaemolyticus*

We examined expression of the  $P_{betI-gfp}$  reporter in wild-type and the  $\Delta opaR$  mutant in *V. parahaemolyticus*. Expression of the reporter was significantly down-regulated in  $\Delta opaR$ , indicating that OpaR is a positive regulator of the glycine betaine biosynthesis operon (**Figure 21A**). We also examined whether regulation of *PbetI* by OpaR was direct utilizing an EMSA with purified OpaR protein. OpaR bound to *PbetI* probes A, B, C and E, and very weakly to probe D, which indicated that regulation of *betIBAprXWV* by OpaR is direct (**Figure 21B**). These results are in agreement with a previous study, which also showed direct positive regulation of *betIBAprVWX* by LuxR in *V. harveyi* (62). Thus, it appears that the quorum sensing master regulator may be a conserved regulatory mechanism of glycine betaine biosynthesis among *Vibrio* species.

**A.**  $P_{betI}$ -*gfp* reporter assay in *V. parahaemolyticus*



**B.** *PbetI* OpaR EMSA

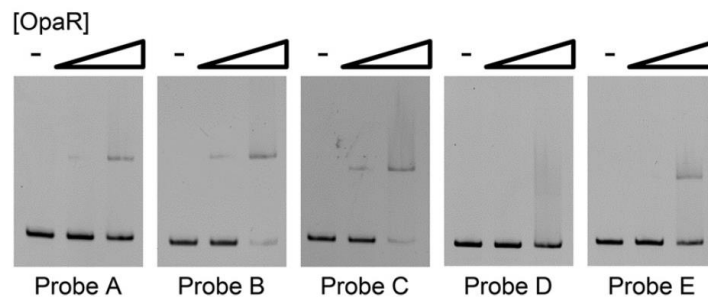


**Figure 21 OpaR binds to *betI* *AProXWV* promoter region.**

(A) Expression of a  $P_{betI}$ -*gfp* transcriptional fusion reporter in wild-type and  $\Delta opaR$  mutant strains. Relative fluorescence intensity (RFU) and  $OD_{595}$  were measured after growth in M9G3%. Specific fluorescence was calculated by dividing RFU by OD. Mean and standard deviation of two biological replicates are shown. Statistics were calculated using a one-way ANOVA with a Tukey-Kramer *post hoc* test (\*\*,  $P < 0.01$ ). (B) An EMSA was performed with 30 ng of each *PbetI* probe A-E utilized previously in the CosR EMSA and purified OpaR protein (0 to 0.41  $\mu$ M) in various DNA:protein molar ratios (1:0, 1:1, and 1:5 for probe A; 1:0, 1:1, 1:10 for all other probes).

Motif identification and phylogenetic distribution of CosR

CosR bound to eight of the probes tested in our DNA binding analyses, including two probes of the *ectABCasp\_ect* regulatory region, as shown previously (108). We utilized these sequences in MEME (multiple EM for motif elicitation) analysis (173), and identified a 24-bp pseudo-palindromic motif present in each of the



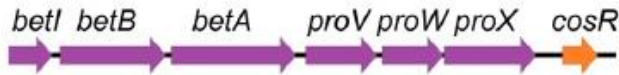
*splendidus*, *V. crassostreae*, *V. cyclitrophicus*, *V. celticus*, *V. lentus* and *Aliivibrio wodanis*, the CosR homolog is present directly downstream of the *betIBAprOXWV* operon and in *V. tasmaniensis* strains and *Vibrio sp.* MED222, the ectoine biosynthesis operon clustered in the same genome location (**Figure 23**). Collectively, these data indicated that CosR function is conserved among this divergent group of species and that CosR is an important regulator of the osmotic stress response. In all strains of *Aliivibrio fischeri*, the *cosR* homolog (which shares 73% amino acid identity with CosR from *V. parahaemolyticus*) clusters with two uncharacterized transporters. A recent phylogenomics study of distribution of ectoine biosynthesis genes and a homolog of CosR showed the presence of this regulator in species of the *Alpha-Proteobacteria*, *Beta-Proteobacteria* and *Gamma-Proteobacteria* (34). This again suggests that the role of CosR in the osmotic stress response is conserved and phylogenetically widespread.

Incidentally, a second MarR-type regulator, a 141 amino acid protein, which we name *ectR*, clusters with the ectoine biosynthesis genes in *Aliivibrio fischeri* (**Figure 23**). EctR shares only 31% identity with less than 60% query coverage to CosR from *V. parahaemolyticus* and a similar level of low amino acid identity to EctR1 from *Methylmicrobium alcaliphilum*. EctR was clustered with the *ectABCasp\_ect* genes in all strains of *Aliivibrio finisterrensis*, *Aliivibrio sifiae*, and most *A. wodanis* strains. Thus, in *Aliivibrio* species, it appears that the ectoine biosynthesis gene cluster has a new uncharacterized MarR-type regulator.

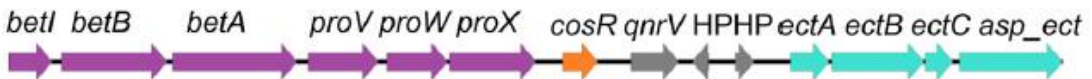
***Vibrio parahaemolyticus* and more than 50 *Vibrio* species**



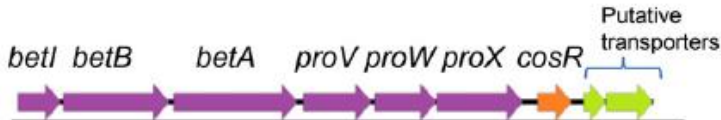
***V. cyclitrophicus/V. splendidus/V. crassotreae/V. lentus/V. celticus***



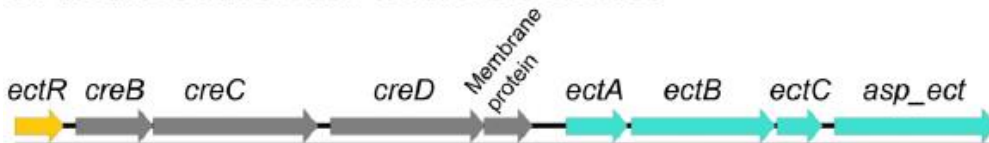
***Vibrio tasmaniensis/Vibrio sp. MED222***



***A. wodanis* AWOD1/*A. wodanis* 06/09/160**



***A. wodanis* AWOD1/*A. wodanis* 06/09/160**



***A. fischeri* MJ11/*A. fischeri* ES114**

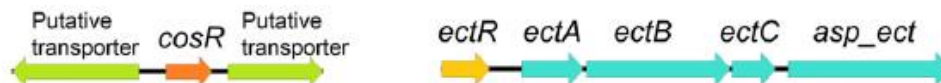


**Figure 23 Genomic context of CosR in Vibrionaceae species.**  
Schematic of the genomic context of CosR homologs from select *Vibrionaceae* species. Open reading frames are designated by arrows.

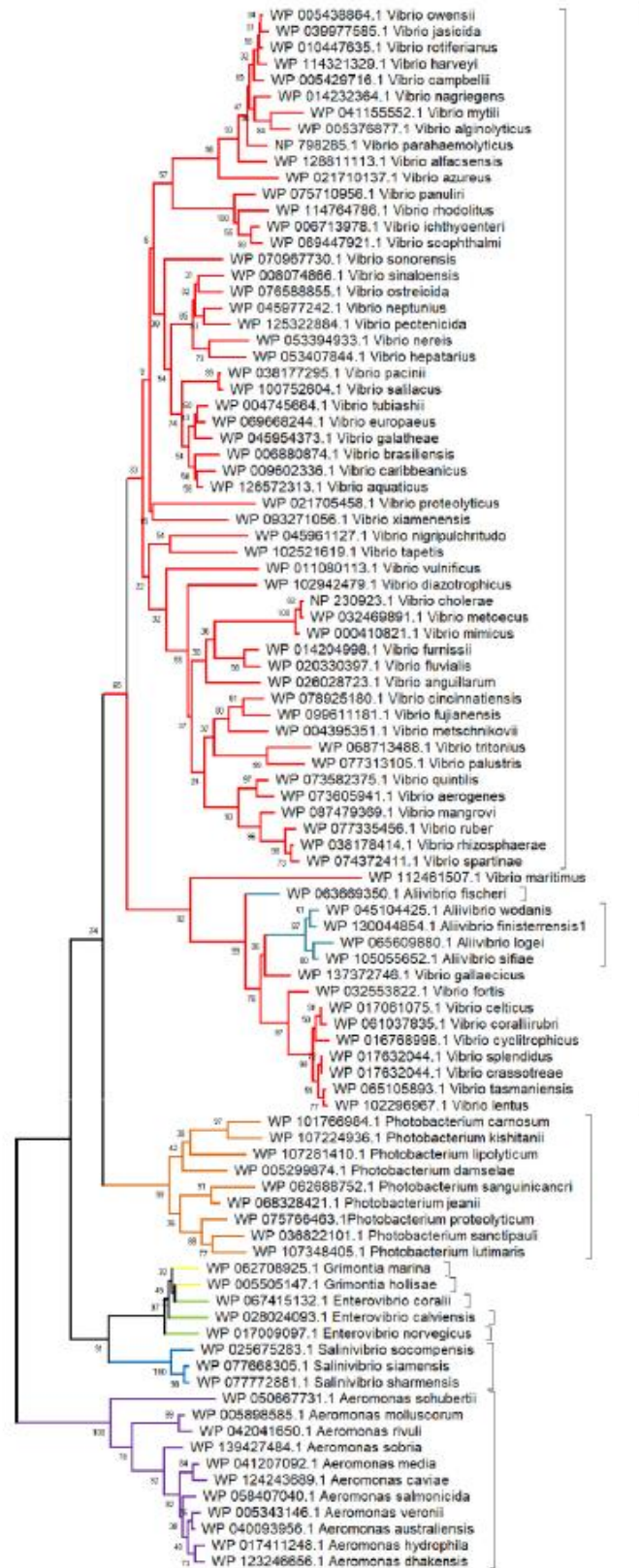


**Figure 24 Phylogenetic analysis of CosR distribution.**

The phylogeny of CosR was inferred using the Neighbor-Joining method. The optimal tree with the sum of branch length = 5.19649696 is shown. The percentage of replicate trees in which the associated taxa clustered together in the bootstrap test (1000 replicates) are shown next to the branches. The tree is drawn to scale, with branch lengths in the same units as those of the evolutionary distances used to infer the phylogenetic tree. Brackets represent groups based on genus.

### Discussion

Here we have shown that the compatible solute biosynthesis and transport genes are downregulated in *V. parahaemolyticus* in low salinity and these genes are de-repressed in a *cosR* mutant. Our genetic analyses, binding analyses, and reporter assays demonstrated that CosR is a regulator of *betI**B**A**proXWV*, *bccT1*, *bccT3*, and *proVWX* (**Figure 25**). Additionally, we showed that under the conditions tested, CosR is not autoregulated. To date, it has now been demonstrated that CosR is a regulator of six different compatible solute systems; two biosynthesis systems ectoine and glycine betaine and four transporters (**Figure 25**). Our phylogenetic and bioinformatics analyses indicated that CosR is universal within the *Vibrionaceae* and widespread in *Gamma-Proteobacteria* in general suggesting a conserved previously unrecognized global regulator of the osmotic stress response in bacteria.

The physiological importance of CosR repression of compatible solute biosynthesis in low salinity is to protect levels of key intracellular metabolites. Ectoine biosynthesis requires the precursor aspartate and this affects the level of glutamate, acetyl-CoA, and oxaloacetate (185, 186). Thus, tight regulation of ectoine biosynthesis is essential for cellular fitness. CosR characterized from *Vibrio* species show ~50% amino acid identity to EctR1 first described in the halotolerant methanotroph *Methylmicrobium alcaliphilum* that repressed ectoine biosynthesis (110). In this

species, *ectRI* is divergently transcribed from the same promoter as *ectABC-ask*. Mustakhimov and colleagues showed that EctR1 repressed expression of the *ectABC-ask* operon in response to low salinity (110). Purified EctR1 bound specifically to the promoter of *ectABC-ask*, indicating direct regulation by EctR1 (110). EctR repression of the ectoine biosynthesis genes was also shown in both *Methylophaga alcalica* and *Methylophaga thalassica*, two moderately halophilic methylotrophs (187, 188). Czech and colleagues showed that CosR/EctR1 was phylogenetically widespread and clustered with *ect* genes in some species (34). In *V. cholerae*, CosR was also identified as a repressor of ectoine biosynthesis genes though it does not cluster with *ectABCasp\_ect* (109). The *cosR* gene in *V. cholerae* is divergently transcribed from the *opuD* gene (a *bccT3* homolog), which was also repressed by CosR (109). Similarly, in *V. parahaemolyticus*, the *cosR* (VP1906) homolog is divergently transcribed from *bccT3* (VP1905) and is a direct negative regulator of both *bccT3* and *ectABCasp\_ect* (108). Our phylogenetic analysis found that the CosR homolog was present in all members of the *Vibrionaceae*, and among many *Vibrio* species was clustered with a *bccT3* homolog. The phylogeny of CosR mirrored the branching pattern of the relationships of members of the group for other housekeeping genes. These data indicate that CosR is ancestral to the group and the conservation of genomic context suggests functional conservation (**Figure 23 and Figure 24**). We used CosR from *Aeromonas* species to root the tree and similar to *Vibrionaceae* species, CosR is present in all members of this group. Indeed, bioinformatics analysis indicated that a CosR homolog is present in many other *Gamma-Proteobacteria* suggesting that it is an unrecognized player in the osmotic stress response in bacteria (data not shown). In several *Vibrio* species, the CosR homolog was clustered with the

*betIB**proXWV* operon, which is further suggestive of its role in regulation of compatible solute biosynthesis among *Vibrio* species.

The MarR family of transcriptional regulators, first characterized in *E. coli*, are important regulators of a number of cellular responses, typically responding to a change in the external environment (189-191). The literature suggests that MarR-type regulators form dimers and bind to a 20-45 bp pseudo-palindromic site in the intergenic region of genes they control (189, 192-194). We utilized the regulatory regions of each of the osmotic stress response genes that CosR regulates and identified a pseudo-palindromic CosR DNA binding motif (**Figure 22**). This motif is similar to the binding sequence of the CosR homolog EctR1 identified previously in *M. alcaliphilum*, which was also pseudo-palindromic with 2 bp separating inverted repeats (110). The activity of MarR-type regulators can be modulated by the presence of a chemical signal, either a ligand, metal ion, or reactive oxygen species. Binding of these signals causes the protein to undergo a conformational change, thereby affecting DNA binding capability (189, 195, 196). We modeled a CosR homodimer using SWISS-MODEL and did not identify a ligand binding pocket (data not shown). In *V. cholerae*, CosR activity was not affected by the presence of exogenous compatible solutes including ectoine, glycine betaine and proline, and *opuD* (*bccT* homolog) transcripts were unchanged in a *cosR* mutant (34). Hence, the environmental or cellular signals that modulate the activity of CosR remain unidentified, as was noted by Czech and colleagues (34). Interestingly, our modelling of the EctR regulator clustered with ectoine genes identified in *Aliivibrio* species indicated it also does not have a ligand-binding pocket (data not shown). Autoregulation was shown for several MarR family regulators, including *ectR1* in *M. alcaliphilum* (110, 189). In *V.*

*parahaemolyticus* we showed CosR does not bind to its own regulatory region, and our reporter assays suggested that CosR does not autoregulate. It is interesting to note that EctR1 does not participate in an autoregulatory feedback loop in *M. thalassica* (188, 197).

Similar to ectoine biosynthesis gene expression, few direct regulators of glycine betaine biosynthesis genes have been identified. In *E. coli*, expression of *betIBA* was repressed by BetI and repression was relieved in the presence of choline (55). BetI was shown to directly regulate transcription at this locus via DNA binding assays (56). ArcA was shown to repress the *betIBA* operon under anaerobic conditions in *E. coli*, although direct binding was not shown (55). In *V. harveyi*, it was shown that *betIBAprWXWV* were repressed 2- to 3-fold when *betI* was overexpressed from a plasmid. Purified BetI bound directly to the regulatory region of the *betIBAprWXWV* operon in DNA binding assays (62, 111). In these studies, it was also shown that the quorum sensing response regulator LuxR, along with the global regulator IHF, activated expression of *betIBAprWXWV* (62, 111). Here, we have shown that BetI represses its own operon in *V. parahaemolyticus*, as expected, and we identified a novel regulator of glycine betaine biosynthesis genes, CosR, which directly represses under low salinity conditions (**Figure 25**). We also confirm that, similar to *V. harveyi*, the quorum sensing master regulator OpaR directly induced *betIBAprWXWV* expression in *V. parahaemolyticus*, indicating this mechanism is likely conserved in *Vibrio* species (**Figure 25**).

Biosynthesis of compatible solutes is an energetically costly process for bacteria (75). *V. parahaemolyticus* does not accumulate compatible solutes in low salinity (45, 59, 60), and therefore the transcription of biosynthesis and transport genes

is unnecessary. CosR represses these genes involved in the osmotic stress response in *V. parahaemolyticus*. The high conservation of the CosR protein across *Vibrionaceae* and *Gamma-Proteobacteria* and its genomic context indicates that regulation by CosR of compatible solute systems is widespread in bacteria.

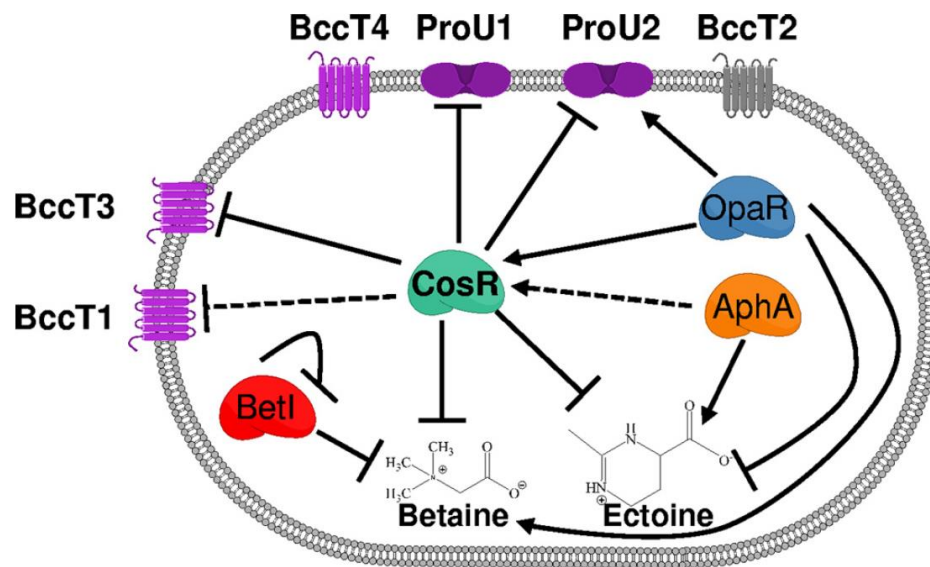


**Figure 25** A model of CosR regulation of the osmotic stress response. Solid arrows indicate direct positive regulation, dashed arrows, indirect positive regulation, solid hammers represent direct repression and dashed hammers, indirect repression. Transporters colored purple are osmotic responsive. The quorum sensing regulators OpaR and AphA were shown in previous studies to directly and indirectly positively regulate CosR, respectively, and in addition, directly regulate ectoine and glycine betaine biosynthesis operons.

Table 4 Strains and plasmids used in this study

Strain	Genotype or description	Reference or Source
<i>Vibrio</i>		
<i>parahaemolyticus</i>		
RIMD2210633	O3:K6 clinical isolate, Str <sup>r</sup>	(104, 157)
$\Delta$ <i>cosR</i>	RIMD2210633 $\Delta$ <i>cosR</i> (VP1906), Str <sup>r</sup>	(108)
$\Delta$ <i>betI</i>	RIMD2210633 $\Delta$ <i>betI</i> (VPA1114), Str <sup>r</sup>	This study
SSK2516 ( $\Delta$ <i>opaR</i> )	RIMD2210633 $\Delta$ <i>opaR</i> (VP2516), Str <sup>r</sup>	(107)
<i>Escherichia coli</i>		
DH5 $\alpha$ $\lambda$ <i>pir</i>	$\Delta$ <i>lac pir</i>	ThermoFisher Scientific
$\beta$ 2155 $\lambda$ <i>pir</i>	$\Delta$ <i>dapA::erm pir</i> for bacterial conjugation	(163)
BL21(DE3)	Expression strain	ThermoFisher Scientific
MKH13	MC4100 ( $\Delta$ <i>betTIBA</i> ) $\Delta$ ( <i>putPA</i> )101 $\Delta$ ( <i>proP</i> )2 $\Delta$ ( <i>proU</i> ); Sp <sup>r</sup>	(94)
<b>Plasmids</b>		
pDS132	Suicide plasmid; Cm <sup>R</sup> Cm <sup>r</sup> ; SacB	(164)
pBBR1MCS	Expression vector; <i>lacZ</i> promoter; Cm <sup>r</sup>	(165)
pBBR <i>cosR</i>	pBBR1MCS harboring full-length <i>cosR</i> (VP1906)	(108)
pRU1064	promoterless- <i>gfpUV</i> , Amp <sup>r</sup> , Tet <sup>r</sup> , IncP origin	(153)
pRU <i>PectA</i>	pRU1064 with <i>PectA-gfp</i> , Amp <sup>r</sup> , Tet <sup>r</sup>	(108)
pRU <i>PbetI</i>	pRU1064 with <i>PbetI-gfp</i> , Amp <sup>r</sup> , Tet <sup>r</sup>	This study
pRU <i>PbccT1</i>	pRU1064 with <i>PbccT1-gfp</i> , Amp <sup>r</sup> , Tet <sup>r</sup>	This study
pRU <i>PbccT3</i>	pRU1064 with <i>PbccT3-gfp</i> , Amp <sup>r</sup> , Tet <sup>r</sup>	This study
pRU <i>proV1</i>	pRU1064 with <i>PproV-gfp</i> , Amp <sup>r</sup> , Tet <sup>r</sup>	This study
pRU <i>cosR</i>	pRU1064 with <i>PcosR-gfp</i> , Amp <sup>r</sup> , Tet <sup>r</sup>	(108)
pET28a+	Expression vector, 6xHis; Kan <sup>r</sup>	Novagen
pET <i>cosR</i>	Pet28a+ harboring <i>cosR</i> , Kan <sup>r</sup>	(108)

Table 5 Primers used in this study

Use	Sequence (5'-3')	bp
<b>Mutant</b>		
VPbetIA	gcttcttagaggtaccgcatgcGCCAGTTTTATGTGCTCACC	580
VPbetIB	atatttatgagaCATCCCCACCTTTGGCATTTTG	
VPbetIC	gatgcctgaaCTCGACAAGCAGCTAACG	688
VPbetID	ggagagctcgatatcgcatgcTCTGCCCTACCCGGTAATC	
VPbetIFL Fwd	AGCATAGCACAATAAGAGTCG	1895
VPbetIFL Rev	CCTGATTCGCCAGTGAACGA	
<b>EMSA</b>		
VPbetIFwdA	CGGTTTTCTGATTCAGGC	125
VPbetIRevA	CTTTTAATGATAAATCGTTTGAGTTCG	
VPbetIFwdB	ATGCCAAAAATTTAGTTCGAAC	112
VPbetIRevB	GGTCTTTGAATGGATGGTAGGG	
VPbetIFwdC	CCCTACCATCCATTCAAAGACC	142
VPbetIRevC	CTAAGGCTTCTACATTGCTTTC	
VPbetIFwdD	GAAAGCAATGTAGAAGCCTTAG	202
VPbetIRevD	GAACTTGGATATGCGTCCATT	
VPbetIFwdE	AATGGACGCATATCCAAGTTC	158
VPbetIRevE	AGCATAGCACAATAAGAGTCG	
VPbcct1FwdA	ACCGCAAACCTCCCGATC	120
VPbcct1RevA	CGGTATTCAGTACAAAAGAA	
VPbcct1FwdB	TTCTTTTGTACTGAATACCG	110
VPbcct1RevB	TGTCTTCAACTCACAAGAAT	
VPbcct1FwdC	ATTCTTGTGAGTTGAAGACA	101
VPbcct1RevC	AGCGAATTTTATCACCAATCACA	
VPbcct3FwdA	CGCTTTTGTAAATGCAAATTACC	107
VPbcct3RevA	CCCGTGAAAGCGGAAGATC	
VPbcct3FwdB	GATCTCCGCTTTCACGGG	108
VPbcct3RevB	TCTATACCCTTTGTCATCGTTCCCTC	
VPcosRFwdA	CAAATCTCCACACCATTAATTAG	105
VPcosRRevA	CGTCTTTGGTGATTTCTTTTTATTTCG	
VPcosRFwdB	GCGAATAAAAAGAAATCACCAAAGACG	142
VPcosRRevB	CCAATTTTTTTCATCCAGTCTGTAGGG	
VPproU1FwdA	TCTTTATTCCATGCGTTG	160
VPproU1RevA	AGAGGCAGAAAGAACAGTGAA	
VPproU1FwdB	TTCACTGTTCTTTCTGCCTCT	134
VPproU1RevB	GGTTATGAATGTGTTTCGTTTGT	
VPproU1FwdC	ACAAACGAACACATTCATAACC	108
VPproU1RevC	TGGCTTGGCTTATTGGTGTTCT	
VPproU1FwdD	GAACACCAATAAGCCAAGCCA	109

Table 5 (continued)

VPproU1RevD	GGGATCCATGTTAATTGTCCTTTG	
VPbcct2Fwd	ACCGAGACATGCCAATTTCTG	233
VPbcct2Rev	CGGTGCTCACGAATAATCTCC	
VPbcct4Fwd	AGAACAGGTTGGCTCAATGT	244
VPbcct4Rev	TTCCCCTCACATCAAGTCG	
<b>Expression</b>		
PbetIFwd	TCTAAGCTTGCATAGCACAATAAGAGTCGC	594
PbetIRev	TATACTAGTTTTGCGTCCTTGTTATTTTTAATTG	
Pbcct1Fwd	tagatagagagagagagagaAAACCGCAAACCTCCCGATC	278
Pbcct1Rev	actcatttttctctccaCAATCACAAATTTATGCAAAAATGAC	
Pbcct3Fwd	tagatagagagagagagagaAATTTTTTCATCCAGTCTGTAGG	397
Pbcct3Rev	actcatttttctctccaCGTTCCTCTCTATTTTTGTATTATTTTTTC	
PproU1Fwd	tagatagagagagagagagaTCTTTATCCATGCGTTG	438
PproU1Rev	actcatttttctctccaGTTAATTGTCCTTTGTTATGTG	
PcosRFwd	tagatagagagagagagagaCGTTCCTCTCTATTTTTGTATTATTTTTTC	397
PcosRRev	cggccgctctagaactagtgTTATTCTGGTTTGGTGATG	
<b>RT-PCR primers</b>		
VPbcct1Fwd	GTTCCGGTCTTGCGACTTCTC	246
VPbcct1Rev	CCCATCGCAGTATCAAAGGT	
VPbcct2Fwd	AACAAAGGGTTGCCACTGAC	167
VPbcct2Rev	TTCAAACCTGTTGCTGCTTG	
VPbcct3Fwd	TGGACGGTATTCTACTGGGC	202
VPbcct3Rev	CGCCTAACTCGCCTACTTTG	
VPectAFwd	TCGAAAGGGAAGCGCTGAG	125
VPectARev	AGTGCTGACTTGGCCATGAT	
VPasp_ectFwd	CGATGATTCCATTTCGCGACG	126
VPasp_ectRev	GTCATCTCACTGTAGCCCCG	
VPproV1Fwd	GCATCGTTTCTCTCGACTCC	163
VPproV1Rev	TGCTCATCGACTACTGGCAC	
VPAbcct4Fwd	CAAGGCGTAGGCCGCATGGT	234
VPAbcct4Rev	ACCGCCCACGATGCTGAACC	
VPAbetIFwd	ACTTCGGTGGTAAGCATGGG	138
VPAbetIRev	TGCCGTCAATAATGGCGTTG	
VPAbetBFwd	TGGAAATCAGCACCAGCACT	160
VPAbetBRev	TCTGCCCTACCCGGTAATCA	
VPAproXFwd	TTCCTTGGTAACTGGATGCC	216
VPAproXRev	ATCGTTACCTGGTTCGATGC	
VPAproWFwd	ATCACAGCGGCACTGGCTTGG	190
VPAproWRev	GGCGATGCGCTGCCATGATC	
16SFwd	ACCGCCTGGGGAGTACGGTC	234
16SRev	TTGCGCTCGTTGCGGGACTT	



## Chapter 4

# **INVESTIGATIONS OF DIMETHYLGLYCINE (DMG), GLYCINE BETAINE AND ECTOINE UPTAKE BY A BCCT FAMILY TRANSPORTER WITH BROAD SUBSTRATE SPECIFICITY IN *VIBRIO* SPECIES**

The work in this chapter was submitted to the Journal of Bacteriology

Investigations of dimethylglycine (DMG), glycine betaine and ectoine uptake by a BCCT family transporter with broad substrate specificity in *Vibrio* species.

Gregory GJ; Dutta A; Parashar V; Boyd EF

### **Introduction**

In order to grow in high osmolarity environments, bacteria accumulate compounds called compatible solutes (osmolytes) within the cytoplasm of the cell, either via uptake or biosynthesis (9, 13, 22, 167). These compounds balance the internal osmolarity with that of the environment and maintain the turgor pressure of the cell (15, 78, 167). Osmolytes also protect proteins, nucleic acids and other vital molecular machinery by increasing the hydration shell around these molecules (23). Osmolytes fall into several classes of compounds including: sugars (trehalose), polyols (glycerol, mannitol), free amino acids (proline, glutamine), amino acid derivatives (ectoine), and quarternary amines (glycine betaine (GB), carnitine) (5, 13-18).

Biosynthesis of compatible solutes is energetically costly and therefore bacteria encode compatible solute transporters to scavenge available osmolytes from

the environment (5, 30, 75). Compatible solute transporters include the multicomponent ATP Binding Cassette (ABC)-family such as ProU (*proVWX*) in *Escherichia coli* and OpuC (*proVWX*) in *Pseudomonas syringae* (88, 91, 170), and the single component betaine-carnitine-choline transporter (BCCT) family which are Na<sup>+</sup> or H<sup>+</sup> dependent. Members of the BCCT family include BetT, in *E. coli*, which transports choline with high affinity, and glycine betaine transporters in *Bacillus subtilis* (OpuD) and *Corynebacterium glutamicum* (BetP), among many others (81-84).

BCCTs are energized by sodium- or proton-motive force symport and are organized into 12 transmembrane (TM) segments (81, 83, 85, 198). Aromatic residues found in TM4 and TM8 make up the glycine betaine binding pocket in BCCT-family transporters examined to date. These residues are highly conserved in BCCTs that transport trimethylammonium compounds such as glycine betaine, L-carnitine and  $\gamma$ -butyrobetaine (82, 85, 86, 199). An additional tryptophan residue is present in TM8 just outside the binding pocket, and is thought to participate in coordination of substrates during conformational changes that occur during transport (86).

*Vibrio parahaemolyticus* is a halophilic bacterium that is found in marine and estuarine environments in association with plankton, fish and shellfish (102, 200-204). *V. parahaemolyticus* is the leading bacterial cause of seafood-related gastroenteritis worldwide, frequently associated with consuming raw or undercooked seafood (101, 102). *Vibrio parahaemolyticus* can grow in a range of salinities and possesses four BCCTs encoded by *bccT1* (VP1456), *bccT2* (VP1723), *bccT3* (VP1905), and *bccT4* (VPA0356), and two ProUs encoded by *proVWX* (VP1726-VP1728) and *proXWV* (VPA1109-VPA1111) for the uptake of compatible solutes (45). In addition to

compatible solute transporters, *V. parahaemolyticus* also possesses biosynthesis systems for compatible solutes ectoine, *ectABC-asp\_ect* (VP1719-VP1722) and glycine betaine, *betIBA-proXWV* (VPA1112-VPA1114) whose expression is induced in high salinity (45). It was demonstrated that the expression of these biosynthesis systems in *Vibrio* species was under tight regulation, controlled by quorum sensing regulators OpaR and AphA, as well as CosR a global regulator of the osmotic stress response (61, 62, 108, 109). We reported previously that in *V. parahaemolyticus* *bccT1*, *bccT3*, *bccT4*, and both *proU* operons, are responsive to salinity, with the exception of *bccT2* (60, 61). Both *bccT1* and *bccT3* and both *proU* operons are repressed in low salinity by CosR (60, 61). Studies have shown that BccT1 in *V. parahaemolyticus* had the broadest substrate specificity, transporting glycine betaine, choline, proline, and ectoine, while BccT2 and BccT3 transport glycine betaine, choline and proline, and BccT4 transports only choline and proline (**Figure 26**) (60). Interestingly, the number of osmolyte transporters present among *Vibrio* species varies, which suggested differences in osmolytes utilized and osmotolerance (45). It was shown that *Vibrio alginolyticus* contained four BCCTs and two ProUs, *Vibrio harveyi* and *Vibrio splendidus* possessed six BCCTs and two ProUs whereas *Vibrio cholerae* and *Vibrio vulnificus* possessed one BCCT, a BccT3 homolog (45).

In this study, we examined the full range of osmolytes utilized by *V. parahaemolyticus* using an osmolyte phenotypic microarray plate, which identified over half a dozen potential osmolytes. We examined the ability of several different *Vibrio* species to utilize dimethylglycine, a compound previously not shown as an osmolyte in these species and one of the most effective osmolytes we identified. How *Vibrio* species uptake DMG is unknown. Therefore, we examined *V.*

*parahaemolyticus* transport of DMG using several osmolyte transporter mutants. These analyses showed that the BCCT carriers were required for efficient DMG uptake, thus representing a new transporter family for the uptake of DMG. In *V. parahaemolyticus*, BccT1 has the broadest substrate uptake ability in terms of number and diversity of compounds. Our *in silico* modelling analysis demonstrated that glycine betaine, DMG, and ectoine docked in the same binding pocket in BccT1. We investigated via mutagenesis and functional complementation the amino acid residues that are required for coordination of glycine betaine, DMG, and ectoine. This analysis describes for the first time the residues that coordinate DMG and ectoine in a BCCT family transporter.

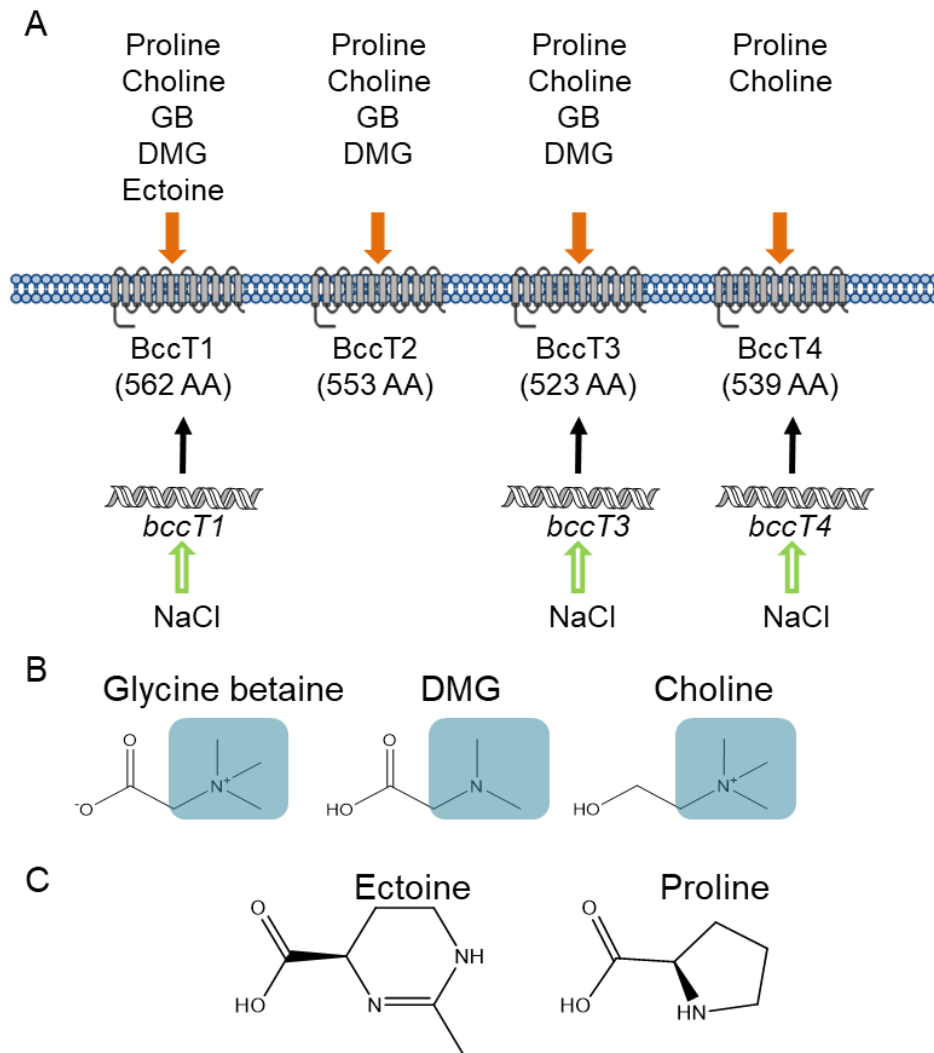


**Figure 26 BCCT-family transporters in *Vibrio parahaemolyticus***  
**(A)** A diagram depicting the BCCT family transporters present in *Vibrio parahaemolyticus* and their known substrates. *bccT1*, *bccT3*, and *bccT4* are induced by salinity. Structures of known substrates of BCCT family transporters in *V. parahaemolyticus* **(B)** with methylated headgroups highlighted in blue boxes or **(C)** substrates that are cyclic compounds.

## Materials and Methods

### Bacterial strains, media and culture conditions

All strains and plasmids used in this study are listed in Table 6. *Vibrio parahaemolyticus* strains were grown either in lysogeny broth (LB) (Fisher Scientific, Fair Lawn, NJ) with 3% (wt/vol) NaCl (LB3%) or M9 minimal media (47.8 mM Na<sub>2</sub>HPO<sub>4</sub>, 22mM KH<sub>2</sub>PO<sub>4</sub>, 18.7 mM NH<sub>4</sub>Cl, 8.6 mM NaCl; Sigma-Aldrich) supplemented with 2mM MgSO<sub>4</sub>, 0.1 mM CaCl<sub>2</sub>, 20 mM glucose as the sole carbon source (M9G) and NaCl (wt/vol), as indicated. Dimethylglycine (DMG) was used at a final concentration of 20 mM when supplied as a carbon source. *E. coli* strains were grown either in LB supplemented with 1% NaCl (LB1%) or M9G supplemented with 1% NaCl (M9G1%). All strains were grown at 37°C with aeration. Chloramphenicol (Cm), was added to the media at 25 µg/mL when necessary.

### Growth analysis

*Vibrio parahaemolyticus* and an in-frame deletion mutant of *ectB* were grown overnight in M9 minimal media supplemented with 1% NaCl and 20 mM glucose as the sole carbon source. Cultures were subsequently diluted 1:50 into fresh medium and grown for five hours. Cultures were pelleted, washed two times with 1X PBS to remove excess salt, and then diluted 1:50 into M9G, and 100 uL was then added to each well of a 96-well Biolog PM9 plate containing different osmolytes and/or salt concentrations (Biolog, Inc., Hayward, CA). The plates were incubated at 37°C with intermittent shaking in a Tecan Sunrise microplate reader and OD<sub>595</sub> was measured every hour for 24 hours. The area under the curve (AUC) was calculated using Origin 2018 for wild type (WT) and the  $\Delta$ *ectB* mutant. Statistics were calculated using a

Student's t-test; growth in 6% NaCl in the presence of a compatible solute was compared to growth in 6% NaCl with no exogenous compatible solutes.

For growth analysis in individual compatible solutes, wild type (WT),  $\Delta ectB$  mutant and quadruple  $\Delta bcct1-\Delta bcct3-\Delta bcct4-\Delta bcct2$  mutant (*bccT* null) strains were grown overnight in M9G 1%NaCl. Cultures were subsequently diluted 1:50 into fresh medium and grown for five hours to late exponential phase. Exponential cultures were then diluted 1:40 into 200  $\mu$ L of M9G 6%NaCl medium with and without exogenous compatible solutes in a 96-well microplate and grown at 37°C with intermittent shaking for 24 hours. Compatible solutes N-N dimethylglycine (DMG), trimethylamine-N-oxide (TMAO) and  $\gamma$ -amino-N-butyric acid (GABA) were added to a final concentration of 500  $\mu$ M. Growth analysis in each compatible solute was repeated following the above procedure with each of four triple *bccT* mutants,  $\Delta bcct2-\Delta bcct3-\Delta bcct4$ ,  $\Delta bcct1-\Delta bcct3-\Delta bcct4$ ,  $\Delta bcct1-\Delta bcct2-\Delta bcct4$ ,  $\Delta bcct1-\Delta bcct2-\Delta bcct3$ .

Growth analyses of *V. cholerae*, *V. harveyi*, *V. vulnificus*, and *V. fluvialis* were conducted by growing strains overnight in M9G supplemented with 2% NaCl (M9G 2% NaCl). Strains were diluted 1:40 into 200  $\mu$ L of M9G 4%NaCl medium, or M9G 5%NaCl for *V. fluvialis*, with and without exogenous DMG, in a 96-well microplate and grown at 37°C with intermittent shaking for 24 hours. To test DMG as a carbon source, *V. cholerae*, *V. vulnificus*, *V. fluvialis* and *V. parahaemolyticus* were grown overnight in LB1%; *V. harveyi* was grown in LB2%. Cells were pelleted, washed two times with 1 X PBS, and diluted 1:40 into 200  $\mu$ L of M9 with 20 mM DMG as the sole carbon source and 1% NaCl (2% NaCl for *V. harveyi*). Strains were grown in

M9G1% NaCl (2% NaCl for *V. harveyi*) as a control. Strains were grown in a 96-well microplate as described above.

Functional complementation of *E. coli* strain MKH13 with VP1456, VP1723, VP1905, and VPA0356

Full-length VP1456 (*bccT1*) or VPA0356 (*bccT4*) were amplified from the *V. parahaemolyticus* RIMD2210633 genome using primers listed in Table 7. Gibson assembly protocol using NEBuilder HiFi DNA Assembly Master Mix (New England Biolabs, Ipswich, MA) was followed to ligate the VP1456 or the VPA0356 fragment with the expression vector pBAD33, which had been linearized with SacI. Regions of complementarity for Gibson assembly are indicated by lowercase letters in the primer sequence in Table 7. The resulting expression plasmids, pBAVP1456 or pBAVPA0356, were transformed into *E. coli* Dh5 $\alpha$  for propagation. Plasmids were then purified, sequenced, and subsequently transformed into *E. coli* strain MKH13, which has large deletions that include all compatible solute transporters (*putP*, *proP*, *proU*) and the choline uptake and glycine betaine biosynthesis loci (*betT*-*betIBA*) (94). *E. coli* MKH13 strains containing pBAVP1456, pBAVP1723, pBAVP1905 or pBAVPA0356 were grown overnight in M9G 1%NaCl with chloramphenicol and subsequently diluted 1:100 into M9G 4% NaCl and 500  $\mu$ M of the indicated compatible solute and chloramphenicol for plasmid maintenance. Expression of each BccT was induced with 0.01% arabinose and functional complementation was determined by measuring OD595 after 24 hours growth at 37°C with aeration. Growth was compared to that of an MKH13 strain harboring empty pBAD33, which cannot grow in M9G 4% NaCl without exogenous compatible solutes. Statistics were calculated using a Student's t-test.

Site-directed mutagenesis was performed on pBPVP1456 with a Q5 site-directed mutagenesis kit (New England Biolabs, Ipswich, MA) and primers listed in Table 7. Primers were designed to create the nucleotide substitutions resulting in the following amino acid changes: Trp203Cys, Trp203Ala, Trp208Leu, Trp208Ala, Tyr211Leu, Tyr211Ala, Trp384Leu, and Trp384Ala. Site-directed mutagenesis was performed following the manufacturers' protocol to create single amino acid substitutions Trp203Cys, Trp208Leu, Tyr211Leu, Trp384Leu. Residues 203, 208, and 211 were mutagenized to encode for alanines, and residue 384 was subsequently mutagenized in this plasmid backbone to encode for an alanine.

Homology modeling of BCCT1 and docking of glycine betaine, DMG and ectoine.

BLAST search of BccT1 sequence against Protein Data Bank (PDB) as the search database showed highest sequence identity with the 3.2 Å X-ray crystal structure of Glycine Betaine transporter from *C. glutamicum* (CgBetP, PDB ID: 4AIN). Homology modeling of BccT1 was done in SWISS-MODEL server using CgBetP structure (PDB ID: 4AIN) as a template (175). CgBetP exists as a trimer in the structure with each protomer showing different states of substrate transport. Two different models resembling protomers from chain B and chain C of CgBetP structure, and therefore representing two different substrate binding states, were treated separately after modeling. Residues showing poor stereo-chemical properties or close-contacts in each monomeric model were fixed manually in COOT (205). Models were then subjected to energy minimization using 3Drefine server to reduce any other structural restraints (206). The quality of the resulting models was finally verified with Verify3D and PROCHECK (207, 208).

For docking studies, ligand models for glycine betaine, DMG and ectoine were obtained from Chemical Entities of Biological Interest (ChEBI) EMBL (209). Polar hydrogens were added to the ligand structures in PRODRG (210). The AutoDoc tools v1.5.6 were used to assign the rotatable bonds in the ligands and to add all polar hydrogens in the BccT1 models to prepare them for the docking. The ligand-centered maps for BccT1 models were assigned a grid size of 20 x 20 x 20 Å<sup>3</sup>. The docking experiments of glycine betaine, DMG and ectoine ligands to the BccT1 receptor model were performed using AutoDock Vina (211). The binding free energies and BccT1 residues making interactions with the ligands are listed in Table 8. The structural illustrations were prepared using PyMOL (The PyMOL Molecular Graphics System, Version 2.0 Schrödinger, LLC).

#### Bioinformatics and phylogenetic analyses

Transmembrane helix probabilities of *C. glutamicum* BetP (CAA63771.1) and BccT1 (Q87PP5.1) were generated using OCTOPUS and aligned via the AlignMe program (<http://www.bioinfo.mpg.de/AlignMe>) (212-214). The *V. parahaemolyticus* protein BccT1 (Q87PP5.1), and CgBetP (CAA63771.1), EctP (CAA04760.1), and LcoP (ASW14702.1) were downloaded from NCBI and aligned using the ClustalW algorithm (180). Aligned sequences were displayed and annotated using ESPript (<http://espript.ibcp.fr/ESPript/cgi-bin/ESPript.cgi>) (215).

Phylogenetic analysis was conducted using BccT1 (VP1456) protein as a seed to identify all homologs within the family Vibrionaceae with completed genome sequences available. Unique protein sequences that had >95% sequence coverage and >70% amino acid identity with BccT1 were obtained from NCBI database and aligned using the ClustalW algorithm (180). The evolutionary history of

BccT1 was inferred by using the Maximum Likelihood method and Le\_Gascuel\_2008 model as determined by best fit model selection in MEGAX (184, 216). The tree with the highest log likelihood (-10453.23) is shown. The percentage of trees in which the associated taxa clustered together is shown next to the branches. Initial tree(s) for the heuristic search were obtained automatically by applying Neighbor-Join and BioNJ algorithms to a matrix of pairwise distances estimated using a Jones-Taylor-Thornton (JTT) model, and then selecting the topology with superior log likelihood value. A discrete Gamma distribution was used to model evolutionary rate differences among sites (5 categories (+G, parameter = 0.4143)). The tree is drawn to scale, with branch lengths measured in the number of substitutions per site. This analysis involved 49 amino acid sequences and a total of 525 positions in the final dataset.

## Results

*V. parahaemolyticus* can utilize a wide range of compatible solutes

To determine the range of compatible solutes that can be utilized by *V. parahaemolyticus*, a Biolog 96-well PM9 osmolyte phenotypic microarray plate was used. Growth analyses were performed using a *V. parahaemolyticus*  $\Delta ectB$  deletion mutant, which is unable to synthesize ectoine *de novo* and therefore has a growth defect in high salinity in the absence of exogenous osmolytes (45, 59). The  $\Delta ectB$  mutant was grown in a Biolog 96-well PM9 osmolyte phenotypic microarray plate, which contains 23 unique osmolytes. A total of 14 of these osmolytes significantly rescue the growth of the  $\Delta ectB$  mutant, which indicated that the substrate was transported and utilized by *V. parahaemolyticus* (**Figure 27**). Previously unrecognized osmolytes for this species included N-N dimethylglycine (DMG),  $\gamma$ -amino-N-butyric

acid (GABA), trimethylamine-N-oxide (TMAO), glutathione, dimethylsulfoniopropionate, MOPS, creatine, N-acetyl L-glutamine, and octopine, in addition to those already known to provide osmoprotection such as trehalose,  $\beta$ -glutamic acid, glycine betaine, ectoine and L-proline (**Figure 27**).

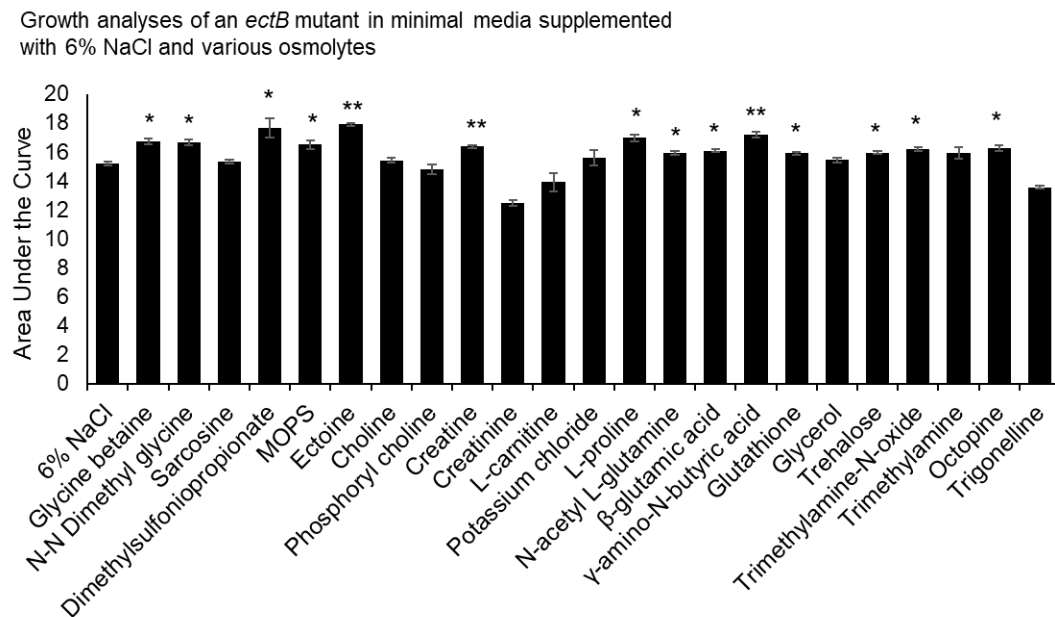


**Figure 27** Growth analyses of  $\Delta$ *ectB* mutant in phenotypic microarray plate  
Area under the curve analysis of growth of an  $\Delta$ *ectB* deletion mutant with a subset of 23 osmolytes from the Biolog phenotypic microarray PM9 plate. Growth in the presence of individual osmolytes is compared to growth in minimal medium with 6% NaCl only. Mean and standard error of at least two biological replicates are shown. Statistics were calculated using a Student's t-test (\*,  $P < 0.05$ ; \*\*,  $P < 0.01$ ).

To validate the phenotypic microarray analysis, we performed growth analyses with the  $\Delta$ *ectB* mutant in the presence of compatible solutes DMG, GABA, or TMAO in in M9 minimal media supplemented with glucose and 6% NaCl (M9G 6%NaCl).

The presence of exogenous DMG, GABA, or TMAO rescued the growth of the  $\Delta ectB$  mutant, which confirmed *V. parahaemolyticus* can utilize these as compatible solutes (**Figure 28**). Growth of the  $\Delta ectB$  mutant was rescued by addition of exogenous DMG with a lag phase of less than one hour (**Figure 28A**), which indicated that DMG is a very effective compatible solute for *V. parahaemolyticus*. The  $\Delta ectB$  mutant was rescued to a greater extent with exogenous DMG as compared to GABA or TMAO (**Figure 28B and 28C**).

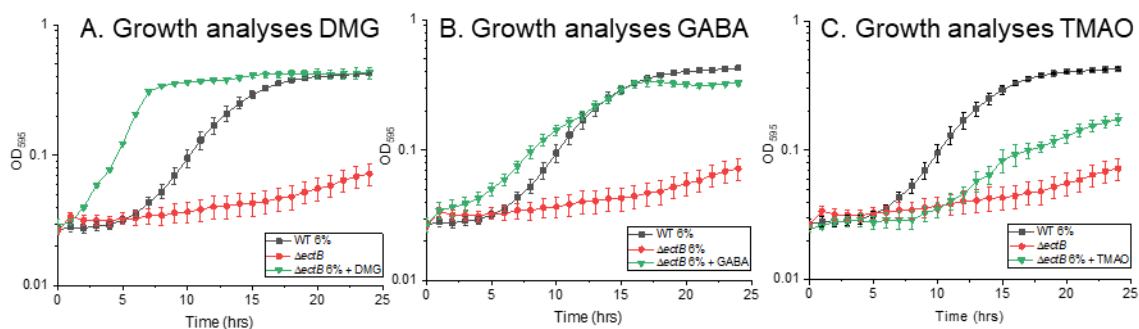


**Figure 28** Growth analyses of  $\Delta ectB$  mutant with selected osmolytes

Growth analyses were conducted in M9G supplemented with 6% NaCl and wild type RIMD2210633 and an  $\Delta ectB$  mutant strain. Media was supplemented with (A) DMG, (B) GABA, or (C) TMAO. Optical density (OD<sub>595</sub>) was measured every hour for 24 hours; the mean and standard error of at least two biological replicates are shown.

DMG is an important compatible solute for *Vibrio* species.

To investigate whether DMG can also act as an osmolyte in other *Vibrio* species, we grew four species representing divergent clades of *Vibrio* in M9G 4%

NaCl or 5%NaCl supplemented with and without DMG at 37C for 24 h. Growth of *V. harveyi*, *V. fluvialis*, *V. vulnificus* and *V. cholerae* were all rescued by exogenous DMG (**Figure 29A-D**). In the absence of DMG, *V. harveyi* grew with a 9 h lag phase and a 3 h lag phase and a shorter doubling time in the presence of DMG (**Figure 29A**), which indicated that DMG is a highly effective compatible solute for this species. Similarly, *V. fluvialis* grown in the presence of DMG had a reduced lag phase and a shorter doubling time (**Figure 29B**), indicating DMG is an effective osmolyte. *V. vulnificus* is unable to grow in M9G 4%NaCl in the absence of DMG, but growth was rescued in the presence of DMG with a 10 h lag phase (**Figure 29C**), indicating this is a highly effective osmolyte for this species. In the presence of DMG the growth rate of *V. cholerae* was significantly increased (**Figure 29D**). These data indicated that all *Vibrio* species tested utilize DMG as an osmoprotectant, with varying degrees of effectiveness.

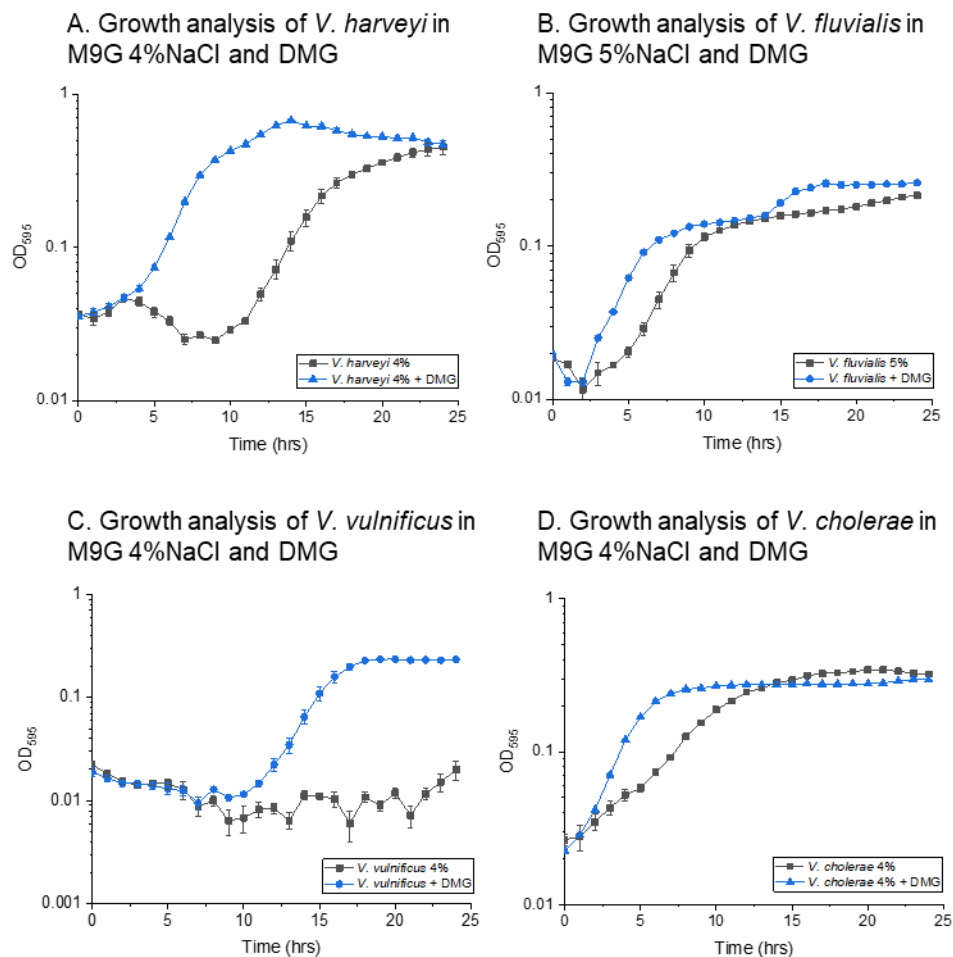


**Figure 29 Growth analyses of *Vibrio* strains with DMG**  
 Growth analyses of (A) *V. harveyi* 393, (B) *V. fluvialis*, (C) *V. vulnificus* YJ016 and (D) *V. cholerae* N16961, were conducted in M9G 4% NaCl (M9G5% for *V. fluvialis*) with and without exogenous DMG. Optical density (OD<sub>595</sub>) was measured every hour for 24 hours. Mean and standard error of two biological replicates are shown.

Because DMG is an intermediate in glycine betaine catabolism, and many bacteria possess genes for the degradation of DMG to sarcosine, there is the possibility that DMG can be used as a carbon source in these species (64, 217, 218). Therefore, we examined whether any *Vibrio* species could utilize DMG as a sole

carbon source by growing strains in M9 supplemented with DMG as the sole carbon source. None of the species tested could utilize DMG as a carbon source, demonstrating that DMG is a *bona fide* compatible solute for *Vibrio* species (Figure 30).

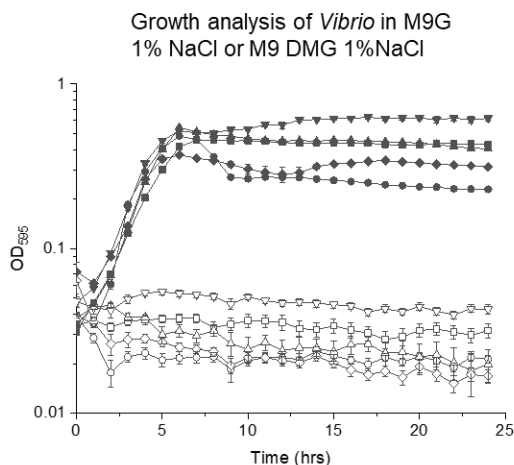


**Figure 30 Growth analyses of *Vibrio* species with DMG as carbon source**  
Growth analyses of *V. parahaemolyticus* RIMD2210633 (down triangles), *V. harveyi* 393 (up triangles), *V. vulnificus* YJ016 (diamonds), *V. cholerae* N16961 (squares), and *V. fluvialis* (circles), were conducted in M9 with DMG (open shapes) as the sole carbon source or M9 with glucose (solid shapes) as the sole carbon source. Optical density (OD<sub>595</sub>) was measured every hour for 24 hours. Mean and standard error of two biological replicates are shown.

#### BCCTs are responsible for transport of DMG

DMG was identified as an alternative substrate of the *E. coli* transporter ProP, which is a member of the major facilitator superfamily (MFS) (219). In *Bacillus subtilis* DMG was transported into the cell as an osmolyte via an ABC-family transporter OpuA (63). We examined whether any of the BCCTs in *V. parahaemolyticus* were responsible for transport of DMG and to accomplish this we

used a *bccT* null mutant (quadruple  $\Delta bccT1-bccT3-bccT4-bccT2$ ). We grew wild type and the *bccT* null mutant in M9G 6%NaCl supplemented with and without DMG at 37°C for 24 h. In the wild-type strain, in the absence of DMG there was a 4 h lag phase whereas in the presence of DMG the lag phase was < 1 h and cells had a faster doubling time, which indicated that DMG is transported into the cell effectively (**Figure 31**). However, the *bccT* null mutant did not exhibit a reduced lag phase or increased growth rate in the presence of DMG (**Figure 31**), which indicated that a BCCT carrier is required for transport of DMG. Although, *V. parahaemolyticus* encodes two ABC-family compatible solute transporters, ProU1 and ProU2, which are present in the *bccT* null mutant, these do not appear to be involved in DMG uptake.

Growth analyses of  $\Delta bcct1342$  in M9G 6%NaCl and DMG

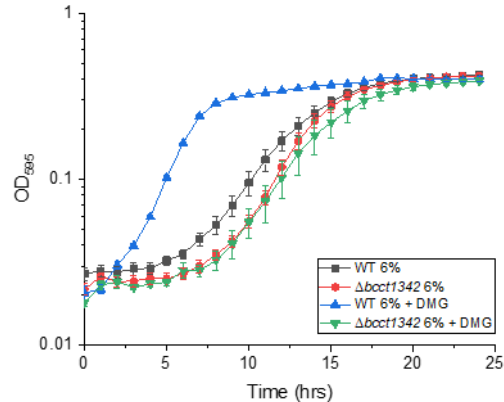


**Figure 31 Growth analyses of quadruple *bccT* mutant with DMG**  
Growth analysis of wild type (WT) and  $\Delta bcct1342$  in M9G6% with and without the addition of exogenous DMG. Optical density (OD<sub>595</sub>) was measured every hour for 24 hours; mean and standard error of at least two biological replicates are displayed.

To determine which of the four BCCTs transports DMG, a set of four triple *bccT* mutants each possessing a single functional *bccT* was utilized in growth assays. The triple  $\Delta bccT2-bccT3-bccT4$  mutant, which contains only *bccT1*, had a slightly reduced lag phase and a slightly faster growth rate through exponential phase in M6G 6%NaCl supplemented with DMG (**Figure 32A**). This suggested that BccT1 transported DMG with low efficiency. In contrast, the triple  $\Delta bccT1-bccT3-bccT4$  mutant, which contains only *bccT2*, had a similar reduction in lag phase and faster growth rate as wild type (**Figure 32B**). This suggested that BccT2 transported DMG as efficiently as the wild-type strain. The triple  $\Delta bccT1-bccT2-bccT4$  mutant, which contains only *bccT3*, grew similar to the *bccT1* only strain, with a very slightly reduced lag phase and grew slightly better through exponential phase in the presence of DMG (**Figure 32C**). This suggested that DMG is transported by BccT3 with low efficiency. The  $\Delta bccT123$  mutant showed no difference in growth in the absence or presence of DMG, which indicated that BccT4 does not transport DMG into the cell (**Figure 32D**).

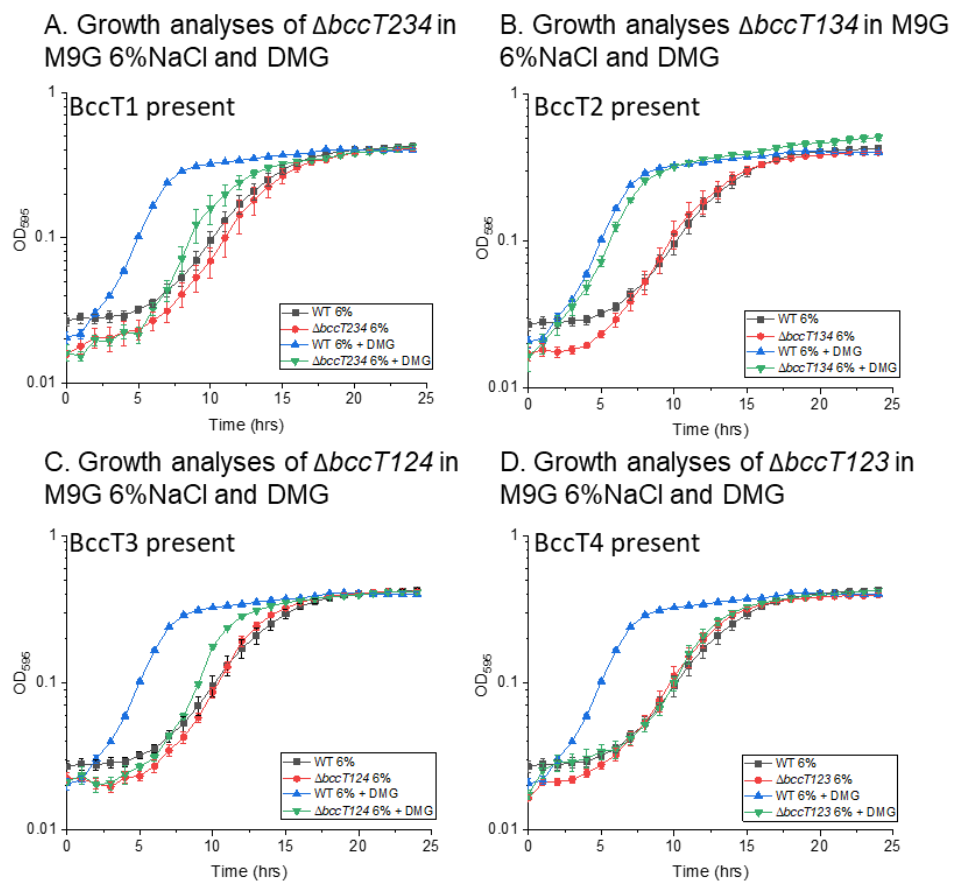


**Figure 32 Growth analyses of triple *bccT* mutants with DMG**  
 Growth analysis of wild type (WT) and (A)  $\Delta bccT234$ , (B)  $\Delta bccT134$ , (C)  $\Delta bccT124$ , or (D)  $\Delta bccT123$  in M9G6% with and without the addition of exogenous DMG. Optical density ( $OD_{595}$ ) was measured every hour for 24 hours; mean and standard error of at least two biological replicates are displayed.

In order to examine DMG uptake by the BCCT transporter further, we used *E. coli* MKH13, a mutant strain that does not contain osmolyte transporters or biosynthesis genes and cannot grow in M9G 4%NaCl. We cloned each of the *bccT* genes into an expression plasmid and used each construct to complement *E. coli* MKH13 and examined growth in M9G 4%NaCl supplemented with DMG (**Figure**

33). *Escherichia coli* MKH13 strains complemented with *bccT1*, *bccT2* and *bccT3* grew in the presence of DMG whereas the *bccT4* complemented strain and the empty expression plasmid did not (**Figure 33**). The *E. coli* MKH13 pBAVP1456 (*bccT1*) and pBAVP1723 (*bccT2*) strains grew significantly better than the strain with pBAVP1905 (*bccT3*) (**Figure 33**). These indicated that BccT1 and BccT2 are more efficient transporters of DMG than BCC3, and BCC4 is not a transporter of this substrate.

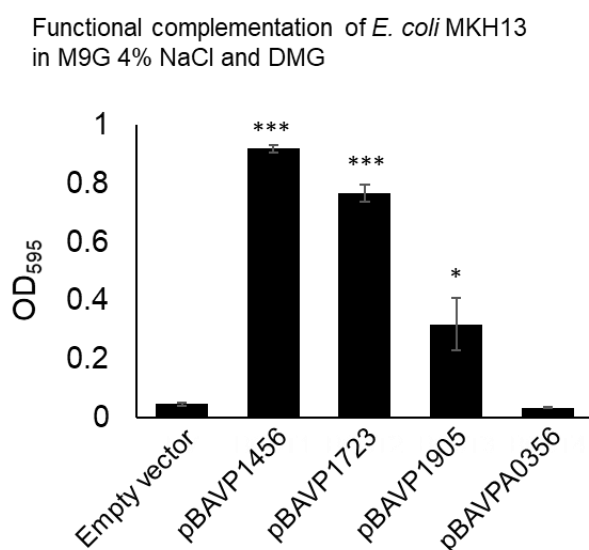


**Figure 33 Functional complementation of *E. coli* with DMG**  
*E. coli* strain MKH13 was grown in M9G supplemented with 4% NaCl and functionally complemented with (A) BccT1 (pBAVP1456), (B) BccT2 (pBAVP1723), (C) BccT3 (pBAVP1905), or (D) BccT4 (pBAVPA0356), each expressed from an arabinose-inducible expression plasmid, pBAD33. Strains were grown for 24 hours in the presence of 500  $\mu$ M DMG and the final optical density (OD<sub>595</sub>) was compared to that of a strain harboring empty pBAD33. Mean and standard error of at least two biological replicates are shown. Statistics were calculated using a Student's t-test (\*\*,  $P < 0.01$ ).

### BccT1 sequence homology to structurally characterized BCCTs

From a structure/function standpoint, BccT1 is of particular interest as it can transport glycine betaine, DMG, and ectoine (**Figure 34**). While glycine betaine and DMG have similar structures with methylated head groups, ectoine is a cyclic compound and may require coordination by different amino acid residues in the transporter (85). Furthermore, transporters of ectoine typically do not possess the conserved aromatic residues located in TM4 and TM8 that coordinate trimethylammonium substrate binding such as glycine betaine (85). Therefore, first we compared BccT1 to structurally characterized BCCT proteins by hydrophathy analysis. The hydrophathy profile of BccT1 was aligned with that of BetP from *Corynebacterium glutamicum* (CgBetP), a glycine betaine transporter whose structure has been studied extensively. We found BccT1 possessed 12 TM segments (TM1 to TM12) along with N- and C-terminal tail extensions. BccT1 shared matched positions with 89% of residues in CgBetP, which indicated the structures were highly conserved (**Figure 35**). In CgBetP, the conserved residues that form the glycine betaine binding pocket in TM4 are Trp189, Trp194, Tyr197 and one residue located in TM8, Trp374. An additional residue located in TM8 below the binding pocket (Trp377) is thought to be involved in substrate coordination during conformational changes (86). In addition, *C. glutamicum* BCCT-family transporters LcoP (CgLcoP) and EctP (CgEctP), have been reported to uptake glycine betaine and ectoine (220, 221). We aligned the protein sequences of each of these transporters with CgBetP and BccT1, in order to compare residues in each protein (**Figure 36**). CgBetP, CgLcoP and BccT1 possessed identical amino acids to residues corresponding to TM4 Trp189, Trp194, Tyr197, and TM8 Trp374 and Trp377 suggesting that these proteins coordinate glycine betaine with the same residues (**Figure 36**).

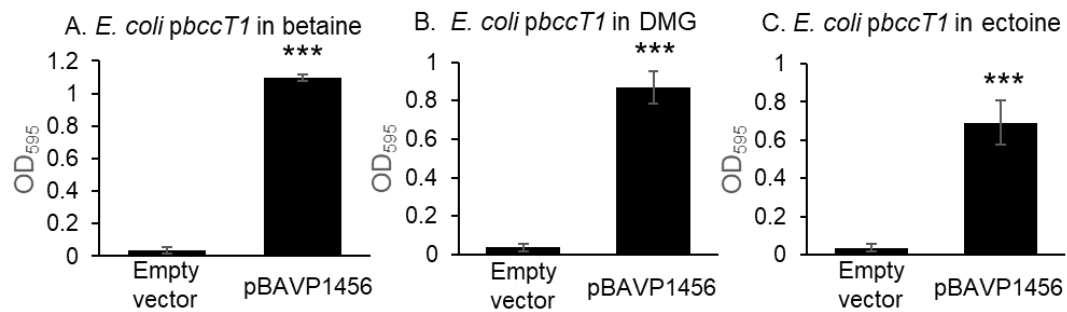


**Figure 34 Functional complementation of *E. coli* with BccT1**

Functional complementation of *E. coli* MKH13 with wild type BccT1 (pBAVP1456) and exogenous (A) glycine betaine, (B) DMG, and (C) ectoine. Strains were grown for 24 hours in the presence of 500  $\mu$ M DMG and the final optical density (OD<sub>595</sub>) was compared to that of a strain harboring empty pBAD33. Mean and standard error of at least two biological replicates are shown. Statistics were calculated using a Student's t-test (\*\*\*, P < 0.001).

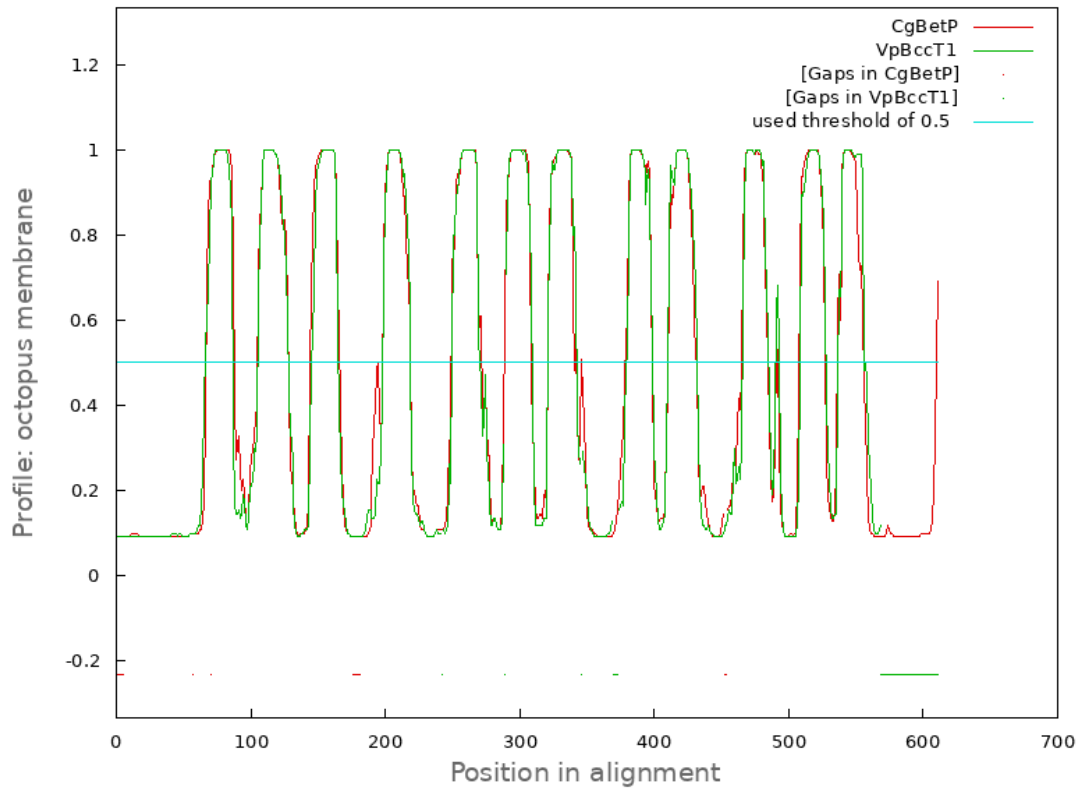


**Figure 35** **Hydropathy profile of *V. parahaemolyticus* BccT1**

The transmembrane helix probability of *V. parahaemolyticus* BccT1 was generated and aligned with *Corynebacterium glutamicum* BetP using AlignMe (<http://www.bioinfo.mpg.de/AlignMe>). Values close to 1 indicate a high probability of that sequence being in the membrane while 0 is a low probability of that sequence being in the membrane. Dots below the plot indicate gaps introduced during alignment.

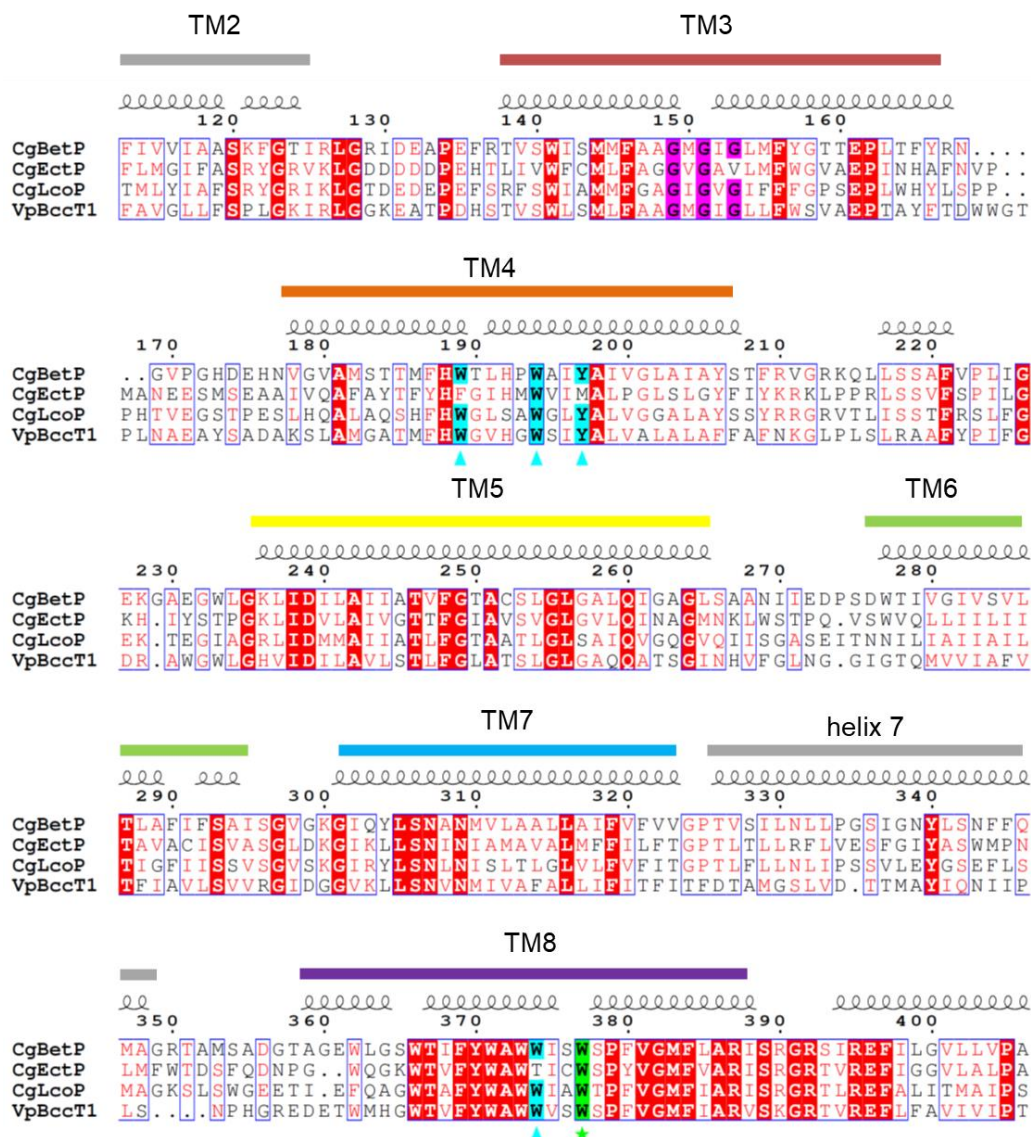


**Figure 36** BccT1 alignment with *Corynebacterium glutamicum* BCCT-family transporters

The *V. parahaemolyticus* BCCT protein BccT1 was aligned with *Corynebacterium glutamicum* transporters BetP, LcoP and EctP and displayed using ESPript. Residues highlighted in red are strictly conserved. Residues highlighted in magenta are conserved in sodium-symporters. Residues marked with a cyan triangle have been demonstrated to be important for glycine betaine binding; residues highlighted in cyan are conserved. A green star denotes residues thought to be important for additional substrate binding; conserved residues are highlighted in green.

## Structural Modelling of BccT1

A BLASTP search of BccT1 sequence against Protein Data Bank (PDB) provided glycine betaine transporter CgBetP (PDB ID 4AIN) as the highest scoring hit with a sequence identity of 37% to BccT1 over 80% query coverage. CgBetP is an active trimer correctly represented in its three-dimensional structure with the three protomers (chains) showing different stages of substrate transport cycle with an alternating-access mechanism (222). More specifically, the chain A of CgBetP structure represents closed apo state ( $C_c$ ) whereas chains B and C represent a closed substrate-bound ( $C_cS$ ) and an open substrate-bound ( $C_iS$ ) state, respectively. The chain B and chain C of CgBetP were used as templates to generate  $C_cS$  and  $C_iS$ -like homology model of BccT1, respectively. The energy-minimized models of BccT1 were verified using a 3D profile method of Verify3D that evaluates the correlation between amino acid sequence (1D) and the model (3D) by comparing it to the other known structures in the database. The  $C_cS$  and  $C_iS$  model of BccT1 showed Verify3D scores of 88.6% and 84.0% respectively, which indicated good quality of the models (**Figure 37**). The stereo-chemical properties of the models were examined by Ramachandran plot using PROCHECK. Both  $C_cS$  and  $C_iS$  BccT1 models contain 99.2% of all the residues in the allowed region and none in the disallowed region (**Figure 38**).

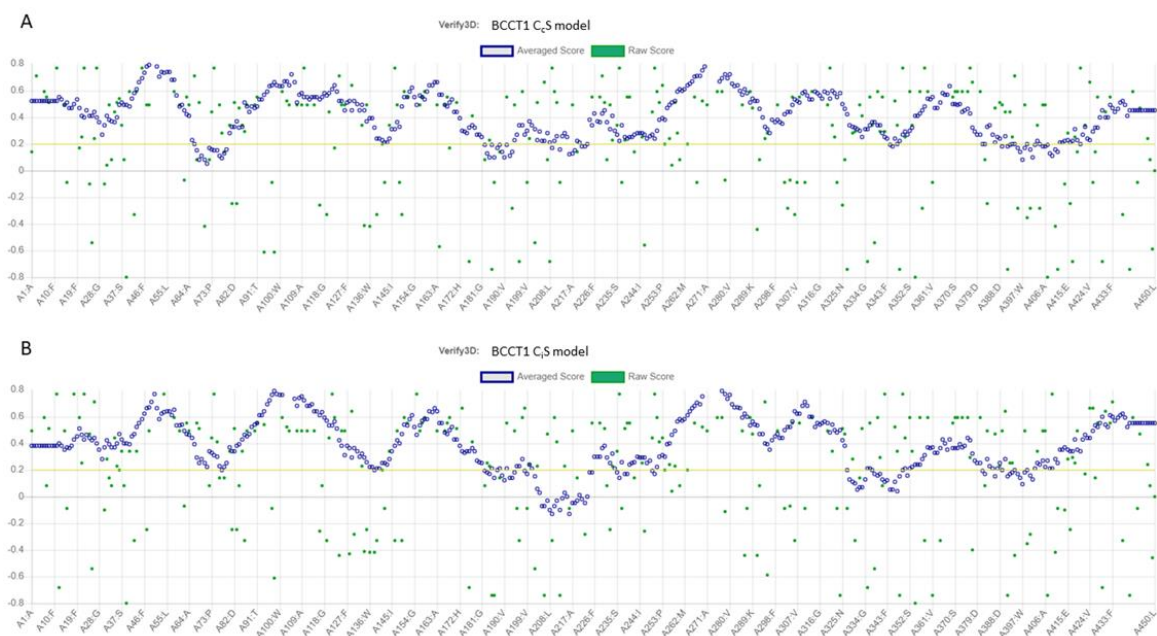


**Figure 37** Verification of the overall quality of our predicted BccT1 models with Verify3D

(A) 88.6% of BccT1 residues in the C<sub>c</sub>S model have a 3D-1D score  $\geq 0.2$ ,  
 (B) 84.0% of BccT1 residues in the C<sub>i</sub>S model have 3D-1D score  $\geq 0.2$ .

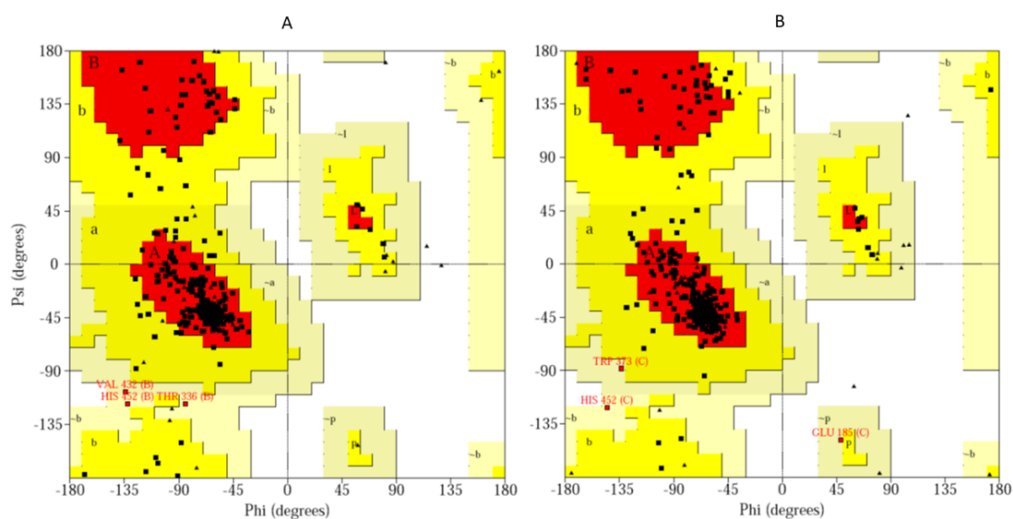


**Figure 38 Ramachandran plots verifying stereochemical properties of our BccT1 models.**

(A) C<sub>c</sub>S model of BccT1 has 90.2% residues in most favored, 9.0% in additionally allowed, and no residues in outlier regions (B) C<sub>i</sub>S model of BccT1 contains 91.5% residues in most favored, 7.7% in additionally allowed, and no residues in outlier regions.

Our structural models of BccT1 have cylindrical shapes and are composed of eleven trans-membrane helices (2-12) and a periplasmic helix (H7) (**Figure 39A**). The first 108 amino acids of BccT1 could not be modeled because of their poor sequence similarity with CgBetP. BccT1 also lacks a cytosolic C-terminal domain (CTD), which is important for osmo-sensing in CgBetP (223). Nonetheless, BccT1 models are very similar to the CgBetP structure with an RMSDs of 0.26Å (399 Ca atoms) and 0.22 Å (391 Ca atoms) for C<sub>c</sub>S and C<sub>i</sub>S models, respectively. The residues involved in the central binding pocket, cytoplasmic and periplasmic gates as well as the rest of the substrate pathway are mostly conserved in BccT1. More specifically, a comparison of BccT1 models with the glycine betaine-bound structure of CgBetP showed that all the

substrate binding residues are conserved and located in TM4 (Trp203, Trp208, Tyr211) and TM8 (Trp380, Trp381 and Trp384) (**Figure 36**).

The closed state ( $C_cS$ ) represents a transition state between outward- and inward-facing open states where the substrate is bound in a central cavity with both substrate entry and exit ports occluded. Unlike open states, the substrate makes optimal interactions with the active site residues in the  $C_cS$  state (222), therefore,  $C_cS$  model of BccT1 was used for our substrate docking studies. The glycine betaine-docked BccT1 model showed binding free energy change ( $\Delta G$ ) of -4.8 kcal/mole (**Table 8**). Briefly, the aromatic rings of Trp380, Trp381 and Trp384 form a small hydrophobic pocket that binds glycine betaine in this BccT1 model (**Table 8 and Figure 39B**). The quaternary amine group of glycine betaine binds to this pocket by cation- $\pi$  and van der Waals interactions. Other aromatic residues Trp203, Trp208 and Tyr211 of BccT1 also contribute to the hydrophobic interactions with glycine betaine. The glycine betaine carboxylic group interacts with the peptide backbones of Ile160 and Gly161 as well as side chain of Ser266 via hydrogen bonding (**Figure 39B**).

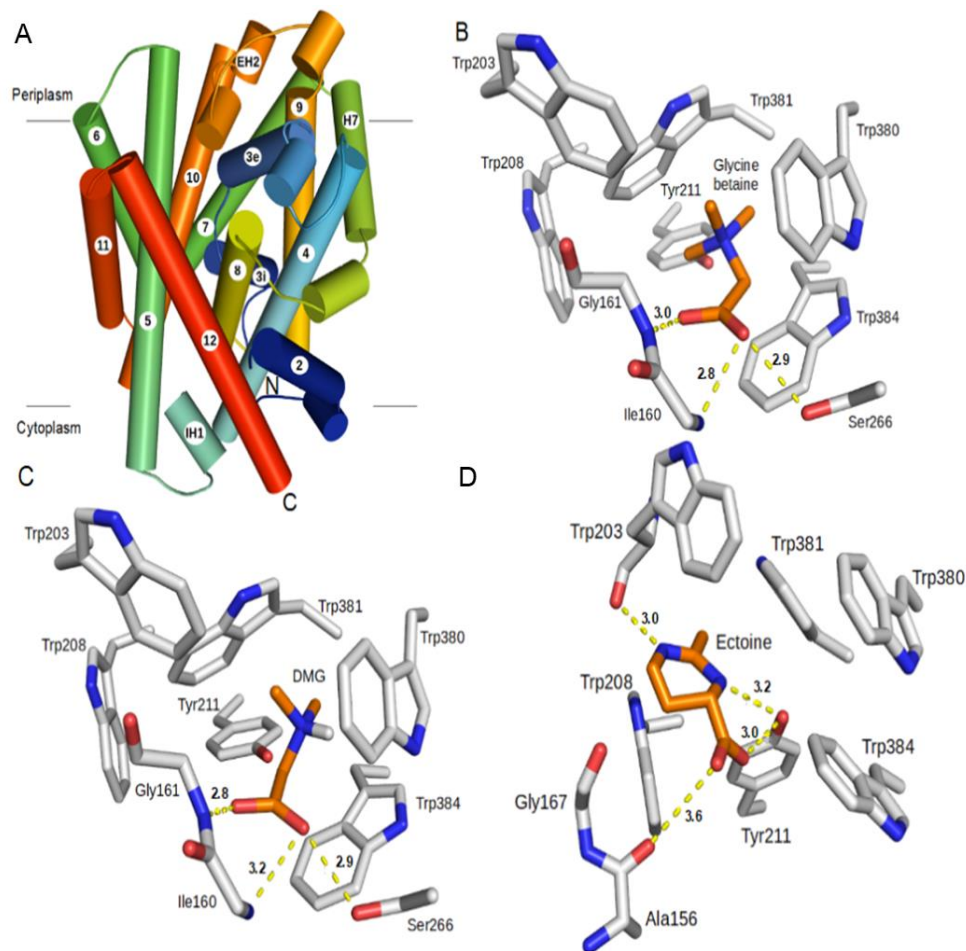


**Figure 39 Predicted overall structure of BCCT1 and its active site interactions with different substrates.**

(A) A side view of the overall structure of BCCT1.  $\alpha$ -helices are depicted by cylinders and directionality of the polypeptide chain is shown by a color gradient from blue (N-terminus) to red (C-terminus). Eleven transmembrane helices (TM2-TM12) and a periplasmic helix (H7) make the core of the structure. Two small helices, IH1 and EH2, connect TM4-TM5 and TM9-TM10 respectively. (B-D) Interactions of the active site residues of BccT1 with the substrates. (B) Interacting residues of BccT1 CcS state with docked glycine betaine and (C) DMG; (D) interactions of BccT1 residues in a CiS state with docked ectoine. Bonds are depicted as sticks; substrates and BccT1 residues are colored orange and gray, respectively. Yellow dashed lines show hydrogen bonding distances between BccT1 residues and various atoms in the substrates. Illustrations are prepared using Pymol (The PyMOL Molecular Graphics System, Version 2.0 Schrödinger, LLC).

Docking analysis of DMG and ectoine binding residues in BccT1.

Since BccT1 is a unique BCCT-family transporter that can transport multiple osmolytes, we sought to determine the DMG and ectoine binding residues in BccT1 by docking. Docking of DMG to the BccT1 C<sub>c</sub>S model (**Figure 39C**) predicted a mode of interaction identical to glycine betaine with a favorable binding free energy change ( $\Delta G$ ) of -4.4 kcal/mole (**Table 8**). This was expected since DMG and glycine betaine have very similar chemical structures.

To identify the mode of ectoine binding to BccT1, ectoine was first docked to the active site of the C<sub>c</sub>S model of BccT1. However, free energy change ( $\Delta G$ ) of ectoine binding to C<sub>c</sub>S model of BccT1 was too low (-2.8 kcal/mol), likely because of spatially constrained fitting of the large ectoine ring into the smaller hydrophobic pocket comprised of the aromatic rings of Trp380, Trp381 and Trp384. Therefore, we turned our attention to the C<sub>i</sub>S model of BccT1 ectoine docking, keeping all other docking parameters constant. The substrate binding site in the C<sub>i</sub>S state differs from C<sub>c</sub>S state in the relative orientations of the Trp380 and Trp381 side chains remodeling the hydrophobic pocket. More specifically, during the C<sub>c</sub>S to C<sub>i</sub>S transition, aromatic rings of Trp380 and Trp381 are known to flip 90 degrees, opening up the hydrophobic pocket (222). Interestingly, ectoine docking to the C<sub>i</sub>S state of BccT1 was accompanied by a significant free energy change ( $\Delta G$ ) of -6.1 kcal/mol (**Table 8**). The ectoine binding in this BccT1 state is stabilized by hydrogen bonding interactions between ectoine carboxyl group and the peptide backbone of Ala157 as well as the side chain of Tyr211 (**Figure 39D**). Further, the ectoine ring nitrogens are involved in hydrogen bonding with Tyr211 and the peptide backbone of Trp203. The bound ectoine also shows van der Waals interactions with the aromatic residues Trp203, Trp208, Trp281 and Trp384 (**Figure 39D**).

Site directed mutagenesis of BccT1 uncovers ectoine binding pocket.

The above-mentioned structural modeling and docking experiments predicted BccT1 residues that are likely involved in binding and transport of glycine betaine, DMG and ectoine. All these residues are conserved in CgBetP, and interestingly, mutations targeting four of the corresponding CgBetP residues, namely Trp189, Trp194, Tyr197, and Trp377, have been shown to significantly abrogate transporter function (86). Therefore, we selected the corresponding residues in BccT1 namely, Trp203, Trp208, Tyr211, and Trp384, for a mutagenesis study. We utilized functional complementation of *E. coli* MKH13 as a readout for uptake of glycine betaine, DMG and ectoine by BccT1 with single amino acid substitutions: Trp203Cys, Trp208Leu, Tyr211Leu and Trp384Leu. Amino acid substitutions corresponding to these positions in CgBetP, which conserve the bulky side chain of the amino acid being substituted, have been demonstrated to affect glycine betaine uptake in CgBetP (86). We also tested a BccT1 mutant with all four of these residues replaced by alanine, which is chemically inert and possesses a non-bulky methyl functional group. Replacement of Trp203 resulted in reduced growth of the *E. coli* MKH13 strain in the presence of glycine betaine, while strains harboring the other three single-replacement mutants Trp208Leu, Tyr211Leu, and Trp384Leu grew similarly to a strain harboring WT BccT1 (**Figure 40A**). This indicates that Trp203 is important, but not essential, for uptake of glycine betaine by BccT1. In the absence of each of the other three residues 208, 211, or 384, glycine betaine may be accommodated by an alternate residue. Replacement of all four residues with alanine resulted in no growth of the *E. coli* MKH13 strain (**Figure 40A**). This indicated that these four residues are involved in coordination of glycine betaine in BccT1.

Replacement of Trp203 or Trp384 resulted in no uptake of DMG, as strains harboring these mutants did not grow (**Figure 40B**). Replacement of Tyr211 resulted in a reduced ability to uptake DMG, as evidenced by growth of this strain to a lower final OD (**Figure 40B**). Replacement of all four residues resulted in no growth of *E. coli* MKH13, which indicated that these residues make up the binding pocket for DMG (**Figure 40B**).

Replacement of residues Trp203, Tyr211 or Trp384 individually was sufficient to completely abolish uptake of ectoine by *E. coli* MKH13, as the strains harboring these mutants were unable to grow (**Figure 40C**). However, replacement of Trp208 did not result in a statistically significant difference in growth from a WT BccT1-expressing strain, indicating that Trp208 is not required for uptake of ectoine (**Figure 40C**). Replacement of all four residues with alanine also resulted in abrogation of ectoine transport (**Figure 40C**). Together these results indicated that DMG and ectoine share a binding pocket with glycine betaine. The coordination of DMG requires Trp203 and Trp384 while coordination of ectoine requires Trp203, Tyr211 and Trp384. These results suggest that coordination of DMG and ectoine cannot be as easily accommodated by alternate residues as can glycine betaine.

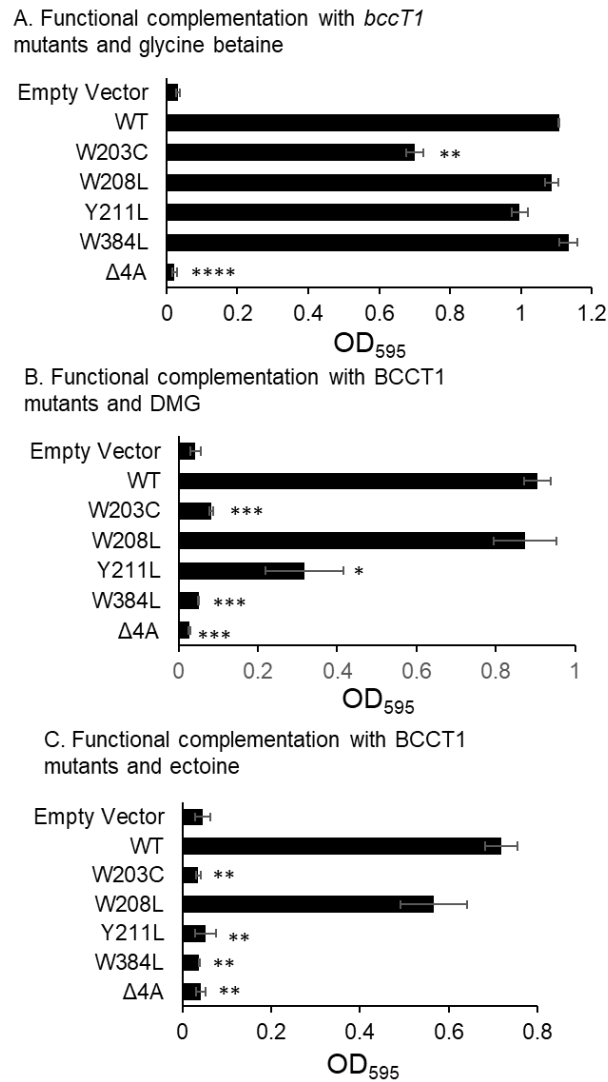


**Figure 40 Functional complementation of *E. coli* with BccT1 mutants**  
 Functional complementation of *E. coli* MKH13 with wild type and BccT1 mutants grown in the presence of (A) glycine betaine, (B) DMG, and (C) ectoine. Strains were grown for 24 hours in the presence of 500  $\mu$ M exogenous compatible solutes and the final optical density (OD<sub>595</sub>) was compared to that that of the strain harboring wild type BccT1 (pBAVP1456). Mean and standard error of at least two biological replicates are shown. Statistics were calculated using a Student's t-test (\*\*,  $P < 0.01$ ; \*\*\*,  $P < 0.001$ ; \*\*\*\*,  $P < 0.0001$ ).

### Distribution of BCCT1

The BccT1 protein is 562 amino acids and is present in all sequenced *V. parahaemolyticus* genomes (>800 genomes). A highly homologous protein is also present in all *V. alginolyticus*, *V. antiquarius*, *V. diabolicus* strains (95% sequence identity), *V. natriegens*, *V. nersis* (90% sequence identity), as well as *V. harveyi* and *V. campbellii* sequenced strains (86% sequence identity). In general, phylogenetic analysis indicated that BccT1 is conserved within the Harveyi clade and when present in other clades it is present in all strains of each species. Overall, within the family *Vibrionaceae*, BccT1 is present in 35 *Vibrio* species and in 11 *Photobacterium* species (**Figure 41**). It is of interest to note that in all species, the residues corresponding to Trp 203, Trp 208, Tyr 211, and Trp 384, which coordinate substrates, are conserved (data not shown), suggesting an ability to uptake a range of osmolytes in these species.

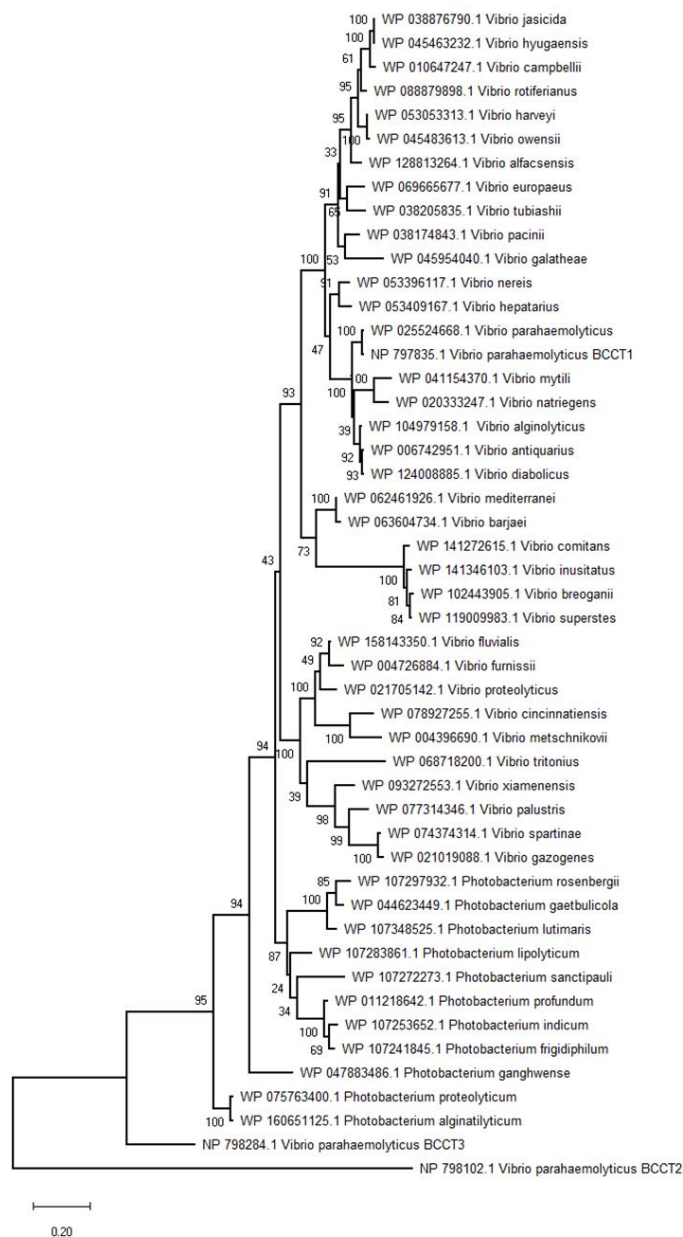


**Figure 41** **Phylogenetic distribution of BccT1**

Phylogenetic tree was inferred by using the Maximum Likelihood method and Le\_Gascuel\_2008 model in MEGAX. The tree with the highest log likelihood (-10453.23) is shown. The percentage of trees in which the associated taxa clustered together is shown next to the branches. This analysis involved 49 amino acid sequences and a total of 525 positions.

## Discussion

Here we have demonstrated that *V. parahaemolyticus* can utilize additional compatible solutes DMG, GABA, TMAO, and creatine amongst others that have not been previously reported as osmolytes for *Vibrio* species. BccT1, BccT2 and BccT3 are capable of uptake of DMG, which is a highly effective osmoprotectant for *V. parahaemolyticus* and also is a potent osmoprotectant for *V. vulnificus*, *V. harveyi*, *V. cholerae* and *V. fluvialis*. DMG is the N-dimethyl derivative of glycine while glycine betaine is the N-trimethyl derivative. Some halophilic bacteria were shown to accumulate DMG, an intermediate compound produced during *de novo* biosynthesis (20, 47-54). Additionally, DMG is an intermediate of aerobic glycine betaine catabolism, therefore should be available in the environment (63-67). DMG was found to be suitable for osmotic adaptation on its own, without modifications by bacteria (20). As stated previously, DMG is known to be transported by MFS family and ABC-family transporters (63, 219). Here, we demonstrated that the BCCT family can also uptake DMG.

BccT1 and BccT2 effectively transport DMG when expressed in a heterologous *E. coli* background (**Figure 33**). However, in the native background, a *V. parahaemolyticus* strain expressing only BccT2 is fully rescued to wild-type levels by the presence of DMG while a strain expressing BccT1 is only partially rescued (**Figure 32A and 32B**). For our growth analyses, cells are first grown in low salinity (1% NaCl) and then upshocked into high salinity (6% NaCl). We have shown previously that *bcct2* is not induced by high salinity and has a basal level of transcription in the cell, whereas *bcct1* expression is repressed in low salinity conditions (60, 61). Therefore, in a strain expressing only *bcct2*, expression is constitutively active in low salinity, which may allow for more rapid adaptation to

high salinity conditions via uptake of DMG, resulting in a reduced lag phase. In *C. glutamicum*, the transporter EctP is not induced by external osmolarity and EctP transport capacity is maximal at low osmolarity and does not increase in high osmolarity conditions (221). EctP also showed a broad substrate spectrum with moderate to low affinity for these substrates, which, taken together, suggested that EctP acts as a rescue system that is available at low osmolarity, ensuring that cells can respond to osmotic stress (221). The same could be true of BccT2 in *V. parahaemolyticus*, which has a broad substrate range, including glycine betaine, choline, DMG, and proline and therefore could act as a rescue system to scavenge available compatible solutes in the event of osmotic stress.

DMG was not shown previously to be transported by the BCCT family of carriers and the amino acid residues important for uptake of DMG by a BCCT are unknown. Our *in silico* docking study showed that glycine betaine was coordinated by identical residues in the binding pocket of BccT1 (**Figure 39B**) as have been previously reported for CgBetP (86, 199). Coordination of DMG by BccT1 was identical to that of glycine betaine (**Figure 39C**). Likewise, an ATP-binding cassette (ABC) transporter, OpuAC, from *Bacillus subtilis* has been reported to interact very similarly with glycine betaine (PDB ID 2B4L) and a sulfonium analog of DMG, dimethylsulfonioacetate (DMSA) (PDB ID 3CHG) (224, 225). Our mutagenesis studies demonstrated that glycine betaine, DMG and ectoine are coordinated in the same binding pocket of BccT1, but the residues required for coordination are strict for DMG and ectoine, while glycine betaine may be accommodated by alternate residues in single amino acid mutants. It was demonstrated previously in an ABC-type transporter, that while replacement of a single aromatic residue in the binding pocket

results in decreased affinity of the protein for glycine betaine, the substrate is still coordinated with reasonable affinity. Only when any combination of two residues was mutated was transport completely abolished (226). We did not see a reduction in the ability of *E. coli* MKH13 to grow when only one residue is mutated, and uptake of glycine betaine was only completely abolished when all four residues were mutated. This is likely due to coordination of glycine betaine at alternate positions within the binding pocket that do not affect the overall growth ability of *E. coli* MKH13, but may affect the affinity of BccT1 for glycine betaine. Comparative protein analyses also demonstrated that in other *Vibrio* species with BccT1 homologs, the residues that coordinate glycine betaine, DMG and ectoine are conserved. There is a very high percent identity shared with BccT1 amongst BCCT-family transporters in these species and therefore the ability of these transporters to uptake a broad range of substrates is most likely conserved.

All of the substrates that *V. parahaemolyticus* was demonstrated to uptake are available in the marine environment, including glycine betaine, choline, DMG, and ectoine (13, 64, 65, 74). Five of the six compatible solute transporters encoded by *V. parahaemolyticus* are induced by high salinity, and collectively take up a broad range of compatible solutes (60, 61). Although there is redundancy in the compounds taken up by each BccT, the ability to uptake many different compatible solutes likely provides *V. parahaemolyticus* and other *Vibrio* species with a fitness advantage.

Members of the BCCT family are widespread among bacteria, present in both Gram-positive and Gram-negative bacteria as well as Archaea. For example, using the Interpro database (<http://www.ebi.ac.uk/interpro/>) and IPR000060 for BccT as a search, 23,000 BccT proteins fall within the domain Bacteria, 604 BccT proteins

within the Archaea and 78 BccTs within the Eukaryota. Of the 604 Archaea representatives, 593 were from the Stenosarchaea group of which 549 were within *Halobacteria* suggesting an important function in osmotolerance. Surprisingly, there have been no studies on BCCT function from representatives of Archaea or Eukaryota to date.

Table 6 Strains and plasmids used in this study

Strain	Genotype or description	Reference or Source
<i>Vibrio</i>		
<i>parahaemolyticus</i>		
RIMD2210633	O3:K6 clinical isolate, Str <sup>r</sup>	(104, 157)
<i>V. cholerae</i> N16961	O1, El Tor strain, Bangladesh, Clinical, 1975	(227)
<i>V. vulnificus</i> YJ016	Clinical isolate	(228)
<i>V. fluvialis</i> 606	[NCTC 11327] Clinical isolate	(229)
<i>V. harveyi</i> 393	Isolated from barramundi in Australia	(230)
<i>ΔectB</i>	RIMD2210633 <i>ΔectB</i> (VP1721), Str <sup>r</sup>	(45)
SOYBCCT124	RIMD2210633 <i>ΔVP1456 ΔVP1723 ΔVPA0356</i> , Str <sup>r</sup>	(60)
SOYBCCT123	RIMD2210633 <i>ΔVP1456 ΔVP1723 ΔVP1905</i> , Str <sup>r</sup>	(60)
SOYBCCT134	RIMD2210633 <i>ΔVP1456 ΔVP1905 ΔVPA0356</i> , Str <sup>r</sup>	(60)
SOYBCCT234	RIMD2210633 <i>ΔVP1723 ΔVP1905 ΔVPA0356</i> , Str <sup>r</sup>	(60)
SOYBCCT1342	RIMD2210633 <i>ΔVP1456ΔVP1723ΔVP1905ΔVPA0356 Str<sup>r</sup></i>	(60)
<i>Escherichia coli</i>		
DH5α λpir	<i>Δlac pir</i>	ThermoFisher Scientific
β2155 λpir	<i>ΔdapA::erm pir</i> for bacterial conjugation	(163)
MKH13	MC4100 ( <i>ΔbetTIBA</i> ) <i>Δ(putPA)101</i> <i>Δ(proP)2 Δ(proU)</i> ; Sp <sup>r</sup>	(94)
<b>Plasmids</b>		
pBAD33	Expression vector; <i>araBAD</i> promoter; Cm <sup>r</sup> ; p15a origin	(231)
pBAVP1456	pBAD33 harboring full-length VP1456	This study
pBAVP1723	pBAD33 harboring full-length VP1723	(60)
pBAVP1905	pBAD33 harboring full-length VP1905	(60)
pBAVPA0356	pBAD33 harboring full-length VPA0356	This study
pBAVP1456W203C	pBAD33 harboring full-length VP1456 with Trp203Cys mutation	This study
pBAVP1456W208L	pBAD33 harboring full-length VP1456 with Trp208Lys mutation	This study
pBAVP1456Y211L	pBAD33 harboring full-length VP1456 with Tyr211Lys mutation	This study
pBAVP1456W377L	pBAD33 harboring full-length VP1456 with Trp377Lys mutation	This study
pBAVP1456-3	pBAD33 harboring full-length VP1456 with Trp203Ala, Trp208Ala, Tyr211Ala mutations	This study

Table 6 (continued)

pBAVP1456-4	pBAVP1456-3 harboring full-length VP1456 with Trp377Ala mutation	This study
-------------	--	------------

---

Table 7 Primers used in this study

Use and Primer	Sequence (5'-3')	Length (bp)
<b>Expression primers</b>		
VP1456 Fwd	tgggctagcgaattcgagctTTTGCTGTAAATATGCAAT AAAAGTG	1740
VP1456 Rev	ggatccccgggtaccgagctTTAGCGGTAAGCGGAAAG	
VPA0356	tgggctagcgaattcgagctAGCGGCTTTTTGAACATC	1671
VPA0356	ggatccccgggtaccgagctTTAAACCAAACCTTGATC C	
<b>Mutagenesis primers</b>		
BCCT1 TRP203CYS F	CATGTTTCACtgcGGTGTTCACGGTTGGAG	7096
BCCT1 TRP203CYS R	GTCGCGCCCATCGCGAGT	
BCCT1 TRP208LEU F	TGTTACAGGTctgAGTATTTACGC	7096
BCCT1 TRP208LEU R	CCCCAGTGAAACATGGTC	
BCCT1 TYR211LEU F	TTGGAGTATTctgGCCCTTGTTGCGTTG	7096
BCCT1 TYR211LEU R	CCGTGAACACCCCAGTGA	
BCCT1 TRP384LEU F	GTGGGTATCTctgTCTCCGTTTG	7096
BCCT1 TRP384LEU R	CAAGCCCAGTAGAACACTG	
BCCT1 203208211ALA F	tgcgagtattgcgGCCCTTGTTGCGTTGGCG	7096
BCCT1 203208211ALA R	ccgtgaacaccgcGTGAAACATGGTCGCGCC	
BCCT1 TRP384ALA F	GTGGGTATCTgcgTCTCCGTTTG	7096
BCCT1 TRP384ALA R	CAAGCCCAGTAGAACACTG	

Table 8 Results of the docking study showing free energy change upon substrate binding and a list of BccT1 residues mediating interactions with each substrate.

	<b>Glycine Betaine</b>	<b>DMG</b>	<b>Ectoine</b>
<b>Binding free energy (kcal/mol)</b>	-4.8	-4.4	-6.1
<b>Hydrogen bonding interactions</b>	Ilu160, Gly161, Ser266	Ilu160, Gly161, Ser266	Trp203, Tyr211
<b>Van der Waals interactions</b>	Trp203, Trp208, Tyr211, Trp380, Trp381, Trp384	Trp203, Trp208, Tyr211, Trp380, Trp381, Trp384	Trp208, Trp380, Trp381, Trp384

## Chapter 5

# UTILIZATION OF DIMETHYLSULFONIOPROPIONATE (DMSP) AS AN OSMOLYTE BY *VIBRIO SPECIES*

The work in this chapter is in preparation for publication in *Applied and  
Environmental Microbiology*

Utilization of Dimethylsulfoniopropionate (DMSP) as an osmolyte by *Vibrio*  
species

Gregory GJ and Boyd EF

### Introduction

Compatible solutes (osmolytes) are accumulated by bacteria to maintain the turgor pressure of the cell in response to high external osmolarity (15, 78, 167). Compatible solutes include sugars and amino acids and include glycine betaine, ectoine, proline, glutamate, glycerol and trehalose (5, 13-18). Compatible solutes, as the name suggests, are compounds that can be accumulated to high levels and are compatible with the molecular machinery and processes of the cell. Osmolytes allow organisms to continue to grow and divide in unfavorable environments that include changes in osmolarity and temperature shifts (10, 63, 157, 158, 232-237). The uptake and biosynthesis of compatible solutes in response to osmotic stress has been studied extensively in *Escherichia coli* and *Bacillus subtilis*, which can biosynthesize glycine

betaine from choline and both species can uptake glycine betaine and choline amongst others (10, 81, 238-249).

Organisms that live in marine environments have adapted to grow optimally in high NaCl conditions and also have adapted to cope with fluctuations in salinity to maintain cellular homeostasis. Members of the family *Vibrionaceae* have the ability to grow optimally at 0.5 M-1.0 M NaCl, but regularly encounter fluctuations in osmolarity ranging from 0.1M to 1.5M (45). One of the key response of *Vibrio* species to fluctuations in osmolarity is the biosynthesis of the osmolytes ectoine and glycine betaine or the rapid uptake of these osmolytes from the environment using as many as six osmolyte transporters (45, 59, 60). *Vibrio parahaemolyticus*, a halophile ubiquitous in the marine environment, biosynthesizes glycine betaine (encoded by *betIBA*) from exogenously supplied choline and ectoine (encoded by *ectABC-aspK*) from aspartic acid *de novo* (45, 59). *Vibrio parahaemolyticus* encodes two osmolyte ATP Binding Cassette (ABC)-family transporters, ProU1 (*proVWX*) and ProU2 (*proXWV*), and four Betaine Carnitine Choline Transporter (BCCT) family transporters, BccT1 (VP1456), BccT2 (VP1723), BccT3 (VP1905), and BccT4 (VPA0356) (45) (**Figure 42**). All BCCTs described have 12 predicted *trans*-membrane (TM)  $\alpha$ -helical domains, TM1 to TM12, which is a defining feature in their classification (81, 83, 85, 198, 250, 251). In addition to the 12 TM domains, these proteins contain hydrophilic N- and C- terminal tails of varying length (81, 83, 85, 198). Homologues of BccT1 to BccT4 are present in many *Vibrio* species such as *V. alginolyticus*, as well as *V. harveyi* and *V. splendidus*, both of which also contain two additional BccTs. However, some species such as *V. vulnificus*, *V. cholerae* and *Aliivibrio fischeri* encode only a homolog of BccT3 (45). We have previously

demonstrated that the *bccT1*, *bccT3*, and *bccT4* genes in *V. parahaemolyticus* are induced by increased salinity (60, 61). Together the BCCTs in *V. parahaemolyticus* transport glycine betaine, choline, dimethylglycine (DMG), ectoine, and proline, with some redundancy in the substrates transported by each BCCT (60).

Dimethylsulfoniopropionate (DMSP) is an organosulfur compound abundant in marine surface waters, produced by phytoplankton and some halophytic vascular plants in large quantities and used by these primary producers as an osmoprotectant, thermoprotectant and antioxidant (69-73). DMSP is an important component of the global geochemical sulfur cycle as a precursor for dimethylsulfide (DMS). DMS is a climate active gas that is produced from the degradation of oceanic DMSP, releasing sulfur-containing aerosols into the atmosphere (71, 72). It was also recently reported that DMSP is abundant in marine and estuarine sediments, and is produced by bacteria in these environments (252). Algal blooms that have high production of DMSP are sources of reduced sulfur and carbon for many marine heterotrophic bacteria (70, 253-257). DMSP-catabolizing bacteria are mainly confined to the marine alpha-proteobacteria, SAR11, SAR116 and Roseobacter (258-265). Given that many species of the *Vibrionaceae* interact and associate with DMSP producers, surprisingly there are no studies on the use of DMSP as an osmoprotectant in these bacteria, or in bacteria in general (19, 78, 266, 267). The first direct evidence that DMSP can be used as an osmoprotectant for bacteria came from a study in *E. coli*, which does not encounter this compound naturally. Osmotically stressed *E. coli* responded to nanomolar amounts of DMSP; the ABC-family ProU transporter was shown to be important for DMSP uptake to relieve salt stress (19). A more recent study in *B. subtilis* showed that DMSP was an osmoprotectant in this species and transported into

the cell with high affinity by the ABC-family OpuC transporter (266). Sun and colleagues demonstrated that BCCT carriers linked to DMSP cleavage pathways could uptake DMSP in a heterologous *E. coli* background as an osmolyte, suggesting that these transporters are potential DMSP transporters in their native background (267). Outside of these studies, little is known about bacterial utilization of DMSP as an osmolyte or the bacterial response to this abundant marine compound.

*Vibrio* species are abundant in marine environments, in the water column, sediments and associated with marine flora and fauna. Many species are halophiles that thrive in high salinity environments. The role of DMSP, an abundant osmolyte especially during algal blooms, as an osmoprotectant in marine bacteria has not been examined previously. We use *V. parahaemolyticus* as a model organism to study marine halophiles, which can grow in 0.1M NaCl to 1.5M NaCl and contains at least six transporters for the uptake of osmolytes. First, we examined whether a *V. parahaemolyticus* *ectB* mutant, which cannot grow in high NaCl in the absence of exogenous osmolyte, could be rescued in M9 minimal media glucose (M9G) supplemented with DMSP. Then we investigated the effectiveness of DMSP as an osmoprotectant in several *Vibrio* species to determine if this was a general trait. We determined the transporters responsible for uptake of DMSP into the cell in *V. parahaemolyticus*. We demonstrated that a BCCT-family transporter BccT2 was required for efficient uptake of DMSP by *V. parahaemolyticus*. Phylogenetic analysis of the distribution of BccT2 indicates that the ability to uptake DMSP is prevalent among the *Vibrionaceae*.



source. *E. coli* strains were grown either in LB supplemented with 1% NaCl (LB1%) or M9G supplemented with 1% NaCl (M9G1%). All strains were grown at 37 C with aeration. Antibiotics were used at the following concentrations, as necessary: chloramphenicol (Cm), 25 µg/mL.

### Growth analysis

Wild type RIMD2210633 or an in-frame deletion mutant of *ectB* were grown overnight in M9G1%. Cultures were subsequently diluted 1:50 into fresh medium and grown for five hours. For growth analysis in individual compatible solutes, WT,  $\Delta ectB$  mutant and quadruple  $\Delta bccT1\Delta bccT3\Delta bccT4\Delta bccT2$  mutant (*bccT* null) strains were grown overnight in M9G1%. Cultures were subsequently diluted 1:50 into fresh medium and grown for five hours to late exponential phase. Exponential cultures were then diluted 1:40 into 200 µL of M9G6% medium with and without exogenous compatible solutes in a 96-well microplate and grown at 37° C with intermittent shaking for 24 hours. Dimethylsulfonylpropionate (DMSP) was added to a final concentration of 500 µM. Growth analysis was repeated following the above procedure with each of four triple *bccT* deletion mutants,  $\Delta bccT2\Delta bccT3\Delta bccT4$ ,  $\Delta bccT1\Delta bccT3\Delta bccT4$ ,  $\Delta bccT1\Delta bccT2\Delta bccT4$ ,  $\Delta bccT1\Delta bccT2\Delta bccT3$ , to determine which BCCT was responsible for transport of DMSP.

### Functional complementation of *E. coli* strain MKH13 with VP1456, VP1723, VP1905, and VPA0356

*E. coli* MKH13 strains containing pBAVP1456, pBAVP1723, pBAVP1905 or pBAVPA0356 were grown overnight in minimal media supplemented with 1% NaCl and 20 mM glucose (M9G1%) with chloramphenicol and subsequently diluted 1:100 into M9G supplemented with 4% NaCl (M9G4%) and 500 µM of the indicated

compatible solute and chloramphenicol. Expression of each BCCT was induced with 0.01% arabinose and functional complementation was determined by measuring OD<sub>595</sub> after 24 hours growth at 37°C with aeration. Growth was compared to that of an MKH13 strain harboring empty pBAD33, which cannot grow in M9G4% without exogenous compatible solutes. Statistics were calculated using a Student's t-test.

### Bioinformatics and phylogenetic analyses

Phylogenetic analysis was conducted using *V. parahaemolyticus* proteins VP1456 (Q87PP5.1), VP1723 (Q87NZ5.1), VP1905 (Q87NG3.1) and VPA0356 (Q87J97.1) as a seeds to identify all homologs within the family Vibrionaceae with completed genome sequences available. Representative strains from each species containing a BCCT homolog were downloaded from NCBI and aligned using the Clustal W algorithm (180). A neighbor-joining tree was constructed in MEGA X using aligned protein sequences with a bootstrap value of 1000 (181, 182). *V. vulnificus* VV0783 (BAC93547.1), *V. fluvialis* (OJ160339.1), *V. harveyi* (WP\_00542005.1), and *Halomonas* sp. HTNK1 (ACV84066.1) were downloaded from the NCBI database and aligned using the Clustal W algorithm (180). Aligned sequences were displayed and annotated using ESPript (<http://esprict.ibcp.fr/ESPript/cgi-bin/ESPript.cgi>) (215).

## Results

*Vibrio parahaemolyticus* can utilize dimethylsulfoniopropionate (DMSP) as a compatible solute.

DMSP is produced in large quantities by phytoplankton and used by these primary producers as an osmolyte. However, the role of DMSP as an osmolyte for

marine bacteria remains largely unknown. We examined the halophile *V. parahaemolyticus* for its ability to grow in high salinity using DMSP as an osmolyte. The *V. parahaemolyticus* *ectB* deletion mutant, which is unable to biosynthesize ectoine *de novo*, cannot grow in high NaCl growth conditions in the absence of exogenous osmolytes. We examined grow of the *ectB* mutant in M9 minimal media supplemented with glucose and 6% NaCl (M9G 6%NaCl), in the presence and absence of DMSP. Growth pattern analysis after 24 h showed that the lag phase of the wild-type strain without exogenous compatible solutes is approximately six hours, while the  $\Delta ectB$  mutant did not grow (**Figure 43**). However, in M9G 6%NaCl supplemented with DMSP the *ectB* mutant grew similarly to wild type, demonstrating that *V. parahaemolyticus* can uptake and utilize DMSP as an osmolyte (**Figure 43**).

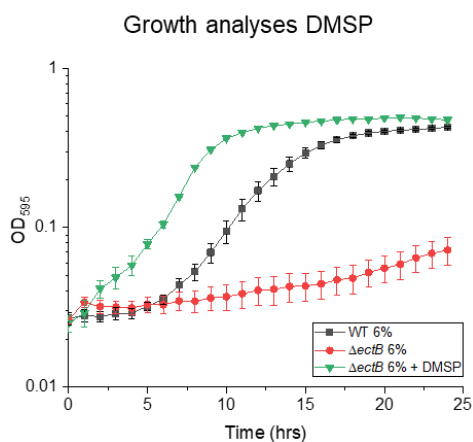


**Figure 43 Growth analyses with DMSP**  
Growth analysis of wild type RIMD and an *ectB* mutant was conducted in M9G supplemented with 6% NaCl and DMSP. Optical density (OD<sub>595</sub>) was measured every hour for 24 hours; mean and standard error of at least two biological replicates are displayed.

### DMSP is utilized as an osmolyte by *Vibrio* species

To determine whether other *Vibrio* species can utilize DMSP as an osmolyte, we tested DMSP uptake in *V. harveyi* 393, *V. fluvialis* NCTC11327, *V. vulnificus* YJ016, and *V. cholerae* N16961. The growth of *V. harveyi* 393, *V. vulnificus* YJ016, and *V. cholerae* N16961 was examined in M9G 4%NaCl and *V. fluvialis* NCTC11327 in M9G 5%NaCl, with and without added DMSP (**Figure 44A-D**). The growth of *V. harveyi* 393 in M9G 4%NaCl showed a 10h lag phase, however the addition of DMSP resulted in a lag phase of less than 2 h (**Figure 44B**). We found that *V. fluvialis* and *V. cholerae* cells has a reduced lag phase and reached a higher OD in the presence of DMSP (**Figure 44A and 44D**). *Vibrio vulnificus* did not grow in M9G 4%NaCl, however the addition of DMSP rescued growth, but cells had a 13h lag phase suggesting uptake was not efficient (**Figure 44C**). These data demonstrated that all *Vibrio* species tested can utilize DMSP as an osmolyte.

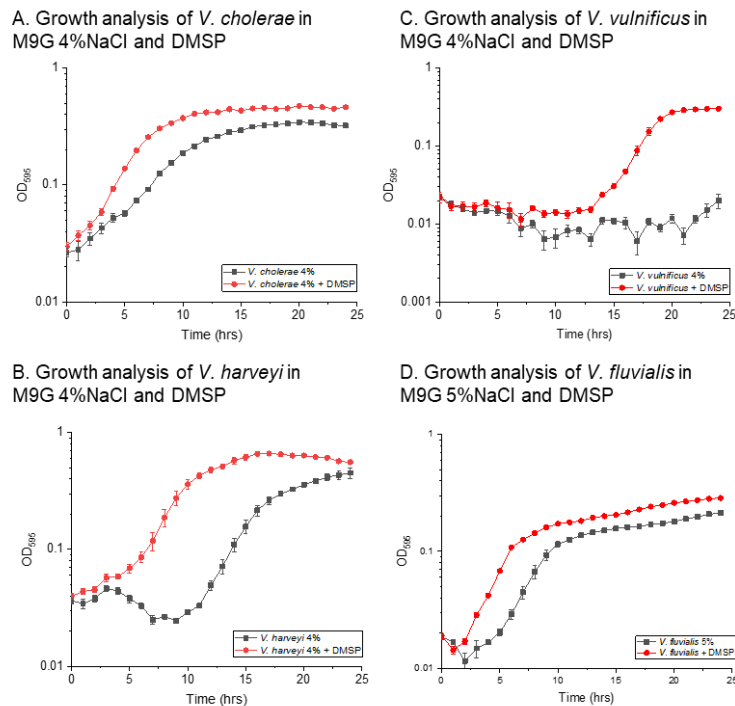


**Figure 44 Growth analyses of *Vibrio* species with DMSP.** Growth analyses of (A) *V. cholerae* N16961, (B) *V. harveyi* 393, and (C) *V. vulnificus* YJ016 were conducted in M9G 4% NaCl with and without exogenous DMSP. Growth analyses of (D) *V. fluvialis* was conducted in M9G 5% NaCl with and without exogenous DMSP. Optical density (OD<sub>595</sub>) was measured every hour for 24 hours. Mean and standard error of two biological replicates are shown.

DMSP is not a carbon source for *V. parahaemolyticus*

Some marine bacteria are able to catabolize DMSP (268-271). To ensure that the reduced lag phase in each *Vibrio* species tested was not due to use of DMSP as a carbon source, we grew each strain in M9 minimal media with DMSP as the sole carbon source, utilizing M9G as a control. None of the *Vibrio* species tested grew with DMSP as the sole carbon source and all grew on M9G, which indicated that they cannot catabolize DMSP (Figure 45). This data demonstrated that DMSP is a *bona fide* compatible solute for the *Vibrio* species tested.

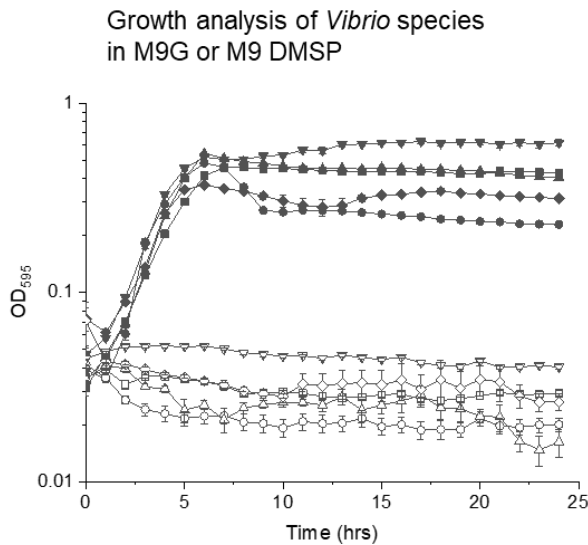


**Figure 45 Growth of *Vibrio* species with DMSP as sole carbon source.** Growth analyses of *V. cholerae* N16961 (squares), *V. fluvialis* (circles), *V. harveyi* 393 (up triangles), *V. parahaemolyticus* RIMD2210633 (down triangles), and *V. vulnificus* YJ016 (diamonds) were conducted in M9 with DMSP (open shapes) as the sole carbon source or M9 with glucose (solid shapes) as the sole carbon source. Optical density (OD<sub>595</sub>) was measured every hour for 24 hours. Mean and standard error of two biological replicates are shown.

#### A BCCT transporter is required for DMSP uptake

Uptake of DMSP as a catabolite by a BCCT-family transporter in *Halomonas* *sp.* HTNK1 has been reported (265). Therefore, we examined whether the four BccTs in *V. parahaemolyticus* were responsible for the uptake of DMSP into the cell. To accomplish this, first we grew wild type and a *bccT* null strain in the presence of DMSP in M9G 6% NaCl. The lag phase of the wild-type strain was reduced from ~6 hours to ~3 hours after growth in the presence of DMSP, which indicates that DMSP is a highly effective osmoprotectant for *V. parahaemolyticus* (**Figure 46**). However, the *bccT* null mutant did not exhibit a reduced lag phase in the presence of DMSP

(**Figure 46**). This indicated that at least one of the BCCTs is responsible for transport of DMSP into the cell. *V. parahaemolyticus* contains two ABC-type osmolyte transporters, ProU1 and ProU2; however, given that a *bcct* null mutant, which encodes wild-type copies of both ProU systems, did not exhibit a reduced lag phase, it is likely that neither ProU plays a role in uptake of DMSP.

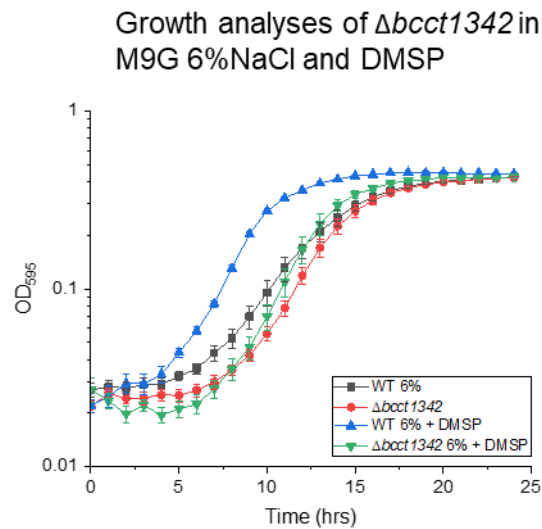


**Figure 46 Growth analysis of *bcct* null strain with DMSP.** Growth analysis of wild-type RIMD and a  $\Delta bcct1\Delta bcct3\Delta bcct4\Delta bcct2$  mutant was conducted in M9G supplemented with 6% NaCl and DMSP. Optical density (OD<sub>595</sub>) was measured every hour for 24 hours; mean and standard error of at least two biological replicates are displayed.

To determine which of the BCCTs were responsible for uptake of DMSP, we utilized four triple *bcct* deletion mutants, each containing only one functional *bcct* gene. The  $\Delta bcct2\Delta bcct3\Delta bcct4$  mutant, which expresses only *bcct1* (VP1456), had a slight reduction in lag phase and had a faster growth rate through the exponential

phase when grown in the presence of DMSP. This suggests that BccT1 can transport DMSP with low efficiency (**Figure 47A**). The  $\Delta bccT1\Delta bccT3\Delta bccT4$  mutant, which expresses only *bccT2* (VP1723), showed a nearly identical reduction in lag phase as the wild-type strain, which indicated that it also transports DMSP into the cell, but with higher efficiency than *bccT1* (**Figure 47B**). The  $\Delta bccT1\Delta bccT2\Delta bccT4$  mutant, which expresses only *bccT3* (VP1905), did not have a reduced lag phase in the presence of DMSP (**Figure 47C**), which indicated that BccT3 is not responsible for transport of DMSP. The  $\Delta bccT1\Delta bccT2\Delta bccT3$  mutant, which expresses only *bccT4* (VPA0356), had a slight reduction in lag phase in the presence of DMSP (**Figure 47D**), which suggested that BccT4 may transport DMSP with very low efficiency.

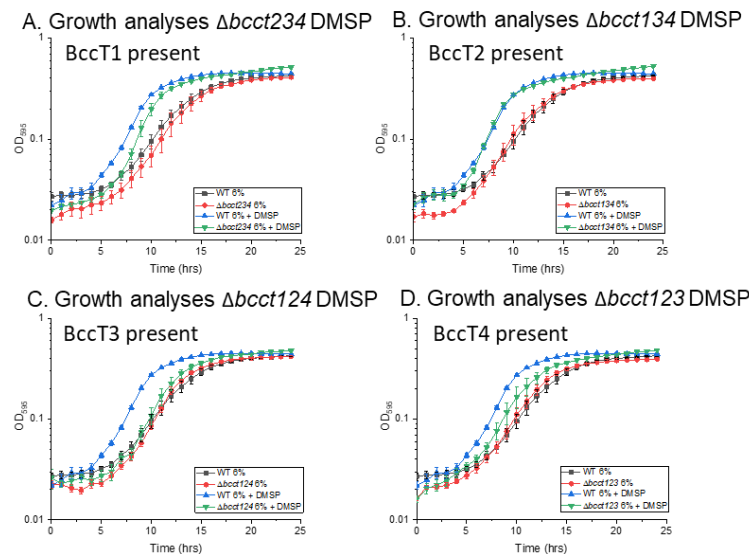


**Figure 47 Growth analyses of triple *bccT* mutants with DMSP.** Growth analysis of wild-type (WT) and (A)  $\Delta bccT2\Delta bccT3\Delta bccT4$ , (B)  $\Delta bccT1\Delta bccT3\Delta bccT4$ , (C)  $\Delta bccT1\Delta bccT2\Delta bccT4$ , or (D)  $\Delta bccT1\Delta bccT2\Delta bccT3$  in M9G6% with and without the addition of exogenous DMSP. Optical density ( $OD_{595}$ ) was measured every hour for 24 hours; mean and standard error of at least two biological replicates are displayed.

Next, we examined DMSP transport capabilities of each BccT using functional complementation in *E. coli* strain MKH13, a strain that lacks any osmolyte transporters or biosynthesis systems (94). Strains were grown in M9G with 4% NaCl in the presence of DMSP, with an arabinose-inducible expression plasmid, pBAD33, harboring a full-length copy of a single *bccT*. We measured the optical density (OD<sub>595</sub>) after 24 hours for each complemented strain and compared to the empty vector strain. Only the BccT2-complemented strain (pBAVP1723) could grow in the presence of DMSP (**Figure 48A**). The BccT1-complemented strain (pBAVP1456) was unable to grow in the presence of DMSP (**Figure 48A**), although the *V. parahaemolyticus* strain only containing BccT1 appeared to transport DMSP, albeit with low efficiency. To confirm that *bccT1* is expressed and produces a functional protein in *E. coli*, we examined the ability of BccT1 to uptake glycine betaine, a known substrate for this transporter. In this assay, *E. coli* MKH13 complemented with *bccT1* (pBAVP1456) grew with the addition of glycine betaine, which indicated BccT1 is functional, and suggested that BccT1 is not an efficient transporter of DMSP (**Figure 48B**). Taken together, this lead us to conclude that BccT2, rather than BccT1, is the main transporter of DMSP into the cell.

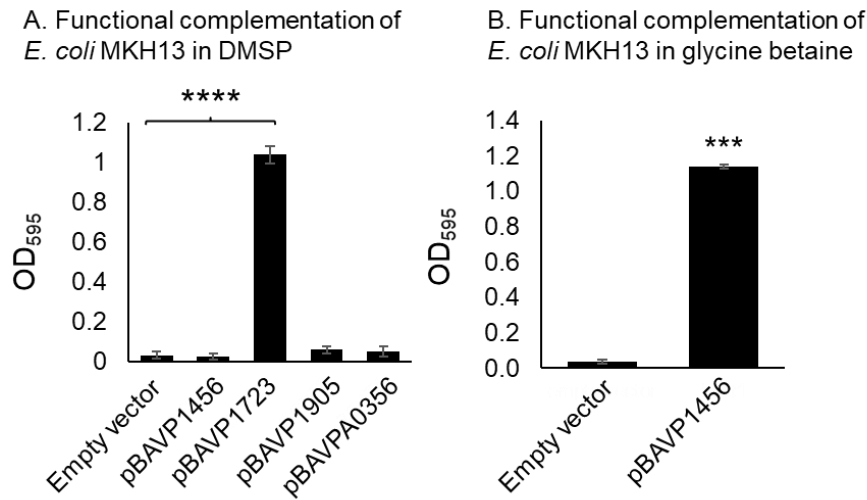


**Figure 48 Functional complementation of *E. coli* MKH13 with *bccT*.** *E. coli* strain MKH13, which has deletions in all compatible solute transporters, was grown in M9G supplemented with 4% NaCl and functionally complemented with (A) BCCT1, BCCT2, BCCT3, or BCCT4, each expressed from an arabinose-inducible expression plasmid, pBAD33. Strains were grown for 24 hours in the presence of 500  $\mu$ M DMSP and the final optical density (OD<sub>595</sub>) was compared to that of a strain harboring empty pBAD33. (B) *E. coli* MKH13 complemented with BCCT1 was grown in presence of 500  $\mu$ M glycine betaine and compared to a strain harboring empty pBAD33. Mean and standard error of at least two biological replicates are shown. Statistics were calculated using a Student's t-test (\*\*\*\*,  $P < 0.0001$ ).

#### Distribution and Phylogenetic Analysis

To the best of our knowledge, there are no reports of DMSP uptake via a BCCT family transporter for use as an osmoprotectant. Only BccT2 is capable of efficiently transporting DMSP in *V. parahaemolyticus*. Here, we have shown that multiple species of *Vibrio* can transport and utilize DMSP as a highly effective osmoprotectant. However, there is limited distribution of BccT2 among *Vibrio* species; for example BccT2 is absent from *V. vulnificus*, which can uptake DMSP (Figure 49). We identified an additional BCCT in *V. vulnificus*, which we named

BccT5 that has less than 30% identity with the BccTs present in *V. parahaemolyticus*. This transporter showed homology to a BCCT transporter from a *Halomonas sp.* strain HTNK1 named DddT, which is required for DMSP uptake for catabolism in this species (**Figure 50**). *V. fluvialis* and *V. harveyi* also possess a transporter that is homologous BccT5. Protein sequences of BccT5 found in *V. vulnificus*, *V. fluvialis*, and *V. harveyi* were aligned with DddT (**Figure 50**). These proteins have substitutions in a residue thought to be responsible for sodium symport and substrate specificity and a residue thought to be an alternate residue for coordination of trimethylammonium compounds in conformational changes during the transport cycle (**Figure 50**) (86). The phylogeny of each of the four BCCTs encoded by *V. parahaemolyticus* and BccT5 present in *V. vulnificus*, was also examined. The phylogeny shows that BccT1 and BccT2 are more closely related to each other than to the other BccT proteins and BccT3 clusters close to BccT1 and BccT2. However, BccT4 is distantly related to the other three. BccT5 is also found on a separate divergent branch and clusters next to DddT (**Figure 51**). These data suggest that the BCCT transporters in *Vibrio* have very different evolutionary histories.

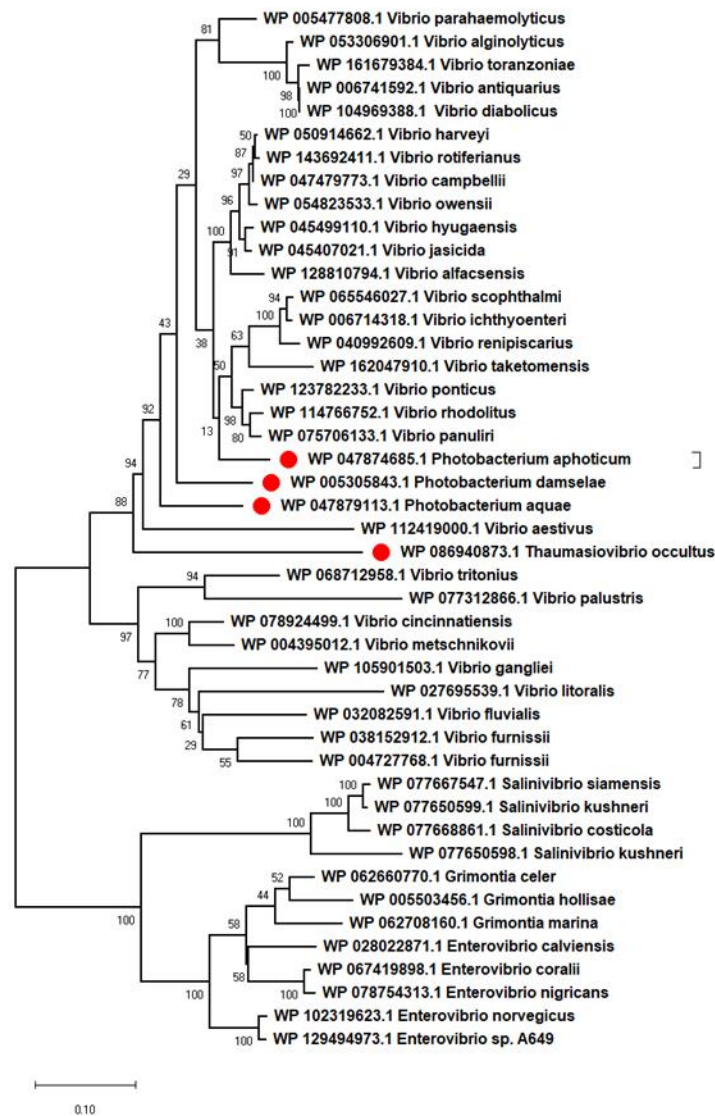


**Figure 49** Phylogenetic analysis of BccT2 distribution within Vibrionaceae. *V. parahaemolyticus* BccT2 sequence was used as a seed for BLASTP to identify homologs within the Vibrionaceae family.

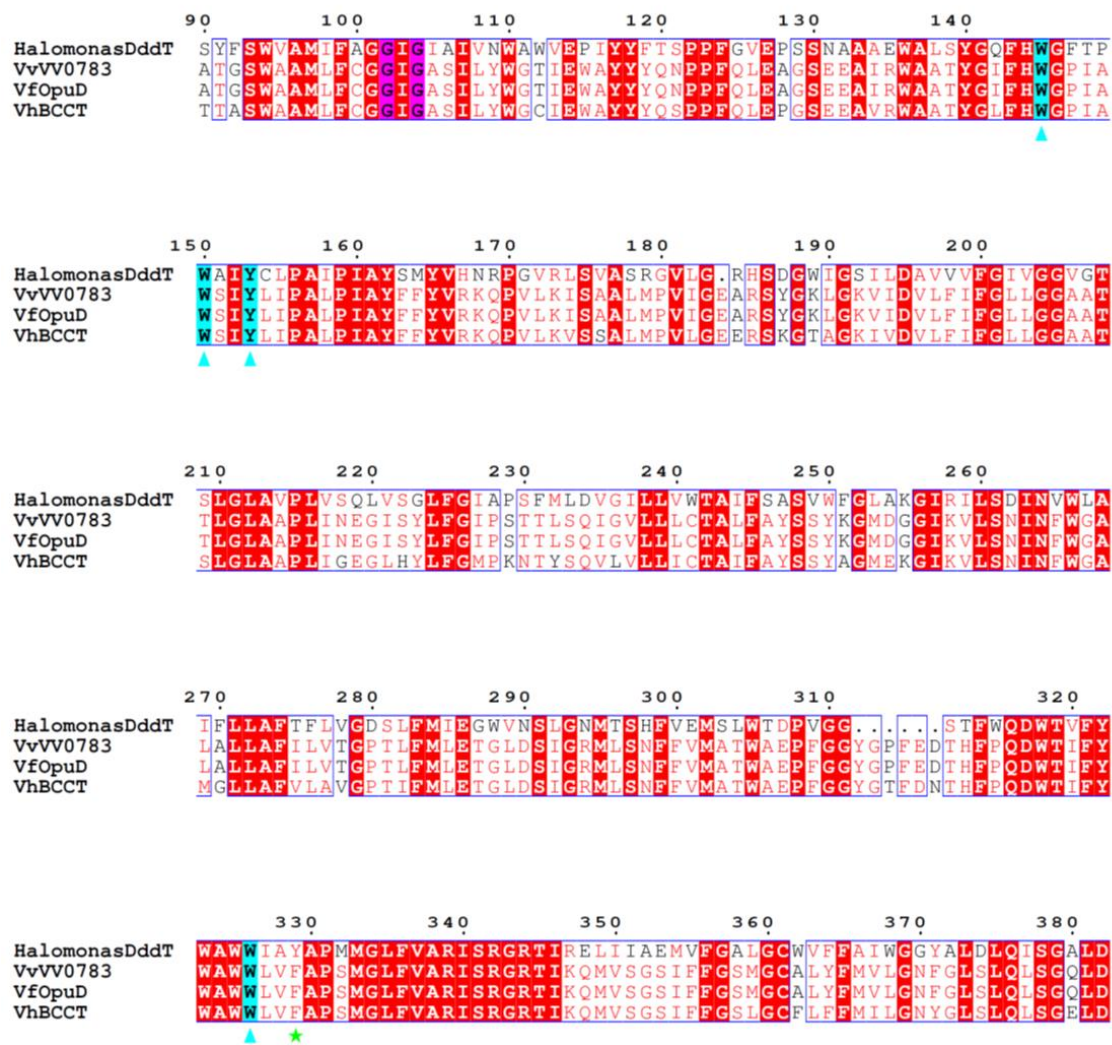


**Figure 50** *Halomonas* sp. HTNK1 DddT alignment with homologs found in *V. vulnificus*, *V. fluviialis* and *V. harveyi*.

Residues highlighted in magenta are conserved in sodium-symporters. Residues marked with a cyan triangle have been demonstrated to be important for trimethylammonium compound binding; residues highlighted in cyan are conserved. A green star denotes residues thought to be important for additional substrate binding; conserved residues are highlighted in green.

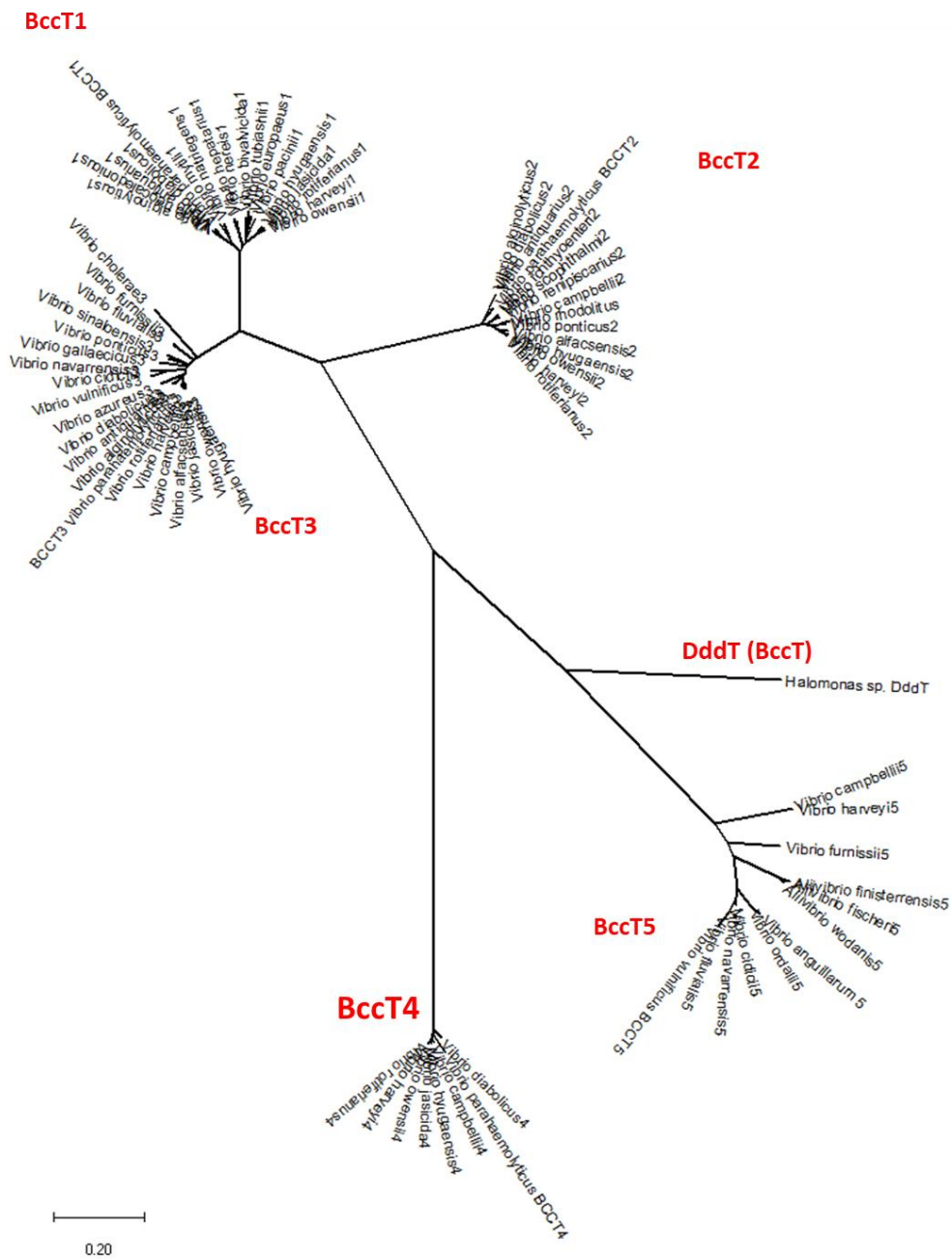


**Figure 51** Phylogenetic analysis of the evolutionary relationships among five BccTs present in *Vibrio* species. BccT1, BccT2, BccT3, BccT4 and BccT5 from *Vibrio* species and DddT from *Halomonas* sp. HTNK1.

## Discussion

Bacteria have adapted to hyper-osmotic conditions by changing the level of osmolytes in their cells to maintain turgor pressure. The most prevalent and energetically effective method to accomplish this is the uptake of osmolytes from the surrounding environment. DMSP is produced in vast quantities by marine phytoplankton as an osmoprotectant and is also an important component of the global sulfur cycle. We show that marine bacteria in the genus *Vibrio* can use DMSP as an effective osmolyte. These are the first studies to demonstrate a more widespread use of DMSP among marine halophiles. We demonstrate the important role BCCT carriers play in this process. BCCT-family transporters were solely responsible for the uptake of DMSP by *V. parahaemolyticus* and most likely BCCTS also play a role in DMSP uptake in other *Vibrio* species based on protein homology analysis.

BccT1 can uptake proline, choline, glycine betaine, ectoine, and DMG. BccT2 can uptake proline, choline, glycine betaine, DMG and DMSP, while BccT3 can transport proline, choline, glycine betaine and DMG, and BccT4 uptakes only proline and choline. The mechanism(s) of substrate specificity for BCCTs are not fully understood. Structural analysis of BetP, a BCCT in *Corynebacterium glutamicum*, has revealed four residues (Trp 189, Trp 194, Tyr 197, and Trp 374) found in TM4 and TM8 are important for coordination of trimethylammonium compounds. BccT1, BccT2 and BccT3 all share the conserved residues in the BCCTs that are important for coordination of trimethylammonium compounds (data not shown); however, they differ in their substrate specificities. To the best of our knowledge, there are no reports of DMSP uptake via a BCCT family transporter for use as an osmoprotectant. DddT in

*Halomonas sp.* HTNK1 was shown to transport DMSP for use as a catabolite (265). Here we have shown that multiple species of Vibrios can transport and utilize DMSP as a highly effective osmoprotectant. DMSP fits loosely into this group of compounds (85), as it has a fully methylated sulfur headgroup. In *V. parahaemolyticus*, only BccT2 is capable of efficiently transporting DMSP, which indicated that additional residues present in BccT2 must be responsible for transporter specificity for DMSP. *V. fluvialis*, *V. harveyi*, and *V. vulnificus* all possess a transporter that is homologous to *Halomonas* DddT, but do not encode *bccT2* homologs. As mentioned above, these proteins possess substitutions in a residues important substrate specificity and coordination of trimethylammonium compounds (86). It should be noted that *V. harveyi* does possess a BccT2 homolog (**Figure 49**), and so may possess two BCCT-family carriers capable of DMSP uptake. Additionally, we demonstrated that *V. cholerae* N16961 can uptake DMSP, but it also does not encode a BccT2 homolog. Therefore, more work needs to be done to elucidate the mechanisms of DMSP coordination by BCCT-family carriers, and to identify the transporters responsible for uptake in *V. fluvialis*, *V. harveyi*, *V. vulnificus*, and *V. cholerae*.

Recently, an increased incidence of algal blooms has led to increased *V. parahaemolyticus* and *V. vulnificus* proliferation (162, 272, 273). Our data shows that *V. parahaemolyticus* is unable to utilize DMSP as a carbon source, but can grow and divide rapidly in high salinity when exogenous DMSP is present. We speculate that the ability of *V. parahaemolyticus* to utilize DMSP as a compatible solute increases its ability to proliferate in algal blooms that occur in both high salinity and in warmer months. Dinoflagellates are some of the main producers of DMSP and *V. parahaemolyticus* proliferation has been found in conjunction with dinoflagellate algal

blooms (272, 273). Likewise, *V. vulnificus* can grow and divide rapidly and can grow in higher salinity when exogenous DMSP is present.

Table 9 Strains and plasmids used in this study

Strain	Genotype or description	Reference or Source
<i>Vibrio parahaemolyticus</i>		
RIMD2210633	O3:K6 clinical isolate, Str <sup>r</sup>	(104, 157)
<i>ΔectB</i>	RIMD2210633 <i>ΔectB</i> (VP1721), Str <sup>r</sup>	(45)
SOYBCCT124	RIMD2210633 <i>ΔVP1456 ΔVP1723 ΔVPA0356</i> , Str <sup>r</sup>	(60)
SOYBCCT123	RIMD2210633 <i>ΔVP1456 ΔVP1723 ΔVP1905</i> , Str <sup>r</sup>	(60)
SOYBCCT134	RIMD2210633 <i>ΔVP1456 ΔVP1905 ΔVPA0356</i> , Str <sup>r</sup>	(60)
SOYBCCT234	RIMD2210633 <i>ΔVP1723 ΔVP1905 ΔVPA0356</i> , Str <sup>r</sup>	(60)
SOYBCCT1342	RIMD2210633 <i>ΔVP1456ΔVP1723ΔVP1905ΔVPA0356</i> Str <sup>r</sup>	(60)
<i>Escherichia coli</i>		
DH5α λpir	<i>Δlac pir</i>	ThermoFisher Scientific
β2155 λpir	<i>ΔdapA::erm pir</i> for bacterial conjugation	(163)
MKH13	MC4100 ( <i>ΔbetTIBA</i> ) <i>Δ(putPA)101</i> <i>Δ(proP)2 Δ(proU)</i> ; Sp <sup>r</sup>	(94)
<b>Plasmids</b>		
pBAD33	Expression vector; <i>araBAD</i> promoter; Cm <sup>r</sup> ; p15a origin	(231)
pBAVP1456	pBAD33 harboring full-length VP1456 ( <i>bccT1</i> )	This study
pBAVP1723	pBAD33 harboring full-length VP1723 ( <i>bccT2</i> )	(60)
pBAVP1905	pBAD33 harboring full-length VP1905 ( <i>bccT3</i> )	(60)
pBAVPA0356	pBAD33 harboring full-length VPA0356 ( <i>bccT4</i> )	(60)

## Chapter 6

# IDENTIFICATION OF NOVEL REGULATORS OF THE ECTOINE BIOSYNTHESIS OPERON

### Introduction

Bacteria require compatible solutes to grow and divide in high osmolarity environments, and can accumulate these compounds utilizing transporters or via biosynthesis (9, 13, 15, 22, 78, 167). Compatible solutes are small, organic compounds that are accumulated in the cytoplasm to maintain the turgor pressure of the cell. Typically compatible solutes carry no net charge at physiological pH and do not interact with proteins or nucleic acids (12). Compatible solutes include compounds such as sugars, polyols, free amino acids, amino acid derivatives, quaternary amines, sulfate esters, N-acetylated amino acids and small peptides (5, 13-18). Examples include trehalose (a sugar), glycerol and mannitol (polyols), proline, glutamate and glutamine (free amino acids), ectoine (amino acid derivative), glycine betaine (GB), and carnitine (quarternary amines), choline-*O*-sulfate (sulfate ester) (5, 13-18).

The amino acid derivative ectoine is an important compatible solute biosynthesized by many aerobic heterotrophic bacteria (28-31). A recent bioinformatics study showed that ectoine genes were present almost exclusively in *Bacteria*. Among 6,428 microbial genomes examined, 440 species (7%) had ectoine biosynthesis genes (32). Among 33 species from the family *Vibrionaceae*, it was shown that nearly 70% of species produced ectoine (59). In *Vibrio parahaemolyticus*, a halophile, ectoine production was shown to be essential for growth in minimal media supplemented with 6% NaCl when no other compatible solutes or precursors are

available (59). Aspartic acid is the precursor for ectoine, which can be biosynthesized *de novo*. Aspartic acid is converted to ectoine by EctA, EctB, and EctC, encoded by the operon *ectABC*, which is evolutionarily conserved in Gram-positive and Gram-negative bacteria (38-40). Several species that produce ectoine also encode a specialized aspartokinase (Ask) specific to the ectoine biosynthesis pathway and clustered with the *ectABC* genes (41-44). *V. parahaemolyticus* encodes an aspartokinase (Asp\_ect) in the same operon as the *ectABC* genes (45). Ask/Asp\_ect converts aspartic acid to  $\beta$ -aspartyl phosphate, which is then converted to L-aspartate- $\beta$ -semialdehyde by aspartate semialdehyde dehydrogenase (Asd). This intermediate product in the aspartic acid pathway, L-aspartate  $\beta$ -semialdehyde, is then funneled into the ectoine biosynthesis pathway and converted to L-2,4-diaminobutyrate by L-2,4-diaminobutyrate transaminase (EctB). This product is then acetylated by L-2,4-diaminobutyrate N<sup>γ</sup>-acetyltransferase (EctA) and N<sup>γ</sup>-acetyldiaminobutyrate is formed. Finally, L-ectoine synthase (EctC) performs the cyclic condensation reaction to produce ectoine (40).

Previously, it was shown in *Vibrio* species that *ectABC-asp\_ect* is repressed by the MarR-type regulator CosR, and this repression is strongest in low salinity conditions (61, 108, 109). Additionally, CosR is regulated by the quorum sensing master regulators AphA and OpaR. AphA activates the *ectABCasp\_ect* operon while OpaR represses these genes. This feed-forward loop results in a tightly controlled gradient of *ectABCasp\_ect* expression across the growth cycle (108). A homolog of CosR, EctR1, also represses ectoine in several halotolerant methanotrophic species (110, 187, 188, 197).

The uptake of exogenous compatible solutes was shown to repress transcription of ectoine biosynthesis genes and the production of ectoine, though no direct mechanism has been demonstrated. Previously, it was shown that ectoine accumulated in exponential phase in the moderate halophile *Chromohalobacter israelensis*, when grown in minimal media with no glycine betaine present, but ectoine production was halted in the presence of exogenous glycine betaine (274). In *Chromohalobacter salexigens*, another halophilic bacterium, it was found that the presence of glycine betaine negatively modulated ectoine biosynthesis gene levels, but did not completely repress transcription (275, 276). In *Vibrio anguillarum*, the presence of choline in the medium repressed ectoine biosynthesis genes under cold stress conditions, suggesting glycine betaine is the preferred cryoprotectant in this species (277). Recently, it was determined that the ectoine promoter of *Pseudomonas stutzeri* is osmotically regulated and induced by both ionic and non-ionic osmolytes, with transcriptional activity increasing linearly with osmolarity (113). CosR appears to be a regulator of ectoine biosynthesis genes in response to salinity and the quorum sensing system plays a role in regulation of these genes across the growth cycle. However, the mechanisms of regulation of ectoine biosynthesis genes in response to environmental cues such as temperature, availability of exogenous compatible solutes, or non-ionic osmolytes is not known.

We therefore set out to identify additional regulators of the ectoine biosynthesis genes by performing a DNA affinity chromatography-pulldown with the regulatory region of the *ectABCasp\_ect* operon. Pulldowns were performed under inducing conditions (minimal medium with no exogenous compatible solutes) and non-inducing conditions (rich medium) to capture both positive and negative

regulators of the *ect* genes. We identified the regulators NhaR, TorR, LeuO, and OmpR and utilized expression analyses of deletion mutants to determine the role of each in ectoine biosynthesis gene regulation under various environmental stresses. Plasmid-based assays were utilized to determine whether control of the regulatory region was direct.

## Materials and Methods

### Bacterial strains, media and culture conditions

All strains and plasmids used in this study are listed in **Table 10**. A streptomycin-resistant *V. parahaemolyticus* RIMD2210633 was used as the wild-type (WT) strain. *Vibrio parahaemolyticus* were grown either in lysogeny broth (LB; Fisher Scientific, Fair Lawn, NJ) with 3% (wt/vol) NaCl (LB3%) or M9 minimal media (47.8 mM Na<sub>2</sub>HPO<sub>4</sub>, 22mM KH<sub>2</sub>PO<sub>4</sub>, 18.7 mM NH<sub>4</sub>Cl, 8.6 mM NaCl; Sigma-Aldrich) supplemented with 2mM MgSO<sub>4</sub>, 0.1 mM CaCl<sub>2</sub>, 20 mM glucose as the sole carbon source (M9G) and 3% NaCl (wt/vol) (M9G3%). *E. coli* strains were grown either in LB supplemented with 1% NaCl (LB1%) or M9G supplemented with 1% NaCl (M9G1%). The diaminopimelic acid (DAP) auxotrophic strain, *E. coli*  $\beta$ 2155 *λpir*, was grown with 0.3 mM DAP. All strains were grown at 37 C with aeration. Antibiotics were used at the following concentrations, as necessary: ampicillin (Amp), 50 µg/mL; chloramphenicol (Cm), 12.5 µg/mL; tetracycline (Tet), 1 µg/mL.

### DNA affinity chromatography/mass spectrometry

DNA affinity chromatography was performed as previously described (111, 278). The assay was performed twice, once after growth in noninducing conditions (LB3%) and once after growth in inducing conditions (M9G3%) in an effort to obtain

both positive and negative regulators of the ectoine biosynthesis operon. The WT RIMD2210633 strain was grown overnight in LB3%, cells were pelleted and washed two times with 1X PBS and diluted 1:50 into 500 mL of LB3% or M9G3%. Cells were then grown to an OD<sub>595</sub> of 0.5, pelleted and stored overnight at -80°C. Cells were resuspended in buffer with Fast-Break cell lysis reagent (Promega) with 1 mM PMSF, 0.5 mM benzamidine, 0.1 µg/mL lysozyme and incubated for 30 min at room temperature. Cells were then sonicated on ice at 30% pulse amplitude for 15 seconds with 1-minute rest to shear genomic DNA. This was repeated five times. The cell lysate was then clarified by centrifuging at 17000 x g for 30 minutes at 4°C. Biotinylated probe was amplified using primer pairs Biotin-PectAFwd/PectARev and Biotin-ectBFwd/ectBRev (**Table 11**) via PCR with Phusion high-fidelity polymerase (ThermoFisher) using 10 reactions. The regulatory region of *ectABCasp\_ect* (including 33 bp of the coding region and the entire 290-bp upstream intergenic region) was used as the target probe, while a portion of the coding region of *ectB* (+533 to +859 relative to ATG) was used as the negative control probe. Reactions were pooled and biotinylated probe was precipitated in ethanol as previously described (279). Streptavidin M280 DynaBeads (ThermoFisher) were incubated two times with 10 µg of biotinylated probe to ensure saturation. Clarified cell lysate was then incubated for one hour with streptavidin-coated beads to remove non-specifically binding proteins. Pre-cleared clarified cell lysate was incubated with streptavidin-coated beads in binding buffer at room temperature for 30 minutes with constant rotation in the presence of 100 µg sheared salmon sperm DNA as a non-specific competitor. Beads were pulled down, gently washed and incubated with additional cell lysate for 30 minutes. Proteins were eluted using a step-wise NaCl gradient from 100

$\mu\text{M}$  to 1 M. Samples were then separated using 12% SDS-PAGE and silver-stained using a Pierce Silver Stain Kit (ThermoFisher). Candidate proteins were selected and the corresponding band was excised from the gel, along with corresponding areas in the negative control lanes. The gel was destained and digested with trypsin. The samples were then loaded onto a Q-exactive Orbitrap mass spectrometer with nano-flow electrospray (Thermo). Proteins were identified using Proteome Discoverer 2.1 software (Thermo).

#### Construction of *nhaR*, *torR*, and *ompR*, deletion mutants

A 692 base pair in-frame deletion of *ompR* (VP0154) was created in *Vibrio parahaemolyticus* RIMD2210633 through Splicing by Overlap Extension (SOE) PCR and homologous recombination (151). Primers were designed to create a 692-bp truncated allele of *ompR* using the primer pair listed in **Table 11**. The product was amplified from the *V. parahaemolyticus* RIMD2210633 genome via PCR and ligated into the cloning vector pJET1.2 via blunt-end ligation with T4 DNA ligase and transformed into *E. coli* Dh5 $\alpha$ . The truncated allele was then cut out of the resulting pJET $\Delta$ *ompR* vector using the restriction enzymes SacI and XbaI and ligated into the suicide vector pDS132, which had been linearized using the same restriction enzymes. The resulting plasmid, pDS $\Delta$ *ompR*, was transformed into *E. coli* Dh5 $\alpha$ , and then the diamino pimelic acid auxotroph strain *E. coli*  $\beta$ 2155  $\lambda$ *pir*, for conjugation into wild-type RIMD2210633. The suicide vector pDS132 must recombine into the genome via homologous recombination in order to be replicated, due to the absence of the necessary replication gene *pir* in the *V. parahaemolyticus* genome. Single-crossover colonies were selected by plating onto chloramphenicol selection plates and screened via PCR for a truncated allele. A double-crossover event was then induced after

overnight growth in liquid medium without chloramphenicol selection. Cultures were spread-plated onto 10% sucrose plates, and healthy colonies were screened. Colonies still containing the plasmid appeared soupy on the plate due to the presence of the *sacB* gene which makes sucrose toxic to the cells. An in-frame deletion was confirmed via sequencing.

In-frame deletion mutants of *nhaR* (VP0527) and *torR* (VP1032) were constructed as previously described via Gibson assembly and allelic exchange (108). Briefly, primers were designed to amplify a 15 bp truncated PCR product of the 891 bp *nhaR* gene and a 54 bp truncated PCR product of the 714 bp *torR* gene using the primer pairs listed in **Table 11**. The truncated alleles were ligated with the suicide vector pDS132, which was linearized with *SacI*, via Gibson assembly protocol and transformed into *E. coli* Dh5 $\alpha$  (150). The resulting plasmids pDS $\Delta$ *nhaR* and pDS $\Delta$ *torR* were purified and transformed into *E. coli*  $\beta$ 2155  $\lambda$ *pir*, and subsequently conjugated with wild-type RIMD2210633. Allelic exchange and selection were performed as described above for the *ompR* mutant. In-frame deletions of *nhaR* and *torR* were confirmed via sequencing.

### Reporter assays

Reporter assays were conducted in *V. parahaemolyticus* deletion mutant strains  $\Delta$ *nhaR*,  $\Delta$ *torR*,  $\Delta$ *leuO*, and  $\Delta$ *ompR*. *E. coli*  $\beta$ 2155  $\lambda$ *pir* harboring the reporter plasmid pRUP<sub>*ectA*</sub>-*gfp* was conjugated with each deletion mutant strain, as previously described (108). Strains were grown overnight in LB3% with tetracycline selection (1  $\mu$ g/mL). Cells were pelleted, washed two times with 1X PBS, and diluted 1:100 in M9G3% with tetracycline and grown for 20 hours. Reporter expression was determined by measuring the relative fluorescence with excitation 385 nm and emission at 509 nm in

black, clear-bottomed 96-well microplates on a Tecan Spark microplate reader with Magellan software (Tecan Systems, Inc., San Jose, CA). Specific fluorescence was calculated by dividing the relative fluorescence units (RFU) by the optical density of each well. At least two biological replicates were performed for each experiment.

Vectors were constructed to express *nhaR* and *torR* from an inducible *araBAD* promoter in the pBAD33 expression vector. Primers were designed to amplify the ribosomal binding site and the full-length coding region of *nhaR* and *torR* from the RIMD2210633 genome (**Table 11**). PCR products were ligated with pBAD33, which had been linearized with SacI, via Gibson assembly protocol and transformed into *E. coli* Dh5 $\alpha$ . Complementary regions for Gibson assembly are indicated in lowercase letters in the primer sequence (**Table 11**). The resulting expression plasmids, pBADnhaR and pBADtorR, were purified, sequenced, and subsequently transformed into the corresponding Keio collection *E. coli* deletion mutant strains JW0019-1 ( $\Delta$ *nhaR738::kan*) and JW0980-1 ( $\Delta$ *torR739::kan*) (280). The expression plasmid pBADleuO was transformed into the corresponding Keio collection *E. coli* deletion mutant strain JW0075-1 ( $\Delta$ *leuO783::kan*) (280). The reporter plasmid pRUP<sub>*ectA*</sub>-*gfp* was transformed into JW0019-1 harboring pBADnhaR to produce strain GJG0019, JW0980-1 harboring pBADtorR to produce strain GJG0980, and JW0075-1 harboring pBADleuO to produce strain GJG0075. GFP reporter assays were conducted, as previously described, by growing GJG0019, GJG0980, and GJG0075 in LB1% overnight with antibiotic selection (chloramphenicol, 12.5  $\mu$ g/mL; ampicillin, 50  $\mu$ g/mL) (108). Cultures were pelleted, washed twice with 1X PBS, and diluted 1:1000 in M9G1% with chloramphenicol and ampicillin. Expression was induced with 0.01% arabinose and cultures were grown for 20 hours to an OD<sub>595</sub> between 0.9 and 1.1.

Specific fluorescence was determined as described above. Two biological replicates were performed for each experiment.

## Results

### Identification of putative novel regulators of the ectoine biosynthesis operon

We have shown previously that ectoine genes are expressed differentially across the growth cycle, in both rich and minimal media (59, 108). Therefore, to identify novel regulators, we isolated proteins after growth to mid-exponential phase in minimal medium (OD 0.5, M9G3%) and stationary phase in rich medium (1.0 OD, LB3%). We speculated that different proteins may be responsible for regulation of the ectoine biosynthesis operon in minimal medium vs rich medium due to the presence of compounds in rich medium that can be utilized as compatible solutes. A promoter pulldown was performed using a 5'-biotin tagged DNA fragment comprising the regulatory region of the ectoine biosynthesis genes bound to streptavidin beads, with a coding region of the downstream gene *ectB* used as a negative control bait. Proteins bound to the DNA were eluted using a step-wise NaCl gradient and separated via SDS-PAGE. Individual bands present in the target lanes that were not present in the negative control lanes were selected for analysis via mass spectrometry (**Figure 52**). Proteins were identified via mass spectrometry after trypsin digestion and were aligned to the *V. parahaemolyticus* genome. Proteins were then sorted by gene class and ranked by score (**Table 12**). Candidate proteins that belonged to the transcriptional regulator gene class or were identified via HHPRED analysis to contain DNA-binding domains were selected (**Table 13**). We chose several candidate proteins to investigate: NhaR, LeuO, OmpR, and TorR. Deletion mutants of *ompR* and *leuO*

had been constructed previously in the lab (106) (Ongagna, unpublished), and we constructed in-frame deletion mutants of *nhaR* and *torR*.

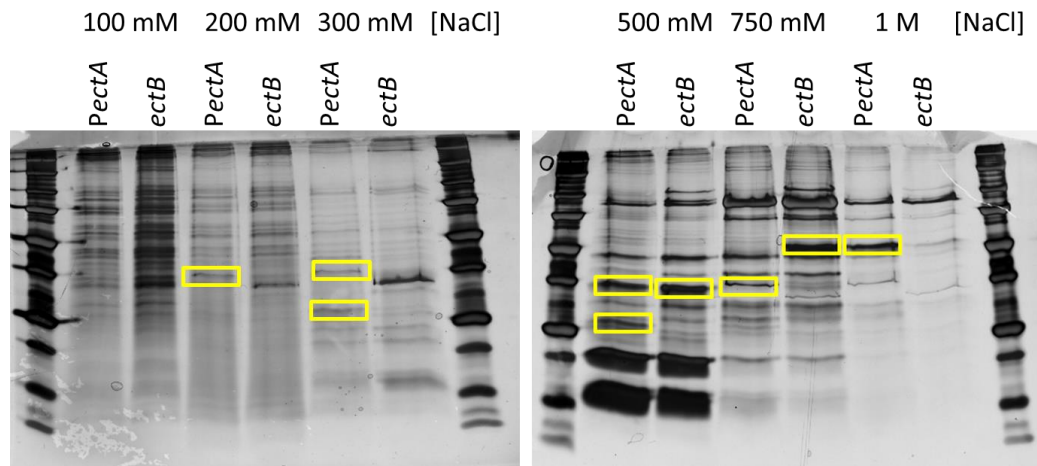


**Figure 52 Protein separation via SDS-PAGE.**

DNA affinity chromatography and mass spectrometry was utilized to identify proteins that bind to the regulatory region of the *ectABCasp\_ect* operon. (A) Experimental flow for DNA affinity chromatography pulldown (Jutras *et al.*, 2012, Chaparian *et al.*, 2016). (B) Candidate proteins identified in pulldown and ranked by score. Highlighted proteins were chosen for further investigation.

LeuO, NhaR, OmpR and TorR are regulators of *ectABCasp\_ect* in *V. parahaemolyticus*

To determine whether LeuO, NhaR, OmpR and TorR play a role in regulation of the ectoine biosynthesis operon, we performed a GFP reporter assay using a reporter plasmid with *gfp* under the control of the ectoine regulatory region ( $P_{ectA-gfp}$ ). We found that activity of the  $P_{ectA-gfp}$  reporter was significantly reduced in a  $\Delta leuO$  mutant, which suggested that LeuO is an activator of ectoine biosynthesis genes (Figure 53). We found that  $P_{ectA-gfp}$  expression was significantly higher in an  $\Delta nhaR$

mutant than in the wild type strain (**Figure 53**), which suggested that NhaR is a repressor of the ectoine biosynthesis genes. The expression of  $P_{ectA}$ -*gfp* in both the  $\Delta ompR$  and  $\Delta torR$  mutants was statistically significantly upregulated over that of wild type but expression changes are lower than for LeuO and NhaR (**Figure 53**), therefore we chose to further characterize the role of LeuO and NhaR in regulation of ectoine biosynthesis gene expression.

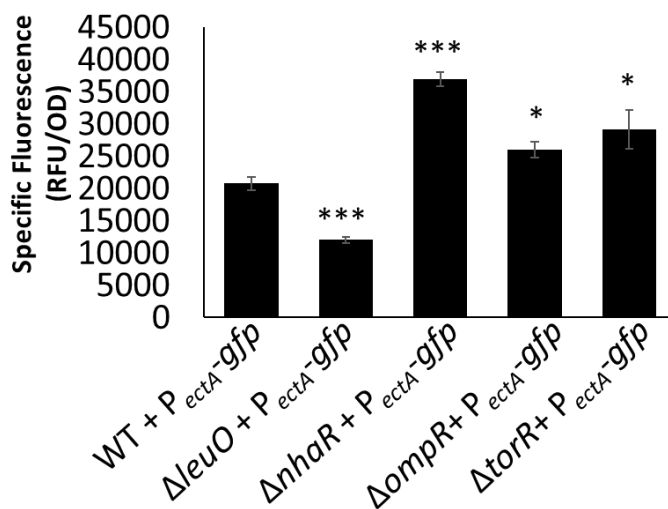


**Figure 53** Expression of a  $P_{ectA}$ -*gfp* transcriptional fusion in wild-type (WT) *V. parahaemolyticus*  $\Delta leuO$ ,  $\Delta nhaR$ ,  $\Delta ompR$ , and  $\Delta torR$  mutants. Cultures were grown overnight in M9G3% and relative fluorescence intensity (RFU) was measured. Specific fluorescence was calculated by dividing RFU by OD. Mean and standard deviation of three biological replicates are shown. Statistics were calculated using a Student's t-test; (\*,  $P < 0.05$ ; \*\*\*,  $P < 0.001$ ).

Investigation of NhaR as a direct regulator of *ectABCasp\_ect* in *V. parahaemolyticus*

We next set out to determine whether NhaR is a direct regulator of the ectoine biosynthesis genes. To test this, we utilized an *E. coli* keio collection  $\Delta nhaR$  mutant and expressed full-length *nhaR* from *V. parahaemolyticus* from an inducible plasmid (*pnhaR*) and measured expression of the  $P_{ectA}$ -*gfp* reporter in this background. There was not a difference in expression of the reporter in the NhaR-expressing strain as compared to the strain harboring empty vector (pBAD33) (**Figure 54**). This indicated that additional proteins may be required for full repression by NhaR in this background. Additionally, NhaR may repress *PectA* under different environmental conditions, such as higher salinity. Additional conditions should be tested to determine if NhaR is a direct repressor of the ectoine biosynthesis genes.

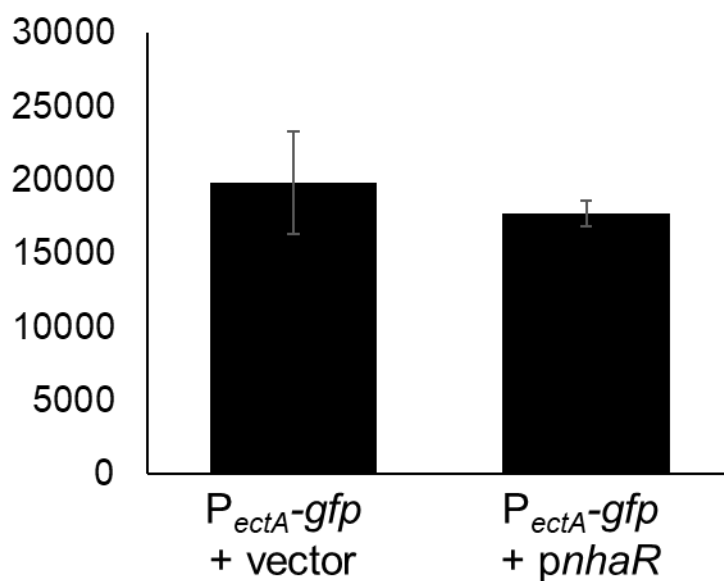


**Figure 54** Expression of a  $P_{ectA-gfp}$  transcriptional fusion in *E. coli* strain  $\Delta nhaR$ .

A reporter assay was conducted in *E. coli*  $\Delta nhaR$  using the  $P_{ectA-gfp}$  reporter plasmid and an expression plasmid, *pnhaR*. Specific fluorescence was calculated by dividing RFU by OD and compared to a strain with empty expression vector, pBAD33. Mean and standard deviation of two biological replicates are shown.

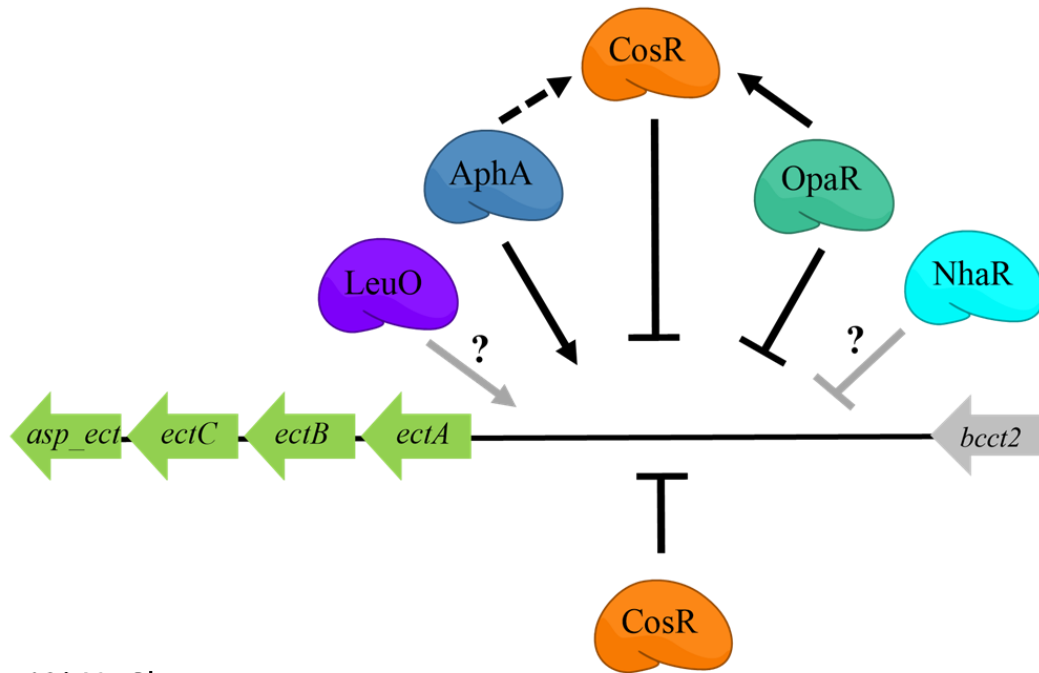
## Discussion

Here we have identified four novel regulators of the ectoine biosynthesis genes in *V. parahaemolyticus*. NhaR, OmpR, and TorR are novel repressors of the ectoine biosynthesis operon while LeuO is a novel activator. We have previously identified the quorum sensing master regulator AphA as a direct activator of the ectoine operon, while OpaR and CosR are also repressors (**Figure 55**) (61, 108). Ectoine is energetically costly to biosynthesize (75), and therefore multiple regulators that tightly control ectoine under various environmental conditions are reasonable. Biosynthesis

of ectoine also drains the intracellular pools of key metabolites, making regulation of ectoine biosynthesis necessary for maximum cellular fitness (185, 186).

NhaR and OmpR are known to play a role in high salt tolerance and osmosensing, respectively (281-285). We have previously demonstrated that LeuO plays a role in acid stress tolerance in *V. parahaemolyticus*, although a connection with osmotic stress has not been demonstrated (106). TorR is a regulator of TorS, which is involved in TMAO sensing and anaerobic respiration in *E. coli* (286, 287). TMAO is also a compatible solute that is used by *V. parahaemolyticus* (**Figure 55**) (68), and so we sought to investigate whether there was cross talk between two compatible solute systems.

3% NaCl



1% NaCl

**Figure 55** Model of regulation of ectoine biosynthesis genes in low salinity and high salinity growth conditions.

Solid lines represent direct regulation while dashed lines represent indirect regulation. Gray lines represent regulators for whom direct regulation has not yet been determined.

Table 10 Strains and plasmids used in this study

Strain	Genotype or description	Reference or Source
<i>Vibrio</i>		
<i>parahaemolyticus</i>		
RIMD2210633	O3:K6 clinical isolate, Str <sup>r</sup>	(104, 157)
$\Delta ompR$	RIMD2210633 $\Delta ompR$ (VP0154), Str <sup>r</sup>	This study
$\Delta ompR\Delta envZ$	RIMD2210633 $\Delta ompR \Delta envZ$ (VP0154/ VP0155), Str <sup>r</sup>	This study
$\Delta nhaR$	RIMD2210633 $\Delta nhaR$ (VP0527), Str <sup>r</sup>	This study
$\Delta torR$	RIMD2210633 $\Delta torR$ (VP1032), Str <sup>r</sup>	This study
$\Delta leuO$	RIMD2210633 $\Delta leuO$ (VP0350), Str <sup>r</sup>	(106)
<i>Escherichia coli</i>		
DH5 $\alpha$ $\lambda$ pir	$\Delta lac$ pir	ThermoFisher Scientific
$\beta$ 2155 $\lambda$ pir	$\Delta dapA::erm$ pir for bacterial conjugation	(163)
JW0019-1 ( $\Delta nhaR$ )	BW25113, $\Delta nhaR738::kan$ , $\Delta(araD-araB)567$ , $\Delta lacZ4787(::rrnB-3)$ , $\lambda$ -, <i>rph-1</i> , $\Delta(rhaD-rhaB)568$ , <i>hsdR514</i>	(280)
JW0980-1 ( $\Delta torR$ )	BW25113, $\Delta torR739::kan$ , $\Delta(araD-araB)567$ , $\Delta lacZ4787(::rrnB-3)$ , $\lambda$ -, <i>rph-1</i> , $\Delta(rhaD-rhaB)568$ , <i>hsdR514</i>	(280)
JW0075-1 ( $\Delta leuO$ )	BW25113, $\Delta leuO783::kan$ , $\Delta(araD-araB)567$ , $\Delta lacZ4787(::rrnB-3)$ , $\lambda$ -, <i>rph-1</i> , $\Delta(rhaD-rhaB)568$ , <i>hsdR514</i>	(280)
GJG0019	JW0019-1 ( $\Delta nhaR$ ) harboring pBADnhaR and pRUpectA; Cm <sup>r</sup> ; Amp <sup>r</sup> ; Tet <sup>r</sup> ; Kan <sup>r</sup>	This study
GJG0980	JW0098-1 ( $\Delta torR$ ) harboring pBADtorR and pRUpectA; Cm <sup>r</sup> ; Amp <sup>r</sup> ; Tet <sup>r</sup> ; Kan <sup>r</sup>	This study
GJG0075	JW0075-1 ( $\Delta leuO$ ) harboring pBADleuO and pRUpectA; Cm <sup>r</sup> ; Amp <sup>r</sup> ; Tet <sup>r</sup> ; Kan <sup>r</sup>	This study
<b>Plasmids</b>		
pJET1.2/blunt	Cloning vector	ThermoFisher Scientific
pJETompR	pJET1.2 harboring truncated <i>ompR</i> allele	This study
pJETenvZ	pJET1.2 harboring truncated <i>envZ</i> allele	This study
pDS132	Suicide plasmid; Cm <sup>r</sup> ; <i>sacB</i> (sucrose intolerant), R6Kg origin	

Table 10 (continued)

pDSompR	pDS132 harboring truncated <i>ompR</i> allele	This study
pDSenvZ	pDS132 harboring truncated <i>envZ</i> allele	This study
pDSnhaR	pDS132 harboring truncated <i>nhaR</i> allele	This study
pDStorR	pDS132 harboring truncated <i>torR</i> allele	This study
pBAD33	Expression vector; <i>araBAD</i> promoter; Cm <sup>r</sup> ; p15a origin	(231)
pBADnhaR	pBAD33 harboring full-length <i>nhaR</i> (VP0527)	This study
pBADtorR	pBAD33 harboring full-length <i>torR</i> (VP1032)	This study
pBADleuO	pBAD33 harboring full-length <i>leuO</i> (VP0350)	(106)
pRU1064	promoterless- <i>gfpUV</i> , Amp <sup>r</sup> , Tet <sup>r</sup> ; IncP origin	(153)
pRUPectA	pRU1064 with <i>PectA-gfp</i> , Amp <sup>r</sup> , Tet <sup>r</sup>	(108)

Table 11 Primers used in this study

Use and Primer	Sequence (5'-3')	Length (bp)
<b>Mutant primers</b>		
ompR FLF	TGGATTAAAACGAGCCCTTG	1329
ompR FLR	TCGATGTGCATCCACAAAAT	
ompR A	TCTAGAGCGCCGAAAGTTAGATGAAG	301
ompR B	CAGCTGAGATCTGGTACCCCTGCATTGAAACATCCTTT	
ompR C	GGTACCAGATCTCAGCTGCCAGACGGCAAAGAGTCGTAA	336
ompR D	GAGCTCTAATAACTGGCGACGCAATG	
envZ FLF	CGCCGAAAGTTAGATGAAGC	2133
envZ FLR	TGGGGTTAGGTATCGCTCAG	
envZ A	TCTAGAAAGGATGTTTCAATGCAGGAA	318
envZ B	CAGCTGAGATCTGGTACCGTAATCGTCCGCACCAACTT	
envZ C	GGTACCAGATCTCAGCTGGAGACGGACTTGAACATGCA	373
envZ D	GAGCTCGGGTTATTTGGTCGGGAAAC	
nhaR FLF	AGACCACCTGCAACTAAGCC	2157
nhaR FLR	GCATTTTCAGTCTGTGCGATCA	
nhaR A gibson	accgcatcgatategagctACAATACTTTTGGCTTGGTCG	553
nhaR B gibson	tttactcaaaATGTGACATCGGCCAATTC	
nhaR C gibson	gatgtcacatTTTGAGTAAACCCGTATCGTTG	490
nhaR D gibson	gtggaattcccgggagagctGTCACGACGAAGCCAAGC	
torR FLF	CCTGAACCCCAAAATCTGCC	2033
torR FLR	ACCAAGCTTCTCATGCCACT	
torR A gibson	accgcatcgatategagctGTTGAGCATCATTGCGGTC	506
torR B gibson	cttcaccgtgGACTAATACGTGATAGCTCATTTAC	
torR C gibson	cgtattagtcCACGGTGAAGGCTACATG	502
torR D gibson	gtggaattcccgggagagctTGATGGTGGCTCTGAGATC	
<b>Expression/GFP reporter primers</b>		
nhaRC Fwd	agggaacaaaagctgggtacTTCCCTACAGACTGGATG	913
nhaRC Rev	cggccgctctagaactagtgTTATTCTGGTTTGGTGATG	
torRC Fwd	tgggctagcgaattcgagctATAGAATACGTCTTGGATAATAAGAAG	757
torRC Rev	ggatccccgggtaccgagctTTAATCACCTGCGAACATG	

Table 12 Candidate proteins ranked by score

Accession no.	Locus tag	Function/Predicted Domains	Score	Coverage	# AAs	MW [kDa]
Q87RV7	VP0669	Succinylglutamate/aspartoacylase	29.64	50.84	356	39.0
Q87K62	VPA0036	N-terminal winged helix, endonuclease-DNA mismatch repair	23.07	65.63	288	33.2
Q87SD5	VP0489	Aerobic respiration control protein FexA	17.15	9.66	238	26.9
Q87S97	VP0527	Na <sup>+</sup> /H <sup>+</sup> antiporter regulatory protein NhaR	15.06	38.18	296	33.9
Q87SS2	VP0350	LysR family transcriptional regulator LeuO	13.64	17.87	319	36.2
Q87HC6	VPA1039	IcmF-related protein, type IV SS	11.73	21.93	1172	133.7
Q87QL6	VP1133	Nucleoid associated protein H-NS	10.40	79.26	135	15.1
Q87JF0	VPA0303	Ribo-5-phosphate isomerase; DNA binding domain	9.94	17.89	246	26.9
Q87M65	VP2393	LacI family transcriptional regulator	7.87	3.31	332	36.2
Q87QW7	VP1032	DNA-binding response regulator TorR	7.74	15.19	237	26.7
Q87FD8	VPA1741	Phosphosugar isomerase; DNA binding domain	7.47	4.95	283	30.8
Q87IK0	VPA0606	Putative AraC-type regulator	6.64	11.61	267	29.9
Q87T18	VP0252	LacI family transcriptional repressor CytR	4.51	9.85	335	36.8
Q87RT5	VP0692	LysR family transcriptional regulator GcvA	4.12	37.25	306	34.5
Q87MQ9	VP2172	Resolvase, recombinase; DNA binding domain	3.92	40.87	252	28.2
Q87N99	VP1976	LysR family transcriptional regulator MetR	3.44	28.38	303	34.1
Q87H16	VPA1149	ABC-transporter, SBP domain	2.41	2.42	414	45.3
Q87JP6	VPA0202	GGDEF family protein	2.36	3.26	337	38.2
Q87QW9	VP1030	PurR purine nucleotide synthesis repressor	2.35	4.19	334	37.7
Q87TB6	VP0154	Osmolarity response regulator OmpR	2.33	3.77	239	27.3
Q87QB4	VP1236	Phosphogluconate repressor HexR	2.33	3.52	284	31.5
Q87FZ8	VPA1522	LysR family transcriptional regulator	2.30	3.56	309	34.4
Q87S55	VP0569	DNA-binding response regulator PhoB	2.20	4.80	229	26.1
Q87M71	VP2387	DeoR family transcriptional regulator	2.15	3.80	263	29.2
Q87J66	VPA0387	LysR family transcriptional regulator	2.09	3.86	311	34.7
Q87P35	VP1683	Hypothetical protein; periplasmic binding domain	2.01	4.31	325	35.0

Table 12 (continued)

Q87GI4	VPA1332	Transcriptional regulator ToxR	1.98	26.88	253	28.9
Q87PW3	VP1387	Unknown	1.85	12.87	3412	363.4
Q87TA3	VP0167	Peptidoglycan endopeptidase (M. tuberculosis, S. pneumoniae)	1.78	49.21	254	28.4
Q87HC0	VPA1045	Lipoprotein nlpI (E. coli)	1.76	4.89	511	57.0
Q87JN2	VPA0216	LysR family transcriptional regulator	1.63	29.32	307	34.1
Q79YT7	VPA1505	Chaperone CsuC	1.49	16.99	259	29.9
Q87HR9	VPA0887	Uncharacterized; putative catalytic domains	1.22	29.46	129	14.2
Q87TB5	VP0155	Osmolarity sensor protein EnvZ	0.00	10.23	430	47.6
Q87JQ8	VPA0190	Oxidase	0.00	29.66	408	45.3

Table 13 Candidate transcriptional regulators

<b>locus tag</b>	<b>Predicted Domains</b>
VP0489	Aerobic respiration control protein FexA
VP0527	Na <sup>+</sup> /H <sup>+</sup> antiporter regulatory protein NhaR
VP0350	LysR family transcriptional regulator LeuO
VP1133	Nucleoid associated protein H-NS
VP2393	LacI family transcriptional regulator
VP1032	DNA-binding response regulator TorR
VPA0606	Putative AraC-type regulator
VP0252	LacI family transcriptional repressor CytR
VP0692	LysR family transcriptional regulator GcvA
VP1976	LysR family transcriptional regulator MetR
VP1236	phosphogluconate repressor HexR
VP0154	Osmolarity response regulator OmpR
VPA1522	LysR family transcriptional regulator
VP0569	DNA binding response regulator
VP2387	DeoR family transcriptional regulator
VPA0387	LysR family transcriptional regulator
VPA1332	Transcriptional regulator ToxR
VPA0216	LysR family transcriptional regulator

## REFERENCES

1. Galinski EA, Trüper HG. 1994. Microbial behaviour in salt-stressed ecosystems. *FEMS Microbiology Reviews* 15:95-108.
2. Rengpipat S, Lowe SE, Zeikus JG. 1988. Effect of extreme salt concentrations on the physiology and biochemistry of *Halobacteroides acetoethylicus*. *J Bacteriol* 170:3065-71.
3. Oren A. 1986. Intracellular salt concentrations of the anaerobic halophilic eubacteria *Haloanaerobium praevalens* and *Halobacteroides halobius*. *Canadian Journal of Microbiology* 32:4-9.
4. Lanyi JK. 1974. Salt-dependent properties of proteins from extremely halophilic bacteria. *Bacteriol Rev* 38:272-90.
5. Kempf B, Bremer E. 1998. Uptake and synthesis of compatible solutes as microbial stress responses to high-osmolality environments. *Arch Microbiol* 170:319-30.
6. Ochrombel I, Becker M, Kramer R, Marin K. 2011. Osmotic stress response in *C. glutamicum*: impact of channel- and transporter-mediated potassium accumulation. *Arch Microbiol* 193:787-96.
7. Epstein W. 1986. Osmoregulation by potassium transport in *Escherichia coli*. *FEMS Microbiology Letters* 39:73-78.
8. Booth IR, Higgins CF. 1990. Enteric bacteria and osmotic stress: intracellular potassium glutamate as a secondary signal of osmotic stress? *FEMS Microbiol Rev* 6:239-46.
9. Wood JM. 1999. Osmosensing by bacteria: signals and membrane-based sensors. *Microbiol Mol Biol Rev* 63:230-62.
10. Wood JM, Bremer E, Csonka LN, Kraemer R, Poolman B, van der Heide T, Smith LT. 2001. Osmosensing and osmoregulatory compatible solute accumulation by bacteria. *Comp Biochem Physiol A Mol Integr Physiol* 130:437-60.
11. Saum SH, Müller V. 2007. Salinity-Dependent Switching of Osmolyte Strategies in a Moderately Halophilic Bacterium: Glutamate Induces Proline Biosynthesis in *Halobacillus halophilus*.
12. Poolman B, Glaasker E. 1998. Regulation of compatible solute accumulation in bacteria. *Mol Microbiol* 29:397-407.
13. da Costa MS, Santos H, Galinski EA. 1998. An overview of the role and diversity of compatible solutes in Bacteria and Archaea. *Adv Biochem Eng Biotechnol* 61:117-53.
14. Galinski EA, Oren A. 1991. Isolation and structure determination of a novel compatible solute from the moderately halophilic purple sulfur bacterium *Ectothiorhodospira marismortui*. *Eur J Biochem* 198:593-598.
15. Galinski EA. 1995. Osmoadaptation in bacteria. *Adv Microb Physiol* 37:272-328.

16. Sleator RD, Hill C. 2002. Bacterial osmoadaptation: the role of osmolytes in bacterial stress and virulence. *FEMS Microbiol Rev* 26:49-71.
17. Roberts MF. 2004. Osmoadaptation and osmoregulation in archaea: update 2004. *Front Biosci* 9:1999-2019.
18. Roberts MF. 2005. Organic compatible solutes of halotolerant and halophilic microorganisms. *Saline Systems* 1:5.
19. Cosquer A, Pichereau V, Pocard JA, Minet J, Cormier M, Bernard T. 1999. Nanomolar levels of dimethylsulfoniopropionate, dimethylsulfonioacetate, and glycine betaine are sufficient to confer osmoprotection to *Escherichia coli*. *Appl Environ Microbiol* 65:3304-11.
20. Menaia J, Duarte J, Boone D. 1993. Osmotic adaptation of moderately halophilic methanogenic Archaeobacteria, and detection of cytosolic N,N-dimethylglycine | SpringerLink. *Experientia* 49:1047-1054.
21. Cayley S, Lewis BA, Record MT, Jr. 1992. Origins of the osmoprotective properties of betaine and proline in *Escherichia coli* K-12. *J Bacteriol* 174:1586-95.
22. Record MT, Jr., Courtenay ES, Cayley DS, Guttman HJ. 1998. Responses of *E. coli* to osmotic stress: large changes in amounts of cytoplasmic solutes and water. *Trends Biochem Sci* 23:143-8.
23. Yancey P. 1994. Compatible and counteracting solutes, p 81-109. *In* Strange K (ed), *Cellular and Molecular Physiology of Cell Volume Regulation*. CRC Press, Boca Raton, FL.
24. Reed RH, Richardson DL, Warr SRC, Stewart WDP. 1984. Carbohydrate accumulation and osmotic stress in cyanobacteria, vol 130, p 1-4. *J General Microbiology*.
25. Galinski EA, Institut für Mikrobiologie der Rheinischen Friedrich-Wilhelms-Universität B, Meckenheimer Allee 168, F.R.G., Trüper HG, Institut für Mikrobiologie der Rheinischen Friedrich-Wilhelms-Universität B, Meckenheimer Allee 168, F.R.G. 1982. Betaine, a compatible solute in the extremely halophilic phototrophic bacterium *Ectothiorhodospira halochloris*. *FEMS Microbiology Letters* 13:357-360.
26. Imhoff JF. 1986. Osmoregulation and compatible solutes in eubacteria. *FEMS Microbiology Letters* 39:57-66.
27. Robertson DE, Noll D, Roberts MF, Menaia JA, Boone DR. 1990. Detection of the osmoregulator betaine in methanogens. *Appl Environ Microbiol* 56:563-5.
28. Severin J, Axel W, Galinski EA. 1992. The predominant role of recently discovered tetrahydropyrimidines for the osmoadaptation of halophilic eubacteria. *J General Microbiology* 138:1629-38.
29. Frings E, Institut für Mikrobiologie und Biotechnologie RFWU, Bonn, FRG, Kunte HJ, Institut für Mikrobiologie und Biotechnologie RFWU, Bonn, FRG, Galinski EA, Institut für Mikrobiologie und Biotechnologie RFWU, Bonn,

- FRG. 1993. Compatible solutes in representatives of the genera *Brevibacterium* and *Corynebacterium*: Occurrence of tetrahydropyrimidines and glutamine. *FEMS Microbiology Letters* 109:25-32.
30. Ventosa A, Nieto JJ, Oren A. 1998. Biology of Moderately Halophilic Aerobic Bacteria. *Microbiol Mol Biol Rev* 62:504-44.
  31. Wohlfarth A, Severin J, Galinski EA. 1990. The spectrum of compatible solutes in heterotrophic halophilic eubacteria of the family Halomonadaceae.
  32. Widderich N, Hoppner A, Pittelkow M, Heider J, Smits SH, Bremer E. 2014. Biochemical properties of ectoine hydroxylases from extremophiles and their wider taxonomic distribution among microorganisms. *PLoS One* 9:e93809.
  33. Widderich N, Czech L, Elling FJ, Konneke M, Stoveken N, Pittelkow M, Riclea R, Dickschat JS, Heider J, Bremer E. 2016. Strangers in the archaeal world: osmostress-responsive biosynthesis of ectoine and hydroxyectoine by the marine thaumarchaeon *Nitrosopumilus maritimus*. *Environ Microbiol* 18:1227-48.
  34. Czech L, Hermann L, Stoveken N, Richter AA, Hoppner A, Smits SHJ, Heider J, Bremer E. 2018. Role of the Extremolytes Ectoine and Hydroxyectoine as Stress Protectants and Nutrients: Genetics, Phylogenomics, Biochemistry, and Structural Analysis. *Genes (Basel)* 9.
  35. Dinnbier U, Limpinsel E, Schmid R, Bakker EP. 1988. Transient accumulation of potassium glutamate and its replacement by trehalose during adaptation of growing cells of *Escherichia coli* K-12 to elevated sodium chloride concentrations. *Arch Microbiol* 150:348-57.
  36. Strom AR, Kaasen I. 1993. Trehalose metabolism in *Escherichia coli*: stress protection and stress regulation of gene expression. *Mol Microbiol* 8:205-10.
  37. Horlacher R, Uhland K, Klein W, Ehrmann M, Boos W. 1996. Characterization of a cytoplasmic trehalase of *Escherichia coli*. *J Bacteriol* 178:6250-7.
  38. Kuhlmann AU, Bremer E. 2002. Osmotically regulated synthesis of the compatible solute ectoine in *Bacillus pasteurii* and related *Bacillus spp.* *Appl Environ Microbiol* 68:772-83.
  39. Reshetnikov AS, Khmelenina VN, Trotsenko YA. 2006. Characterization of the ectoine biosynthesis genes of haloalkalotolerant obligate methanotroph "*Methylobacterium alcaliphilum* 20Z". *Arch Microbiol* 184:286-97.
  40. Louis P, Galinski EA. 1997. Characterization of genes for the biosynthesis of the compatible solute ectoine from *Marinococcus halophilus* and osmoregulated expression in *Escherichia coli*. *Microbiology* 143 ( Pt 4):1141-9.
  41. Lo CC, Bonner CA, Xie G, D'Souza M, Jensen RA. 2009. Cohesion group approach for evolutionary analysis of aspartokinase, an enzyme that feeds a branched network of many biochemical pathways, p 594-651, *Microbiol Mol Biol Rev*, vol 73.

42. Pastor JM, Salvador M, Argandona M, Bernal V, Reina-Bueno M, Csonka LN, Iborra JL, Vargas C, Nieto JJ, Canovas M. 2010. Ectoines in cell stress protection: uses and biotechnological production. *Biotechnol Adv* 28:782-801.
43. Schwibbert K, Marin-Sanguino A, Bagyan I, Heidrich G, Lentzen G, Seitz H, Rampp M, Schuster SC, Klenk HP, Pfeiffer F, Oesterhelt D, Kunte HJ. 2011. A blueprint of ectoine metabolism from the genome of the industrial producer *Halomonas elongata* DSM 2581 T. *Environ Microbiol* 13:1973-94.
44. Vargas C, Argandona M, Reina-Bueno M, Rodriguez-Moya J, Fernandez-Aunion C, Nieto JJ. 2008. Unravelling the adaptation responses to osmotic and temperature stress in *Chromohalobacter salexigens*, a bacterium with broad salinity tolerance. *Saline Systems* 4:14.
45. Naughton LM, Blumerman SL, Carlberg M, Boyd EF. 2009. Osmoadaptation among *Vibrio* species and unique genomic features and physiological responses of *Vibrio parahaemolyticus*. *Appl Environ Microbiol* 75:2802-10.
46. Bursy J, Pierik AJ, Pica N, Bremer E. 2007. Osmotically induced synthesis of the compatible solute hydroxyectoine is mediated by an evolutionarily conserved ectoine hydroxylase. *J Biol Chem* 282:31147-55.
47. Lai MC, Yang DR, Chuang MJ. 1999. Regulatory factors associated with synthesis of the osmolyte glycine betaine in the halophilic methanoarchaeon *Methanohalophilus portucalensis*. *Appl Environ Microbiol* 65:828-33.
48. Roberts MF, Lai MC, Gunsalus RP. 1992. Biosynthetic pathways of the osmolytes N epsilon-acetyl-beta-lysine, beta-glutamine, and betaine in *Methanohalophilus* strain FDF1 suggested by nuclear magnetic resonance analyses. *J Bacteriol* 174:6688-93.
49. Kimura Y, Kawasaki S, Yoshimoto H, Takegawa K. 2010. Glycine betaine biosynthesized from glycine provides an osmolyte for cell growth and spore germination during osmotic stress in *Myxococcus xanthus*. *J Bacteriol* 192:1467-70.
50. Lu WD, Chi ZM, Su CD. 2006. Identification of glycine betaine as compatible solute in *Synechococcus* sp. WH8102 and characterization of its N-methyltransferase genes involved in betaine synthesis. *Arch Microbiol* 186:495-506.
51. Nyysölä A, Kerovuori J, Kaukinen P, Weymarn Nv, Reinikainen T. 2000. Extreme Halophiles Synthesize Betaine from Glycine by Methylation. *J Biol Chem* 275:22196-201.
52. Nyysölä A, Reinikainen T, Leisola M. 2001. Characterization of glycine sarcosine N-methyltransferase and sarcosine dimethylglycine N-methyltransferase. *Appl Environ Microbiol* 67:2044-50.
53. Nyysölä A, Leisola M. 2001. *Actinopolyspora halophila* has two separate pathways for betaine synthesis. *Arch Microbiol* 176:294-300.
54. Waditee R, Tanaka Y, Aoki K, Hibino T, Jikuya H, Takano J, Takabe T. 2003. Isolation and functional characterization of N-methyltransferases that catalyze

- betaine synthesis from glycine in a halotolerant photosynthetic organism *Aphanothece halophytica*. *J Biol Chem* 278:4932-42.
55. Lamark T, Rokenes TP, McDougall J, Strom AR. 1996. The complex bet promoters of *Escherichia coli*: regulation by oxygen (ArcA), choline (BetI), and osmotic stress. *J Bacteriol* 178:1655-62.
  56. Rokenes TP, Lamark T, Strom AR. 1996. DNA-binding properties of the BetI repressor protein of *Escherichia coli*: the inducer choline stimulates BetI-DNA complex formation. *J Bacteriol* 178:1663-70.
  57. Andresen PA, Kaasen I, Styrvold OB, Boulnois G, Strom AR. 1988. Molecular cloning, physical mapping and expression of the bet genes governing the osmoregulatory choline-glycine betaine pathway of *Escherichia coli*. *J Gen Microbiol* 134:1737-46.
  58. Landfald B, Strom AR. 1986. Choline-glycine betaine pathway confers a high level of osmotic tolerance in *Escherichia coli*. *J Bacteriol* 165:849-55.
  59. Ongagna-Yhombi SY, Boyd EF. 2013. Biosynthesis of the osmoprotectant ectoine, but not glycine betaine, is critical for survival of osmotically stressed *Vibrio parahaemolyticus* cells. *Appl Environ Microbiol* 79:5038-49.
  60. Ongagna-Yhombi SY, McDonald ND, Boyd EF. 2015. Deciphering the role of multiple betaine-carnitine-choline transporters in the Halophile *Vibrio parahaemolyticus*. *Appl Environ Microbiol* 81:351-63.
  61. Gregory GJ, Morreale DP, Boyd EF. 2020. CosR is a global regulator of the osmotic stress response with widespread distribution among bacteria. *Appl Environ Microbiol* 86.
  62. van Kessel JC, Rutherford ST, Cong JP, Quinodoz S, Healy J, Bassler BL. 2015. Quorum sensing regulates the osmotic stress response in *Vibrio harveyi*. *J Bacteriol* 197:73-80.
  63. Bashir A, Hoffmann T, Smits SH, Bremer E. 2014. Dimethylglycine provides salt and temperature stress protection to *Bacillus subtilis*. *Appl Environ Microbiol* 80:2773-85.
  64. Casaite V, Poviloniene S, Meskiene R, Rutkiene R, Meskys R. 2011. Studies of dimethylglycine oxidase isoenzymes in *Arthrobacter globiformis* cells. *Curr Microbiol* 62:1267-73.
  65. Wargo MJ, Szwergold BS, Hogan DA. 2008. Identification of two gene clusters and a transcriptional regulator required for *Pseudomonas aeruginosa* glycine betaine catabolism. *J Bacteriol* 190:2690-9.
  66. Incharoensakdi A, Waditee R. 2000. Degradation of glycinebetaine by betaine-homocysteine methyltransferase in *Aphanothece halophytica*: effect of salt downshock and starvation. *Curr Microbiol* 41:227-31.
  67. White RF, Kaplan L, Birnbaum J. 1973. Betaine-homocysteine transmethylase in *Pseudomonas denitrificans*, a vitamin B 12 overproducer. *J Bacteriol* 113:218-23.

68. Gregory G, Dutta A, Parashar V, Boyd E. 2020. Investigations of dimethylglycine (DMG), glycine betaine and ectoine uptake by a BCCT family transporter with broad substrate specificity in *Vibrio* species. bioRxiv.
69. Turner SM, Nightingale PD, Broadgate W, Liss PS. 1995. The distribution of dimethyl sulphide and dimethylsulphoniopropionate in Antarctic waters and sea ice. 42:1059-1080.
70. Keller MD, Bellows WK, Guillard RRL. 1989. Dimethyl sulfide production in marine phytoplankton, p 167-182, *Biog Sulfur Environ*, vol 393. ACS Publications.
71. Burgermeister S, Zimmerman RL, Georgii HW, Bingemer HG, Kirst GO, Janssen M, Ernst W. 1990. On the biogenic origin of dimethylsulfide: Relation between chlorophyll, ATP, organismic DMSP, phytoplankton species, and DMS distribution in Atlantic surface water and atmosphere. *J Geophys Res* 95:607-615.
72. Kiene RP, Linn LJ, Bruton JA. 2000. New and important roles for DMSP in marine microbial communities. *J Sea Research* 43:209-224.
73. Malin GK, G.O. 1997. Algal production of dimethyl sulfide and its atmospheric role. *J Phycol* 33:889-896.
74. King GM. 1984. Metabolism of trimethylamine, choline, and glycine betaine by sulfate-reducing and methanogenic bacteria in marine sediments. *Appl Environ Microbiol* 48:719-25.
75. Oren A. 1999. Bioenergetic aspects of halophilism. *Microbiol Mol Biol Rev* 63:334-48.
76. Youssef NH, Savage-Ashlock KN, McCully AL, Luedtke B, Shaw EI, Hoff WD, Elshahed MS. 2014. Trehalose/2-sulfotrehalose biosynthesis and glycine-betaine uptake are widely spread mechanisms for osmoadaptation in the Halobacteriales. *Isme j* 8:636-49.
77. Wood JM. 2007. Bacterial osmosensing transporters. *Methods Enzymol* 428:77-107.
78. Wood JM. 2011. Bacterial osmoregulation: a paradigm for the study of cellular homeostasis. *Annu Rev Microbiol* 65:215-38.
79. Wood JM, Culham DE, Hillar A, Vernikovska YI, Liu F, Boggs JM, Keates RA. 2005. A structural model for the osmosensor, transporter, and osmoregulator ProP of *Escherichia coli*. *Biochemistry* 44:5634-46.
80. Wood JM. 2010. Osmotic Stress, p 133-56. *In* G. Storz RH (ed), *Bacterial Stress Responses*. ASM, Washington, D.C.
81. Lamark T, Kaasen I, Eshoo MW, Falkenberg P, McDougall J, Strom AR. 1991. DNA sequence and analysis of the bet genes encoding the osmoregulatory choline-glycine betaine pathway of *Escherichia coli*. *Mol Microbiol* 5:1049-64.
82. Kappes RM, Kempf B, Bremer E. 1996. Three transport systems for the osmoprotectant glycine betaine operate in *Bacillus subtilis*: characterization of OpuD. *J Bacteriol* 178:5071-9.

83. Peter H, Burkovski A, Kramer R. 1996. Isolation, characterization, and expression of the *Corynebacterium glutamicum* betP gene, encoding the transport system for the compatible solute glycine betaine. *J Bacteriol* 178:5229-34.
84. Eichler K, Bourgis F, Buchet A, Kleber HP, Mandrand-Berthelot MA. 1994. Molecular characterization of the cai operon necessary for carnitine metabolism in *Escherichia coli*. *Mol Microbiol* 13:775-86.
85. Ziegler C, Bremer E, Kramer R. 2010. The BCCT family of carriers: from physiology to crystal structure. *Mol Microbiol* 78:13-34.
86. Ressler S, Terwisscha van Scheltinga AC, Vonrhein C, Ott V, Ziegler C. 2009. Molecular basis of transport and regulation in the Na(+)/betaine symporter BetP. *Nature* 458:47-52.
87. Eitinger T, Rodionov DA, Grote M, Schneider E. 2011. Canonical and ECF-type ATP-binding cassette importers in prokaryotes: diversity in modular organization and cellular functions. *FEMS Microbiol Rev* 35:3-67.
88. May G, Faatz E, Villarejo M, Bremer E. 1986. Binding protein dependent transport of glycine betaine and its osmotic regulation in *Escherichia coli* K12. *Mol Gen Genet* 205:225-33.
89. Kempf B, Bremer E. 1995. OpuA, an osmotically regulated binding protein-dependent transport system for the osmoprotectant glycine betaine in *Bacillus subtilis*. *J Biol Chem* 270:16701-13.
90. Mahmood NA, Biemans-Oldehinkel E, Patzlaff JS, Schuurman-Wolters GK, Poolman B. 2006. Ion specificity and ionic strength dependence of the osmoregulatory ABC transporter OpuA. *J Biol Chem* 281:29830-9.
91. Chen C, Beattie GA. 2007. Characterization of the osmoprotectant transporter OpuC from *Pseudomonas syringae* and demonstration that cystathionine-beta-synthase domains are required for its osmoregulatory function. *J Bacteriol* 189:6901-12.
92. Kappes RM, Kempf B, Kneip S, Boch J, Gade J, Meier-Wagner J, Bremer E. 1999. Two evolutionarily closely related ABC transporters mediate the uptake of choline for synthesis of the osmoprotectant glycine betaine in *Bacillus subtilis*. *Mol Microbiol* 32:203-16.
93. Biemans-Oldehinkel E, Mahmood NA, Poolman B. 2006. A sensor for intracellular ionic strength. *Proc Natl Acad Sci U S A* 103:10624-9.
94. Haardt M, Kempf B, Faatz E, Bremer E. 1995. The osmoprotectant proline betaine is a major substrate for the binding-protein-dependent transport system ProU of *Escherichia coli* K-12. *Mol Gen Genet* 246:783-6.
95. Haardt M, Bremer E. 1996. Use of *phoA* and *lacZ* fusions to study the membrane topology of ProW, a component of the osmoregulated ProU transport system of *Escherichia coli*. *J Bacteriol* 178:5370-81.
96. Gowrishankar J, Manna D. 1996. How is osmotic regulation of transcription of the *Escherichia coli* proU operon achieved? A review and a model. *Genetica* 97:363-78.

97. Lucht JM, Bremer E. 1994. Adaptation of *Escherichia coli* to high osmolarity environments: osmoregulation of the high-affinity glycine betaine transport system proU. *FEMS Microbiol Rev* 14:3-20.
98. Gul N, Poolman B. 2013. Functional reconstitution and osmoregulatory properties of the ProU ABC transporter from *Escherichia coli*. *Mol Membr Biol* 30:138-48.
99. Nair GB, Ramamurthy T, Bhattacharya SK, Dutta B, Takeda Y, Sack DA. 2007. Global dissemination of *Vibrio parahaemolyticus* serotype O3:K6 and its serovariants. *Clin Microbiol Rev* 20:39-48.
100. Su YC, Liu C. 2007. *Vibrio parahaemolyticus*: a concern of seafood safety. *Food Microbiol* 24:549-58.
101. Daniels NA, MacKinnon L, Bishop R, Altekruze S, Ray B, Hammond RM, Thompson S, Wilson S, Bean NH, Griffin PM, Slutsker L. 2000. *Vibrio parahaemolyticus* infections in the United States, 1973-1998. *J Infect Dis* 181:1661-6.
102. McLaughlin JB, DePaola A, Bopp CA, Martinek KA, Napolilli NP, Allison CG, Murray SL, Thompson EC, Bird MM, Middaugh JP. 2005. Outbreak of *Vibrio parahaemolyticus* gastroenteritis associated with Alaskan oysters. *N Engl J Med* 353:1463-70.
103. CDC. 2017. Questions and Answers | *Vibrio* Illness (Vibriosis) | CDC. <https://www.cdc.gov/vibrio/faq.html>.
104. Makino K, Oshima K, Kurokawa K, Yokoyama K, Uda T, Tagomori K, Iijima Y, Najima M, Nakano M, Yamashita A, Kubota Y, Kimura S, Yasunaga T, Honda T, Shinagawa H, Hattori M, Iida T. 2003. Genome sequence of *Vibrio parahaemolyticus*: a pathogenic mechanism distinct from that of *V. cholerae*. *Lancet* 361:743-9.
105. Burdette DL, Yarbrough ML, Orvedahl A, Gilpin CJ, Orth K. 2008. *Vibrio parahaemolyticus* orchestrates a multifaceted host cell infection by induction of autophagy, cell rounding, and then cell lysis. *Proc Natl Acad Sci U S A* 105:12497-502.
106. Whitaker WB, Parent MA, Boyd A, Richards GP, Boyd EF. 2012. The *Vibrio parahaemolyticus* ToxRS regulator is required for stress tolerance and colonization in a novel orogastric streptomycin-induced adult murine model. *Infect Immun* 80:1834-45.
107. Kalburge SS, Carpenter MR, Rozovsky S, Boyd EF. 2017. Quorum Sensing Regulators Are Required for Metabolic Fitness in *Vibrio parahaemolyticus*. *Infect Immun* 85:e00930-16.
108. Gregory GJ, Morreale DP, Carpenter MR, Kalburge SS, Boyd EF. 2019. Quorum sensing regulators AphA and OpaR control expression of the operon responsible for biosynthesis of the compatible solute ectoine. *Appl Environ Microbiol* 85.

109. Shikuma NJ, Davis KR, Fong JN, Yildiz FH. 2013. The transcriptional regulator, CosR, controls compatible solute biosynthesis and transport, motility and biofilm formation in *Vibrio cholerae*. *Environ Microbiol* 15:1387-99.
110. Mustakhimov, II, Reshetnikov AS, Glukhov AS, Khmelenina VN, Kalyuzhnaya MG, Trotsenko YA. 2010. Identification and characterization of EctR1, a new transcriptional regulator of the ectoine biosynthesis genes in the halotolerant methanotroph *Methylobacterium alcaliphilum* 20Z. *J Bacteriol* 192:410-7.
111. Chaparian RR, Olney SG, Hustmyer CM, Rowe-Magnus DA, van Kessel JC. 2016. Integration host factor and LuxR synergistically bind DNA to coactivate quorum-sensing genes in *Vibrio harveyi*. *Mol Microbiol* 101:823-40.
112. Eshoo MW. 1988. lac fusion analysis of the bet genes of *Escherichia coli*: regulation by osmolarity, temperature, oxygen, choline, and glycine betaine. *J Bacteriol* 170:5208-15.
113. Czech L, Poehl S, Hub P, Stoeveken N, Bremer E. 2018. Tinkering with osmotically controlled transcription allows enhanced production and excretion of ectoine and hydroxyectoine from a microbial cell factory. *Appl Environ Microbiol* 84:e01772-17.
114. Rao NV, Shashidhar R, Bandekar JR. 2013. Comparative analysis of induction of osmotic-stress-dependent genes in *Vibrio vulnificus* exposed to hyper- and hypo-osmotic stress. *Can J Microbiol* 59:333-8.
115. Scholz A, Stahl J, de Berardinis V, Muller V, Averhoff B. 2016. Osmotic stress response in *Acinetobacter baylyi*: identification of a glycine-betaine biosynthesis pathway and regulation of osmoadaptive choline uptake and glycine-betaine synthesis through a choline-responsive BetI repressor. *Environ Microbiol Rep* 8:316-22.
116. Malek AA, Chen C, Wargo MJ, Beattie GA, Hogan DA. 2011. Roles of Three Transporters, CbcXWV, BetT1, and BetT3, in *Pseudomonas aeruginosa* Choline Uptake for Catabolism. *J Bacteriol* 193:3033-41.
117. Khodr A, Fairweather V, Bouffartigues E, Rimsky S. 2015. IHF is a trans-acting factor implicated in the regulation of the proU P2 promoter. *FEMS Microbiol Lett* 362:1-6.
118. Kernell Burke A, Guthrie LT, Modise T, Cormier G, Jensen RV, McCarter LL, Stevens AM. 2015. OpaR controls a network of downstream transcription factors in *Vibrio parahaemolyticus* BB22OP. *PLoS One* 10:e0121863.
119. Gode-Potratz CJ, McCarter LL. 2011. Quorum sensing and silencing in *Vibrio parahaemolyticus*. *J Bacteriol* 193:4224-37.
120. McCarter LL. 1998. OpaR, a homolog of *Vibrio harveyi* LuxR, controls opacity of *Vibrio parahaemolyticus*. *J Bacteriol* 180:3166-73.
121. Henke JM, Bassler BL. 2004. Quorum sensing regulates type III secretion in *Vibrio harveyi* and *Vibrio parahaemolyticus*. *J Bacteriol* 186:3794-805.
122. Ng WL, Bassler BL. 2009. Bacterial quorum-sensing network architectures. *Annu Rev Genet* 43:197-222.

123. Cao JG, Meighen EA. 1989. Purification and structural identification of an autoinducer for the luminescence system of *Vibrio harveyi*. *J Biol Chem* 264:21670-6.
124. Freeman JA, Lilley BN, Bassler BL. 2000. A genetic analysis of the functions of LuxN: a two-component hybrid sensor kinase that regulates quorum sensing in *Vibrio harveyi*. *Mol Microbiol* 35:139-49.
125. Swem LR, Swem DL, Wingreen NS, Bassler BL. 2008. Deducing receptor signaling parameters from in vivo analysis: LuxN/AI-1 quorum sensing in *Vibrio harveyi*. *Cell* 134:461-73.
126. Bassler BL, Wright M, Showalter RE, Silverman MR. 1993. Intercellular signalling in *Vibrio harveyi*: sequence and function of genes regulating expression of luminescence. *Mol Microbiol* 9:773-86.
127. Bassler BL, Wright M, Silverman MR. 1994. Multiple signalling systems controlling expression of luminescence in *Vibrio harveyi*: sequence and function of genes encoding a second sensory pathway. *Mol Microbiol* 13:273-86.
128. Schauder S, Shokat K, Surette MG, Bassler BL. 2001. The LuxS family of bacterial autoinducers: biosynthesis of a novel quorum-sensing signal molecule. *Mol Microbiol* 41:463-76.
129. Neiditch MB, Federle MJ, Miller ST, Bassler BL, Hughson FM. 2005. Regulation of LuxPQ receptor activity by the quorum-sensing signal autoinducer-2. *Mol Cell* 18:507-18.
130. Neiditch MB, Federle MJ, Pompeani AJ, Kelly RC, Swem DL, Jeffrey PD, Bassler BL, Hughson FM. 2006. Ligand-induced asymmetry in histidine sensor kinase complex regulates quorum sensing. *Cell* 126:1095-108.
131. Surette MG, Miller MB, Bassler BL. 1999. Quorum sensing in *Escherichia coli*, *Salmonella typhimurium*, and *Vibrio harveyi*: a new family of genes responsible for autoinducer production. *Proc Natl Acad Sci U S A* 96:1639-44.
132. Higgins DA, Pomianek ME, Kraml CM, Taylor RK, Semmelhack MF, Bassler BL. 2007. The major *Vibrio cholerae* autoinducer and its role in virulence factor production. *Nature* 450:883-6.
133. Miller MB, Skorupski K, Lenz DH, Taylor RK, Bassler BL. 2002. Parallel quorum sensing systems converge to regulate virulence in *Vibrio cholerae*. *Cell* 110:303-14.
134. Freeman JA, Bassler BL. 1999. Sequence and function of LuxU: a two-component phosphorelay protein that regulates quorum sensing in *Vibrio harveyi*. *J Bacteriol* 181:899-906.
135. Freeman JA, Bassler BL. 1999. A genetic analysis of the function of LuxO, a two-component response regulator involved in quorum sensing in *Vibrio harveyi*. *Mol Microbiol* 31:665-77.
136. Lenz DH, Mok KC, Lilley BN, Kulkarni RV, Wingreen NS, Bassler BL. 2004. The small RNA chaperone Hfq and multiple small RNAs control quorum sensing in *Vibrio harveyi* and *Vibrio cholerae*. *Cell* 118:69-82.

137. Feng L, Rutherford ST, Papenfort K, Bagert JD, van Kessel JC, Tirrell DA, Wingreen NS, Bassler BL. 2015. A Qrr noncoding RNA deploys four different regulatory mechanisms to optimize quorum-sensing dynamics. *Cell* 160:228-40.
138. Rutherford ST, van Kessel JC, Shao Y, Bassler BL. 2011. AphA and LuxR/HapR reciprocally control quorum sensing in vibrios. *Genes Dev* 25:397-408.
139. Zhang Y, Qiu Y, Tan Y, Guo Z, Yang R, Zhou D. 2012. Transcriptional regulation of *opaR*, *qrr2-4* and *aphA* by the master quorum-sensing regulator OpaR in *Vibrio parahaemolyticus*. *PLoS One* 7:e34622.
140. Tu KC, Waters CM, Svenningsen SL, Bassler BL. 2008. A small-RNA-mediated negative feedback loop controls quorum-sensing dynamics in *Vibrio harveyi*. *Mol Microbiol* 70:896-907.
141. Shao Y, Feng L, Rutherford ST, Papenfort K, Bassler BL. 2013. Functional determinants of the quorum-sensing non-coding RNAs and their roles in target regulation. *Embo j* 32:2158-71.
142. Tu KC, Bassler BL. 2007. Multiple small RNAs act additively to integrate sensory information and control quorum sensing in *Vibrio harveyi*. *Genes Dev* 21:221-33.
143. van Kessel JC, Rutherford ST, Shao Y, Utria AF, Bassler BL. 2013. Individual and combined roles of the master regulators AphA and LuxR in control of the *Vibrio harveyi* quorum-sensing regulon. *J Bacteriol* 195:436-43.
144. Waters CM, Bassler BL. 2006. The *Vibrio harveyi* quorum-sensing system uses shared regulatory components to discriminate between multiple autoinducers. *Genes Dev* 20:2754-67.
145. Pompeani AJ, Irgon JJ, Berger MF, Bulyk ML, Wingreen NS, Bassler BL. 2008. The *Vibrio harveyi* master quorum-sensing regulator, LuxR, a TetR-type protein is both an activator and a repressor: DNA recognition and binding specificity at target promoters. *Mol Microbiol* 70:76-88.
146. Lin W, Kovacicova G, Skorupski K. 2007. The quorum sensing regulator HapR downregulates the expression of the virulence gene transcription factor AphA in *Vibrio cholerae* by antagonizing Lrp- and VpsR-mediated activation. *Mol Microbiol* 64:953-67.
147. Lin W, Kovacicova G, Skorupski K. 2005. Requirements for *Vibrio cholerae* HapR Binding and Transcriptional Repression at the hapR Promoter Are Distinct from Those at the aphA Promoter. *J Bacteriol* 187:3013-9.
148. Sun F, Zhang Y, Wang L, Yan X, Tan Y, Guo Z, Qiu J, Yang R, Xia P, Zhou D. 2012. Molecular characterization of direct target genes and cis-acting consensus recognized by quorum-sensing regulator AphA in *Vibrio parahaemolyticus*. *PLoS One* 7:e44210.
149. Lilley BN, Bassler BL. 2000. Regulation of quorum sensing in *Vibrio harveyi* by LuxO and sigma-54. *Mol Microbiol* 36:940-54.

150. Gibson DG. 2011. Enzymatic assembly of overlapping DNA fragments. *Methods Enzymol* 498:349-61.
151. Horton RM, Ho SN, Pullen JK, Pease LR. 1989. Engineering hybrid genes without the use of restriction enzymes: gene splicing by overlap extension. *Gene* 77:61-68.
152. Livak KJ, Schmittgen TD. 2001. Analysis of relative gene expression data using real-time quantitative PCR and the  $2^{-\Delta\Delta C_T}$  method. *Methods* 25:402-8.
153. Karunakaran R, Mauchline TH, Hosie AH, Poole PS. 2005. A family of promoter probe vectors incorporating autofluorescent and chromogenic reporter proteins for studying gene expression in Gram-negative bacteria. *Microbiology* 151:3249-56.
154. Korhonen J, Martinmaki P, Pizzi C, Rastas P, Ukkonen E. 2009. MOODS: fast search for position weight matrix matches in DNA sequences. *Bioinformatics* 25:3181-2.
155. Joelsson A, Kan B, Zhu J. 2007. Quorum sensing enhances the stress response in *Vibrio cholerae*. *Appl Environ Microbiol* 73:3742-6.
156. Kang Y, Goo E, Kim J, Hwang I. 2017. Critical role of quorum sensing-dependent glutamate metabolism in homeostatic osmolality and outer membrane vesiculation in *Burkholderia glumae*. *Sci Rep* 7:44195.
157. Whitaker WB, Parent MA, Naughton LM, Richards GP, Blumerman SL, Boyd EF. 2010. Modulation of responses of *Vibrio parahaemolyticus* O3:K6 to pH and temperature stresses by growth at different salt concentrations. *Appl Environ Microbiol* 76:4720-9.
158. Kalburge SS, Whitaker WB, Boyd EF. 2014. High-salt preadaptation of *Vibrio parahaemolyticus* enhances survival in response to lethal environmental stresses. *J Food Prot* 77:246-53.
159. Harvell CD, Kim K, Burkholder JM, Colwell RR, Epstein PR, Grimes DJ, Hofmann EE, Lipp EK, Osterhaus AD, Overstreet RM, Porter JW, Smith GW, Vasta GR. 1999. Emerging marine diseases--climate links and anthropogenic factors. *Science* 285:1505-10.
160. CDC. 2017. FoodNet 2015 Annual Foodborne Illness Surveillance Report | FoodNet | CDC.
161. Turner JW, Paranjpye RN, Landis ED, Biryukov SV, Gonzalez-Escalona N, Nilsson WB, Strom MS. 2013. Population structure of clinical and environmental *Vibrio parahaemolyticus* from the Pacific Northwest coast of the United States. *PLoS One* 8:e55726.
162. Paranjpye R, Hamel OS, Stojanovski A, Liermann M. 2012. Genetic diversity of clinical and environmental *Vibrio parahaemolyticus* strains from the Pacific Northwest. *Appl Environ Microbiol* 78:8631-8.
163. Dehio C, Meyer M. 1997. Maintenance of broad-host-range incompatibility group P and group Q plasmids and transposition of Tn5 in *Bartonella henselae* following conjugal plasmid transfer from *Escherichia coli*. *J Bacteriol* 179:538-40.

164. Philippe N, Alcaraz JP, Coursange E, Geiselmann J, Schneider D. 2004. Improvement of pCVD442, a suicide plasmid for gene allele exchange in bacteria. *Plasmid* 51:246-55.
165. Kovach ME, Phillips RW, Elzer PH, Roop RM, 2nd, Peterson KM. 1994. pBBR1MCS: a broad-host-range cloning vector. *Biotechniques* 16:800-2.
166. Liu J, Li F, Rozovsky S. 2013. The intrinsically disordered membrane protein selenoprotein S is a reductase *in vitro*. *Biochemistry* 52:3051-61.
167. Csonka LN. 1989. Physiological and genetic responses of bacteria to osmotic stress. *Microbiol Rev* 53:121-47.
168. Culham DE, Henderson J, Crane RA, Wood JM. 2002. Osmosensor ProP of *Escherichia coli* Responds to the Concentration, Chemistry, and Molecular Size of Osmolytes in the Proteoliposome Lumen. *Biochemistry* 42:410-20.
169. Rübenhagen R, Morbach S, Krämer R. 2001. The osmoreactive betaine carrier BetP from *Corynebacterium glutamicum* is a sensor for cytoplasmic K<sup>+</sup>. *EMBO J* 20:5412-20.
170. van der Heide T, Stuart MC, Poolman B. 2001. On the osmotic signal and osmosensing mechanism of an ABC transport system for glycine betaine. *EMBO J* 20:7022-32.
171. Cairney J, Booth IR, Higgins CF. 1985. Osmoregulation of gene expression in *Salmonella typhimurium*: proU encodes an osmotically induced betaine transport system. *J Bacteriol* 164:1224-32.
172. Pfaffl MW. 2001. A new mathematical model for relative quantification in real-time RT-PCR. *Nucleic Acids Res* 29:e45.
173. Bailey TL, Elkan C. 1994. Fitting a mixture model by expectation maximization to discover motifs in biopolymers. *Proc Int Conf Intell Syst Mol Biol* 2:28-36.
174. Sullivan MJ, Petty NK, Beatson SA. 2011. Easyfig: a genome comparison visualizer. *Bioinformatics* 27:1009-10.
175. Waterhouse A, Bertoni M, Bienert S, Studer G, Tauriello G, Gumienny R, Heer F, de Beer T, Rempfer C, Bordoli L, Lepore R, Schwede T. 2018. SWISS-MODEL: Homology Modelling of Protein Structures and Complexes. *Nucleic acids research* 46:W296-W303.
176. Guex N, Peitsch MC, Schwede T. 2009. Automated comparative protein structure modeling with SWISS-MODEL and Swiss-PdbViewer: a historical perspective. *Electrophoresis* 30 Suppl 1:S162-73.
177. Bienert S, Waterhouse A, de Beer TA, Tauriello G, Studer G, Bordoli L, Schwede T. 2017. The SWISS-MODEL Repository-new features and functionality. *Nucleic Acids Res* 45:D313-d319.
178. Benkert P, Biasini M, Schwede T. 2011. Toward the estimation of the absolute quality of individual protein structure models. *Bioinformatics* 27:343-50.
179. Bertoni M, Kiefer F, Biasini M, Bordoli L, Schwede T. 2017. Modeling protein quaternary structure of homo- and hetero-oligomers beyond binary interactions by homology. *Sci Rep* 7:10480.

180. Thompson JD, Higgins DG, Gibson TJ. 1994. CLUSTAL W: improving the sensitivity of progressive multiple sequence alignment through sequence weighting, position-specific gap penalties and weight matrix choice. *Nucleic Acids Res* 22:4673-80.
181. Saitou N, Nei M. 1987. The neighbor-joining method: a new method for reconstructing phylogenetic trees. *Mol Biol Evol* 4:406-25.
182. Felsenstein J. 1985. Confidence limits on phylogenies: An approach using the bootstrap. *Evolution* 39:783-791.
183. Jones DT, Taylor WR, Thornton JM. 1992. The rapid generation of mutation data matrices from protein sequences. *Comput Appl Biosci* 8:275-82.
184. Kumar S, Stecher G, Li M, Knyaz C, Tamura K. 2018. MEGA X: Molecular Evolutionary Genetics Analysis across Computing Platforms. *Mol Biol Evol* 35:1547-1549.
185. Shao Z, Deng W, Li S, He J, Ren S, Huang W, Lu Y, Zhao G, Cai Z, Wang J. 2015. GlnR-Mediated Regulation of ectABCD Transcription Expands the Role of the GlnR Regulon to Osmotic Stress Management. *J Bacteriol* 197:3041-7.
186. Pastor JM, Bernal V, Salvador M, Argandona M, Vargas C, Csonka L, Sevilla A, Iborra JL, Nieto JJ, Canovas M. 2013. Role of central metabolism in the osmoadaptation of the halophilic bacterium *Chromohalobacter salexigens*. *J Biol Chem* 288:17769-81.
187. Mustakhimov, II, Reshetnikov AS, Khmelenina VN, Trotsenko YA. 2009. EctR--a novel transcriptional regulator of ectoine biosynthesis genes in the haloalcaliphilic methylotrophic bacterium *Methylophaga alcalica*. *Dokl Biochem Biophys* 429:305-8.
188. Mustakhimov, II, Reshetnikov AS, Fedorov DN, Khmelenina VN, Trotsenko YA. 2012. Role of EctR as transcriptional regulator of ectoine biosynthesis genes in *Methylophaga thalassica*. *Biochemistry (Mosc)* 77:857-63.
189. Perera IC, Grove A. 2010. Molecular mechanisms of ligand-mediated attenuation of DNA binding by MarR family transcriptional regulators. *J Mol Cell Biol* 2:243-54.
190. Sulavik MC, Gambino LF, Miller PF. 1995. The MarR repressor of the multiple antibiotic resistance (mar) operon in *Escherichia coli*: prototypic member of a family of bacterial regulatory proteins involved in sensing phenolic compounds. *Mol Med* 1:436-46.
191. Cohen SP, Hachler H, Levy SB. 1993. Genetic and functional analysis of the multiple antibiotic resistance (mar) locus in *Escherichia coli*. *J Bacteriol* 175:1484-92.
192. Hong M, Fuangthong M, Helmann JD, Brennan RG. 2005. Structure of an OhrR-ohrA operator complex reveals the DNA binding mechanism of the MarR family. *Mol Cell* 20:131-41.
193. Kumarevel T, Tanaka T, Umehara T, Yokoyama S. 2009. ST1710-DNA complex crystal structure reveals the DNA binding mechanism of the MarR family of regulators. *Nucleic Acids Res* 37:4723-35.

194. Dolan KT, Duguid EM, He C. 2011. Crystal structures of SlyA protein, a master virulence regulator of Salmonella, in free and DNA-bound states. *J Biol Chem* 286:22178-85.
195. Hao Z, Lou H, Zhu R, Zhu J, Zhang D, Zhao BS, Zeng S, Chen X, Chan J, He C, Chen PR. 2014. The multiple antibiotic resistance regulator MarR is a copper sensor in *Escherichia coli*. *Nat Chem Biol* 10:21-8.
196. Deochand DK, Grove A. 2017. MarR family transcription factors: dynamic variations on a common scaffold. *Crit Rev Biochem Mol Biol* 52:595-613.
197. Reshetnikov AS, Khmelenina VN, Mustakhimov, II, Kalyuzhnaya M, Lidstrom M, Trotsenko YA. 2011. Diversity and phylogeny of the ectoine biosynthesis genes in aerobic, moderately halophilic methylophilic bacteria. *Extremophiles* 15:653-63.
198. Farwick M, Siewe RM, Kramer R. 1995. Glycine betaine uptake after hyperosmotic shift in *Corynebacterium glutamicum*. *J Bacteriol* 177:4690-5.
199. Perez C, Koshy C, Ressler S, Nicklisch S, Kramer R, Ziegler C. 2011. Substrate specificity and ion coupling in the Na<sup>+</sup>/betaine symporter BetP. *Embo j* 30:1221-9.
200. Chiou CS, Hsu SY, Chiu SI, Wang TK, Chao CS. 2000. *Vibrio parahaemolyticus* serovar O3:K6 as cause of unusually high incidence of food-borne disease outbreaks in Taiwan from 1996 to 1999. *J Clin Microbiol* 38:4621-5.
201. Joseph SW, Colwell RR, Kaper JB. 1982. *Vibrio parahaemolyticus* and related halophilic Vibrios. *Crit Rev Microbiol* 10:77-124.
202. Kaneko T, Colwell RR. 1973. Ecology of *Vibrio parahaemolyticus* in Chesapeake Bay. *J Bacteriol* 113:24-32.
203. Kaneko T, Colwell RR. 1974. Distribution of *Vibrio parahaemolyticus* and related organisms in the Atlantic Ocean off South Carolina and Georgia. *Appl Microbiol* 28:1009-17.
204. Kaneko T, Colwell RR. 1975. Incidence of *Vibrio parahaemolyticus* in Chesapeake Bay. *Appl Microbiol* 30:251-7.
205. Emsley P, Cowtan K. 2004. Coot: Model-Building Tools for Molecular Graphics. *Acta crystallographica Section D, Biological crystallography* 60.
206. Bhattacharya D, Nowotny J, Cao R, Cheng J. 2016. 3Drefine: An Interactive Web Server for Efficient Protein Structure Refinement. *Nucleic acids research* 44:W406-9.
207. Bowie J, Lüthy R, Eisenberg D. 1991. A Method to Identify Protein Sequences That Fold Into a Known Three-Dimensional Structure. *Science* 253:164-70.
208. Laskowski RA, MacArthur MW, Moss DS, Thornton JM, IUCr. 1993. PROCHECK: a program to check the stereochemical quality of protein structures. *Journal of Applied Crystallography* 26:283-291.
209. Hastings J, Owen G, Dekker A, Ennis M, Kale N, Muthukrishnan V, Turner S, Swainston N, Mendes P, Steinbeck C. 2016. ChEBI in 2016: Improved

- Services and an Expanding Collection of Metabolites. *Nucleic acids research* 44:D1214-9.
210. Schüttelkopf A, van Aalten D. 2004. PRODRG: A Tool for High-Throughput Crystallography of Protein-Ligand Complexes. *Acta crystallographica Section D, Biological crystallography* 60:1355-63.
  211. Trott O, Olson AJ. 2010. AutoDock Vina: improving the speed and accuracy of docking with a new scoring function, efficient optimization and multithreading. *J Comput Chem* 31:455-61.
  212. Khafizov K, Staritzbichler R, Stamm M, Forrest L. 2010. A Study of the Evolution of Inverted-Topology Repeats From LeuT-fold Transporters Using AlignMe. *Biochemistry* 49:10702-13.
  213. Stamm M, Staritzbichler R, Khafizov K, Forrest L. 2013. Alignment of Helical Membrane Protein Sequences Using AlignMe. *PloS one* 8:e57731.
  214. Stamm M, Staritzbichler R, Khafizov K, Forrest L. 2014. AlignMe--a Membrane Protein Sequence Alignment Web Server. *Nucleic acids research* 42:W246-51.
  215. Robert X, Gouet P. 2014. Deciphering key features in protein structures with the new ENDscript server. *Nucleic Acids Res* 42:W320-4.
  216. Le SQ, Gascuel O. 2008. An improved general amino acid replacement matrix. *Mol Biol Evol* 25:1307-20.
  217. Meskys R, Harris RJ, Casaite V, Basran J, Scrutton NS. 2001. Organization of the genes involved in dimethylglycine and sarcosine degradation in *Arthrobacter spp.*: implications for glycine betaine catabolism. *Eur J Biochem* 268:3390-8.
  218. Smith LT, Pocard JA, Bernard T, Le Rudulier D. 1988. Osmotic control of glycine betaine biosynthesis and degradation in *Rhizobium meliloti*. *J Bacteriol* 170:3142-9.
  219. MacMillan SV, Alexander DA, Culham DE, Kunte HJ, Marshall EV, Rochon D, Wood JM. 1999. The ion coupling and organic substrate specificities of osmoregulatory transporter ProP in *Escherichia coli*. *Biochim Biophys Acta* 1420:30-44.
  220. Steger R, Weinand M, Kramer R, Morbach S. 2004. LcoP, an osmoregulated betaine/ectoine uptake system from *Corynebacterium glutamicum*. *FEBS Lett* 573:155-60.
  221. Weinand M, Kramer R, Morbach S. 2007. Characterization of compatible solute transporter multiplicity in *Corynebacterium glutamicum*. *Appl Microbiol Biotechnol* 76:701-8.
  222. Perez C, Koshy C, Yildiz O, Ziegler C. 2012. Alternating-access Mechanism in Conformationally Asymmetric Trimers of the Betaine Transporter BetP. *Nature* 490:126-30.
  223. Schiller D, Rübenhagen R, Krämer R, Morbach S. 2004. The C-terminal Domain of the Betaine Carrier BetP of *Corynebacterium Glutamicum* Is

- Directly Involved in Sensing K<sup>+</sup> as an Osmotic Stimulus. *Biochemistry* 43:5583-91.
224. Horn C, Sohn-Bösser L, Breed J, Welte W, Schmitt L, Bremer E. 2006. Molecular Determinants for Substrate Specificity of the Ligand-Binding Protein OpuAC From *Bacillus Subtilis* for the Compatible Solutes Glycine Betaine and Proline Betaine. *J Mol Biol* 357:592-606.
  225. Smits SHJ, Höing M, Lecher J, Jebbar M, Schmitt L, Bremer E. 2008. The Compatible-Solute-Binding Protein OpuAC from *Bacillus subtilis*: Ligand Binding, Site-Directed Mutagenesis, and Crystallographic Studies. *J Bacteriol* 190:5663-71.
  226. Tschapek B, Pittelkow M, Sohn-Bosser L, Holtmann G, Smits SH, Gohlke H, Bremer E, Schmitt L. 2011. Arg149 is involved in switching the low affinity, open state of the binding protein AfProX into its high affinity, closed state. *J Mol Biol* 411:36-52.
  227. Kaper J, Lockman H, Baldini M, Levine M. 1984. Recombinant Nontoxinogenic *Vibrio cholerae* Strains as Attenuated Cholera Vaccine Candidates. *Nature* 308:655-8.
  228. Chen C, Wu K, Chang Y, Chang C, Tsai H, Liao T, Liu Y, Chen H, Shen A, Li J, Su T, Shao C, Lee C, Hor L, Tsai S. 2003. Comparative Genome Analysis of *Vibrio vulnificus*, a Marine Pathogen. *Genome Res* 13:2577-87.
  229. Lee J, Shread P, Furniss A, Bryant T. 1981. Taxonomy and Description of *Vibrio fluvialis* Sp. Nov. (Synonym Group F Vibrios, Group EF6). *J Appl Bacteriol* 50:73-94.
  230. Pedersen KV, L., Austin B, Austin DA, Blanch AR, Grimont PAD, Jofre J, Koblavi S, Larsen JL, Tiainen T, Vigneulle M, Swings J. 1998. Taxonomic evidence that *Vibrio carchariae* Grimes et al, 1985 is a junior synonym of *Vibrio harveyi* (Johnson and Shunk 1936) Baumann et al. 1981. *Intern J Syst Bacteriol* 48:749-748.
  231. Guzman LM, Belin D, Carson MJ, Beckwith J. 1995. Tight regulation, modulation, and high-level expression by vectors containing the arabinose PBAD promoter. *J Bacteriol* 177:4121-30.
  232. Hoffmann T, Bremer E. 2011. Protection of *Bacillus subtilis* against Cold Stress via Compatible-Solute Acquisition. *J Bacteriol* 193:1552-62.
  233. Browne N, Dowds B. 2001. Heat and Salt Stress in the Food Pathogen *Bacillus Cereus*. *J Appl Microbiol* 91:1085-94.
  234. Holtmann G, Bremer E. 2004. Thermoprotection of *Bacillus subtilis* by Exogenously Provided Glycine Betaine and Structurally Related Compatible Solutes: Involvement of Opu Transporters. *J Bacteriol* 186:1683-93.
  235. Budde I, Steil L, Scharf C, Völker U, Bremer E. 2006. Adaptation of *Bacillus Subtilis* to Growth at Low Temperature: A Combined Transcriptomic and Proteomic Appraisal. *Microbiology* 152:831-53.
  236. Bashir A, Hoffmann T, Kempf B, Xie X, Smits S, Bremer E. 2014. Plant-derived Compatible Solutes Proline Betaine and Betonicine Confer Enhanced

- Osmotic and Temperature Stress Tolerance to *Bacillus Subtilis*. *Microbiology* 160:2283-2294.
237. Bursy J, Kuhlmann AU, Pittelkow M, Hartmann H, Jebbar M, Pierik AJ, Bremer E. 2008. Synthesis and uptake of the compatible solutes ectoine and 5-hydroxyectoine by *Streptomyces coelicolor* A3(2) in response to salt and heat stresses. *Appl Environ Microbiol* 74:7286-96.
  238. May G, Faatz E, Lucht JM, Haardt M, Bolliger M, Bremer E. 1989. Characterization of the osmoregulated *Escherichia coli proU* promoter and identification of ProV as a membrane-associated protein. *Mol Microbiol* 3:1521-31.
  239. Lucht J, Bremer E. 1991. Characterization of Mutations Affecting the Osmoregulated proU Promoter of *Escherichia Coli* and Identification of 5' Sequences Required for High-Level Expression. *J Bacteriol* 173:801-9.
  240. Hengge-Aronis R. 1996. Back to Log Phase: Sigma S as a Global Regulator in the Osmotic Control of Gene Expression in *Escherichia Coli*. *Mol Microbiol* 21:887-93.
  241. Gunasekera T, Csonka L, Paliy O. 2008. Genome-wide Transcriptional Responses of *Escherichia Coli* K-12 to Continuous Osmotic and Heat Stresses. *J Bacteriol* 190:3712-20.
  242. Belitsky BR, Brill J, Bremer E, Sonenshein AL. 2001. Multiple Genes for the Last Step of Proline Biosynthesis in *Bacillus subtilis*. *J Bacteriol* 183:4389-92.
  243. Boch J, Kempf B, Bremer E. 1994. Osmoregulation in *Bacillus Subtilis*: Synthesis of the Osmoprotectant Glycine Betaine From Exogenously Provided Choline. *J Bacteriol* 176:5364-71.
  244. Boch J, Kempf B, Schmid R, Bremer E. 1996. Synthesis of the Osmoprotectant Glycine Betaine in *Bacillus Subtilis*: Characterization of the gbsAB Genes. *J Bacteriol* 178:5121-9.
  245. Boch J, Nau-Wagner G, Kneip S, Bremer E. 1997. Glycine Betaine Aldehyde Dehydrogenase From *Bacillus Subtilis*: Characterization of an Enzyme Required for the Synthesis of the Osmoprotectant Glycine Betaine. *Arch Microbiol* 168:282-9.
  246. Brill J, Hoffmann T, Bleisteiner M, Bremer E. 2011. Osmotically Controlled Synthesis of the Compatible Solute Proline Is Critical for Cellular Defense of *Bacillus Subtilis* Against High Osmolarity. *J Bacteriol* 193:5335-46.
  247. Hahne H, Mäder U, Otto A, Bonn F, Steil L, Bremer E, Hecker M, Becher D. 2010. A Comprehensive Proteomics and Transcriptomics Analysis of *Bacillus Subtilis* Salt Stress Adaptation. *J Bacteriol* 192:870-82.
  248. Steil L, Hoffmann T, Budde I, Völker U, Bremer E. 2003. Genome-wide Transcriptional Profiling Analysis of Adaptation of *Bacillus Subtilis* to High Salinity. *J Bacteriol* 185:6358-70.
  249. Schroeter R, Hoffmann T, Voigt B, Meyer H, Bleisteiner M, Muntel J, Jürgen B, Albrecht D, Becher D, Lalk M, Evers S, Bongaerts J, Maurer K, Putzer H, Hecker M, Schweder T, Bremer E. 2013. Stress Responses of the Industrial

- Workhorse *Bacillus Licheniformis* to Osmotic Challenges. *PLoS One* 8:e80956.
250. Saier MH, Jr. 2001. Evolution of transport proteins. *Genet Eng (N Y)* 23:1-10.
  251. Saier MH, Jr., Paulsen IT. 2001. Phylogeny of multidrug transporters. *Semin Cell Dev Biol* 12:205-13.
  252. Williams BT, Cowles K, Bermejo Martinez A, Curson ARJ, Zheng Y, Liu J, Newton-Payne S, Hind AJ, Li CY, Rivera PPL, Carrion O, Spurgin LG, Brearley CA, Mackenzie BW, Pinchbeck BJ, Peng M, Pratscher J, Zhang XH, Zhang YZ, Murrell JC, Todd JD. 2019. Bacteria are important dimethylsulfoniopropionate producers in coastal sediments. *Nat Microbiol* 4:1815-1825.
  253. Gonzalez JM, Simo R, Massana R, Covert JS, Casamayor EO, Pedros-Alio C, Moran MA. 2000. Bacterial community structure associated with a dimethylsulfoniopropionate-producing North Atlantic algal bloom. *Appl Environ Microbiol* 66:4237-46.
  254. Buchan A, LeClerc GR, Gulvik CA, Gonzalez JM. 2014. Master recyclers: features and functions of bacteria associated with phytoplankton blooms. *Nat Rev Microbiol* 12:686-98.
  255. Archer SD, Widdicombe CE, Tarran GA, Rees AP. 2001. Production and turnover of particulate dimethylsulphoniopropionate during a coccolithophore bloom in the northern North Sea. *Aquatic Microbial Ecology* 24:225-241.
  256. Howard EC, Henriksen JR, Buchan A, Reisch CR, Burgmann H, Welsh R, Ye W, Gonzalez JM, Mace K, Joye SB, Kiene RP, Whitman WB, Moran MA. 2006. Bacterial taxa that limit sulfur flux from the ocean. *Science* 314:649-52.
  257. Stefels J. 2000. Physiological aspects of the production and conversion of DMSP in marine algae and higher plants. *Journal of Sea Research* 43:183-197.
  258. Ansedé J, Pellechia P, Yoch D. 2001. Nuclear Magnetic Resonance Analysis of [1-<sup>13</sup>C]dimethylsulfoniopropionate (DMSP) and [1-<sup>13</sup>C]acrylate Metabolism by a DMSP Lyase-Producing Marine Isolate of the Alpha-Subclass of Proteobacteria. *Appl Environ Microbiol* 67:3134-9.
  259. Ansedé J, Friedman R, Yoch D. 2001. Phylogenetic Analysis of Culturable Dimethyl Sulfide-Producing Bacteria From a *Spartina*-Dominated Salt Marsh and Estuarine Water. *Appl Environ Microbiol* 67:1210-7.
  260. Todd J, Curson A, Kirkwood M, Sullivan M, Green R, Johnston A. 2011. DddQ, a Novel, Cupin-Containing, Dimethylsulfoniopropionate Lyase in Marine Roseobacters and in Uncultured Marine Bacteria. *Environ Microbiol* 13:427-38.
  261. Todd J, Kirkwood M, Newton-Payne S, Johnston A. 2012. DddW, a Third DMSP Lyase in a Model Roseobacter Marine Bacterium, *Ruegeria Pomeroyi* DSS-3. *ISME J* 6:223-6.
  262. Hehemann J, Law A, Redecke L, Boraston A. 2014. The Structure of RdDddP From Roseobacter Denitrificans Reveals That DMSP Lyases in the DddP-family Are Metalloenzymes. *PLoS One* 9:e103128.

263. Burkhardt I, Lauterbach L, Brock N, Dickschat J. 2017. Chemical Differentiation of Three DMSP Lyases From the Marine Roseobacter Group. *Org Biomol Chem* 15:4432-4439.
264. Onda D, Azanza R, Lluisma A. 2015. Potential DMSP-degrading Roseobacter Clade Dominates Endosymbiotic Microflora of *Pyrodinium bahamense* Var. *Compressum* (Dinophyceae) in Vitro. *Arch Microbiol* 197:965-71.
265. Todd JD, Curson AR, Nikolaidou-Katsaraidou N, Brearley CA, Watmough NJ, Chan Y, Page PC, Sun L, Johnston AW. 2010. Molecular dissection of bacterial acrylate catabolism--unexpected links with dimethylsulfoniopropionate catabolism and dimethyl sulfide production. *Environ Microbiol* 12:327-43.
266. Broy S, Chen C, Hoffmann T, Brock NL, Nau-Wagner G, Jebbar M, Smits SH, Dickschat JS, Bremer E. 2015. Abiotic stress protection by ecologically abundant dimethylsulfoniopropionate and its natural and synthetic derivatives: insights from *Bacillus subtilis*. *Environ Microbiol* 17:2362-78.
267. Sun L, Curson ARJ, Todd JD, Johnston AWB. 2011. Diversity of DMSP transport in marine bacteria, revealed by genetic analyses. *Biogeochemistry* 110:121-130.
268. Lidbury I, Murrell JC, Chen Y. 2014. Trimethylamine N-oxide metabolism by abundant marine heterotrophic bacteria. *Proc Natl Acad Sci U S A* 111:2710-5.
269. Curson AR, Todd JD, Sullivan MJ, Johnston AW. 2011. Catabolism of dimethylsulphoniopropionate: microorganisms, enzymes and genes. *Nat Rev Microbiol* 9:849-59.
270. Moran MA, Reisch CR, Kiene RP, Whitman WB. 2012. Genomic insights into bacterial DMSP transformations. *Ann Rev Mar Sci* 4:523-42.
271. Reisch CR, Moran MA, Whitman WB. 2011. Bacterial Catabolism of Dimethylsulfoniopropionate (DMSP). *Front Microbiol* 2:172.
272. Greenfield DI, Moore JG, Steward JR, Hilborn ED, George BJ, Li Q, Dickerson J, Keppler CK, Sandifer PA. 2017. Temporal and environmental factors driving *Vibrio vulnificus* and *V. parahaemolyticus* populations and their associations with harmful algal blooms in South Carolina detention ponds and receiving tidal creeks. *GeoHealth* 1:306-317.
273. Thickman JD, Goble CJ. 2017. The ability of algal organic matter and surface runoff to promote the abundance of pathogenic and non-pathogenic strains of *Vibrio parahaemolyticus* in Long Island Sound, USA. *PLoS One* 12:e0185994.
274. Regev R, Peri I, Gilboa H, Avi-Dor Y. 1990. <sup>13</sup>C NMR study of the interrelation between synthesis and uptake of compatible solutes in two moderately halophilic eubacteria. *Bacterium Ba1* and *Vibrio costicola*. *Arch Biochem Biophys* 278:106-12.
275. Calderon MI, Vargas C, Rojo F, Iglesias-Guerra F, Csonka LN, Ventosa A, Nieto JJ. 2004. Complex regulation of the synthesis of the compatible solute ectoine in the halophilic bacterium *Chromohalobacter salexigens* DSM 3043T. *Microbiology* 150:3051-63.

276. Vargas C, Jebbar M, Carrasco R, Blanco C, Calderon MI, Iglesias-Guerra F, Nieto JJ. 2006. Ectoines as compatible solutes and carbon and energy sources for the halophilic bacterium *Chromohalobacter salexigens*. *J Appl Microbiol* 100:98-107.
277. Ma Y, Wang Q, Xu W, Liu X, Gao X, Zhang Y. 2017. Stationary phase-dependent accumulation of ectoine is an efficient adaptation strategy in *Vibrio anguillarum* against cold stress. *Microbiol Res* 205:8-18.
278. Jutras BL, Verma A, Stevenson B. 2012. Identification of novel DNA-binding proteins using DNA-affinity chromatography/pull down. *Curr Protoc Microbiol Chapter 1:Unit1F.1*.
279. Jutras BL, Liu Z, Brissette CA. 2010. Simultaneous isolation of Ixodidae and bacterial (*Borrelia* spp.) genomic DNA. *Curr Protoc Microbiol Chapter 1:Unit1E.2*.
280. Baba T, Ara T, Hasegawa M, Takai Y, Okumura Y, Baba M, Datsenko KA, Tomita M, Wanner BL, Mori H. 2006. Construction of *Escherichia coli* K-12 in-frame, single-gene knockout mutants: the Keio collection. *Mol Syst Biol* 2:2006.0008.
281. Williams SG, Carmel-Harel O, Manning PA. 1998. A functional homolog of *Escherichia coli* NhaR in *Vibrio cholerae*. *J Bacteriol* 180:762-5.
282. Rahav-Manor O, Carmel O, Karpel R, Taglicht D, Glaser G, Schuldiner S, Padan E. 1992. NhaR, a Protein Homologous to a Family of Bacterial Regulatory Proteins (LysR), Regulates nhaA, the Sodium Proton Antiporter Gene in *Escherichia Coli*. *J Biol Chem* 267:10433-8.
283. Krol JE. 2018. Regulatory loop between the CsrA system and NhaR, a high salt/high pH regulator. *PLoS One* 13:e0209554.
284. Pratt L, Hsing W, Gibson K, Silhavy T. 1996. From Acids to osmZ: Multiple Factors Influence Synthesis of the OmpF and OmpC Porins in *Escherichia Coli*. *Mol Microbiol* 20:911-7.
285. Kenney L, Bauer M, Silhavy T. 1995. Phosphorylation-dependent Conformational Changes in OmpR, an Osmoregulatory DNA-binding Protein of *Escherichia Coli*. *Proc Natl Acad Sci U S A* 92:8866-70.
286. Ansaldi M, Théraulaz L, Baraquet C, Panis G, Méjean V. 2007. Aerobic TMAO Respiration in *Escherichia Coli*. *Mol Microbiol* 66:484-94.
287. Simon G, Méjean V, Jourlin C, Chippaux M, Pascal M. 1994. The torR Gene of *Escherichia Coli* Encodes a Response Regulator Protein Involved in the Expression of the Trimethylamine N-oxide Reductase Genes. *J Bacteriol* 176:5601-6.
288. Shikuma NJ, Yildiz FH. 2009. Identification and characterization of OscR, a transcriptional regulator involved in osmolarity adaptation in *Vibrio cholerae*. *J Bacteriol* 191:4082-96.
289. Yang L, Zhan L, Han H, Gao H, Guo Z, Qin C, Yang R, Liu X, Zhou D. 2010. The low-salt stimulon in *Vibrio parahaemolyticus*. *Int J Food Microbiol* 137:49-54.



## Appendix A

### THE ROLE OF OSCR AND LEUO IN LOW SALT REGULATION IN *VIBRIO* *PARAHAEMOLYTICUS*

We sought to further investigate the role of two regulators, OscR and LeuO, in the low salt stress response in *V. parahaemolyticus*. We identified LeuO as a regulator of the ectoine biosynthesis gene cluster in our promoter pulldown. We previously demonstrated that LeuO is a negative regulator of the T3SS, but its role in osmotic stress has not been investigated (106). OscR regulated biofilm formation and motility in *V. cholerae* (288). Furthermore, *oscR* was found to be upregulated under low salt conditions in *V. cholerae*, while both *oscR* and *leuO* are upregulated under low salt conditions in *V. parahaemolyticus* (288, 289). We therefore investigated the role of each regulator in motility and CPS production assays, in both low and optimal salt conditions. We have previously demonstrated that the quorum sensing regulator OpaR plays a role in regulation of the osmotic stress response (108), and so we also investigated whether OpaR regulates *oscR* or *leuO*.

To characterize these regulators, we first constructed a 663 base pair in-frame deletion of the 735-bp *oscR* gene (VPA0593) in *Vibrio parahaemolyticus* RIMD2210633 through Splicing by Overlap Extension (SOE) PCR and homologous recombination (151). Primers were designed to create a 72-bp truncated allele of *oscR* using the primer pair listed in **Table 14**. The product was amplified from the *V. parahaemolyticus* RIMD2210633 genome via PCR and ligated into the cloning vector pJET1.2 via blunt-end ligation with T4 DNA ligase and transformed into *E. coli* Dh5 $\alpha$ . The truncated allele was then cut out of the resulting pJET $\Delta$ *oscR* vector using the restriction enzymes SacI and XbaI and ligated into the suicide vector pDS132, which

had been linearized using the same restriction enzymes. The resulting plasmid, pDS $\Delta$ *oscR*, was transformed into *E. coli* Dh5 $\alpha$ , and then the diaminopimelic acid auxotroph strain *E. coli*  $\beta$ 2155  $\lambda$ *pir*, for conjugation into wild-type RIMD2210633. The suicide vector pDS132 must recombine into the genome via homologous recombination in order to be replicated, due to the absence of the necessary replication gene *pir* in the *V. parahaemolyticus* genome. Single-crossover colonies were selected by plating onto chloramphenicol selection plates and screened via PCR for a truncated allele. A double-crossover event was then induced after overnight growth in liquid medium without chloramphenicol selection. Cultures were spread-plated onto 10% sucrose plates, and healthy colonies were screened. Colonies still containing the plasmid appeared soupy on the plate due to the presence of the *sacB* gene which makes sucrose toxic to the cells. An in-frame deletion was confirmed via sequencing.

We assayed the swarming motility of wild type,  $\Delta$ *oscR*,  $\Delta$ *leuO* and  $\Delta$ *rpoN*, which does not swarm, on swarming plates with either 0.5% NaCl or 3% NaCl. The  $\Delta$ *oscR* mutant had a smaller colony size as compared to wild type and  $\Delta$ *leuO* when grown on media supplemented with 0.5% NaCl (**Figure 56**). When grown on media supplemented with 3% NaCl, the  $\Delta$ *oscR* and  $\Delta$ *leuO* mutants were more proficient at swarming than the wild-type strain (**Figure 57**). All colonies had a rugose colony morphology when grown on 0.5% NaCl media but not when grown on 3% NaCl media (**Figure 56 and 57**). CPS production was also assayed on Congo Red media. The  $\Delta$ *oscR* mutant produces CPS similar to wild type, while the  $\Delta$ *leuO* mutant produces a more compact rugose structure that covers a smaller area (**Figure 58**).

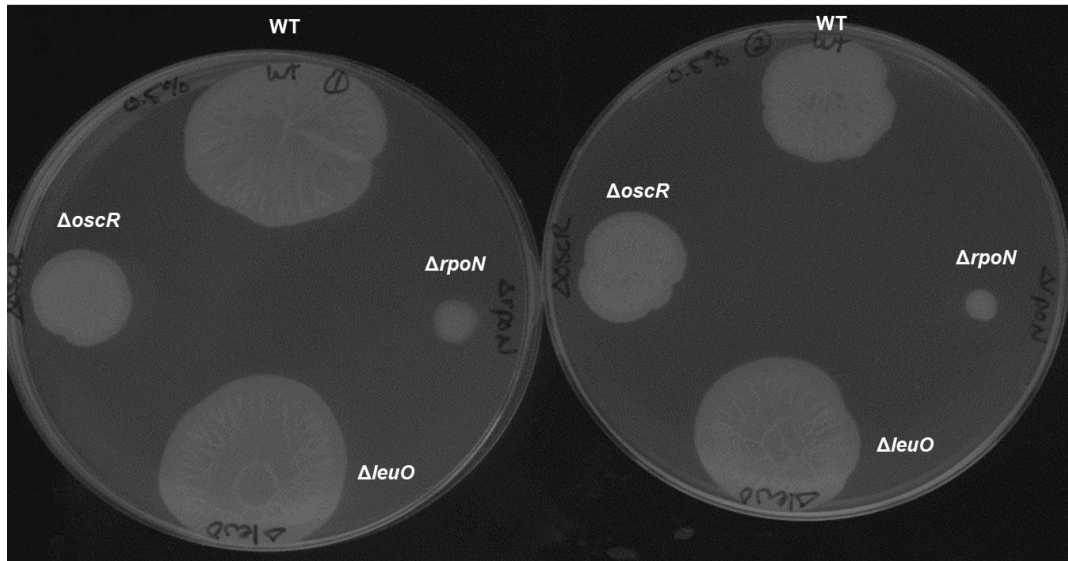


**Figure 56** Swarming assay on HI plates supplemented with 0.5% NaCl *Vibrio parahaemolyticus* wild type,  $\Delta oscR$ ,  $\Delta leuO$  and  $\Delta rpoN$ , as a negative control, were grown on HI swarming plates supplemented with 0.5% NaCl at 30°C for 48 hours.

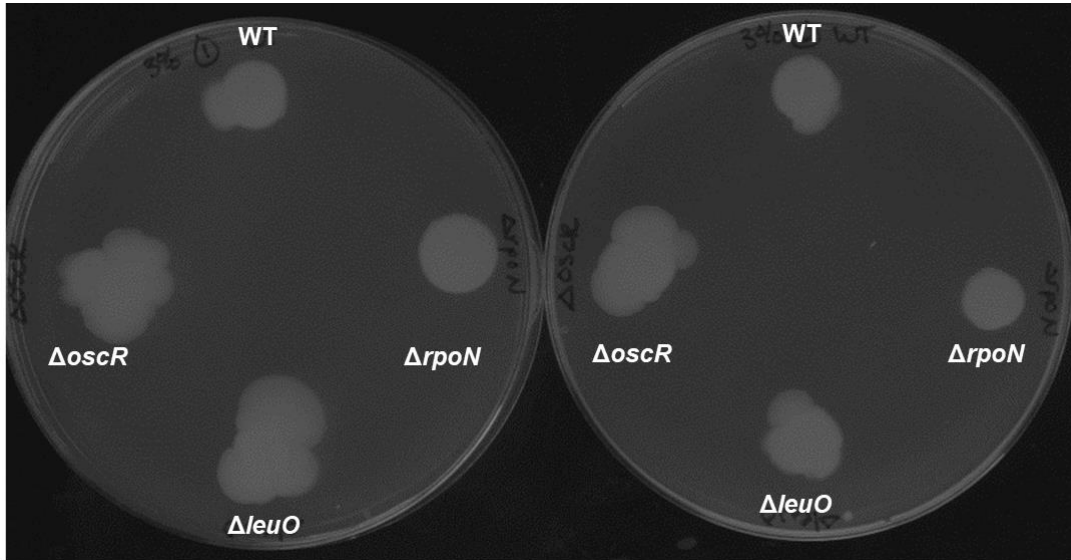
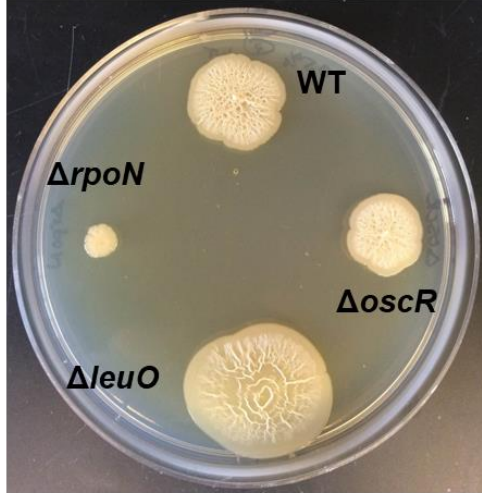
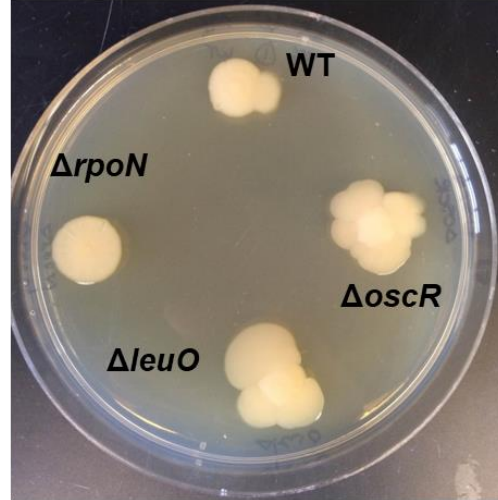


**Figure 57** Swarming assay on HI plates supplemented with 3% NaCl *Vibrio parahaemolyticus* wild type,  $\Delta oscR$ ,  $\Delta leuO$  and  $\Delta rpoN$ , as a negative control, were grown on HI swarming plates supplemented with 3% NaCl at 30°C for 48 hours.

**A. Colony morphology LB 0.5% NaCl**



**B. Colony morphology LB 3% NaCl**



**C. CPS Production**

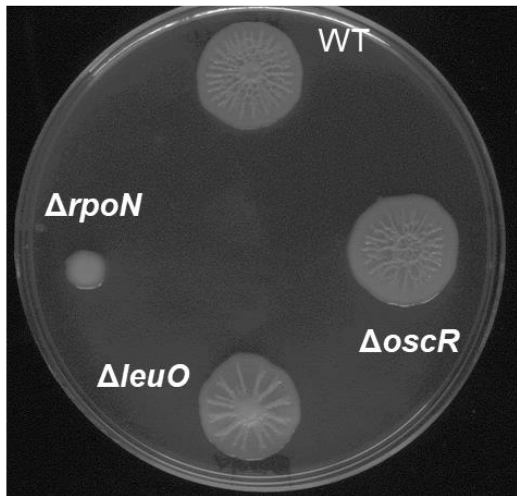
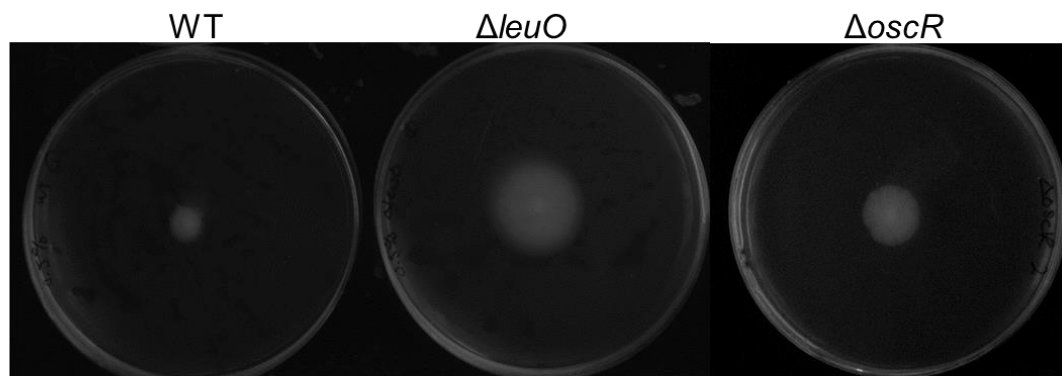


**Figure 58 Colony morphology and CPS production**

*Vibrio parahaemolyticus* wild type,  $\Delta oscR$ ,  $\Delta leuO$  and  $\Delta rpoN$ , as a negative control, were grown on HI swarming plates supplemented with (A) 0.5% NaCl, (B) 3% NaCl or (C) Congo Red plates to visualize capsule polysaccharide production. All plates were incubated at 30°C for 48 hours.

**A. Swimming assay on soft-agar LB 0.5% NaCl**



**B. Quantification of swimming assay**

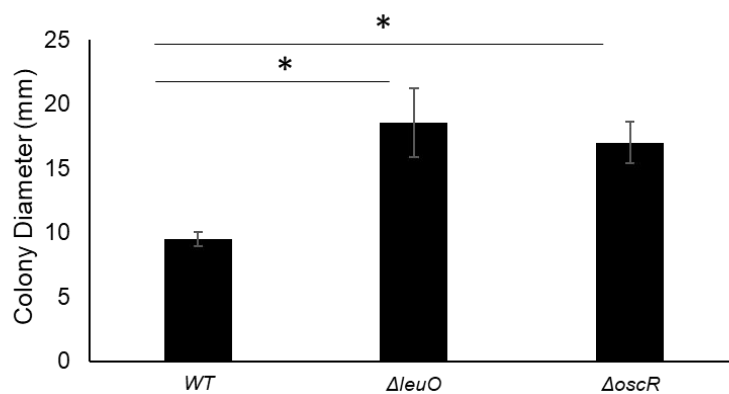


**Figure 59** **Swimming assay on soft-agar 0.5% NaCl plates**  
*Vibrio parahaemolyticus* wild type,  $\Delta oscR$ , and  $\Delta leuO$  were grown on soft-agar (0.3%) swimming plates supplemented with 0.5% NaCl. **(A)** Images of representative swimming plates. **(B)** Quantification of the colony diameter. All plates were incubated at 37°C for 24 hours.

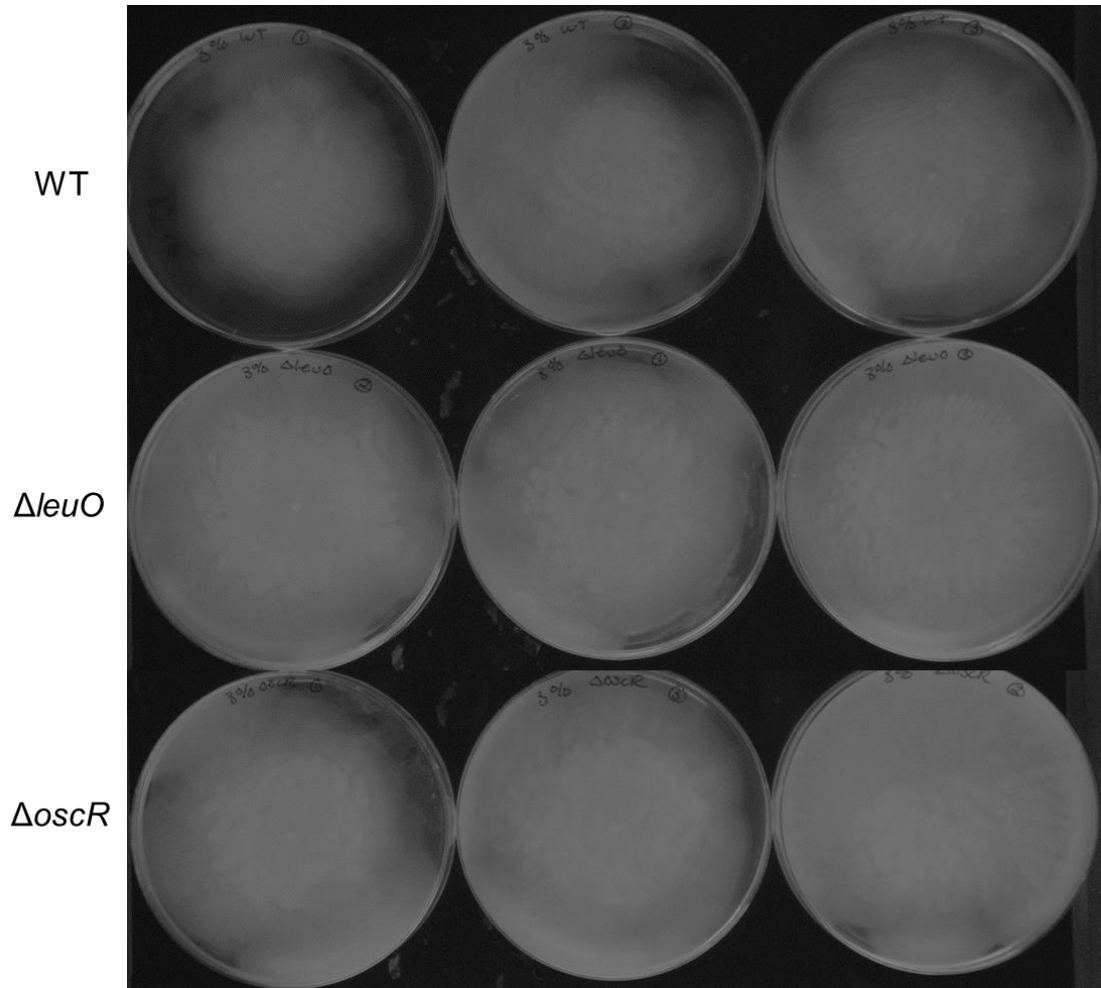


**Figure 60** **Swimming assay on soft-agar 3% NaCl plates**  
*Vibrio parahaemolyticus* wild type,  $\Delta oscR$ , and  $\Delta leuO$  were grown on soft-agar (0.3%) swimming plates supplemented with 3% NaCl. All plates were incubated at 37°C for 24 hours.

Swimming motility of wild type,  $\Delta oscR$ , and  $\Delta leuO$  was assayed on soft-agar plates with either 0.5% NaCl or 3% NaCl. The  $\Delta oscR$  and  $\Delta leuO$  mutants were significantly more proficient at swimming than the wild-type strain when grown in media supplemented with 0.5% NaCl (**Figure 59**), indicating that OscR and LeuO negatively regulate swimming motility in low salinity. Swimming motility assays in

media supplemented with 3% NaCl had a similar trend, with  $\Delta oscR$  and  $\Delta leuO$  swimming to the outside edge of all plates (**Figure 60**). Wild type did not always reach the edge (**Figure 60**). This assay should be repeated with shorter time points or larger plates.

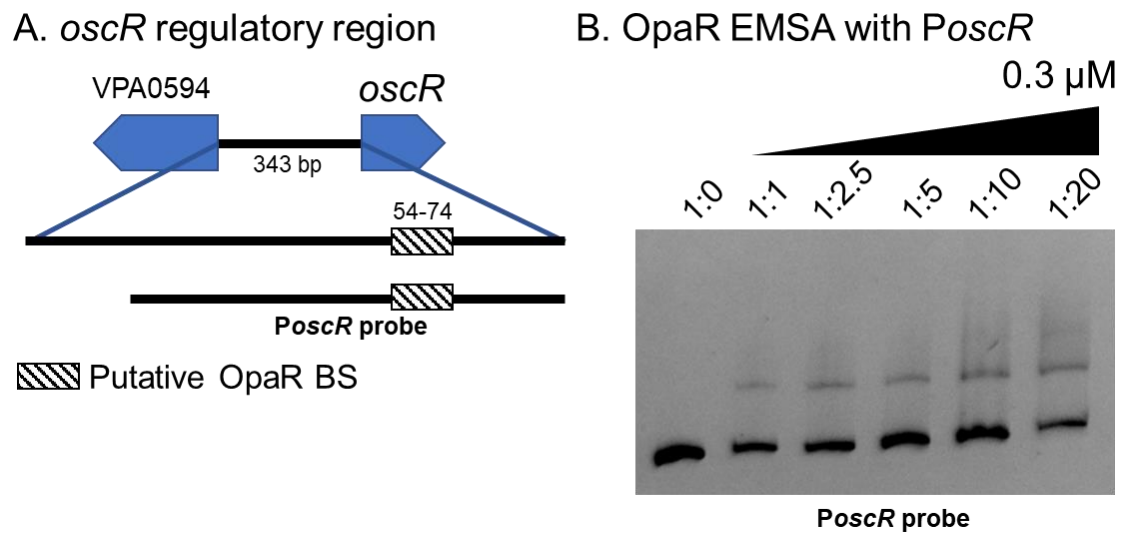


**Figure 61 OpaR binds *oscR* promoter region.** (A) The region upstream of *oscR* (*PoscR*) is shown with a putative OpaR binding site 54 bp upstream of the translational start. *PoscR* probe extends from the translational start to 313 bp upstream. (B) An EMSA was performed with various concentrations of purified OpaR protein (0 to 0.3  $\mu$ M) and 30 ng of probe with DNA:protein ratios of 1:0, 1:1, 1:2.5, 1:5, 1:10, and 1:20.

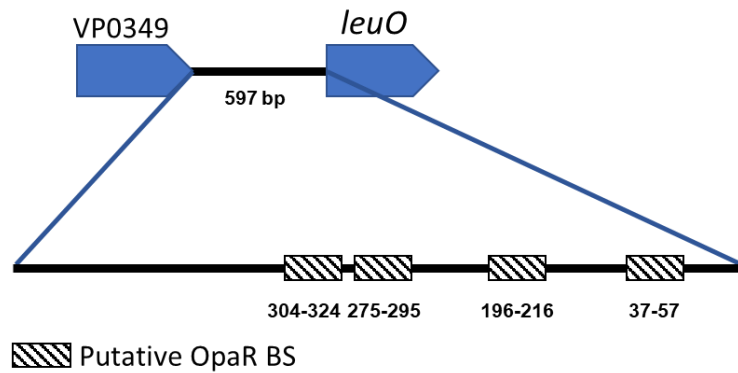


**Figure 62 Putative OpaR binding sites in *leuO* regulatory region**  
 Putative OpaR binding sites were identified in the regulatory region of *leuO* using MOODS and the position frequency matrix of OpaR.

We next investigated whether the quorum sensing regulator OpaR may directly regulate *oscR* or *leuO*. We used the Motif Occurrence Detection Suite (MOODS) to identify putative binding sites of OpaR in the regulatory regions of each gene. We identified a single OpaR binding site in the regulatory region upstream of the *oscR* gene (**Figure 61**). We confirmed that OpaR does bind to the regulatory region of *oscR* via a DNA binding assay (**Figure 61**). We also identified four putative OpaR binding sites upstream of the *leuO* gene (**Figure 62**). Direct binding of OpaR to this region needs to be tested.

Table 14 Primers used in this study

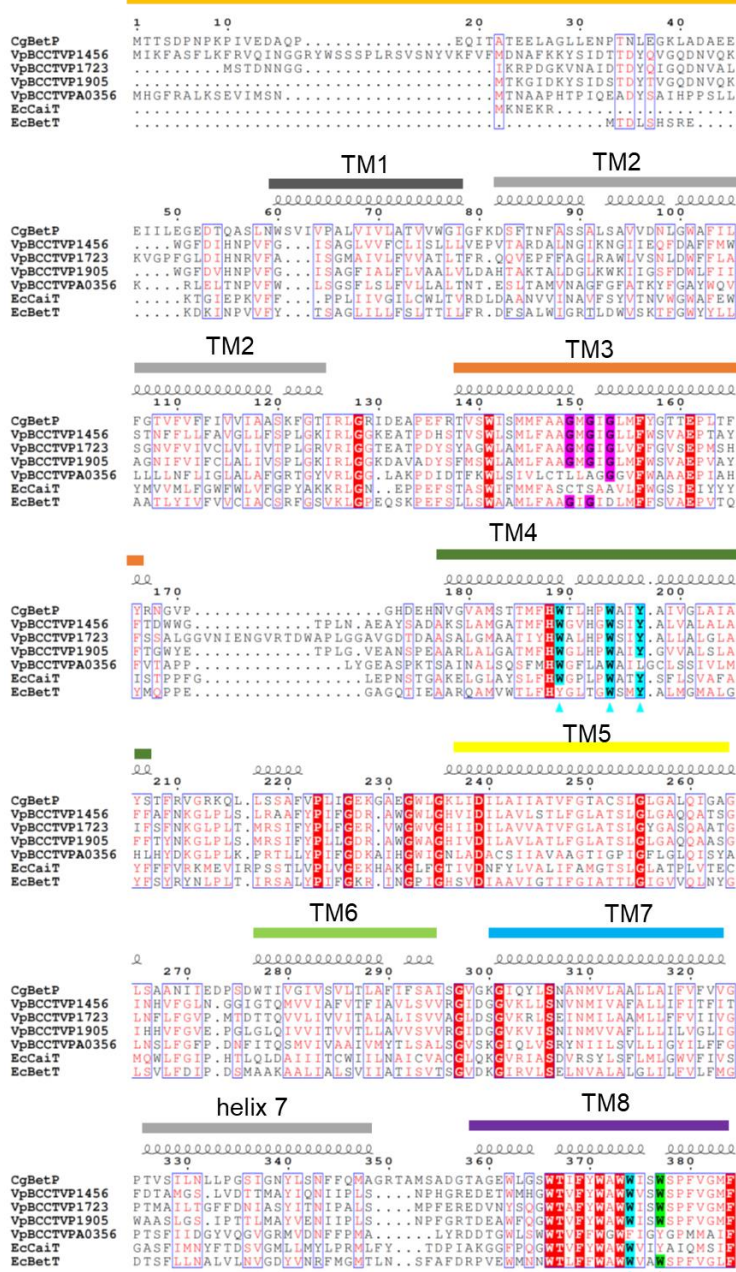
Use and Primer	Sequence (5'-3')	Length (bp)
<b>Mutant primers</b>		
oscR FLF	GCCCTTGAGTCACCACTAGC	2001
oscR FLR	CTTGATCTTCGGCGTATTCC	
oscR A	<u>TCTAGACGAGCAAGTGATCGAGGTTA</u>	503
oscR B	CAGTGCCTTTTTCGTTTACC	
oscR C	<u>GGTAAACGAAAAGGCACTGAGGGCACTACCACCAGAAAG</u>	516
oscR D	<u>GAGCTCTTTCGTGTCTTGCTCGCTTA</u>	

**Appendix B**

**ALIGNMENT OF *VIBRIO PARAHAEMOLYTICUS***

**BCCT-FAMILY TRANSPORTERS**

N-term



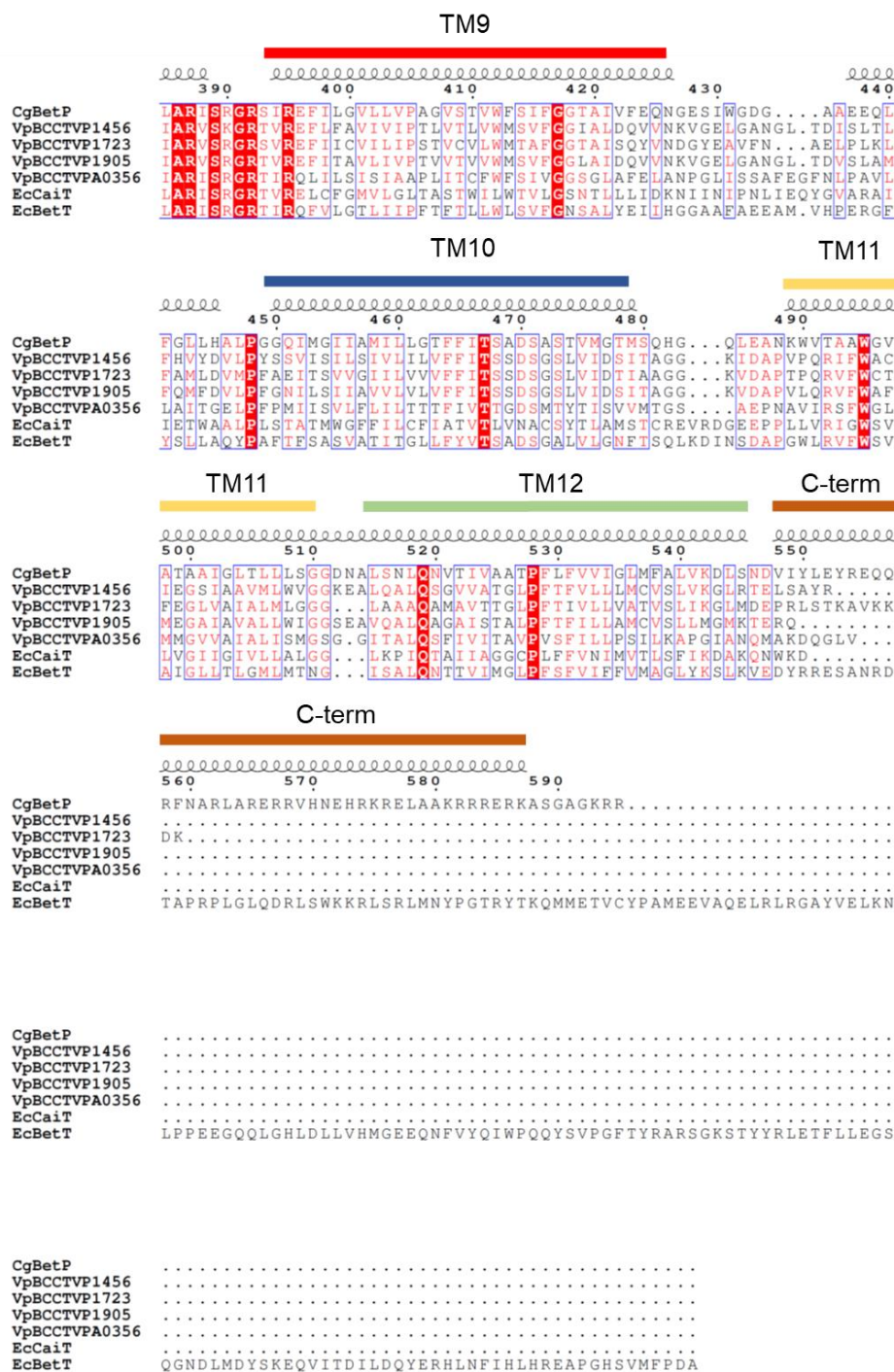


**Figure 63** Alignment of BccTs with structurally-characterized BCCT-family transporters

The *V. parahaemolyticus* BCCT proteins VP1456, VP1723, VP1905 and VPA0356 were aligned with *Corynebacterium glutamicum* BetP, *E. coli* CaiT and *E. coli* BetT and displayed using ESPript. Residues highlighted in red are strictly conserved. Residues highlighted in magenta are conserved in sodium-symporters. Residues marked with a cyan triangle have been demonstrated to be important for glycine betaine binding; residues highlighted in cyan are conserved. A green star denotes residues thought to be important for additional substrate binding; conserved residues are highlighted in green.

## Appendix C

### PERMISSION LETTER



AMERICAN  
SOCIETY FOR  
MICROBIOLOGY

#### **Quorum Sensing Regulators AphA and OpaR Control Expression of the Operon Responsible for Biosynthesis of the Compatible Solute Ectoine**

**Author:**

Gwendolyn J. Gregory, Daniel P. Morreale, Megan R. Carpenter, Sai S. Kalburge, E.  
Fidelma Boyd

**Publication:**

Applied and Environmental Microbiology

**Publisher:**

American Society for Microbiology

**Date:**

Oct 30, 2019

*Copyright © 2019, American Society for Microbiology*

**Permissions Request**

Authors in ASM journals retain the right to republish discrete portions of his/her article in any other publication (including print, CD-ROM, and other electronic formats) of which he or she is author or editor, provided that proper credit is given to the original ASM publication. ASM authors also retain the right to reuse the full article in his/her dissertation or thesis. For a full list of author rights, please see: [http://journals.asm.org/site/misc/ASM\\_Author\\_Statement.xhtml](http://journals.asm.org/site/misc/ASM_Author_Statement.xhtml)

## Appendix D

### PERMISSION LETTER



AMERICAN  
SOCIETY FOR  
MICROBIOLOGY

#### **CosR Is a Global Regulator of the Osmotic Stress Response with Widespread Distribution among Bacteria**

**Author:**

Gwendolyn J. Gregory, Daniel P. Morreale, E. Fidelma Boyd

**Publication:**

Applied and Environmental Microbiology

**Publisher:**

American Society for Microbiology

**Date:**

May 5, 2020

*Copyright © 2020, American Society for Microbiology*

**Permissions Request**

Authors in ASM journals retain the right to republish discrete portions of his/her article in any other publication (including print, CD-ROM, and other electronic formats) of which he or she is author or editor, provided that proper credit is given to the original ASM publication. ASM authors also retain the right to reuse the full article in his/her dissertation or thesis. For a full list of author rights, please

see: [http://journals.asm.org/site/misc/ASM\\_Author\\_Statement.xhtml](http://journals.asm.org/site/misc/ASM_Author_Statement.xhtml)